Cell Replacement and *Ex Vivo* Gene Therapy for Photoreceptor Regeneration

Alona Cramer
Merton College

Supervisor: Professor Robert E. MacLaren

Thesis submitted for the degree of Doctor of Philosophy
University of Oxford, Nuffield Department of Clinical Neurosciences

Trinity Term 2015

Declaration

I declare that this thesis is my own original work. Where I have consulted or quoted the work of others, this is clearly attributed. No part of this thesis has previously been submitted for a degree or any other qualification at this University or any other institution.

Alona Cramer
University of Oxford
2015

Dedication

To my husband Nim; my light.

Acknowledgments

I thank my supervisor, Professor Robert MacLaren, for his mentorship and encouragement throughout my DPhil; for always making time to discuss research and offer valuable perspectives. I am grateful to him for providing a unique example of team-leadership and cultivating a supportive and collaborative research environment, and for his calm nature and sense of humour in discussion of potential challenges. I have been privileged to learn from his vast experience, his dedication to scientific pursuit and his keenness for pushing the boundaries of experimental and clinical research.

I would like to thank my colleagues at the Nuffield Laboratory of Ophthalmology for their generosity with their time and guidance in a multitude of techniques: Dr Mandeep Singh, Dr Dominik Fischer and Major Sher Aslam for direction and assistance in transplantation surgeries; Dr Alun Barnard for his invaluable guidance in experimental design and help with pupilometry, scanning laser ophthalmoscopy and electroretinogram experiments; Dr Michelle McClements for her direction in cloning, primer design and vector production; Dr Samantha de Silva for her advice in set up of the optomotor response experiments; and past and present members of the MacLaren research group, in particular Dr Doron Hickey and Dr Daniyar Dauletbekov for their experience and advice.

I am grateful to our collaborators at Ocata Therapeutics, MA, USA, for their work in differentiation of human stem cells for transplantation studies, primarily to Professor Robert Lanza, Dr Wei Wang and Dr Shi-Jiang Lu for their valued contribution to the research and enthusiasm for discussion.

I am thankful to The Oxford University Clarendon fund for awarding me the Clarendon Scholarship and providing a fantastic opportunity to pursuit this DPhil.

For financial support in presenting this research at international conferences I thank Merton College for the award of the Graduate Research Grant 2012 and 2013, The ARVO association for Research in Vision and Ophthalmology for the MIT Outstanding Poster Award for the ARVO Annual Meeting 2014 and the Asia-ARVO travel Grant Award 2015.

I am also grateful to the European Gateway for Vision Research; Pro Retina Germany; the Young Researcher Vision Camp; ARVO Ocular Cell Biology Conference; EURETINA European Society of Retina Specialists and the Oxford Stem Cell Institute for inviting me to present this research to the scientific community.

For counsel and support of my scientific career I thank Professor Tamar Makin and Professor Heidi Johansen-Berg, my college advisor Professor Kieran Clarke, Professor Robert Lanza and Professor Zila Zuckerman.

Finally, I sincerely thank my family for being a source of inspiration; my parents who are an example of true kindness and wisdom, my wonderful sisters for their endless love, my mother and father in-law for their loving support and my wonderful husband for inspiring me every day.

Abstract

Cell Replacement and *Ex Vivo* Gene Therapy for Photoreceptor Regeneration

Alona Cramer, Merton College, University of Oxford
Trinity 2015

Photoreceptor degeneration due to retinitis pigmentosa (RP) is a primary cause of inherited retinal blindness. Photoreceptor cell-replacement therapies may hold the potential for repair in a degenerate retina, by reinstating light sensitive cells to project and form connections with downstream retinal cells and finally the visual cortex. Patient-specific induced pluripotent stem cells (iPSc) could provide an autologous source of cells to replace lost tissue. However, the use of patient-derived iPSc would require that the disease-causing gene mutation be corrected in cells before transplantation.

Ex vivo gene therapy of mouse photoreceptor precursor (PhRP) cells and subretinal transplantation of treated cells are here studied in a disease-specific animal model of RP; rhodopsin was ectopically expressed *ex vivo* in rod precursor cells, sourced from a transgenic model lacking the rhodopsin gene. Treated rod precursors were here transplanted in mice of the same disease model and are shown to gain expression of rhodopsin and mature to regenerate the absent outer nuclear layer (ONL) of degenerate mice. Visual function, assayed in the same animals before and after transplantation, was restored in animals which had no rod function at baseline.

Delivery of the rhodopsin gene by both an adeno associated viral (AAV) vector and a non-viral minicircle DNA vector developed here for *ex vivo* gene delivery to rod photoreceptor precursors showed comparable efficiency and sustained expression. The non-viral minicircle method provides a novel system for efficient photoreceptor therapy and may offer a platform of genetic treatment of photoreceptor degenerations in which the gene in focus exceeds the size limit for packaging in AAV.

Human embryonic stem cell (ESC) and human iPSC-derived PhRPs were also transplanted in mice with complete ONL degeneration and were able to reform the lost photoreceptor layer and mature in the host retina. Human cells developed light-sensitive outer segments, and reconnect with host neurons downstream to improve vision in previously blind mice.

Efficient transplantation of *ex vivo* genetically treated rod precursors and human stem cell-derived PhRPs in animal models of progressive RP may provide a clinically-relevant model for the investigation of cell-replacement therapy for photoreceptor regeneration in retinal disease.

Table of Contents

List of Tables

List of Figures

List of Abbreviations

AAV	Adeno associated viral
AMD	Age related macular degeneration
BLA	Behavioural Light Aversion
CBA	chicken β-actin
CG	Ciliary ganglia
CHM	choroideremia
CNS	Central nervous system
CRISPR	Clustered regularly interspaced short palindromic repeats
DMEM	Dulbecco's Modified Eagle's Medium
EGFP	enhanced green fluorescent protein
ER	Endoplasmic reticulum
ESC	Embryonic stem cell
EWN	Edinger Westphal nuclei
FACS	Fluorescence-activated cell sorting
GCL	Ganglion cell layer
GFAP	Glial fibrillary acidic protein
GFP	green fluorescent protein
HNA	Human nuclear antigen
HSC	Haematopoietic stem cells
INL	Inner nuclear layer
iPSC	induced Pluripotent Stem cells
IRES	Internal ribosome entry site
IS	Inner segments
ISI	Inter-stimulus interval
ipRGC	intrinsically photosensitive retinal ganglion cell

ITR	Inverted terminal repeat
LCA	Leber's congenital amaurosis
LGN	Lateral geniculate nucleus
MACS	Magnetic-activated cell sorting
MAK	Male germ cell-associated kinase
MC	minicircle
MFRP	Membrane Frizzle-related Protein
MOI	Multiplicity of infection
NACWO	Named Animal Care and Welfare Officer
NRL	Neural retina leucine zipper
NSC	Neural stem cell
NVS	Named Veterinary Surgeon
OCT	Optimal cutting temperature
OMR	Optomotor Response
ONL	Outer nuclear layer
OPL	Outer plexiform layer
ORF	Open reading frames
OS	Outer segment
PBS	Phosphate-buffered saline
PCR	Polymerase chain reaction
PhRP	photoreceptor precursor
PI	Proteasome inhibition
PLR	Pupil light reflex
PN	Post natal
PN	Pretectal nuclei
PP	Parental plasmid
PSC	Pluripotent stem cell
QPCR	Quantitative polymerase chain reaction
RGC	Retinal ganglion cells
RHOK	Rhodopsin kinase
RNPC	Retinal neural progenitor cells

RP	Retinitis pigmentosa
RPE	Retinal pigment epithelium
RT	Room temperature
SB	Sleeping beauty transposon
SEM	Standard error of the mean
SLO	Scanning Laser Ophthalmoscopy
SPLICE	Swift PCR for ligating in vitro constructed exons
TALEN	Transcription activator-like effector nucleases
TR	Terminal repeats
TRID	Translational read-through inducing drugs
WT	Wild-type

1. Introduction

1.1. Overview

Vision is perceived when photons are captured by the light sensing neurons of the eye, the rod and cone photoreceptors, which comprise the retinal outer nuclear layer (ONL). Photoreceptors convert light signals into electrical impulses, sending information to further retinal layers and through the optic nerve to be processed in the brain.

Retinitis pigmentosa (RP) is one of the leading causes of untreatable genetic blindness, and is characterised by degeneration of rod photoreceptors followed by a gradual loss of cones. Mammalian photoreceptor cells do not have the capacity to regenerate and, once they are lost, light is no longer perceived. At present, there is no treatment to regenerate lost photoreceptors in RP.

Cell replacement could provide a promising therapy for patients who have lost all photoreceptor cells due to degeneration, and thus has been widely researched using primary animal cells as well as photoreceptors differentiated from mouse and human pluripotent stem cells (PSC). Patient-specific induced pluripotent stem cells (iPSC) could provide an autologous, readily expandable, and immunologically attuned source of cells for transplantation. However, due

to their derivation from an individual who has a genetic disease, the inherent genetic mutation would be present in the newly-differentiated photoreceptors and thus cells would require genetic repair before being delivered back to the patient. In this study, visual rescue in an animal model of severe retinal degeneration was investigated by transplantation following *ex vivo* gene correction of a genetic mutation in primary neonatal photoreceptor cells. Additionally, human stem cell-derived photoreceptors were transplanted to assess their potential for *in vivo* maturation and visual repair in a mouse model of severe retinal degeneration.

In considering a complex and multi-staged therapy method, it is helpful to start from the clinical need and gain perspective on possible therapeutic approaches.

In this chapter, an introduction to the retina in health (Section 1.2) and RP disease (Section 1.3) will be presented, followed by an overview of photoreceptor cell replacement strategies (Section 1.4) and the potential of *ex vivo* gene therapy for rescue of genetic mutations in photoreceptor cells (Section 1.5). Then, strategies for gene replacement using viral and non-viral gene delivery (Section 1.6), and the aims and outline of the thesis (Section 1.7) will be presented.

1.2. The retina

1.2.1. Anatomy

The retina is a multi-layered, light-sensitive neuronal structure lining the posterior hemisphere of the globe internally (Fig 1.1). Photoreceptor cell bodies in the outer nuclear layer (ONL) extend inner segments (IS) and outer segments (OS) toward the retinal pigment epithelium (RPE) at the posterior margin, and form proximal synaptic connections with bipolar and horizontal cells in the outer plexiform layer (OPL). Bipolar cell bodies, together with the horizontal, amacrine, and Müller cell bodies, construct the inner nuclear layer (INL) and make afferent synaptic connections with the ganglion cell layer (GCL). Axons of the GCL form the nerve fibre layer, which extends through the optic nerve out of the retina and towards the brain.[1,2]

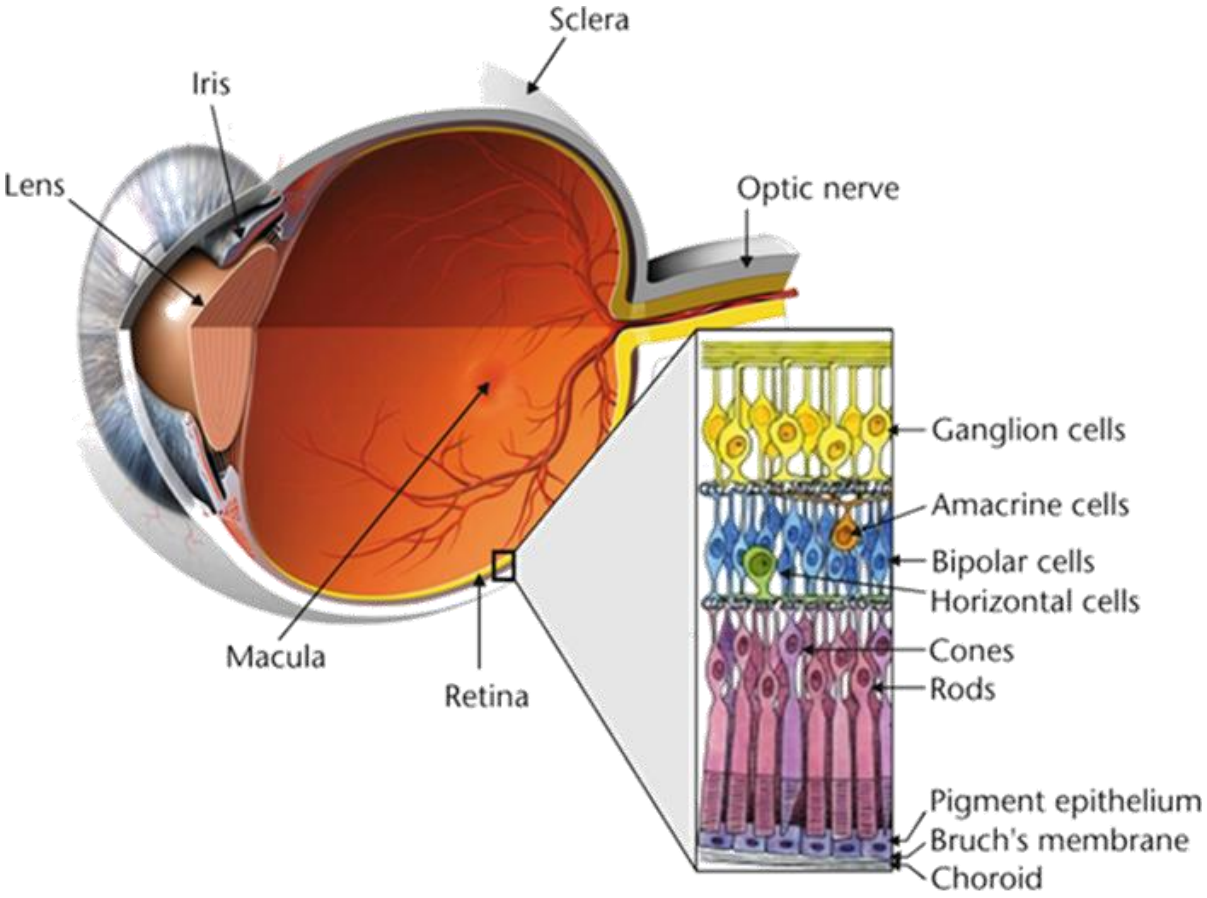

Figure 1.1: The layered structure of the retina.

The first order sensory neurons of the visual system, cone and rod photoreceptors, reside in the outer nuclear layer bordering on RPE cells. Light signals are transferred to the bipolar cells of the inner nuclear layer and pass through ganglion cells and the optic nerve to reach the brain.

Adapted from Bretillion et al., 2011[3].

1.2.2. Photoreceptors and phototransduction

Perception of visual stimuli is dependent on light signals passing through the retinal layers described above, being transmitted through the optic nerve and lateral geniculate nucleus (LGN), and being processed by the visual cortex in the occipital lobe of the brain. The first neurons in this pathway are the light sensitive rod and cone photoreceptors in the ONL. A third class of photoreceptors located in the inner retina, are the intrinsically photosensitive retinal ganglion cell (ipRGC)[4,5], which contain melanopsin as their photosensitive pigment. The latter class of photoreceptors likely does not contribute to image forming vision, but is mainly involved in circadian entrainment and other non-image forming visual functions.

The centre of the human retina is cone-dominated; cone photoreceptors are responsible for high visual acuity in bright-light conditions and colour vision, and represent less than 5% of the total number of photoreceptors (approximately 5 million cells).[6] The peripheral retina is predominantly comprised of rod photoreceptors, which are present in far greater numbers (approximately 125 million cells) and sensitive to low-light conditions. In retinitis pigmentosa, rod cells are the first neurons to degenerate and are thus the focus of cell replacement therapy, as will be further discussed in the coming sections.

Photoreceptors have four major functional structures: the synaptic terminal, the cell body, the IS, and the OS. The IS contains mitochondria and provides energy for photoreceptor metabolism through the production of adenosine

triphosphate (ATP). It is connected by a thin cilium to the OS, which is densely packed with disks containing visual pigments. Photoreceptors instigate the visual transduction cascade by converting light signals into an electrochemical response. This process begins in the outer segment structures. In rod cells the outer segment is stacked with membrane discs containing the visual pigment rhodopsin, which consists of a G-protein coupled receptor opsin, covalently bound to a chromophore, the molecule 11-cis retinal.

The photopigment in rods and cones differs in the protein portion of the molecule, which tunes retinal to be sensitive to specific wavelengths of light. When a photon of light is absorbed by 11-cis retinal, a component of its bond breaks, changing its configuration to the all-trans retinal isomer, which triggers changes in the opsin molecule structure. The altered rhodopsin promotes activation of the G-protein transducin, which is bound to GDP in its inactive state, allowing transducin to exchange its GDP for GTP. The alpha subunit of transducin then activates the phosphodiesterase (PDE) in the disk membrane. PDE hydrolyzes cGMP, thus lowering cytoplasmic free cGMP concentration throughout the outer segment. cGMP in the inactive state holds membrane ion channels open; thus, a reduction in its concentration leads to closing of these channels and hyperpolarisation of the rod photoreceptor, in turn decreasing glutamate release at the synaptic terminal, which is present in the inactive state.[7]

Mutations in the genes encoding proteins involved in the visual cascade may cause retinal disease (as will be further described in Section 1.3) and are thus

a target for gene therapy. OS can be identified using immunohistochemical techniques to tag OS-specific proteins, which are absent in disease models, and to determine their restoration after cell replacement therapy, as described in Chapter 5 and 6.

1.2.3. The retina as a model for central nervous system regeneration

The retina has emerged as an increasingly promising frontier for investigation of central nervous system (CNS) regeneration and stem cell transplantation, owing to its unique features as a surgically accessible, immune privileged organ which can be non-invasively imaged. Grafted cells can be observed directly through the clear ocular media and functional assessment of the transplantation can be achieved using an array of established visual tests. Moreover, retinal degenerations are commonly bilateral, and hence pre-clinical and clinical trials may be applied to only one eye, while making use of the fellow eye as a control. Finally, unlike the long tracts of the brain and cerebellum, transplanted photoreceptors need only to make short synaptic connections to their immediate neighbouring cells in the INL across non-myelinated tissues in order to restore function. This facilitates physiological assessment of transplanted cells.[8]

Retinal neurons, like other neurons of the CNS, degenerate progressively throughout life and show limited capacity for regeneration and repair after injury. But while single retinal neurons do not regenerate (except in specific

circumstances, such as during development[9]) the visual system as a whole does exhibit quite encouraging signs of neuroplasticity and preservation, even after severe retinal degeneration. Post-mortem studies in human patients with advanced retinal degeneration due to retinitis pigmentosa (the disease in focus in this thesis, which will be discussed in Section 1.3 below) revealed that, although only 4% of photoreceptors were present in the severely degenerate eyes, 66% of the normal bipolar cell population remained in the degenerate tissue[10]. Furthermore, observations that ganglion cells in rodents can regenerate to restore function through peripheral nerve grafts demonstrate the plastic potential of the central targets of the visual pathway[11,12]. Compelling evidence for the regenerative capacities of the human visual system was heralded by the subretinal implantation of electronic photoreceptor arrays[13,14], after which patients with visual impairments regained a degree of vision, to the extent that one patient could read large print after the transplant[14]. This implies the potential of an exogenous source to relay signals to a preserved and functioning visual pathway downstream of the lost photoreceptors; or, alternatively, suggests the possibility of neuronal regeneration and reorganisation in the visual pathway following treatment.

In light of this, photoreceptor cell-replacement therapies may hold the potential for repair in a degenerating or completely degenerate retina, by reinstating light sensitive cells to project and form connections with downstream retinal cells and finally the visual cortex.

1.3. Retinitis pigmentosa

1.3.1. Clinical characteristics

Retinitis pigmentosa (RP) refers to a set of hereditary retinal degenerative diseases characterised by the progressive loss of rod photoreceptors and the potential subsequent secondary degeneration of cone photoreceptors, loss of lamination of the outer retina, and invasion of RPE cells into the neural retina, which are visible as bone-spicule shaped pigmented structures – hence 'pigmentosa'[15].

RP is the leading cause of inherited retinal blindness in young patients, with an overall estimated prevalence of approximately 1:3,500-1:5,000, or over 1 million patients worldwide[16-22]. In most forms of the disease, an initial loss of rod photoreceptors leads to a cellular cascade that promotes the gradual secondary degeneration of cone photoreceptors[23]. Retinitis pigmentosa is a highly variable disorder in terms of genetics and onset; some patients develop visual loss in childhood, whereas others remain asymptomatic until mid-adulthood[16]. Typically, affected individuals first experience nyctalopia or 'night blindness' in adolescence, due to defective dark adaptation caused by the degeneration of rod cells. In young adulthood the peripheral visual field constricts, creating 'tunnel vision' with a loss of up to half the visual field before the age of 25[24] and rendering most patients legally blind by the age of 40 due to severely constricted visual fields. These symptoms are attributed to the progressive degeneration of rod cells, which are specialised for vision in low

light conditions and abundant in the retinal periphery. In later life cone photoreceptors progressively degenerate, causing loss of visual acuity and central vision, usually by the age of 60[16]. Progressive loss of all light-sensing rod and cone photoreceptor cells eventually leads to complete blindness.

1.3.2. Genetic mechanisms and the rhodopsin gene in RP

RP can be inherited as an autosomal-dominant (adRP), autosomal-recessive (arRP), or X-linked trait[25-27]. Most cases of retinitis pigmentosa are monogenic, but the disease is nevertheless very heterogeneous genetically. Over 200 loci of mutation have been mapped so far, of which more than 170 genes have been identified (from RetNet; http://www.sph.uth.tmc.edu/retnet/).

Most genes implicated in RP cause only a fraction of cases, with the exception of the rhodopsin gene (RHO), which leads to about 25% of adRP; the USH2A gene, which might cause about 20% of arRP; and the RPGR gene, which accounts for about 70% of X-linked RP. Mutations in these three genes account for approximately 30% of total cases of retinitis pigmentosa[16,17,28-31].

Non-Mendelian inheritance patterns, such as digenic inheritance and maternal (mitochondrial) inheritance, have been reported, but are probably implicated in only a small proportion of cases[32-36].

The rhodopsin (*RHO*) gene was the first gene linked to RP[37,38]. Rhodopsin is the first molecule to initiate the visual transduction cascade (see Section 1.2.2) and accounts for nearly 50% of protein in the OS and 80% of proteins in rod photoreceptor discs.[39] The *RHO* gene holds extensive structural and functional

importance and has been central in animal models of RP, as without this gene no rod function is possible; thus, rhodopsin was chosen as the gene of focus for proof-of-concept gene correction studies in this thesis.

Over 100 different mutations of the *RHO* gene have been identified. Although some mutations in *RHO* cause recessive RP and congenital stationary night blindness, the vast majority of *RHO* mutations are involved in adRP[40-42]. The different mutations in *RHO* have been associated with considerable phenotypic heterogeneity; *in vitro* studies have clustered *RHO* mutations by level of expression, amount of chromophore regeneration, glycosylation pattern, and cell surface targeting, but these did not correspond to a common phenotype[43]. Classification of disease severity, rate of progression, and clinical–functional phenotypes associated with specific RHO mutations are lacking.[44] Genetic heterogeneity implies that diverse mechanisms underpin the different subtypes of the disease, making drug treatment extremely difficult to fit to a patient whose underlying genetic causes for the disease are unknown, as patients with different underlying mutations may require different drugs.[45] Furthermore, the vast number of genetic causes and expression patterns implies that animal models of RP will unavoidably lack in translational characteristics for the different subtypes of the disease. Study of this disease in the context of gene therapy and cell replacement is therefore attained by use of animal models that present similar progression of photoreceptor dysfunction and ONL degeneration as pre-clinical proofs of concept. Insight into specific mutations

and their treatment may be attained by patient-specific reprogrammed cells, as will be discussed in Section 1.5.

1.3.3. Therapeutic approaches for RP

Treatment for patients with RP is currently limited, and the development of therapeutic approaches would rely on an understanding of the disease mechanism and on the stage of intervention.

In the early stages of retinal degeneration before severe degeneration of photoreceptor occurs, delivery of gene therapy or neuroprotective agents could provide a promising option to slow or halt photoreceptor cell loss and rescue the remaining cells of the ONL from further degeneration. Interventions in the late stages of RP, when loss of rod and cone photoreceptors has become severe, would focus on replacement rather than rescue. In late stages, the majority of photoreceptors are lost and strategies to replace photoreceptor cells or their photosensitive role are being developed. Optogenetic strategies aim to introduce novel light-sensing proteins into the degenerate retina, targeting retinal neurons such as bipolar or ganglion cells and prompting these cells to function as light-sensing cells in place of lost photoreceptors.[46,47] Further treatment for the late stages of disease progression and end-stage degeneration may be achieved through direct stimulation by electrodes of the ganglion cells of the inner retina.[48,49] Similarly, implantation of subretinal electronic photodiode arrays has been shown to restore basic vision to formerly blind patients.[13,14]

The ability of electronic devices to stimulate the retina provides proof of the feasibility of visual restoration by reinstating light sensing receptors. The use of biological material to replace cells would be preferable to the implantation of an electronic device. A large number of cells could be transplanted in order to replace lost photoreceptors and potentially reconstruct the degenerate ONL, form connections with the remaining INL, and restore natural input to the INL. Pre-clinical studies of photoreceptor cell replacement for the treatment of RP, as well as challenges in transplantation and potential cell sources, will be presented in Section 1.4.

1.3.4. Animal models of end stage RP

Animal models of RP have been used extensively for the study of retinal degeneration and for pre-clinical assessment of both gene therapy and cell replacement. Mouse models have been an invaluable model system for the development of retinal therapies. The mouse retina presents limitations to the study of human disease—mice do not have a fovea, which is the area in the human retina which is cone-rich and in charge of central vision—but the layered structure and cell types are similar, and the peripheral ONL is largely similar to the human structure and contains predominantly rod photoreceptors.

For studies of RP, the most relevant mouse models are those in which rod photoreceptors degenerate followed by cones, as such models may be assessed at different time-points by relevance to treatment. For example, gene therapy treatments would target early stages of degeneration and aim at the

rescue of rods or cones, while for transplantation studies the most relevant time-point is end stage degeneration, when the ONL is completely lost and would need to be replaced by exogenous cells.

Two models which lead to photoreceptor degeneration and eventual blindness were assessed in this thesis at end stages of degeneration. The rhodopsin knockout ($Rho^{-/-}$) mouse is a model of relatively slow degeneration culminating in complete loss of photoreceptor cells, and the rd1 mouse is a fast degeneration model culminating in complete degeneration of the ONL.

1.3.4.1. The rhodopsin knockout mouse

Homozygous rhodopsin knockout ($Rho^{-/-}$) mice carry a hereditary null mutation in exon 2 of the rhodopsin gene; they are characterised by a complete absence of the rhodopsin gene and do not develop normal rod outer segments (OS).[50] Eventually, degeneration of rods leads to progressive cone degeneration,[51] a common feature of human RP.

$Rho^{-/-}$ mice lose their photoreceptors within a period of approximately 3 months. Due to the absence of the *rho* gene, phototransduction in this model is compromised[52] and rod function is completely absent from birth.[50] Rod degeneration in this model starts at approximately PN24, by postnatal week 6 cone photoreceptors begin degenerating, and the barely-detectable cone-mediated photopic electroretinogram (ERG) signal is completely lost by 8

weeks of age. By approximately 3 months of age near-complete absence of photoreceptor OS is observed.[51]

The $Rho^{-/-}$ model was used in the current work both to provide donor cells for *ex vivo* gene replacement of the rhodopsin gene and as an adult blind host for transplantation of treated cells after loss of host photoreceptors (to be detailed in Chapters 4 and 5).

1.3.4.2. The rd1 mouse

The *rd1* mice carry a null mutation in the rod photoreceptor cyclic GMP (cGMP) phosphodiesterase β subunit (pde6b) gene.[53,54] This mouse model is the most extensively studied animal model for human autosomal recessive RP[55] and mutations in the *PDE6B* gene have also been found in patients with this condition.[54,56]

Mice homozygous for the *rd1* mutation display heredity photoreceptor degeneration and progressive thinning of the ONL, followed by complete loss of this layer. The mutation causes abnormal accumulation of cGMP in the retina and subsequent rapid rod degeneration, followed by degeneration of cone photoreceptors through secondary mechanisms as cones do not express *PDE6B*. In this model, rod photoreceptors begin to degenerate around PN8,[50] and by PN17 only about 2% of rods remain in the posterior region of the retina. Cone photoreceptors degenerate less rapidly, with 75% of cones remaining at PN17 and progressively degenerating thereafter.[57]

By 3-4 weeks of age, all rod cells and the majority of cone cells are lost.[53,57-59] Although approximately 1.5% of cone nuclei are still detectable in the posterior retina at 18 months of age,[57] OS are absent in these cones, the size of their inner segments (IS) is reduced, as is the number of mitochondria, and they are engulfed by RPE processes.[60] Normal ERGs are not elicited at any stage in this model; however, detection of rod and cone a- and b-waves are still attainable in this model at PN18, steadily decline over 90% by 2 months of age,[61] and continue to degenerate thereafter, so that by week 10 the ONL is completely lost and the mice display no visual function.[62]

The *rd1* model was used in this study as a blind host for transplantation of human stem cells (Chapter 6).

1.4. Cell replacement therapies

1.4.1. Cell replacement in animal models of RP

Mouse photoreceptors and photoreceptors derived from animal and human pluripotent stem cells (PSC) have been extensively researched as candidates for cell replacement. Early studies in mammals first attempted to replace lost cells by immature retinal tissue.[63-66] Substantial proof of photoreceptor integration and rescue of function was achieved following the discovery that the ontogenetic stage of donor cells was critical for successful cell transplantation, so that survival and integration were best accomplished by using post-mitotic rod photoreceptor precursor (PhRP) cells at the neural

leucine zipper (*Nrl*)-expressing stage.[62,67-69] Cell-replacement by rod photoreceptors is in line with the pattern of degeneration in severe RP, as transplantation of cone photoreceptors into a rodless animal would culminate in the degeneration of cones in the absence of supporting rods. Rod precursors, however, can potentially mature to become functioning rod cells in the degenerate retina and rescue remaining cones or completely replace lost photoreceptors in severe cases of degeneration. Improvement of visual function following rod PhRP transplantation in animal models with a varied range of retinal dysfunction or degeneration has been described,[62,67,70-75] including a demonstration that transplanted mouse PhRPs were able to construct a new ONL, restoring some visual function to blind mice in complete absence of host photoreceptors;[62] this highlights cell replacement as a potential tool for vision repair after complete degeneration of the ONL, which is the most clinically relevant scenario for the use of cell replacement to treat late-stage RP.

Similarly staged human cells have not been studied in the context of complete photoreceptor absence and will be addressed in Chapter 6.

1.4.2. Challenges in transplantation of photoreceptor cells

When generating photoreceptors for therapeutic application, it is important to consider the physical challenges of transplanting them into the retina.

In the healthy intact human retina, photoreceptors are positioned in the ONL of the outer retina in a laminated and polarised manner, with OS projecting discs

towards the RPE, and adjoining a layer of Müller cells at the outer limiting membrane. Orientation and integration of these cells is important for their function and survival, and loss of connection in the adherent junctions between photoreceptors and Müller cells is linked to photoreceptor degeneration.[76,77,78]

Single-cell suspensions of retinal cells are predominantly used in current transplantation studies, perhaps due to their ease of surgical delivery and high likelihood of forming direct connections with the host INL. While PhRPs have been shown to integrate and form connections with host retina when transplanted as a single-cell suspension,[62,67,70,72,79] the average percentage of synapse-forming grafted precursor cells is extremely low (in the region of 0.1% of transplanted cells)[79] and the integration of photoreceptors in the correct orientation within the ONL is infrequently accomplished.[80]

In order to promote integration of the transplanted photoreceptors into the retina, a method that would ensure their polarised integration post-transplant would be ideal. Transplantation of embryonic, neonate, or adult retinal sheets, where photoreceptors are transplanted within a matrix of neighbouring retinal cells, have been proposed.[81-84] A consideration supporting this strategy for RP is that this disease does not have a constant trajectory of degeneration, but rather manifests differently in different patients. In some diseases that are caused by RPE specific genes, loss of photoreceptors is sometimes accompanied by secondary retinal degeneration or RPE loss, and in such cases transplanting photoreceptors with RPE cells may have additional therapeutic effect (e.g. MerTK, RPE65, choroideremia). However, such studies

face the problem of the donor INL being interposed between the host retina and transplanted photoreceptors, which presents a physical barrier for synaptic integration. Furthermore, gliosis associated with outer retinal degeneration may pose a significant limitation to connectivity between the graft and host, even when outer retinal sheets are transplanted without INL (photoreceptor sheets or photoreceptors with RPE).[85,86] However, disruption of glial barriers may increase integration of immature single cells.

Advancements in stem cell differentiation, and the recent generation of a self-forming optic cup in a 3D *in vitro* culture system from both human embryonic stem cells (ESC) and induced pluripotent stem cells (iPSC),[87,88] may provide advances in transplantation of photoreceptor cells polarised within their ocular environment. Indeed, such retinal structures have shown a degree of integration with the host retina in a model of complete retinal degeneration.[89] Biodegradable polymer scaffolds have also been suggested to promote cell integration and survival in areas of the damaged retina.[90,91] This method may represent an important step forward in cell replacement transplantations and prove to be applicable to the expansion and transplantation of differentiated stem cell-derived photoreceptors.

1.4.3. ESC and iPSC for cell replacement

Stem cell therapies represent a potential therapeutic approach for replacement and repair of non-functioning neuroretinal cells[92-95]. Several types of stem cells are currently being investigated in the field of retinal repair, including retinal

progenitor cells (RPCs)[96-98], brain-derived neural stem and progenitor cells[99-102], mesenchymal stem cells (MSCs)[103], embryonic stem cells (ESCs)[73], and induced pluripotent stem cells (iPSCs)[89]. The differentiation of retinal tissue and, specifically, photoreceptor precursors (PhRPs), from stem cells has been widely researched as an expandable cell source for transplantation[75,87,104-106].

Photoreceptor precursors ideally integrate into the host retina of mice when obtained from donor mice around postnatal day 3,[62,67,78,107] a period which is developmentally comparable with the second trimester of pregnancy in humans.[108,109] Therefore, obtaining significant numbers of the analogous human primary cells is fraught with ethical issues.

Embryonic stem cells (ESC) are cells harvested from the inner cell mass of the embryo blastocyst, and can differentiate into the three germ layers (endoderm, ectoderm and mesoderm). ESCs represent an important research avenue for cell replacement; as they can be differentiated to generate a vast array of target cell types for transplantation, however ethical obstacles and the challenge of obtaining meaningful numbers of cells from human blastocysts limit their use for retinal cell transplantation.

Furthermore, the use of ESC-derived retinal precursor cells in clinical trials entails a risk of immune rejection; although the retina is protected by the blood-retina barrier, in advanced stages of retinal degeneration the RPE monolayer is injured, compromising this protective barrier.[86,110] The surgical manipulation required to transplant cells compromises this barrier to some extent and introduces circulating immune cells, such as T-cells, into the subretinal space.

Foreign transplanted tissue, even if allogeneic, runs a higher risk of rejection in the degenerate retina and requires constant immune suppression post-transplant, which in itself is associated with severe health risks to the patient. A need is evident for a readily expandable, immunologically attuned source of cells for basic and clinical research.

Challenges for cell replacement by cells derived from ESC may potentially be addressed through the use of autologous induced pluripotent stem cells (iPSC). First developed in mammalian vertebrates in 2006[108] and contingent on breakthroughs in cell reprogramming in lower vertebrates in 1962[111], iPSC technology allows the reprogramming of adult somatic cells by chemically altering extrinsic signalling pathways. This reinstitutes the re-differentiation of the adult somatic cell into cell lineages of the three germ layers, generating cells that are similar to ESC. *In vitro* retinal differentiation protocols have been established for the generation of photoreceptor precursors from both ESC and iPSC,[45,75,88,105,112-120] largely echoing the developmental landmarks of *in vivo* differentiation in health and disease [45,121,122].

The possibility of subverting the unidirectional course of differentiation by cell-reprogramming and thus reinstituting the capacity for a differentiated cell to adopt a new fate, is conceptually intriguing and entails a prospective paradigm shift in medicine and research. Disease-specific and patient-specific iPSC would be highly attractive and relevant for both research and clinic.

Patient-specific iPSC may reduce the need for extensive immune suppression after cell transplantation, as the autologous cells are a near-perfect

immunological match for the patient. However, this advantage becomes a drawback in the case of unintentional transplantation of undifferentiated cells, which can lead to tumour formation[123,124]. In the scenario of tumour formation after transplantation of ESC-derived tissue, immune suppression can be removed, permitting the immune cells of the host retina to attack the foreign growth. However, if malignancy occurs after transplanting patient-specific iPSC, proliferating cells are less likely to be identified and removed via circulating immune cells.

In preclinical studies conducted in mice, cell sorting and enrichment of human iPSC-derived photoreceptors prior to transplantation were achieved by fluorescence-activated cell sorting (FACS) after lentiviral transduction of cells with GFP driven from a photoreceptor specific promoter,[114] producing a cell suspension in which 90% of cells could be histologically labelled as rod or cone photoreceptors. However, this method of sorting reduced cell viability and efficacy; and moreover, fluorescent tagging of cells is not desirable for human application. These problems may be addressed by magnetic-activated cell sorting (MACS), in which magnetic beads are attached to surface markers on the target cells and subsequently sorted by a magnet. Enrichment of transplanted rods by this method, using the CD73 rod cell surface marker,[125,126] has been shown to increase the integration of mouse primary rod photoreceptor cells. MACS sorting has also been used successfully to remove unwanted proliferating cells from mouse iPSC-derived photoreceptors prior to transplantation, by depletion of proliferative cells expressing stage-specific

embryonic antigen 1 (SSEA1) from the transplantation suspension.[75] Such methods have not yet been successful in the enrichment of human stem cell-derived photoreceptors prior to transplantation. A method for cell purification or complete differentiation of cells prior to transplantation would critically increase the safety and potential clinical use of stem cells for treatment in humans.

A further consideration specific to autologous iPSC-derived cells for cell replacement therapy is that the newly differentiated autologous cells would be predisposed to the same disease-causing genetic degeneration that is present in the patient, leading to the need for the genetic mutation to be corrected in these cells *ex vivo* before transplantation. *Ex vivo* gene correction will be discussed in the next section.

In a model scenario, cells are obtained from the somatic tissue of a patient with inherited retinal degeneration, reprogrammed to a pluripotent state, expanded *in vitro,* and differentiated to reach an appropriate developmental state for transplantation or research. These iPSC-derived differentiated cells could subsequently be used either as *in vitro* models of genetic diseases and therapy development ('disease in a dish') or subjected to *ex vivo* gene therapy in order to correct the genetic mutation causing blindness. Subsequently, corrected autologous cells would be purified and transplanted back into the patient. Figure 1.2 presents a schematic representation of this process.

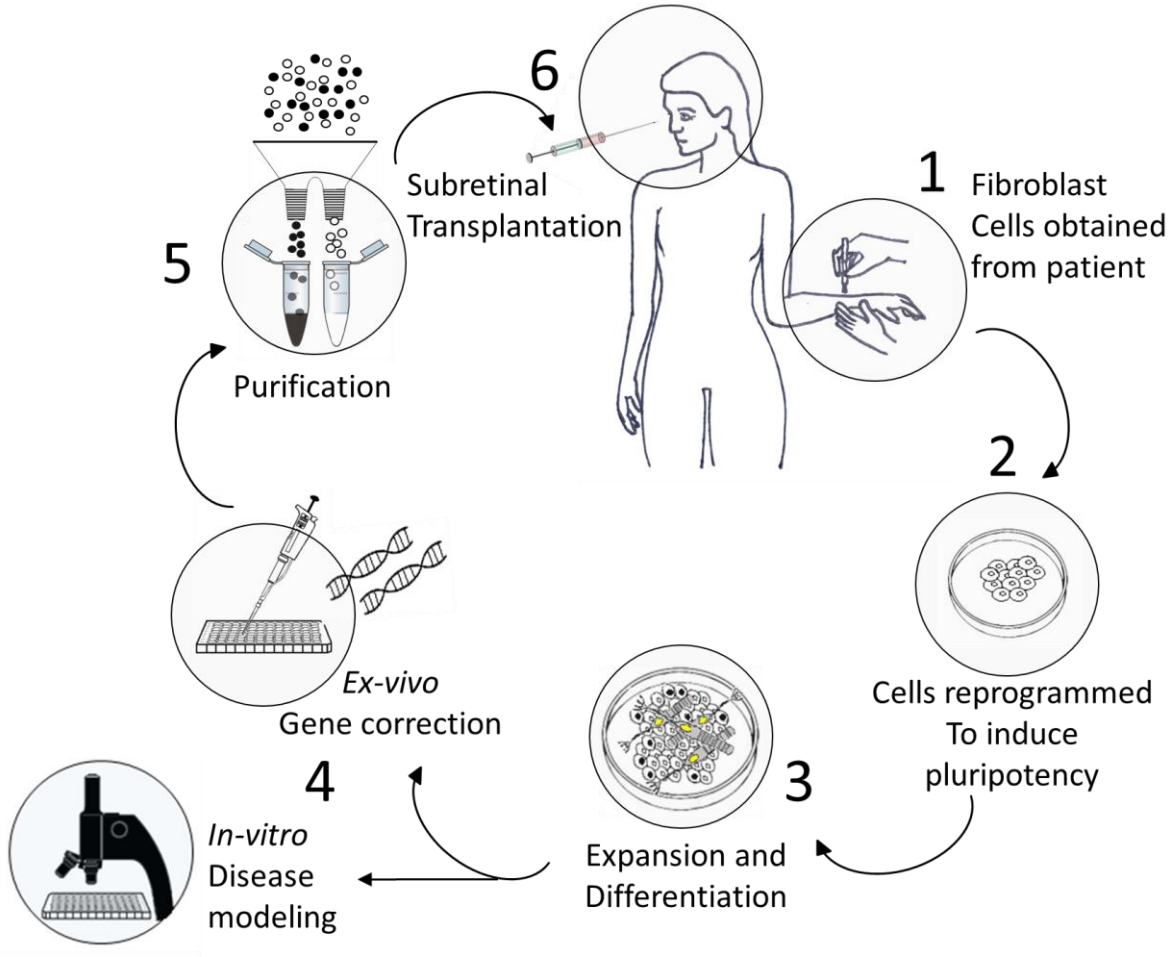

Figure 1.2: Patient Specific Cell Replacement

1. Somatic cells, such as skin fibroblasts are obtained from a patient with a genetic retinal degeneration. **2.** Cells are reprogrammed to an ES-like pluripotent state. **3.** Cells are expanded *in vitro* and differentiated to reach an appropriate developmental state. **4.** Developing cells may provide an *in vitro* model of disease development and treatment or may be subjected to gene therapy with the aim of correcting the genetic source of degeneration *ex vivo*. **5.** cell-colonies which are not homogenously differentiated would need be purified of potentially malignant cells. **6.** Patient receives a subretinal injection to replace degenerate cells with reprogrammed, suitably differentiated, corrected and purified autologous cells. Adapted from Cramer & MacLaren, 2013[127] .

1.5. *Ex vivo* gene correction

Gene therapy has been demonstrated as a promising *in vivo* strategy for rescue of retinal degeneration by gene replacement or gene silencing in pre-clinical animal studies[128-144] and clinical trials[145,146] of retinal disease. Gene therapy may be used *in vivo* for patients diagnosed in the early stages of disease progression, when gene delivery vectors are able to target and rescue cells from further degeneration. In the late stages of disease, when degeneration is excessive and there is no remaining tissue to rescue, cell replacement is necessary. Retinal cells derived from patient-specific iPSC provide an immunologically identical source of cells for transplantation and thus give the cells a high chance of survival with no or little need for immune modulation. However, being autologous, patient-specific cells also harbour the disease-causing mutation and require *ex vivo* gene therapy prior to transplantation if they are to provide long-term restoration of vision.

Due to the vast clinical and genetic heterogeneity of RP, the ability to offer gene therapy *in vivo* or *ex vivo* depends on the understanding of the causative genetic mutation and the pathophysiology of the disease in the specific patient. Furthermore, in order to offer *ex vivo* gene correction prior to cell transplantation, it is important to show that degeneration is recapitulated *in vitro* and is not caused solely through *in vivo* interaction or exposure to exogenous stress from nearby cells, the vascular system, or the immune system.

1.5.1. Modelling RP using patient specific iPSC: 'Disease in a dish'

Patient-specific iPSC are likely to be extremely beneficial in retinal research, as they allow an inexpensive model system for recapitulation of the patient's disease phenotype for *in vitro* drug discovery, drug screening, gene therapy optimisation, or indeed gene correction prior to transplantation.

Several groups have pursued RP disease models, and iPSc have accordingly been generated from patients with RP for assessment of disease mechanisms and therapeutic potential. Rod photoreceptors (Rho+/Nrl+) were differentiated from five RP patients with identified gene mutations (RP1, RP9, PRPH2 or RHO gene) to model retinal degeneration *in vitro.*[45] Unlike photoreceptors similarly derived from healthy human iPSC, in RP patient-specific iPSC derived rods a significant reduction of Rho expression was evident by *in vitro* day 150, and rods exhibited oxidation or endoplasmic reticulum (ER) stress in culture after differentiation. Photoreceptor cells derived from patients with different gene mutations in this study responded differently to antioxidant drugs, supporting the argument that drug treatment for RP must be considered in the context of the causative genetic mutation.

Over 60 genes have been implicated in RP, but identified genes account for possibly less than half of all cases of this disease;[147] thus, patient-specific disease modelling may be instrumental in identifying new genes in RP.

Genetic analysis after exome sequencing of iPSC derived from skin cells of patients with RP lead to identification of the cilia-related gene male germ cell-associated kinase (MAK) as a cause of RP.[148] The potential for identification of

rare or undiscovered genes and mutations in RP by use of patient-specific iPSC is evident from this study and paves the way for further research into mechanisms and treatment of this heterogeneous disease.

1.5.2. *In vitro* gene correction of RP mutations

In patients with a known mutation, iPSC can be used to further understand and treat the disease *in vitro*. In a recent study,[149] iPSC generated from a patient with RP who carried a mutation in the *RHO* gene (E181K) were used to derive rod photoreceptor-like cells with the same mutation, indicating a causal relationship between the mutation and disease phenotype which was associated with higher expression of ER stress and apoptotic markers. By use of a helper-dependent adenoviral vector (HDAdV), the mutant *RHO* gene was replaced by wild type *RHO*, thus repairing the mutation *in vitro* in the patient's iPSC and rescuing the cellular phenotype. Uncorrected patient iPSC were used in this study for drug screening for chemical reagents for rescue of the ER stress phenotype in the patient's iPSC derived photoreceptor cells.

Rescue of RPE cellular phenotype via restoration of actin organisation in iPSC derived from RP patients was achieved by adeno-associated virus (AAV) 8 mediated delivery of the Membrane Frizzle-related Protein (MFRP) *in vitro* to RPE cells from a patient with MFRP-associated RP[150]. Repair of patient-specific iPSC derived RPE cells was also achieved in cells generated from an RP patients carrying a premature stop mutation in the RP2 gene by restoring

the presence and function of RP2 proteins in iPSC and RPE cells *in vitro* using translational read-through inducing drugs (TRIDs).[151]

Recently, Photoreceptor precursors derived from CEP290-associated Leber's congenital amaurosis (LCA) patient-iPSC were treated *In vitro* by lentivirus-mediated CEP290 gene delivery, reporting dose dependent rescue of photoreceptor phenotype in these cells[122].

In vitro modelling of patient-specific gene mutations naturally focuses on specific genes and would need to be standardised to be applicable to varied mutations; however, the ability to study and manipulate patient-specific cells in culture conditions would benefit not only drug development and screening, but could be used as an *ex vivo* model in which patient-specific iPSC would be differentiated, treated, and transplanted back into the patient. While *in vitro* correction of cells provides the first step in this process, it is not yet known if these cells can mature normally *in vivo* post-transplantation to restore visual function in blind animals. This question will be explored using an animal model of RP in Chapter 5, by assessing transplantation of $Rho^{-/-}$ mouse rod precursor cells following *ex vivo* gene therapy.

1.5.3. *Ex vivo* gene correction and cell transplantation in an animal model of RP

Modelling of disease-specific and patient-specific retinal degeneration suggests that genetic mechanisms at play *in vivo* in RP are mimicked *in vitro* after cell reprogramming. This is empirical evidence of the basic defining barrier to

patient-specific cell replacement — that cells derived from patients with retinal disease will inevitably express the same genetic phenotype. Modelling of retinal degeneration and evidence of rescue of cellular phenotype *in vitro* together provide a step towards crossing this barrier, as patient-specific autologous cells could undergo *ex vivo* gene correction in culture to produce healthy tissue for cell replacement therapy. IPSC generated from patients with identified genetic mutations, or whose cellular degeneration has been studied *in vitro*, could be corrected and used to produce healthy cells for retinal transplantation.

Animal models of RP, and specifically well-established mouse models, have been extensively used as hosts for cell transplantation[62,70-75,152,153] and gene therapy.[154-159]

The remarkably varied inherited genetic mutations and expression patterns involved in RP imply that animal models will unavoidably lack in translational characteristics for the different subtypes of the disease. Despite this, development of a successful delivery method for *ex vivo* gene therapy of identified genetic mutations in mice, and attainment of visual rescue through transplantation of treated cells, may provide an important stepping-stone for translational research in humans.

Ex vivo gene correction of iPSC and transplantation of corrected cells was first achieved in a mouse model of sickle cell anaemia,[160] whereby mice were rescued after transplantation of corrected autologous iPSC-derived hematopoietic progenitors. Gene-specific targeting of the sickle haemoglobin allele was carried out with the use of a retrovirus, providing notable proof of

concept for such a procedure in a clinical setting. This pioneering study has set the stage for the development of autologous corrected iPSC for transplantation in humans with genetic diseases, although the method of gene correction will need to be reconsidered for a clinical setting. Retroviral vectors introduce external DNA into the cells, and hence bring with them the hazard of inserting novel variation and mutagenesis into the genome. Development of genetic therapies for patient-specific or disease-specific cells should attempt to use techniques that preserve genomic integrity and do not introduce oncogenic or foreign material into cells. Furthermore, transplantation of iPSC-derived cells that have also undergone gene therapy will require overcoming additional regulatory restrictions when seeking approval for clinical trials.

1.6. Viral and non-viral gene augmentation strategies for targeting photoreceptor cells

1.6.1. Ocular gene delivery and challenges in the use of viral and non-viral vectors.

Gene therapy strategies against inherited retinal diseases have been widely studied and recognised as effective treatments for these diseases.[161] Particularly promising is gene augmentation, in which the mutation is identified in a small gene that can be easily packaged into adeno-associated viral (AAV) vectors. For treatment of autosomal recessive RP, which is usually caused by a missense or null mutation, the gene of interest can be replaced by

administration of the healthy gene by a viral or non-viral vector. For dominant RP, which is usually caused by an abnormal accumulation of protein, gene therapy can be used to introduce a healthy copy of the gene or to knock down the abnormal gene. The greatest advancements in the study of RP have been achieved by the use of AAV vectors for replacement of an absent gene.

Gene therapy may be classified into two broad categories: viral and non-viral gene delivery. Viral vectors deliver nucleic acids into the cell nucleus after a specific interaction with a membrane receptor, followed by internalisation by the receiving cell.[162] A number of viruses have evolved strategies to transduce cells in the eye, and this ability is being exploited in pre-clinical and clinical trials to deliver genes to the retina. These viruses include AAV, lentivirus (LV),[163] adenovirus (Ad)[164] and herpes simplex virus.[165] AAV vectors are the most commonly used viral vectors in retinal research, as they represent an efficient and non-pathogenic strategy for gene delivery.

Despite its evolutionary advantages, viral gene delivery faces potential limitations, including restricted packaging ability, possible immune reaction against the viral capsid, or insertional mutagenesis by ectopic chromosomal integration of viral DNA which can disrupt tumour suppressor genes or activate an oncogene.[166] Safety concerns surrounding viral gene therapy have not restricted the use of AAV, as clinical trials using AAV vectors have proven to be extremely effective and safe in patients.[167] However, the limited packaging capacity of AAV vectors, which are approximately 4.7kb, remains a challenge

for gene delivery in many ocular diseases (Figure 1.3) and thus non-viral gene therapy is gaining interest as an alternative strategy.

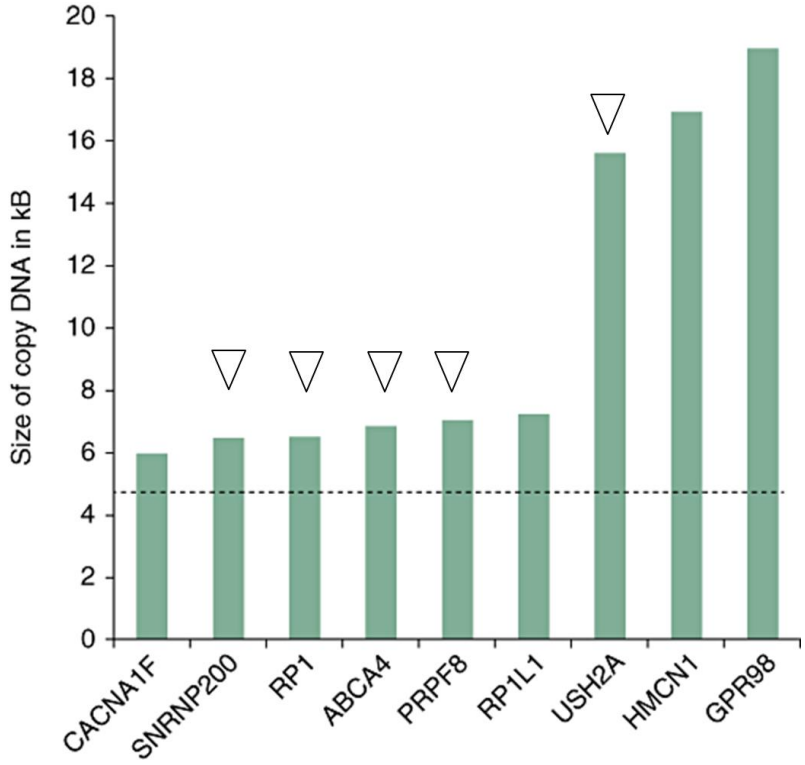

Figure 1.3: Examples of large genes associated with retinal diseases.

The dashed line marks the approximate transgene limit of 4.7 kb for adeno-associated viral (AAV) vectors. White arrows indicate genes that have been implicated in RP.
Mutations in the presented genes may cause the following diseases: CACNA1 (calcium channel, voltage-dependent, L type, alpha 1F subunit): congenital stationary night blindness type 2. SNRNP200 (small nuclear ribonucleoprotein 200 kDa (U5)): autosomal-dominant retinitis pigmentosa (ad RP). RP1 (retinitis pigmentosa 1): ad or autosomal recessive (ar) RP. ABCA4 (ATP-binding cassette, subfamily A, member 4): Stargardt disease, ar cone-rod dystrophy, ar RP. PRPF8 (pre-mRNA processing factor 8 homologue): ad RP. RP1L1 (retinitis pigmentosa 1-like 1): occult macular dystrophy. Ush2A: Usher syndrome, type 2A and ar RP. HMCN1 (hemicentin 1): ad macular dystrophy. GPR98 (G protein-coupled receptor 98): Usher syndrome, type 2. Adapted from Charbel Issa & MacLaren, 2012[168].

Non-viral strategies for gene delivery include naked DNA or DNA combined with liposomes, polymers, or compact nanoparticles.[166,169] Non-viral vectors may be beneficial for gene therapy as they have low immunogenicity and a low risk of insertional mutagenesis, are easy to produce on a large scale, and, most relevantly, have a large packaging capacity that allows delivery of large transgenes and entire genomic DNA fragments. However, non-viral gene therapies are less adapted than viruses to provide persistent expression in cells, and face extracellular degradation and intracellular barriers to gene transfer, and are thus less efficient than viral vectors for gene delivery.[170] To be expressed in the cell, exogenous DNA must avoid cytoplasmic enzymatic breakdown and cross both the cell membrane and nuclear envelope, which are not permeable in post-mitotic cells. In ocular gene therapy, *in vivo* delivery of non-viral vectors faces physical barriers in the eye, such as the vitreous, limiting membranes, and high concentrations of glycosaminoglycans that are present throughout the eye. These barriers lead to aggregation and cellular uptake and thus low expression.[168] Non-viral gene transfer to the eye has been studied *in vivo* and has typically been facilitated by either chemical (nanoparticles,[171] cationic lipids[171] or cationic polymers) or physical (electroporation[172,173] or ionoporation[174,175]) means; however, to date these physical methods have only shown success in delivery to neural retina of neonatal mice[160,161], and their relevance is limited for gene therapy in the adult neural retina[172,173]. Currently, the majority of non-viral delivery methods are not applicable for clinical gene delivery, due to low efficiency or toxicity.[168,176] A

recent method showing potential promise for sustained gene expression is gene delivery by compact nanoparticles[171,177-179]; these have been used to rescue cellular phenotype rds+/- (slow retinal degeneration) mice by subretinal delivery of the *Peripherin 2* gene which is mutated in these mice[177,178], and do not induce an immune responses or toxic effects to the retina[177,180]. However, direct comparisons with viral delivery have not been reported.

Administration of gene therapy to photoreceptor cells *in vitro* instead of *in vivo* can overcome some of the barriers and extracellular challenges of gene delivery, and thus opens an opportunity for long term *in vivo* assessment of gene therapy administered to cells prior to transplantation. Successful *ex vivo* administration may be beneficial for further application to *in vivo* delivery of non-viral gene therapy.

In order for non-viral gene therapy to provide a viable alternative to viral delivery in the retina, enhancement of the efficiency of plasmid uptake into cells and the nucleus must be achieved, gene expression must be enhanced, and the time of gene expression should be extended.[181]

Minicircle DNA technology, a method designed to avoid transcriptional silencing of the transgene and produce sustained gene expression,[182] is receiving growing interest as a non-viral-based therapeutic tool.[183] Minicircles are plasmid derivatives with the same expression cassette but devoid of a bacterial backbone, produced as circular expression cassettes and reduced to the minimal size required for transgene expression. To date, this technology has

not been used in ocular gene therapy or as a means of transfection of photoreceptor cells.

AAV gene delivery is assessed in this study alongside minicircle DNA gene delivery as a potential non-viral therapeutic strategy for *ex vivo* correction of photoreceptor cells. These two delivery methods will be presented below and further discussed in Chapters 4 and 5.

1.6.2. Adeno-associated viruses

Adeno-associated viruses (AAV) are single stranded non-enveloped small viruses(25 nm).[184] AAV serotype 2 (AAV-2) is a human parvovirus (Dependovirus) that has gained increasing interest because of its successful use for gene transfer in a variety of animal models and clinical trials[185] and its capacity for site-specific integration.

Wild type AAV2 consists of two open reading frames (ORFs), each containing a single gene; OFR-1 contains rep, which is required for DNA replication and encodes four proteins (Rep40, Rep52, Rep68 and Rep78), and ORF-2 contains cap, which encodes the structural proteins (VP1, VP2 and VP3) that form the capsid and the proteins essential for capsid assembly within the nuclease. The AAV genome is flanked on either side by 145bp-long palindromic inverted terminal repeats (ITRs), which form hairpin-loop secondary structures at the strand terminal[186] (Figure 1.4). The ITR is the origin for AAV replication and primes second-strand DNA synthesis by DNA polymerase, it is central for AAV packaging and transcription, and negatively regulates non-permissive

conditions by preventing recognition of the single-stranded DNA genome by the host cell immunity, thus directing sustained transcription.[176] ITRs are also important for site-specific integration into the host genome.

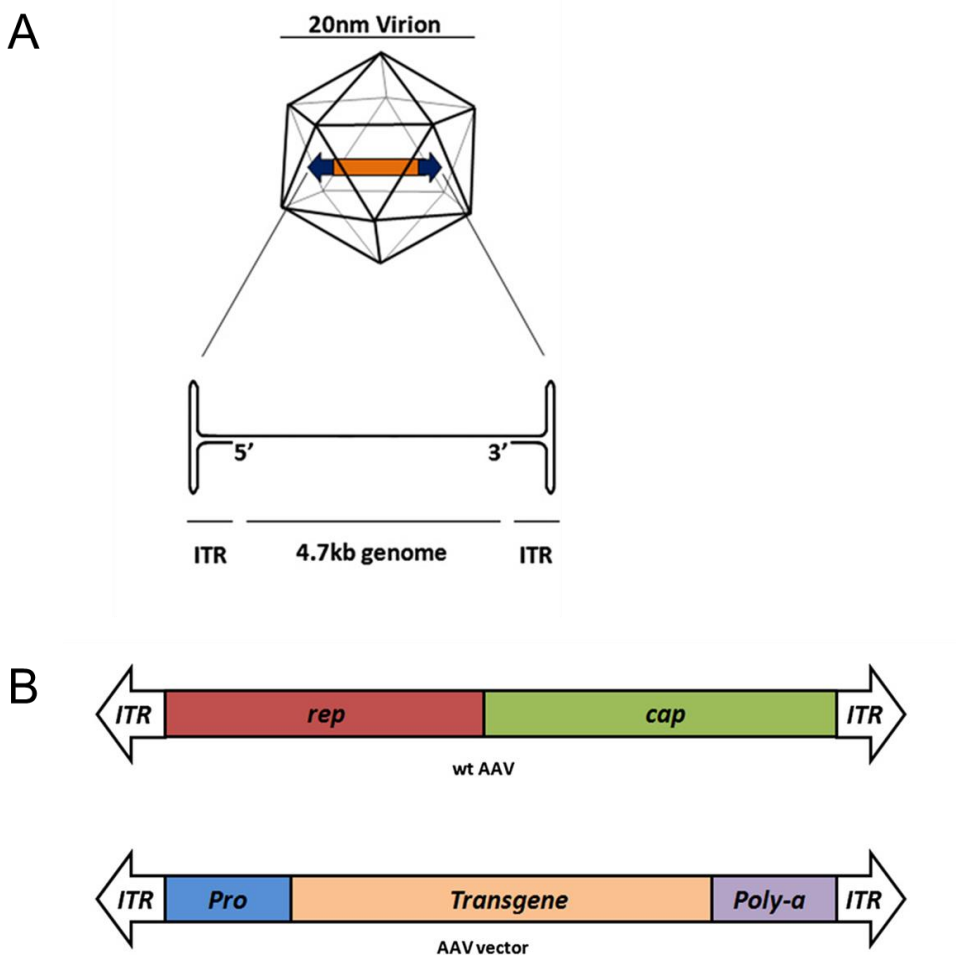

Figure 1.4: Schematic representation of an AAV vector and inverted terminal repeats (ITR).

(A) 20 nm icosahedral capsid of the AAV virion containing a single-stranded DNA AAV genome. (B) Removal of the viral Rep and Cap genes allows the insertion of an expression cassette with a maximum size of 4.7 kb; note the 146 bp inverted terminal repeats (TR) which form T-shaped hairpin loops at both the 5' and 3' termini which facilitates genome packaging, second strand synthesis and genome replication. The transgene cassette minimally contains a promoter, a transgene and poly-a tail signal: regulatory elements which are required for gene expression. Figure adapted from Lipinski et al., 2013[176].

1.6.2.1. Construction of AAV for gene therapy

Construction of a recombinant AAV (rAAV) vector for gene therapy requires modification of the wild-type viral genome (usually done using AAV2). The ORFs containing rep and cap genes are removed and replaced with a transgene cassette. The transgene cassette depends on the therapy being delivered, but consists of at least a promoter, the therapeutic gene or fluorescent reporter gene, and a poly-adenylation (poly-a) tail. The ITRs remain the only viral regions necessary for cis-packaging or a recombinant vector genome.[187] The requirement for the ITRs reduces the total size of AAV vector and limits the packaging capacity for a therapeutic gene for delivery to approximately 4.7kb[188].

While wild type AAV viruses integrate into the host genome (specifically at the AAVS1 locus c19q13.3),[189] deletion of the Rep during rAAV vector construction considerably reduces the level of integration, with more than 99.5% of rAAV vector DNA remaining episomal following transduction.[190] Without the preferential integration of rep into chromosome 19, AAV integrates randomly; however, this is a rare event and random integration has not been linked to increased mutagenesis in human cells.[191]

DNA is packaged within the rAAV as a single-stranded DNA genome, and rate of transduction by rAAV vectors is limited by synthesis of a second strand on the single-stranded genomic AAV DNA[192].

1.6.2.2. AAV pseudotyping

At least 11 naturally occurring AAV serotypes (AAV1-11) have been identified thus far.[176] Each serotype has a distinct external capsid protein, and these can be exchanged among the various AAV serotypes to produce hybrid vectors that contain a genome with an ITR from one serotype (usually AAV2) and the capsid from a different variant.[193] Such pseudotyped AAV vectors are termed AAV2/n, with the first number referring to the ITR origin serotype and the second number to the capsid. The different AAV serotypes have unique transduction characteristics, as the different capsids interact with different receptors and thus target different cell types in the retina.

In the retina, pseudotyped AAV vectors have been studied extensively following *in vivo* delivery.[161] Most relevant for targeted AAV transduction to photoreceptor cells are rAAV2/2, rAAV2/5, rAAV2/7, rAAV2/8, and rAAV2/9, which have been shown to transduce photoreceptors and RPE cells in mice.[194] The choice of AAV pseudotype for *ex vivo* gene therapy in primary mouse $Rho^{-/-}$ PhRPs will be further discussed in Chapter 4.

1.6.2.3. Capsid mutant AAV

AAV2 enters the cell through binding to the specific cell surface receptor heparan sulphate[195] and is internalised by the cell through endocytosis. A conformational change in the capsid structure most probably leads to the release of the virion from the endosome and transport to the cell nucleus.[196,197]

A limiting factor of rAAV transduction efficiency is that prior to release, the AAV capsid frequently undergoes phosphorylation of exposed surface-tyrosine residues, which triggers ubiquitin-mediated degradation by the proteasome and considerably decreases the number of viral genomes delivered to the nucleus for expression.[198] In order to enhance transduction efficiency of rAAV vectors, tyrosine-mutant vectors have been developed, in which tyrosine (Y) residues on the AAV capsid are converted to phenylalanine (F). Phenylalanine lacks the para-hydroxyl group which enables tyrosine to be phosphorylated, and hence this mutation is thought to prevent ubiquitination of the virus in the target cell, avert proteosomal degradation, and improve transduction efficacy.[199]

Indeed, capsid mutant AAV vectors have been shown to significantly improve transduction of all retinal layers and diffusion between retinal layers *in vivo*. Administration of the rAAV2/2 Y444F capsid mutant resulted in consistent transfection of photoreceptor cells, even when injected intravitreally[200] (meaning the virus diffused through the cells of the INL to reach the photoreceptors of the ONL). Following subretinal injection, the rAAV2/8 Y733F tyrosine mutant induced the onset of transgene expression sooner and with increased efficiency compared to rAAV2/8.[201] The ability to generate capsid mutant AAV vectors allows for more efficient transduction of a wider variety of cell types and may require a lower dose of virus to be administered for therapy, thus reducing the potential for toxicity in cells.

1.6.3. Minicircle DNA

Minicircle (MC) DNA vectors are small, supercoiled molecules derived from a parent plasmid by removal of the bacterial backbone[202] and have been suggested as a promising DNA vehicle for gene replacement.[182] Minicircles contain a minimal expression cassette consisting of a promoter, transgene, and polyadenylation signal, but are devoid of prokaryotic plasmid DNA elements. Some studies have suggested that MCs are superior to plasmid DNA vectors for gene delivery, as they offer increased and persistent gene expression compared to plasmid DNA both *in vitro* and *in vivo.*[203-208] MCs have been shown to be capable of sustained expression for months, with expression levels that are eventually 10- to 1000-fold higher than their corresponding plasmids.[202,209,210]

Plasmids are routinely used as vectors for non-viral gene expression due to their ease of construction and amplification. They are episomal, non-integrating vectors[211] and can be subdivided into a transcription unit and a bacterial backbone. The transcriptional unit includes the gene of interest and regulatory elements. The bacterial backbone includes an origin of replication and an antibiotic resistance gene sequence, in addition to immunogenic unmethylated CpG motifs;[212] these components reduce gene transfer and expression and pose a potential risk for clinical application.[181] Minicircles are derived from plasmids by removing such sequences to improve performance and reduce the size of the DNA to be transferred into cells.[213]

1.6.3.1. Minicircle production from plasmid DNA

The production of MCs from plasmids involves the generation of a parental plasmid that includes the gene of interest and regulatory elements, as well as a bacterial backbone. The core principle for generation of MCs is the inclusion of a site-specific recombination between attB and attP sites mediated by the bacteriophage Phie31 integrase. Upon induction of the bacteria with L-arabinose, the plasmid recombines into two circular fragments: the minicircle, containing the expression cassette and attR fragment, and the bacterial backbone (Figure 1.5). The bacterial backbone is subsequently digested by the I-SceI endonuclease and degraded. The process of production has been optimised in a genetically modified *E. coli* strain that stably expresses a set of inducible PhieC31 integrase and I-SceI endonuclease enzymes, which subsequently reduces the time and cost involved in these methods and makes the production and purification of MCs comparable to plasmid production protocols.[214,215]

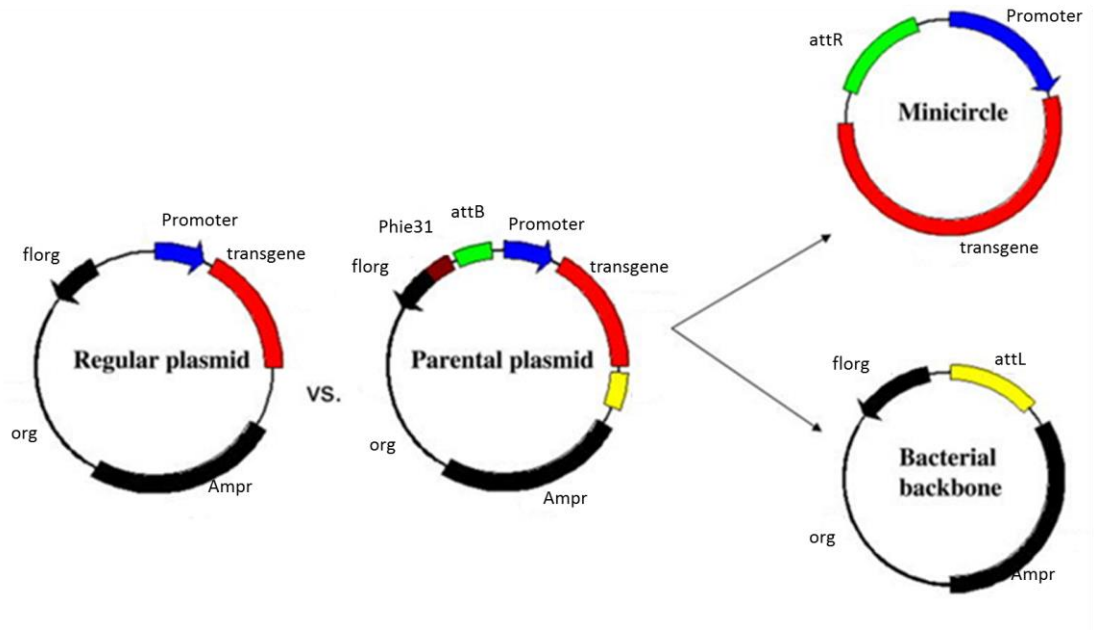

Figure 1.5: Schematic representation of minicircle production from plasmid DNA

Minicircles are the product of site-specific recombination, separating a parental plasmid into two parts: 1.The minicircle which includes the expression cassette. 2. The bacterial backbone which is then subject to degradation. Adapted from Huang et al., 2009[205].

1.6.3.2. Improved transgene expression by minicircle DNA

The bacterial backbone has been shown to be responsible for silencing episomal transgene expression;[209] unmethylated CpG motifs are significantly less frequent in vertebrate DNA, and it seems that these sequences act as an alarm signal to trigger an immune response in the host during bacterial infection.[216,217] Thus, the removal of the bacterial backbone – which consists of a significant portion of plasmid DNA without a therapeutic effect – avoids the

occurrence of CpG related silencing and reduces the vector to the minimal required components for therapy.

In order for the minicircle-encoded gene to be expressed, it needs to pass several barriers; it must diffuse into the tissue, enter through the cell membrane, escape the endosome/lysosome during internalisation via endocytosis, diffuse through the cytoplasm, and cross the nuclear membrane. The most obvious characteristic of minicircle vectors is their small size compared to plasmids. The size of MCs is an advantage for overcoming obstacles on the way to gene expression. Small vectors have better bioavailability characteristics than larger ones; thus, minicircle DNA molecules have been proposed to be better suited for gene transfer and expression[181] than plasmids, as a reduction in size is strongly associated with increased expression.[218,219] The size of MCs is reduced in comparison to AAV vectors as well, and may prove advantageous in bioavailability for gene transfer.

An additional advantageous feature of minicircle DNA is its structure. The supercoiled structure remains unchanged through recombination, and it has been proposed that supercoiled plasmids are superior to linear plasmids in transduction efficiency.[203,220] Supercoiled molecules are better suited to reach the perinuclear region and prevail in a higher intracellular concentration compared to linear plasmids.[220]

1.6.3.3. Minicircles for gene therapy

Minicircles may represent an appealing tool for *ex vivo* gene therapy in the eye, as they are able to transfect both dividing and non-dividing cells and are episomal non-integrating vectors with a potentially unlimited loading capacity.

Minicircles have been predominantly studied in the liver,[182,202,209,210,214,221,222] but also have been used to achieve gene transfer in multiple tissue types *in vivo* and *in vitro*, including heart and skeletal muscle[136,208] and neural stem cells,[223] and have been used as a non-viral system for cancer research[181,213] and for tissue reprogramming and generation of iPSC.[224]. Because the backbone of plasmids is removed together with the origin of replication minicircles may provide sustained expression in quiescent cells but lose expression in dividing cells with cell division. Further improvements have been suggested for persistent expression, including the addition of a scaffold/matrix attachment region (S/MAR) to enhance and prolong transgene expression in dividing cells by reinstating replication capacities in minicircles.[225]

Minicircles have not been studied for gene delivery in the context of ocular gene therapy, and have not been assessed for gene delivery to retinal cells, with the exception of transfection of an RPE cell line among other non-ocular cell lines (HeLa, F9, and HaCaT) for assessment of wide-ranging transfection with a MC-based delivery system of the sleeping beauty (SB) transposon.[226]

The use of minicircle DNA, combined with a cell-specific promoter in retinal cells and photoreceptors, may offer a novel and safe method for delivery of gene therapy for retinal degeneration. Investigation of *ex vivo* gene delivery

provides a unique case for the study of non-viral gene therapy, as it overcomes limitations associated with delivering non-viral particles to cells.

1.7. Aims and outline of thesis

In the work presented here, the main aim is to assess the feasibility of cell replacement in the severely degenerate retina, by use of *ex vivo* genetically treated, disease-specific murine rod photoreceptor cells, or by human ESC- and iPSC-derived photoreceptor cells. A further aim is the investigation of viral and non-viral methodologies for *ex vivo* gene delivery to rod PhRPs and assessment of corresponding *in vivo* therapeutic outcomes following transplantation of treated cells.

This approach addresses the clinical goal of visual restoration by cell replacement in end-stage RP, and provides a model for autologous cell replacement therapy following treatment of patient-specific cells in hereditary disease. The potential of human ESC- and iPSC-derived photoreceptors for transplantation in end-stage degeneration is investigated to assess the achievability of ONL reconstruction and photoreceptor maturation via human cells.

A stepwise approach is presented in the following chapters, detailing the levels of investigation pursued in relation to these aims. First, an *in vitro* system was established for prolonged cultivation of murine rod PhRP cells, and assessment of cell survival *in vitro* and *in vivo* was conducted (Chapter 3).

Next, the adeno-associated virus (AAV) serotype was selected for *ex vivo* gene delivery to primary rod PhRP cells, and minicircle DNA was assessed as a method for gene transfer to retinal cells. A construct for delivery of the wild-type rhodopsin gene was cloned, and both viral (AAV) and non-viral (minicircle) vectors were developed for *ex vivo* delivery of rhodopsin to rod PhRP obtained from rhodopsin knockout mice ($Rho^{-/-.Nrl\text{-}GFP}$) (Chapter 4).

Subsequently, viral and non-viral gene therapies were administered *ex vivo* to rod precursor cells from $Rho^{-/-.Nrl.gfp}$ mice. Treated rods were subretinally transplanted into adult $Rho^{-/-}$ mice with end-stage degeneration for evaluation of ONL reconstruction, gene expression, and *in vivo* visual repair (Chapter 5) (see Figure 1.6 for a schematic illustration of the outline aims of Chapters 3-5).

In order to consider the feasibility of similar studies in iPSC from patients with hereditary disease, it would be essential to show that healthy stem cell-derived human photoreceptors have the capacity to mature in a completely degenerate retina. Photoreceptor precursors—derived from human ESC and iPSC by a protocol suitable for future regulatory approval of clinical trials—were subretinally transplanted into adult *rd1* mice to assess their potential for cell replacement and visual repair in a model of end-stage RP (Chapter 6) (see Figure 1.7 for a schematic illustration of the outline of Chapter 6).

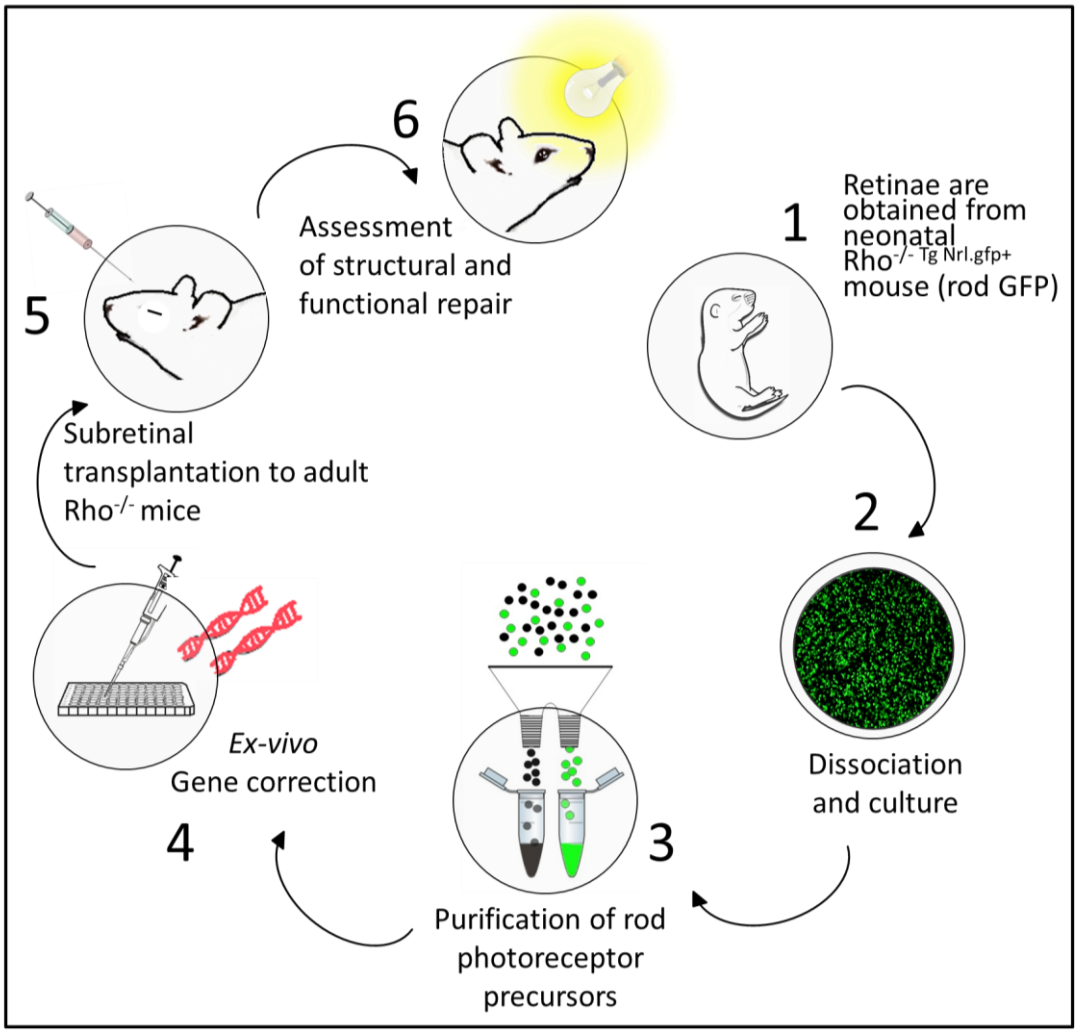

Figure 1.6: Schematic illustration of outline for Chapters 3-5

1-3. Retinae were harvested from neonatal mice to obtain rod photoreceptor precursor cells. Retinae were dissociated and a system for prolonged culture and enrichment of rod precursor cells was established using rod precursor cells which intrinsically express GFP through the Nrl promoter. The prolonged culture system was developed to allow investigation and *ex vivo* treatment of cells carrying the rhodopsin knockout (*rho*$^{-/-}$) mutation (Chapter 3). 4. Methods for viral and non-viral gene therapy were assessed *in vitro* in cells and vectors for *ex vivo* delivery of the rhodopsin gene to *rho-/-* rod precursor cells were developed (Chapter 4). 5-6. Nrl.GFP+ rod precursors with the *rho*$^{-/-}$ mutation were treated *ex vivo* to replace the missing rhodopsin gene by viral and non-viral gene therapy and subretinally injected to blind adult Rho$^{-/-}$ mice for assessment of structural and functional repair post transplantation (Chapter 5).

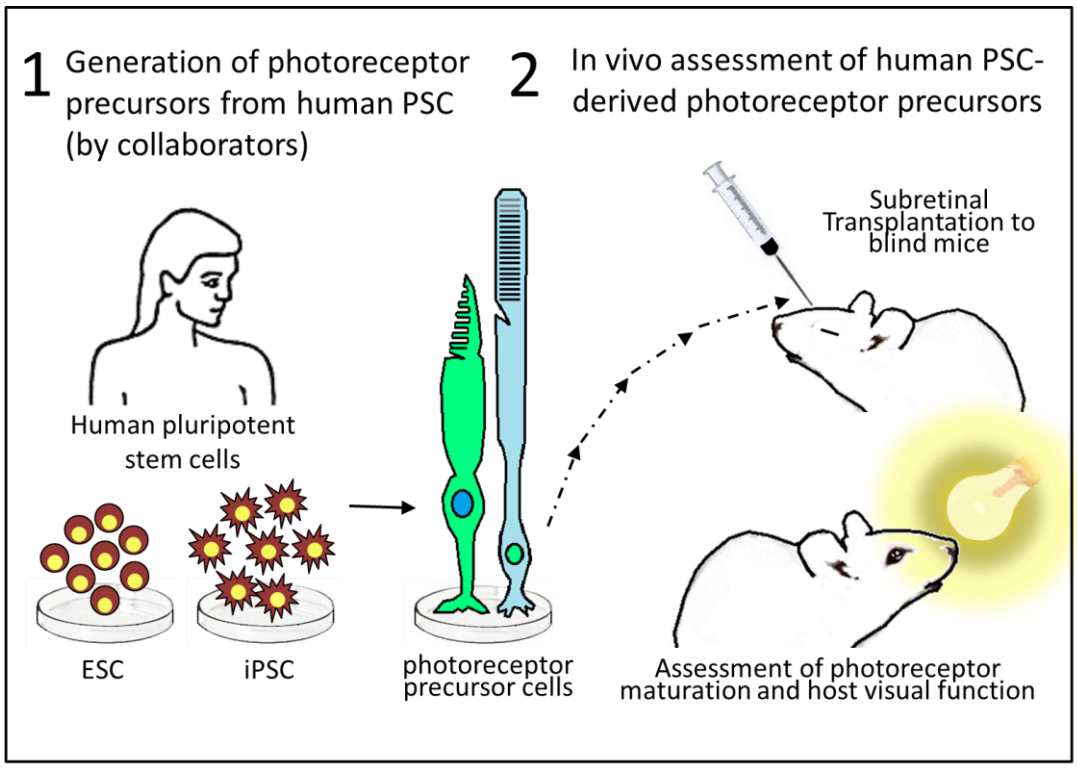

Figure 1.7: Schematic illustration of outline for Chapter 6

1. Pluripotent stem cells (PSC) from healthy humans were generated and differentiated to photoreceptor precursor stage by our collaborators at the biotechnology company Ocata therapeutics. Cells were cryopreserved and sent to our laboratory for *in vivo* evaluation.

2. In Chapter 6 the recovery of cryopreserved human PSC-derived photoreceptor precursors, their characterisation and transplantation into adult blind *rd1* mice is presented. Reconstruction of the degenerate *rd1* ONL by human photoreceptors, *in vivo* maturation and functional repair were assessed.

ESC; Embryonic stem cells, iPSC; induced pluripotent stem cells, ONL; Outer nuclear layer

2. Materials and Methods

2.1. Animals

All animals were housed under standard 12:12 hour light/ dark cycle, with food and water available *ad libitum*. Procedures were performed according to the UK Home Office Guidelines on the Animal (Scientific Procedures) Act of 1986 and were approved by the University of Oxford Animal Ethics Committee and in accordance with the Association for Research in Vision and Ophthalmology statements on the care and use of animals in ophthalmic research. As required by the Act, the project was overseen by the holder of Project Licence 30/280, and the welfare of the animals was ensured with the cooperation of the Named Animal Care and Welfare Officer (NACWO) and Named Veterinary Surgeon (NVS). The work described in this thesis was done under Personal Licence PIL 30/9432.

2.1.1. Host Animals

The host animals used for transplantation studies were neonatal and adult wild-type (WT) mice of the C57BL/6 strain (referred to herein as wild-type), provided by the Biomedical Sciences division of the University of Oxford. Neonatal mice were used at postnatal (PN) day 0-1 and adult mice were at 8-12 weeks.

Animal disease model strains used as hosts for transplantation studies included adult rhodopsin knockout mice (C57B/6.129 Rho^{tm1Phm}, referred to herein as $Rho^{-/-}$) which were a kind gift obtained under a material transfer agreement from Jane Farrar (Trinity College, Dublin, Ireland) and adult C3H/HeNHsd mice which carry the retinal degeneration $Pde6b^{rd1/rd1}$ mutation (referred to herein as *rd1*), obtained from Harlan Laboratories, UK. Adult mice were aged 10-14 weeks to ensure progression of retinal degeneration to end-stage photoreceptor loss in each model.

2.1.2. Anaesthesia

For intraocular injections and *in vivo* imaging procedures general anaesthesia was induced by a single intraperitoneal injection of a mixture of

medetomidine (Dormitor 1 mg/ml; Pfizer, Sandwich, UK), ketamine (Ketaset 100 mg/ml; Fort Dodge, Southampton, UK) and sterile water at a ratio of 1:0.6:84 for PN 0-1 pups or Vetalar (Ketamine Hydrochloride, 80 mg/kg), Rompun (xylazine , 10 mg/kg) and sterile water at a ratio of 5:3:42 for adult mice. Anaesthesia was reversed when needed by intraperitoneal injection of antisedan (Atipamezole, 2mg/kg body weight) in sterile water for injection in the ratio of 1:9.

2.1.3. Pupil dilation

To facilitate transpupillary visualization during subretinal injections and *in vivo* imaging, pupils of adult mice were dilated with a mixture of 1% tropicamide and 2.5% phenylephrine hydrochloride eye drops (both Bausch & Lomb, Kingston-

Upon-Thames, UK) and were allowed approximately 5 minutes for full pupil dilation before commencing a procedure.

2.1.4. Immune suppression

For transplantation of PhRP derived from human stem cells, animals were immune suppressed by addition of cyclosporine A (50 mg/kg/day) and 5% fruit cordial to the drinking water[227] for 2 days prior to and 3 weeks following transplantation. No immune suppression was used for transplantation of primary mouse cells.

2.1.5. Donor animals

Tissue for primary rod precursor culture and transplantations was obtained from the following strains:

1. Tg(Nrl-l-EGFP)Asw/Tg(Nrl-l-EGFP)Asw transgenic mice (referred to herein as Nrl.GFP) in which EGFP is expressed specifically in rod photoreceptors via the neural retina leucine zipper (Nrl) promoter.

2. $Rho^{-/-\ Tg(Nrl\text{-}EGFP+/+)}$ transgenic mice. These mice express EGFP in rod photoreceptors (as above) and have a primary rod specific degeneration.

These mice were obtained by crossing the Rhodopsin Knockout C57B/6.129 Rho^{tm1Phm} ($Rho^{-/-}$) with the Tg(Nrl-l-EGFP)Asw/Tg(Nrl-l-EGFP)Asw, followed by backcrossing of progeny (Rho+/-TgNrl-EGFP+/+) to the parental $Rho^{-/-}$ line. Breeding pairs were genotyped by PCR and confirmed to be homozygous for rhodopsin gene disruption and off-spring were genotyped to confirm the

rhodopsin gene disruption and EGFP expression and EGFP expression was confirmed *ex vivo* in cells in culture. All off-spring had the $Rho^{-/-}Nrl.GFP^{+/+}$ genotype (referred to herein as $Rho^{-/-.Nrl.GFP}$).

2.1.6. Genotyping

DNA samples for genotyping were obtained from tissue pieces from the ears of adult mice or from the tail tips of P1 pups. A polymerase chain reaction (PCR) assay was used to detect the GFP and Rhodopsin alleles in $Rho^{-/-}$ and $Rho^{-/-.Nrl.GFP}$ mice and to detect the proviral *Xmv-28* insertion in intron 1 in the $Pde6b_{rd1}$ allele in *rd1* mice. Tissue samples were collected in PCR tubes and digested by incubation with 100µl of 50 mM NaOH (pH 12) for 1 hour at 95 °C followed by the addition of 10µl 1 M Tris-HCl (pH 5). The genomic DNA obtained was diluted 1:5 and stored at -20 °C until use. Primers for genotyping were ordered from Sigma UK, and are shown in Table 2.1. The PCR conditions used for genotyping are shown in Table 2.2.

Gene	Forward (5' to 3')	Reverse (5' to 3')
GFP	CAATTAAGAGATCAGGTAGTGT	AGTTCACCTTGATGCCGTTCTT
Rhodopsin	GAGGGCTTCTTTGCCACACTTG	AGCGGAAGTTGCTCATCGGCTT
$Pde6b^{rd1}$	GTAAACAGCAAGAGGCTTTATTGGGAAC*	TGACAATTACTCCTTTTCCCTCAGTCTG
	TACCCACCCTTCCTAATTTTTCTCACGC**	

Table 2.1: Primers used for genotyping

*Forward primer used to detect mutant allele, **Forward primer used to detect WT allele.

Temperature	Time	Cycles
95^{o}C	5 min	1
94^{o}C	30 sec	30-40 Cycles (as determined for each set of primers)
55^{o}C	30 sec	
72^{o}C	1 min	
72^{o}C	10 min	1
10^{o}C	hold	1

Table 2.2: PCR conditions for Genotyping

The resultant amplified fragments were run on a 1.5% agarose gel.

.

2.2. Preparation and culture of donor cells

2.2.1. Neonate cell dissociation

In order to prepare donor tissue for cell culture and transplantation studies, animals at PN day 0-4 were sacrificed by decapitation. Eyes were immediately extracted and retinae were dissected free from surrounding tissues in 0.01M sterile phosphate-buffered saline (PBS) at room temperature. Retinal dissociation was performed by papain dissociation system (Worthington Biochemical, USA). The manufacturer's instruction was optimized for the dissociation of neonatal retina. Briefly, preparation of papain solution contained a concentration of 20 units/ml papain and 0.005% DNase. Dissected whole retinae were placed into 250µl papain solution and incubated at 37 °C for 7-15 minutes. Cells were triturated with a 1ml pipette to break cell clumps and then

centrifuged for 5 min at 300g at room temperature (RT). The supernatant was discarded and the cell pellet was re-suspended in a mixture of 450µl of EBSS,50µl of albumin-ovomucoid inhibitor solution and 25µl of DNase solution. The cell suspension was carefully layered on top of 500µl of albumin-inhibitor solution in a 2ml centrifuge tube creating a discontinuous density gradient. The tube was then centrifuged for 6 min at 70g at RT. The supernatant was discarded and the cell pellet was immediately re-suspended in 250µl-1ml (determined by the number of dissociated retinae) complete Neurobasal A media (as described below) for cell counting and culture.

2.2.2. Cell culture

Cells were plated at a seeding density of approximately $3x10^4$/well in 96 well plates with 180µl complete media; $2x10^5$/well in 24 well plates with 500µl complete media or suspended at 10^5/µl PBS for transplantation. Cell counting was performed using a haemocytometer and viability of retinal cells was confirmed using the trypan blue assay. Following optimisation of culture conditions (chapter 3.1) for all future experiments dissociated primary cells were cultured in neuronal growth medium (Neurobasal-A) supplemented with B27 (2%), N2 (1%), L-glutamine (0.8 mM), penicillin (100 U/ml), and streptomycin (100 µg/ml) (all Invitrogen Ltd., Paisley, UK)[157] and maintained at

34˚ C (details of cell culture optimisation are described in chapter 3). Half of the media were changed on *in vitro* day 2 and every second day thereafter.

2.2.3. Preparation for transplantation

For transplantation studies, prior to transplantation cells were lifted from culture wells by light pipetting and dissociated a second time (but with a 5 min incubation period in papain at 37˚ C instead of 15min as described above) to ensure a single cell suspension for transplantation.

2.2.4. Recovery and dissociation of human stem cells

Photoreceptor precursors were obtained as neural Photoreceptor precursor (PhRP) spheres from Ocata therapeutics and maintained in liquid nitrogen (cell lines and details of stem cell differentiation are described in chapter 6).

72 hours prior to transplantation cells were removed from liquid nitrogen into dry ice in vials ($6x10^6$/vial) and thawed in a 37 °C water bath, constantly agitating for approximately 50 seconds or until only a small piece of ice remained in the vial. Vials were then sprayed with 70% isopropanol and the contents was immediately transferred into a 15 ml tube with warm ND medium and centrifuged at 200g for 5 minutes. Supernatant was removed completely, without touching the pellet and 1 ml of ND medium was used to gently re-suspend the cells for 2-4 repetitions before adding an additional 9 ml of ND

medium. Cells were then transferred to a 10cm Ultralow binding plate (Corning® Cat# 3262) and maintained at 37 °C, 5% CO_2 and 90% humidity to form PhRP neural spheres.

PhRP neural spheres were collected 48 hours following thawing and centrifuged at 200g for 2 minutes. Spheres were washed with 10 ml of PBS buffer and spun down at 200g for an additional 2 minutes. PBS was removed and 1 ml of warm Accutase (Innovative Cell Technologies, Inc.) was added. Cells were gently re-suspended for 2-4 repetitions and incubated in a 37 °C water bath for 3 minute. Cells were further dissociated by titration and incubated for an additional 2 minutes at room temperature before stopping dissociation by addition of 9 ml ND medium and centrifugation at 200g for 5 minute. Cells were then re-suspended in 5ml ND medium and filtered through a 40 µm cell strainer (BD FalconTM), centrifuged at 200g for 5min and re-suspended to a final concentration of 10^5 cells/µl balanced salt buffer for transplantation.

2.2.5. Viability assessment

In primary cells expressing GFP through a reporter gene (Nrl.GFP), intrinsic fluorescence was used as a proxy marker of cell viability[159,228,229]. In cultured cells, assessment of cell viability was also determined by use of Trypan blue (0.4%, Life technologies) by mixing 20µl trypan blue with 20µl 1:100 cell suspension. In viable cells, the trypan blue dye does not pass through the cell membrane and is not absorbed, however it traverses the membrane of dead

cells, and these are shown labelled with a blue dye under the microscope. The percent of viable cells was quantified using a haemocytometer and were established as >95% viable if no blue staining was observed.

2.3. Magnetic-activated cell sorting (MACS)

MACS separation system and Anti-Rat IgG MicroBeads (Miltenyi Biotec, Germany) were used in this study. Dissociated primary retinal cells were labelled with 10µg/µl primary Rat IgG anti-mouse CD73 antibody (R&D Systems) and incubated for 10 minutes at 4°C. Cells were then washed in phosphate-buffered saline (PBS), 0.5% BSA, 2mM EDTA), and magnetically labelled with 20µl anti-rat IgG microbeads by incubation for 15 minutes at 4°C. Next, cells were washed, centrifuged (300g for 5 min) and filtered through a 30µm pre-separation filter. 5% of cells were removed at this point and cultured as an unsorted control. Cell suspension was applied through an MS column (Miltenyi Biotec, Germany) attached to a magnet and flow-through was collected (CD73 negative cells). The column was then removed from the magnet and buffer solution was applied to the column to collect CD73 Positive cells in a new collection tube (Figure 2.1).

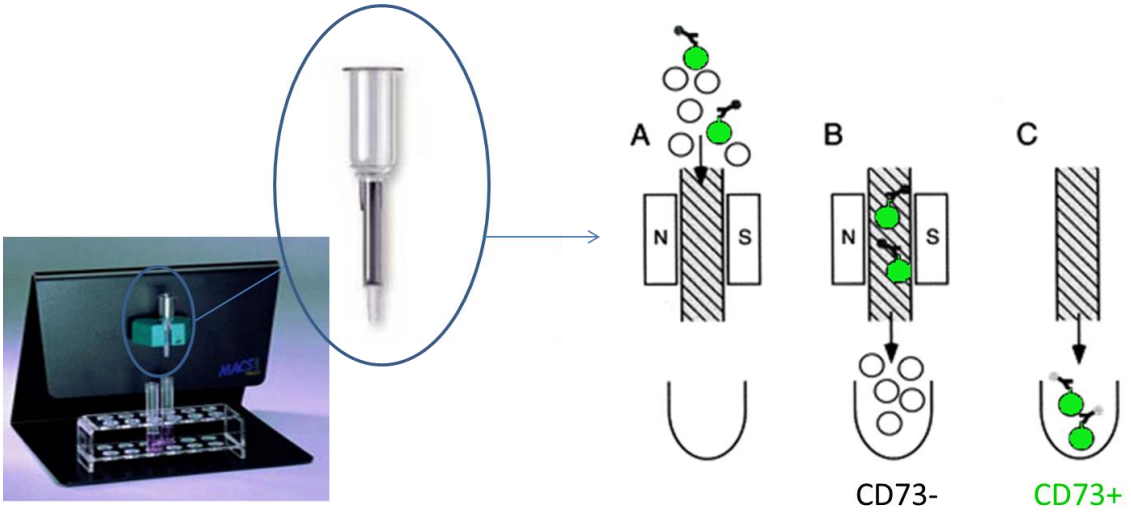

Figure 2.1: Magnetic-activated Cell Sorting (MACS)

Dissociated primary retinal cells were labelled with primary Rat IgG anti-mouse CD73 antibody and magnetic microbeads were attached by a secondary anti-rat IgG. Cell suspension was applied through an MS column attached to a magnet. The cells labelled by magnetic beads are drawn to the magnet and flow-through includes predominantly CD73 negative cells (CD73-). The column was then removed from the magnet and buffer solution was applied to the column to collect CD73 Positive rod cells (CD73+).

2.4. Vector generation

2.4.1. Design of gene construct and plasmid generation

2.4.1.1. Preparation of RHOK.RHO.IRES.DsRed construct

Using polymerase chain reaction (PCR) the Rhodopsin kinase promoter (RHOK) also known as the G protein-coupled receptor kinase 1 (GRK1) sequence, and human rhodopsin (RHO) were isolated from existing plasmids

produced by our laboratory. The IRES sequence had previously been isolated in our laboratory from pIRES2 AcGFP plasmid (Clontech, USA) and joined to the DsRed sequence (from pSIREN DNR DsRed Express plasmid, Clontech, USA). PCR primers were designed manually (Table 2.3) and manufactured by Sigma Aldrich (Dorset, UK). KOD polymerase was selected due to its proofreading activity and low PCR mutation frequency.

Target	Forward	Reverse
RHOKpr	GTCAATTGCTCGGTACCGGG CCCCAGAAG	GTGCCATTCATGGTGGTCCCG GGGCTGACACAG
RHO	ACGGTACCACCACCATGAAT GGCACAGAAG	GGGAGAGGGGCTTAGGCCGG GCCACCTG
IRES DsRed	GACCCCAGGATGTAGGCCCC TCTCCCTCCC	AAAGCGGCCGCCTACAGGAAC AG

Table 2.3: Primers for generation of RHOK.RHO.IRES.DsRed construct

* RHOKpr primers were designed with the Mfe1 restriction site (CAATTG) inserted at 5'end)
** DsRed primers were designed with Not1 restriction site (GCGGCCGC) inserted at 3' end

Standard PCR mix is described in Table 2.4

Forward primer	1.5 µl
Reverse primer	1.5 µl
DNA	1 µl
10x reaction buffer	5 µl
dNTPs	5 µl
$MgSO_4$	3 µl
KOD polymerase	1 µl
Molecular biology grade water	32 µl
Total	**50** µl

Table 2.4: PCR reaction mix for construct ligation

Standard PCR conditions are described in Table 2.5

PCR step	temperature	time	cycles
Initial denaturation	95^{o}C	2 min	1
denaturation	95^{o}C	20 sec	35
annealing	64^{o}C	10 sec	
extension	70^{o}C	45 sec	
Extension	4^{o}C	10 min	1

Table 2.5: Standard PCR conditions for isolation of DNA fragments

PCR products were identified by fragment size using gel electrophoresis and gel extraction was performed to isolate PCR products as detailed below.

Swift PCR for ligating *in vitro* constructed exons (SPLICE) reaction was performed to join the RHOKpr with RHO and IRES-DsRed to a full construct (see PCR conditions in Table 2.6) with Mfe1 and Not1 restriction sites.

	temperature	time	cycles
initial denaturation	95^{o}C	2 min	1
denaturation	95^{o}C	20 sec	40
annealing	64^{o}C	10 sec	
extension	70^{o}C	1.10 min	
extension	4^{o}C	10 min	1

Table 2.6: PCR conditions for generation of full length construct

Next, the full RHOKpr.RHO.IRES.DsRed construct was digested at the Mfe1, Sac1 restriction sites to be inserted into a AAV-CAG AAV-production plasmid. The plasmid contained wild type AAV inverted terminal repeats (ITRs) (Vector Biolabs) and was digested at the same sites to remove the CAG promoter. The construct was ligated using T4 DNA ligase (New England Biolabs) and left for ligation over a period of at least 48 hours.

Following plasmid cloning the presence of the construct was confirmed by the Mfe1, Not1 restriction enzymes and the size of the full construct and residual bacterial backbone was confirmed by gel electrophoresis.

2.4.1.2. Electrophoresis and gel extraction

DNA products were separated by gel consisting of 1%-1.5% agorose in 1x TAE buffer with 1% ethidium bromide. A 1KB DNA ladder was run in parallel to provide size markers (New England Biolabs). Samples were loaded using gel loading dye(New England Biolabs). Gels were run at 180 volts for different times depending on the size of the DNA product and were viewed and photographed on a ultravilot (UV) transilluminator. Relevant bands were excised using a sterile scalpe under UV light. DNA was isolated using a gel extraction kit (Qiagen, UK) and DNA concentration was determined by spectrophotometry using NanoDrop spectrophotometer (Thermo Scientific, USA). The ratio of absorbance at 280nm/260nm was examined, with a ratio of 1.7 to 1.9 indicating acceptable purity.

2.4.1.3. Amplification in bacteria

75µl of XL-10 bacteria (AgilentTechnologies) were thawed on ice for 5 min. 5µl ligation product was added to bacteria and incubated on ice for 30 min for complete thawing of competent cells. A 30sec heat shock was applied to cells in a heated water bath, followed by 2 min recovery on ice.1 ml of SOC medium (Invitrogen) was warmed to 37˚C and added to the culture and cells were incubated at 37˚C on a shaker rotating at 225 rpm for one hour. The resultng

culture was spread on LB-agar plates containing 100µg/ml ampicillin and incubated at 37˚ C for 14 hours.

For initial testing, single colonies were picked and placed in 4 ml LB and 8 µl of ampicillin and incubated on a shaker rotating at 225rpm for 16 hours. Plasmids were isolated using Miniprep kit (Gen Elute plasmid Miniprep Kit, Sigma Aldrich, UK). For vector production, single colonies were picked and placed in 2L LB and 4 ml of ampicillin and similarly incubated before being isolated using Megaprep kit (Qiagen, UK). In brief, cells were centrifuged and cell pellet was re-suspended and lysed. The cell lysate was added to a binding column and DNA absorbed onto a silica membrane within the column. This was then washed to remove contaminants and cell debris, and the DNA eluted in molecular biology grade water.

The resulting plasmid was sequenced for the presence of the full RHOKpr.RHO.IRES.DsRed construct using primers as detailed above to ensure no mutations were created during the cloning process (sequencing was performed by Source Bioscience, Oxford, UK). The resulting plasmid was then used in both AAV vector production (section 2.4.2) and minicircle vector production (section 2.4.3).

2.4.2. AAV vector production

Production of AAV involved the following steps:

1. Transfection of a stable cell line (HEK 293T) with three plasmids: a) the plasmid containing the AAV ITR's and the full transgene construct (as described in 2.2.1), b) a plasmid containing AAV rep and cap genes, c) a plasmid containing helper genes identified from adenovirus (helper plasmid)
2. Harvesting and lysing transfected cells
3. Isolation of the AAV particles using an Iodixanol gradient
4. Virus purification and concentration
5. Virus tittering

The methods used for these steps are detailed below:

2.4.2.1. Plasmid transfection of HEK293T cells for AAV production

Two 75cm2 T75 flasks were used for initial cell seeding. 17x106 HEK293T cells were seeded in 500ml Dulbecco's Modified Eagle's Medium (DMEM) with 4.5g/litre glucose, 10% Foetal Bovine Serum (FBS), 5ml L-Glutamine, 200mM solution, 103 units/ml Penicillin-Streptomycin, 10mg streptomycin/ml (all Sigma-Aldrich). Cells were cultured at 37oC till ~80% confluent (~72 hours). Media was then removed and cells were washed with PBS, loosened from T75 flasks by gentle agitation and re-suspended in 200ml culture media as above. Cell

suspensions from the two T75 culture flasks were transferred into two multi-layered HyperFlasks (Corning) and the flasks were filled with media with attention to dividing cells evenly between the layers of the flask and removing any air bubbles in the layers. HyperFlasks were incubated at 37^{o}C for 72 hours.

After 72 hours, cells were transfected in HyperFlasks with the transgene plasmid, rep-cap plasmid and helper plasmid with a total of 500µg DNA. The ratio is dependent on the size of the plasmids being used and was determined as depicted in Table (2.7).

Plasmid	**Size(kb)**	**Amount per transfection (µg)**
pΔF6 Helper plasmid	15.4	267.3611111
AA2/2 Y444F Rep-Cap plasmid	7.5	130.2083333
RHOK.RHO.IRES.DsRed plasmid	5.9	102.4305556
Total	28.8	500

Table 2.7: Ratio of plasmids used for transfection of HEK293T cells for AAV production

The plasmid mix was made up in a 50ml Falcon tube and the volume was made up to 10ml with addition of Sodium chloride (NaCl) 150mM (Sigma-Aldrich). In a separate tube 1.125ml of Polyethylenimine (PEI) 10mM was mixed with 8.075ml NaCl 150mM. PEI mix was complexed with DNA by slow

dropwise addition of PEI mix into the tube containing DNA. The mixture was incubated at room temperature for 20 minutes.

The DNA/PEI/NaCl complex was added to 500ml media containing DMEM with 4.5g/litre glucose, 2% FBS, 5ml L-Glutamine, 200mM solution, 5ml 103 units/ml Penicillin-Streptomycin, 10mg streptomycin/ml (all Sigma-Aldrich). This transfection media was used to replace media in each HyperFlask and HyperFlasks were incubated at 37^{o}C, for 72 hours for transfection.

2.4.2.2. Harvesting and lysing transfected HEK293T cells

Cells were loosened from HyperFlasks by vigorous shaking and collected into 500ml centrifuge tube (corning) and spun in a centrifuge for 10 minutes at 1,000rpm, 20^{o}C. The media was partially removed and the cell pellets were re-suspended in 30ml of media, transferred to a 50ml tube (Corning) and spun for 10 minutes at 1,000rpm, 20^{o}C. Media was discarded and the cell pellets from both Hyperflasks were re-suspended in 15ml lysis buffer containing 1M Tris(hydroxymethyl)aminomethane (AnalaR NORMAPUR), 150mM NaCl, (Sigma-Aldrich), Molecular biology grade water (buffer autoclaved before use). The lysis buffer was supplemented with 500µl of protease inhibitor mix containing 0.5ml lysis buffer and 0.5 complete mini EDTA-free protease inhibitor cocktail tablet (Roche). Four freeze-thaw cycles were carried out (-80^{o}C freeze for one hour followed by 15min thaw in 37^{o}C) and lysate was stored in 80^{o}C until ready for Isolation of the AAV particles.

2.4.2.3. Isolation of the AAV particles using an Iodixanol gradient

Lysate was thawed at 37^{o}C for 15 minutes and Benzonase (Merck Millipore) was added to the lysate to give a final concentration of 50U/ml. Following incubation of 45 minutes at 37^{o}C (with periodic vigorous shaking of the tube every 15 min) lysate was spun at 3,700g for 20 minutes at room temperature.

Four iodixanol gradient fractions (15%, 25%, 40%, 60%) (15%, 25%, 40%, 60%) were prepared in 50ml falcon tubes using Iodixanol OptiPrep Density Gradient Medium (60%) (Sigma Aldrich), Phenol Red solution (Sigma Aldrich) and autoclaved 5X PBS-MK (250ml PBS 10X (Gibco), 2.5ml 1M magnesium chloride (MgCl2), 6.25ml 1M potassium chloride (KCl)(both Sigma-Aldrich) in 500ml Molecular biology grade water). The ratio of each component in the different Iodixanol gradient fractions is shown in Table 2.8.

Fraction	**Iodixanol**	**5M NaCl**	**5X PBS-MK**	**H_2O**	**Phenol Red**
15%	4.0ml	3.2ml	3.2ml	5.6ml	-
25%	5.0ml	-	2.4ml	4.6ml	20µl
40%	6.7ml	-	2.0ml	1.3ml	-
60%	10ml	-	-	-	20µl

Table 2.8: Preparation of iodixanol gradient fractions

The iodixanol fractions were loaded in layers into Quick-seal Ultra-Clear 25x89 mm centrifuge tubes (Beckman) using a Pasteur pipette.

In each tube 7.2ml of iodixanol 15% was placed directly into the tube followed by careful layering of 4.8ml of iodixanol 25%, then 4ml of iodixanol 40% and finally 4ml of iodixanol 60% (Figure 2.2). The cell lysate was added dropwise on top of the iodixanol gradient and the tube was spun in Beckman 70Ti ultra-centrifuge rotor at 59000rpm for 90 minutes at 20°C. The tube was gently removed from the ultracentrifuge and the tube wall was pierced with an 18 gauge needle on a 5ml syringe at the junction between the 40% and 60% fractions. 2-3 ml of the 40% fraction containing the virus was drawn with the syringe and stored overnight at 4°C.

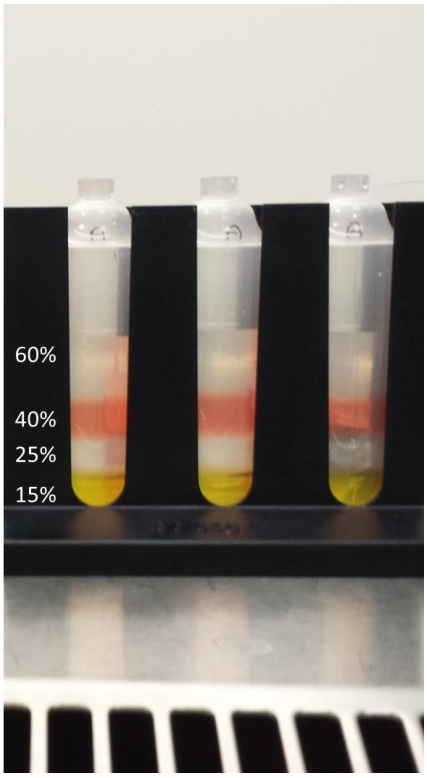

Figure 2.2: Preparation of iodixanol gradient fractions for AAV production

In each Quick-seal Ultra-Clear centrifuge tube iodixanol gradients were prepared by layering iodixanol fractions (15%,25%,40%,60%) . Cell lysate from transfected HEK293T cells was added dropwise on top of the iodixanol gradient for centrifugation and isolation of AAV particles.

2.4.2.4. Virus purification and concentration

Amicon Ultra 100K filter was placed in Amicon Ultra-15 tubes (Millipore) and prepared for virus concentration by rinsing the filter in 5ml PBS and spinning the centrifugation at 3000g for 15 min at 20^{o}C. Supernatant was discarded.

5ml PBS was added to the collected iodixanol fraction and the mix was placed on the filter of the centrifuge tube and spun3000g at 20^{o}C until the volume above the filter was reduced to 500µl. The filter was washed three times by adding 15ml PBS and spinning at 3000g for 45-120minutes. On the final wash the tube was centrifuged until the volume was reduced to 350µl. This final volume contained the purified AAV. Using a 200µl pipette, the AAV was repeatedly drawn up and dispensed back over the filter 20 times on each side to rinse and loosen any AAV remaining on the filter. The virus was then aliquoted and stored at -80^{o}C.

2.4.2.5. Virus tittering

The tittering of the virus was performed to determine the concentrating of AAV concentrated in previous steps. Primers for the RHO gene were used to determine the titre of RHOK.RHO.IRES.DsRed AAV (Table 2.9). A dilution series (10ng, 1ng, 100pg and 10pg) of the RHOK.RHO.IRES.DsRed plasmid was used as a positive template control. The virus was diluted 1:100 in molecular grade water and triplicate reactions were set up with 1µl diluted virus added to each reaction.

	Forward	Reverse
RHO	TAAGCCCATGAGCAACT	GACCACGAACATGTAG

Table 2.9: Primers used for AAV tittering

The SYBR green Nucleic Acid Gel Stain method was used, in which DNA amplified in the QPCR reaction binds to SYBR green dye, thus allowing a reading of the corresponding increase in SYBR green fluorescence intensity. A threshold was set incorporating the log phase of each reaction and a comparative cycle threshold (ct) value was determined for each sample at the same threshold.

To determine a titre, a standard curve was generated after converting the positive template control from nanograms into copies of amplicon by dividing the mass (g) of template by the molecular weight of the amplicon (g/mol) and multiplying by Avogadro's constant (a proportionality factor that relates the molar mass of a material to its mass) to generate the number of molecules in the template. The results were converted into log values and plotted against the ct values from the plasmid dilution series to generate a standard curve. Ct values of the diluted AAV were then compared to the standard curve to determine equivalent molecules. Log value was then converted back to the number of molecules and the dilution factor was corrected by x1000 multiplication for a virus titre of genome AAV particles/ml.

2.4.3. Minicircle vector generation

The minicircle (MC) vector was generated from the RHOK.RHO.IRES.DsRed plasmid described above (2.2.1).

Production of the minicircle vector was performed by PlasmidFactory (Germany).

50µl of the transgene plasmid and the plasmid restriction site map was sent to

PlasmidFactory. The methods they used to generate the MC vector are here summarized. To produce minicircle DNA, the plasmid was cut at Mfe1 Sac1 restriction sites to remove the bacterial backbone and ITRs from the AAV plasmid and inserted into a minicircle-specific parental plasmid (PP) including the eukaryotic expression unit, the transgene expression cassette and polyA signal, flanked by recognition sites of a site-specific recombinase.

Minicircles were generated by site-specific recombination. The PP included the eukaryotic expression unit, the transgene expression cassette, and polyA signal, flanked by recognition sites of a site-specific recombinase.

The parental plasmid is grown in an engineered E. coli K12 bacteria strain which harbours an Arabinose-inducible system to express the bacteriophage PhiC31, a serine recombinase and I-SceI endonuclease simultaneously. MC were generated from the PP by expression of inducible phi-C31 integrase via intramolecular (cis-) recombination. Upon arabinose induction, the phi-C31 integrase separates the MC DNA from the PP backbone, which contains a number of engineered I-SceI restriction sites that are subject to the digestion

and degeneration of the backbone by linearization and E. coli exonucleases. The MC DNA does not include these restriction sites and thus remains intact, including only the expression cassette, a polyA signal and a small residual sequence including one of the two recombination sites.

MC DNA was then purified by chromatographic purification technology to remove all PP residues as well as other contaminants and quality control tests were performed to reduce chromosomal bacterial DNA to less than 1% and produce a purified supercoiled covalently closed circular (ccc) minicircle.

Quality tests were performed at PlasmidFactory and results regarding homogeneity, purity and contamination were sent for evaluation with completion of vector production.

Sequencing to verify the construct integrity in the vector was performed on receipt of MC DNA.

2.5. *In vitro* transfection of cells

2.5.1. *In vitro* transfection of cells by AAV

Primary retinal cells were dissociated and cultured as described above (section 2.2). 24 hours post dissociation virus was added to cells in culture at a multiplicity of infection (MOI) of approximately 10^5 viral genomes (vg)/cell. The media were changed every 48 hours thereafter and cells were imaged daily to detect GFP/DsRed expression. Prior to transplantation cells were rinsed in 5ml

PBS centrifuged in sterile tube at 70g (x2) to eliminate free AAV particles from media prior to transplantation.

2.5.2. *In vitro* transfection of cells by plasmid and minicircle DNA

HEK293T were transfected by use of GeneJuice transfection reagent and primary cell cultures were transfected by NanoJuice transfection reagent and transfection booster (all Novagen). Transfection took place 24 hours after cell seeding and a complete media change was applied to primary cultures to remove antibiotics from media prior to transfection. For each well, transfection reagents were mixed with 20μl of serum free media and incubated at room temperature (RT) for 5 minutes. Subsequently transfection reagents were combined with plasmid or minicircle DNA and incubated for further 15 minutes at RT. In cell lines transfection concentration was 1μg DNA : 1μl GeneJuice and in primary culture 1μg DNA: 2μl NanoJuice: 2μl NanoJuice booster. Transfection mixture was added to cells drop-wise.

2.6. Gene expression analysis

Gene expression analysis was measured by quantitative real time PCR (qPCR). RNA was isolated and purified, followed by reverse transcription to cDNA and subsequent mRNA analysis.

2.6.1. RNA preparation

Ribonucleic acid (RNA) was isolated from cell suspensions from cultured cells or from retinas which were dissected free of all surrounding tissue in RNAlater (Ambion, Huntingdon, United Kingdom). RNA was isolated with an extraction reagent (Trizol; Gibco, NY, USA) and purified (RNeasy Mini Kit; Qiagen, CA, USA) according to the manufacturer's instructions and with buffers supplied in the kit. Briefly, the lysate resulting from RNA isolation was centrifuged for 3min at 13,000rpm; supernatant was removed and transferred to a new microfuge tube. An equal volume of 70% ethanol was added and mixed by pipetting. Up to 700 µl of the mixed sample was transferred to an RNeasy spin column placed in a 2 ml collection tube and centrifuged for 15 sec at 10,000g. Flow-through was discarded and 700 µl Buffer RW1 was added to the column before being further centrifuged for 15 sec at 10,000 g. Flow-through was discarded. 500µl Buffer RPE was added to the column which was then centrifuged for 2 min at 10,000 g. Flow-through was discarded. The spin column was placed in a new 1.5 ml collection tube and 30µl RNase-free water was added directly to the membrane. The tube was then centrifuged for 1 min at 10,000g to elute the RNA. Eluate was immediately placed on ice and RNA yield and purity was assessed by use of NanoDrop spectrophotometer (Thermo Scientific, USA).Purity was determined by the ratio of sample absorbance at 260 and

280nm, with a ratio of approximately 2.0 indicating acceptable purity of RNA and absence of protein, phenol or other significant contaminants.

2.6.2. Reverse transcription (cDNA synthesis)

Complementary DNA (cDNA) was synthesised from 1µg total RNA, using SuperScript III Reverse Transcriptase(Invitrogen, Paisley, UK), according to the manufacturer's instructions. For each reaction a 30.5 µl mixture was prepared by adding 5µl Oligo dT, 1µg total RNA (in 5µl water), and 20.5 µl RNase-Free water. The RNA mixture was placed in a heat block at 85˚C for 15 min and then chilled on ice for 2 min. In a separate tube a mixture was prepared containing 10µl 5x First Strand buffer, 5µl 0.1M DTT, 2.5µl dNTP mixture (10mM of each nucleotide), and 1µl RNAseOUT Inhibitor. The mixture was added to the RNA sample and incubated at room temperature (RT) for 2 min, followed by addition of 1 µl SuperScript III Reverse Transcriptase and further incubation at RT for 8 min. Then, the sample was heated at 50˚C for 1 hour, followed by addition of another 1µl SuperScript III Reverse Transcriptase and further1 hour incubation at 50˚C. cDNA samples were then purified using QIAquick PCR purification system and eluted in 50µl RNase-Free water. Samples were used immediately or stored at -20˚C.

2.6.3. qPCR conditions and primers

Quantitative polymerase chain reaction (qPCR) was performed on the Applied Biosystems 7500 Real-Time PCR System.

1 µl of cDNA was added to each well of the qPCR plate with 9 µl of SYBR Green PCR Master Mix as follows: 5 µl iTaq,1 µl forward primer (2 µM), 1 µl reverse primer (2 µM), 2 µl dH2o. Primers used are detailed in Table 2.10.

Gene	Forward (5' to 3')	Reverse (5' to 3')
Rhodopsin*	AGCAGCAGGAGTCAGCCACC	CCGAAGTTGGAGCCCTGGTG
Pde6b	TGGAGAACCGTAAGGACATCGC	TCCTCACAGTCAGCAGGCTCTT
Cnga1	CGGATGGAAAATGGAGCGTGCA	CTCTGTGATGGTCCTCGCCTTT
Gnat1	GCTTGTGGAAGGACTCGGGTAT	AACGCAACACGTCCTGCTCAGT
Arp	GATCATCCAGCAGGTGTTTGAC	GTGTACTCAGTCTCCACAGACAATG
Beta-actin	GCTGTGCTATGTTGCTCTAGACTTC	CATAGAGGTCTTTACGGATGTCAAC

Table 2.10: Primers used for gene expression analysis

* The rhodopsin primer pair was designed to amplify both mouse and human rhodopsin mRNA[230].

To establish a standard curve, a dilution series of a control sample or plasmid was made in dH_2O as follows: 0, 0.1ng, 1ng, 10ng, 20ng DNA. All qPCR

experiments were performed in triplicate wells. The settings for qPCR reaction are detailed in Table 2.11.

PCR step	Temperature	Time	Cycles
Initial denaturation	95^{o}C	2 min	1
denaturation	95^{o}C	30 sec	40
annealing	60^{o}C	30 sec	
extension	72^{o}C	30 sec	
Extension	4^{o}C	10 min	1

Table 2.11: qPCR conditions for gene expression analysis

2.6.4. mRNA analysis

Values obtained for the target genes were normalised to the geometric mean of the housekeeping genes acidic repeat protein (Arp) and beta-actin to reach a ΔCT (cycle threshold) value. Results were calculated by differences in gene expression between normalized target genes (ΔΔCT) and expressed as a relative quantity value ($2^{-\Delta\Delta CT}$).

2.7. Cell transplantation

Transplantations in adult mice were performed by subretinal injection under direct visualisation using an operating microscope (M620 F20, Leica, Wetzlar,

Germany). Pupils were dilated as described above and a liquid gel (Viscotears, Novartis, Frimley, UK) was applied to the eye. A 6mm circular cover glass was positioned over the cornea to allow retinal visualization through the cornea. Cells were transplanted subretinally using a Hamilton syringe and a 10mm 34-gauge needle (65N, Hamilton AG) inserted into the subretinal space though the sclera. The bevelled tip of the needle was inserted into the subretinal space and guided by the retinal vessels to prevent disruption of the retina. The needle was directed posteriorly and cells were slowly injected into the subretinal space with the bevel entirely placed in the subretinal space before injection and removed slowly after transplantation to form a self-sealing tunnel and prevent reflux of cells (see Figure 2.3). 2µl of diluted cells (approximately 2×10^5 cells) were transplanted in each injection and delivered unilaterally.

In neonatal mice (PN0) the eyelids of host pups were opened by an incision along the palpebral fissure and cells were injected intraocularly using a Hamilton syringe and a 10mm 34-gauge needle (65N, Hamilton AG) under visualisation of an operating microscope. The needle was inserted through the sclera and 1µl of diluted cells (approximately 10^4 cells) were transplanted in each injection and delivered bilaterally. Subretinal injections in early postnatal mice were achieved by rotating the eye and tangentially entering the globe, thereby minimizing reflux of injected cells.

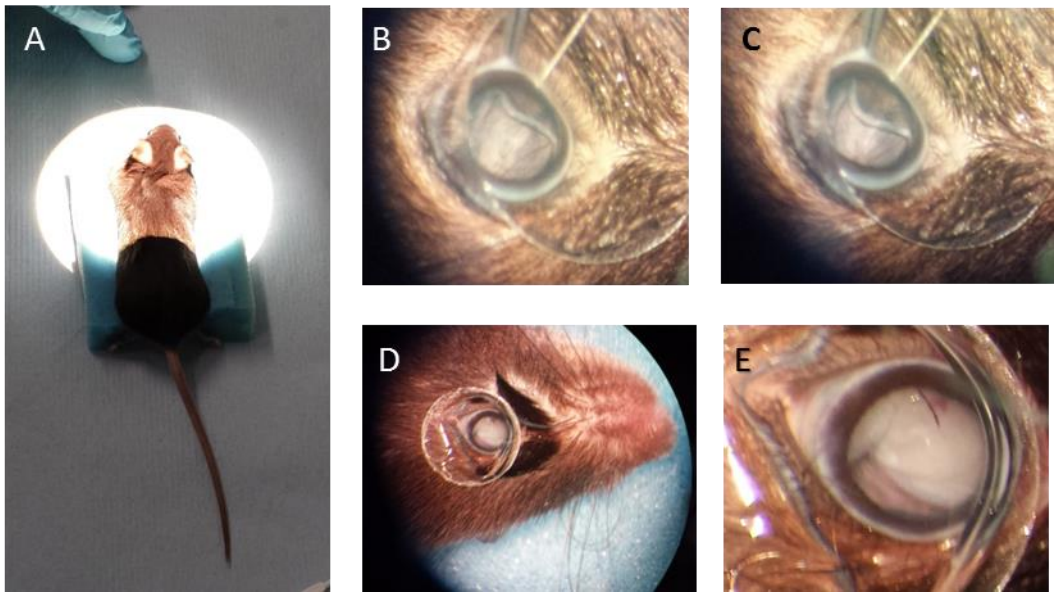

Figure 2.3: Subretinal transplantation of cells

Colour photographs showing the technique of subretinal injection. A. Subretinal transplantation was performed in anaesthetised mice under the visualisation of an operation microscope. B-C. Entry of the needle into the subretinal space was marked by penetration of the RPE by the bevel and the needle was inserted to detach the retina without injuring it. D-E. The injection of cell suspension was performed to create a subretinal bleb that extended to the optic disc.

2.8. Behavioral and functional assessment of vision

2.8.1. Optomotor response (OMR)

The animal's behavioural response to a visual stimulus was assessed by measuring the OMR to a rotating grating by adapting a previous protocol[158]. In response to a moving repetitive stimulus pattern, mice display compensatory eye movements, with a smooth pursuit in the direction of the pattern movement followed by a fast saccadic movement in the opposite direction[231]. Head

tracking behaviour follows the same pattern and can be used as a measure of visual detection of the moving pattern[232].

Mice were placed on a raised platform in the centre of a custom built rotating cylinder with a square-wave grating of black and white vertical stripes corresponding to 0.1 cycles per degree (cpd) spatial frequency (for a schematic representation of the OMR arena see Figure 2.4). In order to isolate a rod mediated response, mice were dark adapted for >12 hours prior to the procedure and testing was conducted in a dark room, with the cylinder illuminated from above by a custom LED array emitting a dim 510-nm green light (150nW·cm^{-2}·s^{-1}, approximately 10 lux at the platform). Thorough cleaning with 70% ethanol was conducted before each test and the tester was masked to treatment conditions. Mice were first habituated to the environment for 1 min during which the drum remained stationary and mice were free to explore the platform. Each experimental run consisted of 1 minute clockwise and 1 minute anti-clockwise rotation, divided into alternating 30 second periods[158]. The experimental run was repeated three times for each animal. An OMR to the rotation of the square-wave grating was assigned by the number of times an animal tracked the rotating stripes per trial, as determined by a slow head-tracking motion in the direction of the drum's rotation followed by a rapid repositioning of the head to a central position. Tracking in each direction is independently driven by one eye[233-235]; so that a head track elicited by the grating rotation in a clockwise direction is driven by the left eye, and a head track elicited by anti-clockwise rotation is driven by the right eye, allowing

comparison between the treatment groups as well as comparison between paired treated and untreated eyes. Behaviour was recorded by use of a digital camera mounted directly above the central platform. The number and direction of head tracks per trial was quantified manually by two independent scorers, blinded with regards to treatment and averaged between the three experimental runs.

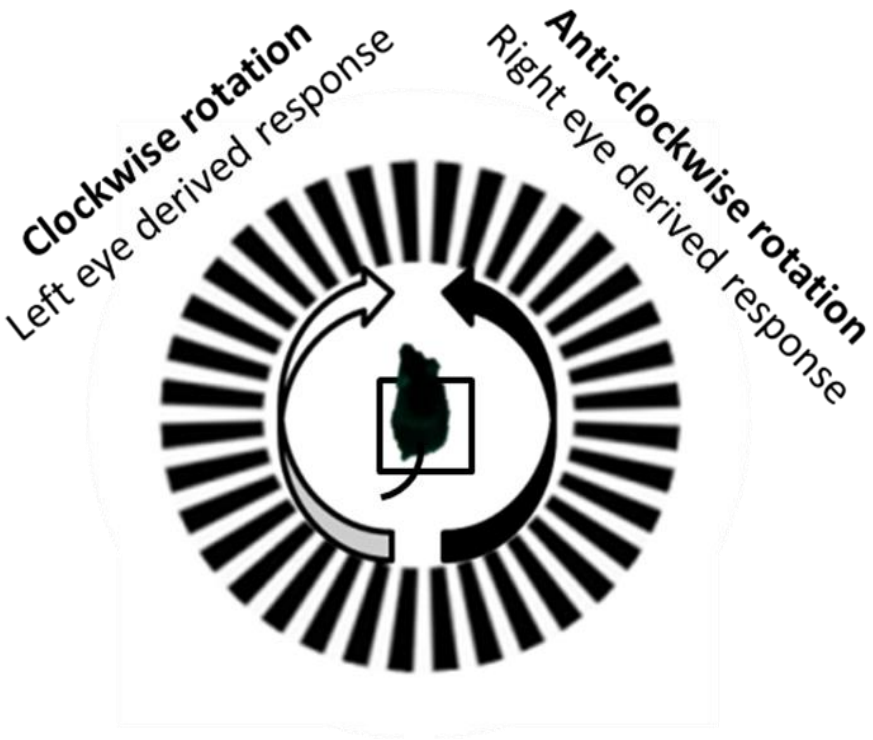

Figure 2.4: Optomotor response test

The apparatuses used was a rotating drum lined with black and white vertical stripes corresponding to 0.1 cycles per degree (cpd) spatial frequency. Mice were placed unconstricted on a raised platform in the centre of the drum and the arena was illuminated with a custom LED array emitting a dim 510 nm green light (approximately 10 lux at the platform). Each trial consisted of 1 minute clockwise and 1 minute anti-clockwise rotation, divided into alternating 30 second periods. The number and direction of head tracks displayed by each mouse were measured and averaged across trials.

2.8.2. Behavioural Light Aversion (BLA)

Behavioural light aversion was measured by animal's tendency to avoid light. Mice were tested in a partitioned arena measuring 26 cm x 26 cm x 26 cm[236] with equally sized dark and light chambers connected by a 4 cm x 5 cm aperture in the partition through which the animals were able to transition freely (for a schematic representation of the BLA area and test criteria see Figure 2.5). The assay was specifically adapted to assess rod-mediated function[62]; to this end mice were dark adapted >12 h before experiments and testing was conducted in a dark room. The light chamber was lit by a LED array suspended from above and emitting dim green light centred at 510 nm (close to the rhodopsin peak of approximately 500 nm) providing a maximal illumination of 150 $nW.cm^{-2}.s^{-1}$ (approximately 10lux at the arena floor). Both pupils were dilated 10 min prior to testing with one drop of 1% atropine. Mice were placed in the middle of the lit chamber facing away from the connecting aperture. Each trial lasted 10 min. Entrance to a chamber was recorded only when all four paws had crossed into that chamber. Light avoidance was measured by the percentage of time spent in the dark chamber. The number of full body transitions between chambers and distance travelled while in the lit chamber were recorded as a measure of anxiety-related behaviour. Both chambers were thoroughly cleaned with 70% ethanol before each test and the tester was masked to treatment group. Data were recorded by a digital camera mounted above the lit chamber and calculated by ANY-Maze video tracking software (Version 4.5 http://www.anymaze.com/).

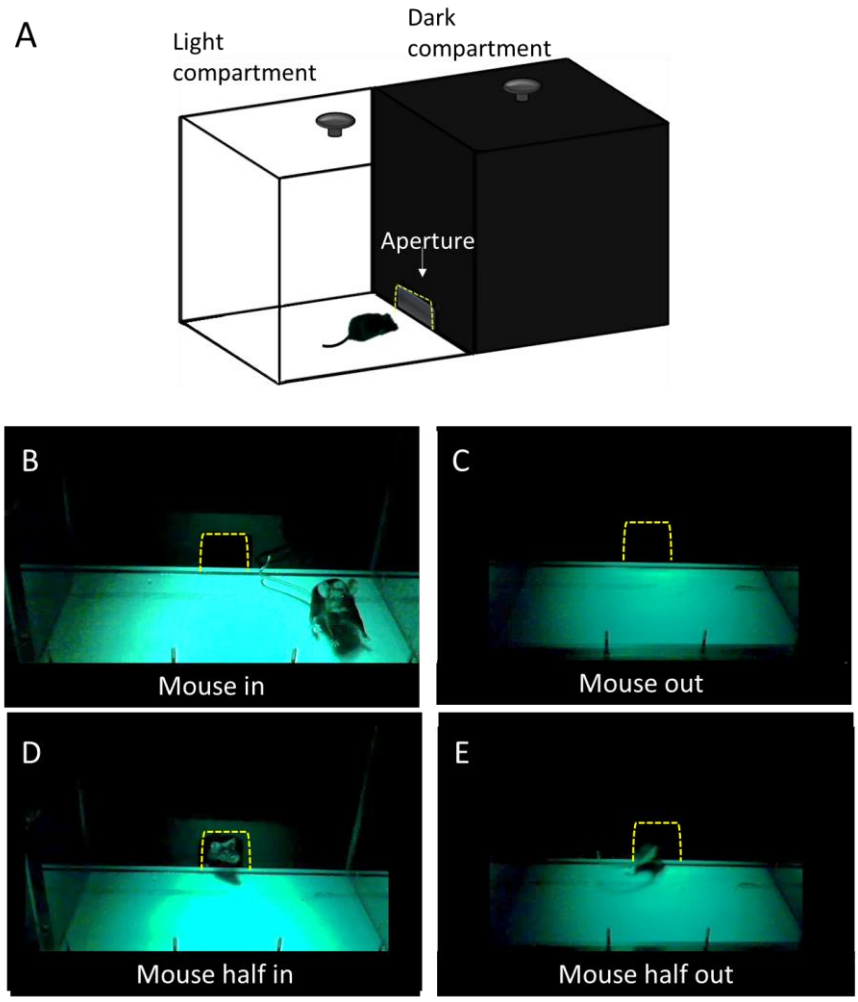

Figure 2.5: Behavioural Light Avoidance

A. Schematic representation of the BLA arena. Similarly sized dark and light compartments were connected by an aperture through which the mouse could move freely during the test period. The amount of time spent in the light and dark compartments and number of transitions between compartments was measured. B-E. Appearance of the light compartment illuminated by a LED array emitting a dim 510 nm green light (approximately 10 lux at the centre of the arena floor). The location of the aperture between the chambers in marked with a dashed line. The criteria for quantification of BLA included strict definitions of when a transition had taken place from one compartment to the other. A transition was recorded only when a mouse had crossed with all four paws into a chamber, as shown in B and C. In cases where the mouse did not fully transition before returning to the same chamber, as shown in D and E, the behaviour was deemed exploratory and was not quantified as a transition.

2.8.3. Pupil light reflex

The principle of this assay was to assess pupil constriction in response to a light stimulus in animals. Because pupil constriction in the treated eye could be impaired by mechanical factors following surgery, such as scarring following inflammation, the rod-mediated pupil response was recorded from the untreated eye in response to light stimulation of the treated eye, as resulting from the bilateral pupil light reflex (PLR). Unilateral retinal stimulation results in signal transmission to both pretectal nuclei (PN) and Edinger Westphal nuclei (EWN), and subsequently to both irides via the left and right ciliary ganglia (CG) in the posterior orbit of the eye. Therefore, the constriction response that results from a unilateral ocular stimulation with light is bilaterally equal (for schematic of the PLR see Figure 2.6).

The rod-mediated PLR was assessed by a custom pupillometry assay. Following dark adaptation for >12 hours, unanesthetised animals were assessed with the treated eye (left eye) stimulated by a 100ms duration white light pulse, while the resulting PLR was recorded from the untreated (right) eye by use of an infrared camera. A Ganzfeld sphere was used for light stimulation in order to ensure reproducible and directionally independent full field retinal illumination. Image capture was synchronised with the light exposure using an electronic shutter.

Light stimuli were presented in ascending order of irradiance, controlled by neutral density filters, and animals were exposed to testing at light intensity of 10^{14} 10^{15} or 10^{16} Photons/cm^2/s. with a period of at least 30 minutes of dark

adaptation between recordings for each animal. The pupil area was measured 1 sec after stimulus offset and was normalized to the pre-stimulus pupil area for comparison between individuals. In each group, the pupil area was assessed before and three weeks or two months after transplantation.

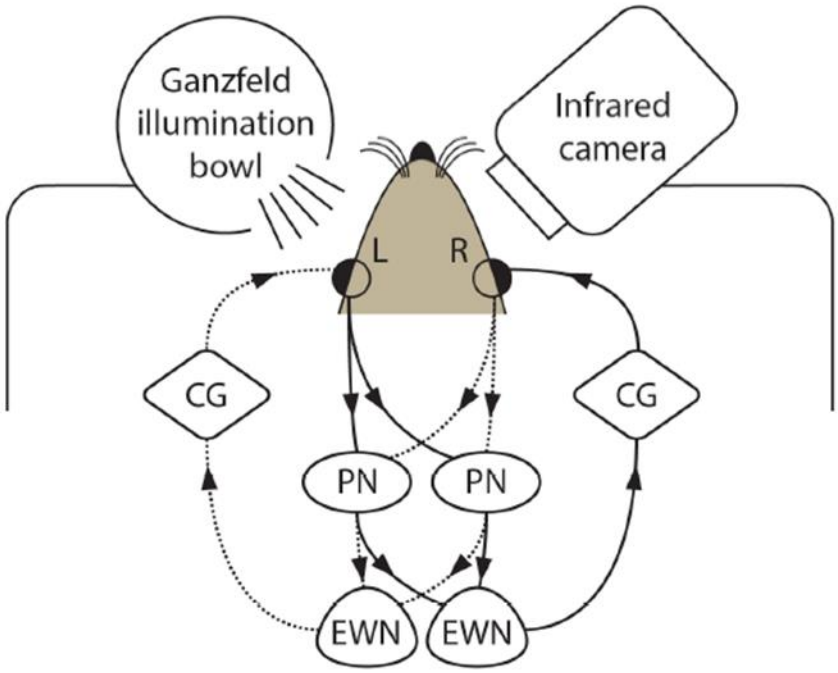

Figure 2.6: Schematic of the pupil light reflex test and consensual light response

A light stimulus is presented to the treated eye and pupil constriction is measured by infrared camera in the non-treated eye. Retinal illumination results in transmission of signals to both pretectal nuclei (PN) and Edinger–Westphal nuclei (EWN). Efferent impulses are transmitted via the ciliary ganglia (CG) and both pupils constrict. Adapted from Singh et al., 2013[62].

2.8.4. Electroretinography

ERGs were obtained by adapting previously described procedures[51]. Mice were dark adapted overnight (at least 12 hours) before the experiments. Mice were anaesthetised and their pupils dilated as described above. Silver needle electrodes served as reference (forehead) and ground (tail) and gold wire ring electrodes as active electrodes. Methylcellulose (Methocel; Ciba Vision, Wessling, Germany) was applied to eyes to ensure good electrical contact and to keep the eye hydrated during the procedure. The recording setup included a Ganzfeld bowl, a DC amplifier, and a computer-based control and recorded using an Espion V5 system (Diagnosys LLC, Cambridge, UK). ERGs were recorded from each eye separately after the mice were placed in the Ganzfeld bowl. Band-pass filter width was 1 to 300 Hz for single-flash and flicker-stimuli recordings. Single-flash and flicker recordings were obtained both under dark-adapted (scotopic) and light-adapted (photopic) conditions. Single-flash stimuli were presented with increasing intensities, reaching from 10^{-4} candelas.second per m^2 (cds/m^2) to 10 cds/m^2, divided into four steps of 10^{-4}, 10^{-2}, 1 ,10 cds/m^2. 16 responses were averaged with an inter-stimulus interval (ISI) of 5 seconds (for 10^{-4}, 10^{-2} cds/m^2) or 17 seconds (for 1 and 10 cds/m^2). Flicker stimuli had an intensity of 1-10 cds/m^2 with frequencies of 6, 20 and 30 Hz. Light-adaptation was performed with a background illumination of 30 cds/m^2 presented for 10 minutes to reach a stable level of the photopic responses[237].

2.8.5. Scanning Laser Ophthalmoscopy (SLO)

In order to assess cell survival and retinal spread of cells *In vivo*, imaging was performed using a confocal scanning laser ophthalmoscope (cSLO; Spectralis HRA, Heidelberg Engineering, Heidelberg, Germany). Imaging protocols adhered to those previously presented in adaptation of SLO imaging for mouse research[166]. Animals were anaesthetised and pupils were dilated as described above. A contact lens was placed on the cornea using a viscous gel (0.3% w/v hypromellose, Matindale Pharmaceuticals, Romford, UK) to improve image quality, and the mouse was place on an imaging platform. The near-infrared (NIR) mode (820nm laser) was used to achieve camera alignment at the confocal plane of the neural retina. GFP expressing cells were imaged using the autofluorescence (AF) mode (480 nm) using a 55° lens with a standardized detector sensitivity of 700nm and automated real-time averaging, which tracked respiration movements and averaged 100 consecutive frames. Images were recorded at a rate of 4.8 frames/s.

2.9. Histology

2.9.1. Cryosections

Following sacrifice and enucleation, eyes were fixed in 4% paraformaldehyde (PFA, Thermo Fisher, Loughborough, UK) in PBS. The cornea was excised and the lens was removed, and eye cups were fixed in 4% PFA overnight. Fixed eyes were cryoprotected in a 10-30% sucrose gradient, then washed in PBS

and embedded in optimal cutting temperature (OCT) compound (Tissue-Tek, Sakura Finetek, The Netherlands) and frozen in liquid nitrogen. Cryosections (18 µm) were cut and affixed to poly-L-lysine coated glass slides (Polysine®; Thermo Scientific, Loughborough, UK).

2.9.2. Retinal Immunohistochemistry

Retinal sections collected on polylysine-coated slides were rinsed 3 x 5 minutes with PBS 0.01M and permeabilised for 20 minutes with 0.3% Triton-X in PBS. Sections were then blocked for 1 hour at room temperature in PBS and 0.1% Triton X-100 with 10% normal donkey or goat serum before overnight incubation at 4°C with PBS containing 0.1% Triton-X, 2% normal donkey serum, and primary antibody at the appropriate concentration. Following overnight incubation, slides were rinsed (3 × 5 min with PBS) and incubated for 2 hours with species–appropriate Alexatagged secondary antibody in PBS containing 0.1% Triton-X, 2% normal donkey serum at room temperature. Slides were then rinsed (2 × 5 min with PBS), counterstained with 1:5000 Hoechst 33342 (Molecular Probes, UK) in PBS for 5 min and mounted using an antifade reagent (Prolong Gold; Invitrogen).

The primary and secondary antibodies used are summarised in Table 2.12 and Table 2.13 respectively.

Antibody	Source	Concentration	Localization
Rb anti Rho	Abcam	1:1000	ROS
Rb anti ROM1	Abcam	1:300	ROS
Rb anti Pde6b	Abcam	1:100	ROS
Rb anti Recoverin	Millipore	1:1000	photoreceptors
Rb anti Cone Arrestin	Millipore	1:1000	Cone photoreceptors
Rb anti Synaptophysin	Abcam	1:200	between host INL and the donor-derived ONL
Rb anti GFAP	Abcam	1:1000	Host Müller cells

Table 2.12: Primary antibodies used for Immunohistochemistry

Rb; Rabbit, Rho; rhodopsin, ROM1, rod outer segment membrane protein 1, Pde6b; phosphodiesterase β6, GFAP; Glial fibrillary acidic protein, ROS; rod outer segments

Reactivity	Host	Fluorescent label	source	concentration
Rabbit	Donkey	Alexa Fluor 555	Invitrogen	1:250
Rabbit	Donkey	Alexa Fluor 635	Invitrogen	1:250

Table 2.13: Secondary antibodies used for Immunohistochemistry

2.10. Image analysis

2.10.1. Confocal Microscopy

Retinal sections were viewed on a confocal microscope (LSM710; Zeiss, Jena, Germany). The fluorescence of Hoechst, GFP, Alexa-555 and Alexa-635 was excited using 350-nm UV, 488-nm argon, and the 543-nm HeNe lasers, as appropriate. GFP-positive cells were first located using epifluorescence illumination and then a series of XY optical sections (approximately 0.5µm thickness) were taken in succeeding stacks to give XY projection images. Image processing was performed using Image J (Version 1.47, National Institute of Health, http://rsb.info.nih.gov/ij/index.html).

2.10.2. Light microscopy

Analysis of fluorescent protein expression in cell culture plates and retinal sections was achieved by light microscopy imaging, using Leica DM IL inverted epifluorescence microscope and QImaging Retiga 2000R camera with

QCapture pro 7.0 software. Images were obtained using identical acquisition setting and exposure time for comparable plates or slides and were saved at a resolution of 1200x1600 pixels. Image processing was performed using Image J (Version 1.47, National Institute of Health, http://rsb.info.nih.gov/ij/index.html).

2.10.3. *In vitro* cell counts

Cells in culture were imaged every 24-48 hours by light microscope and counted using imageJ software as above. Average of cells per field of view was calculated as the mean number of cells counted per view on a 20x microscope objective, with 4 fields of view assessed per well to determine a mean cell count.

2.10.4. Retinal cell counts

The number of surviving cells in eyes was determined by counting GFP positive cells in serial 18µm non-overlapping sections through each eye. Cells were considered for analysis if they resided in the subretinal space or within the outer nuclear layer. Cells residing in the vitreous were excluded from quantification, indicating accidental penetration of the retina with resultant intravitreal injection.

2.11. Statistical Analyses

All measures are presented as mean and standard error of the mean (SEM) with a significance level of $p<0.05$. The Shapiro-Wilk test was used to determine normality of distribution and the Levene's test was used to assess

homogeneity of variance in experimental groups. Means were compared using one-way or two-way ANOVA as appropriate with Bonferroni post hoc test for multiple comparisons, or Tukey's post hoc test for multiple comparisons if comparing more than three groups (α=0.05). Paired or unpaired, two-tailed Student's t test were performed as appropriate when comparing two groups. Due to low sample size, non-parametric Kruskal-Wallis test (Dunn's test for multiple comparisons) was performed to compare responses elicited by the subgroups of animals with a high number of surviving human cells. Linear regression analysis was used to correlate behaviour with numbers of surviving cells, with F-test to determine significance. Statistical analyses were carried out using SPSS version 22 (IBM).

3. Prolonged Cultivation of Rod Photoreceptor Precursor Cells

3.1. Introduction

Rod and cone photoreceptor degeneration is amongst the most common causes of blindness in humans. Restoration of vision in end stages of the disease may be achieved by replacing lost photoreceptors by transplantation of healthy cells. Embryonic stem cells (ESC) cells and induced pluripotent stem cells (iPSC) are two possible sources from which healthy photoreceptors may be derived.

Patient-specific iPSC could provide an autologous source for cell replacement, however cells differentiated from a patient with retinitis pigmentosa (RP) or other forms of hereditary photoreceptor degeneration would have the same mutation and therefore be predisposed to degeneration, limiting their ability for

long term visual repair. To produce healthy cells, the genetic mutation leading to degeneration would need to be treated prior to transplantation, either after iPSC generation of following differentiation of the target cell population.

In pre-clinical studies, transplantation of post mitotic rod precursor cells from neonatal mice has been extensively researched[67,69,70,72,75,78,79,114,153,227] to investigate the efficiency and mechanism of cell replacement. As *in vitro* retinal differentiation from ESC or iPSC largely imitates developmental landmarks of normal *in vivo* differentiation[45,121], studies using primary neonatal photoreceptor cells may provide the defining steps towards therapeutic application of patient-derived photoreceptors.

Well characterised mouse models of disease may be used to achieve pre-clinical data by providing appropriately differentiated cells with a known genetic mutation for large scale treatment of a disease-specific gene prior to transplantation in mice of the same disease model. In order to treat mouse rod precursor cells prior to transplantation, a reliable system for prolonged rod cell culture would be essential for maintaining viable cells throughout a period that would allow testing and application of therapeutic agents. Expression of genes following non-viral transfection is relatively rapid, with expression observed in cell lines within hours. However the onset of gene expression by use of Adeno associated virus (AAV) is delayed by the rate of internalization and time required for synthesis of a complementary strand from the single stranded DNA genome. In the neonate retina, peak expression by AAV is detected on approximately day 5 *in vitro* [238], and may thus require a prolonged window of *in*

vitro cell survival of primary photoreceptor cells in order to assess initial expression and further sustained expression with either therapeutic strategy.

In cell replacement studies employing dissociated photoreceptor precursors (PhRPs), cells are typically prepared for transplantation on the day of injection and maintained for the minimal time required prior to transplantation; there are no reports to date of dissociated mouse PhRPs being maintained in culture for a prolonged period prior to transplantation.

In an *in vitro* model assessing neuroprotection[23], adult retinal explants were reported to survive long term *in vitro* when cultured at 34˚C in serum free Neurobasal A media with B27 and N2 supplements, with up to 80% viable cone photoreceptors on day 10 and over 50% cone viability at day 30[159]. Similar prolonged survival has not been reported in early postnatal ex plants or dissociated cells.

In vitro survival was investigated in young rat dissociated photoreceptor cells at postnatal (PN) day 5-15, finding that while PN10-15 photoreceptors died rapidly, duration of cell survival in PN5 cells was increased from 24 hours to 5 days in the presence of FGF-2 in Dulbecco's Modified Eagle's Medium (DMEM) culture media containing serum, with 62% photoreceptor surviving at day 5[239]. In recent transplantation studies, PN3-4 rod precursor cells were cultured for up to 4 days in DMEM containing serum and B27 supplement[126], or for 14 days in DMEM containing serum[62]. However measures of cell viability were not included in these investigations and cultured cells were not used for

transplantation. Further investigation of prolonged survival and characterisation of rod PhRP cells *in vitro* is thus required.

A further direction of consideration for *ex vivo* studies aimed at transplantation is a method of enriching the culture in a target cell type. Enrichment of early postnatal dissociated retinal cell suspensions in rod PhRP cells has been achieved by sorting fluorescence reporter expressing cells by flow cytometry (fluorescence-activated cell sorting ,FACS)[72] and by magnetic activated cell sorting (MACS) using antibodies against the cell surface molecule cluster of differentiation (CD)73[69,125,126], which is highly expressed in young rod photoreceptors[126,240]. Selection and purification methods are particularly important in photoreceptors generated from stem cells, as the inclusion of proliferating cells in the transplantation entails risk of tumour formation post transplantation. In this chapter the feasibility of MACS enrichment of rod precursor cells was investigated in cells following prolonged culture in order to increase efficiency of future transplantation[125,126] and to provide a simple method of rod precursor enrichment to allow reliable investigation of therapeutic strategies in rod enriched cultures which do not express a fluorescent reporter.

3.2. Aim

The aim was to develop a reliable system for prolonged *ex vivo* culture and rod PhRP enrichment prior to transplantation, and to assess the initial feasibility of post-transplantation survival of cells which have been cultured for a prolonged period.

Specifically, the objectives included the following:

1. To establish an *in vitro* culture system for prolonged survival of rod PhRP cells
2. To assess changes in gene expression throughout the culture period
3. To attain rod enrichment in prolonged cultures prior to transplantation
4. To assess the ability of prolonged cultured cells to survive *in vivo* post transplantation

3.3. Methods

3.3.1. Animals

Retinae were harvested from TgNrl-L-EGFP mice (referred to as Nrl.GFP) at postnatal (PN) day 0-3. Transplantation experiments were performed in C57/BL6 (referred to as WT) neonatal mice at age PN0.

3.3.2. Retinal cell culture

Retinae were dissected free of surrounding tissue and dissociated as described in Chapter 2. Cells were plated in 96 well plates at $3x10^4$ cells/well. For assessment of temperature and growth media (section 1.4.1.1) cell cultures were maintained in humidified incubators at either 34° or 37° in one of two complete culture media conditions:

a. Dulbecco's Modified Eagle Medium (DMEM) supplemented with foetal bovine serum (FBS) (10%) (both from Gibco Ltd. Life Technologies), B27 (2%), L-glutamine (0.08 mM), penicillin (100 U/ml), streptomycin (100 U/ml) (all from Invitrogen Ltd., Paisley, UK). This culture media condition will herein be referred to as DMEM/FBS/B2.

b. Neuronal growth medium (Neurobasal-A) supplemented with B27 (2%), N2 (1%), L-glutamine (0.8 mM), penicillin (100 U/ml), and streptomycin (100 µg/ml)[157] (all Invitrogen Ltd., Paisley, UK). This culture media condition will herein be referred to as NeuroA/B27/N2.

For assessment of supplementation requirements (section 1.4.1.2) dissociated cell cultures were maintained in humidified incubators at 34° Celsius in one of four complete culture media conditions:

a. Complete NeuroA/B27/N2 (as described above)
b. NeuroA/B27 (as described above without addition of N2)
c. NeuroA/N2 (as described above without addition of B27)
d. NeuroA (as described above without addition of B27/N2 supplements)

3.3.3. Cell viability

Cell survival was determined through the use of the GFP reporter gene by which intrinsic fluorescence acts as a proxy marker of cell viability[159,228,229].

For *In vitro* studies, biological replicas were assessed by averaging four fields per well at each time point (field size ~300μm). Number of GFP positive cells and total cells per field of view were counted both manually and automatically using imageJ software. Results of manual and automatic counts were compared and averaged. Viability was further assessed with trypan blue dye exclusion test as described in Chapter 2.

3.3.4. Gene expression analysis

Gene expression was determined by messenger RNA (mRNA) levels measured by quantitative PCR (qPCR) (detailed methods in chapter 2). mRNA analysis was assessed for the following genes: Rhodopsin (Rho), Guanine Nucleotide Binding Protein (G Protein), Alpha Transducin Activity Polypeptide 1

(Gnat1, also known as transducin), Phosphodiesterase 6B (PDE6b) and Cyclic Nucleotide Gated Channel Alpha 1 (Cnga1). RNA was extracted from PN0-3 Nrl.GFP mice which had been maintained in culture for 7, 14 or 30 days (N=7 wells each). To account for changes in gene expression throughout the culture period results are expressed in terms of change in mRNA expression relative to freshly dissociated PN3 Nrl.GFP retina (N = 7).

3.3.5. Magnetic-activated cell sorting (MACS)

To prepare a single cell suspension for cell sorting, at the end of the selected culture period cultured cells were lifted from wells and lightly dissociated a second time (as described in Chapter 2 but with only 3 min incubation in papain+ DNase at 37˚C). MACS was performed by use of an antibody to CD73 rod cell surface marker. Unsorted CD73- and CD73+ cell cohorts were analysed and the latter were used for cell transplantation.

3.3.6. Cell transplantation

PN0 C57/BL6 (WT) hosts were anaesthetised intraperitoneally and received a bilateral subretinal transplantation of 10^4 rod precursor cells which had been either freshly dissociated (n=6) or maintained in culture for 14 days (n=6).

3.3.7. Histology

Mice were sacrificed 14 days post transplantation and eyes were processed as described in Chapter 2. Sections were stained with Hoechst 33342 (Molecular Probes, UK) for confocal microscopy.

3.4. Results

3.4.1. Establishing a prolonged culture system for dissociated rod RhRPs

The primary aim was the development of an *in vitro* culture system in which rod photoreceptor precursors could be maintained in a viable state for a period of time sufficient for *ex vivo* modification and analysis prior to transplantation. Retinae were extracted from early postnatal mice and dissected free of surrounding tissues (Figure 3.1). Retinae were then dissociated enzymatically as described in Chapter 2 and cells were cultured for a prolonged period of time under varied conditions for optimal survival of rod precursor cells.

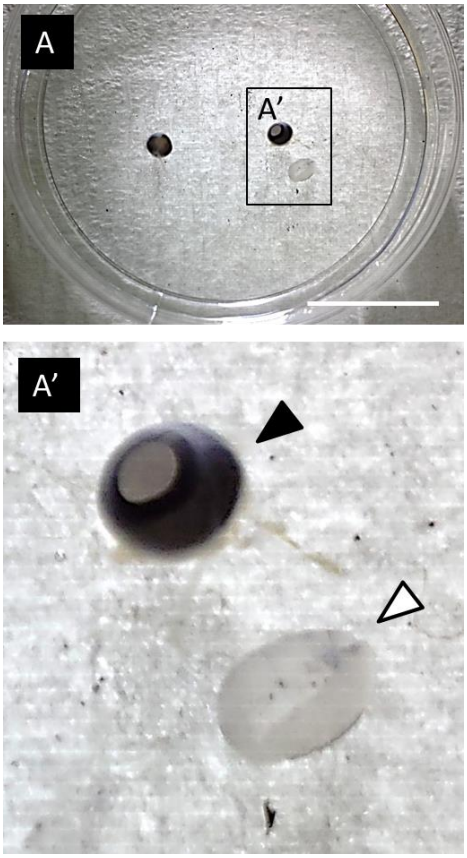

Figure 3.1: Neonatal retina dissection

A. Neonatal (PN0) eyes were extracted and dissected in sterile PBS under direct visualisation of an operating microscope. A’) Enlarged image of whole eye (black arrow) and retina dissected free from surrounding tissues (white arrow). Scale bar= 1cm. PBS; phosphate-buffered saline.

3.4.1.1. Establishing optimal temperature and growth media.

To investigate the effect of media and temperature on cell viability, four conditions were compared throughout a culture period of 16 days. The media additives and temperatures were selected according to previously published

data[126] and established cell culture protocols in our lab[62,159]. Dissociated Nrl.GFP+ cells cultured in DMEM/FBS/B27 survived for up to 7 days at 37° and up to 10 days at 34°. Rods cultured in NeuroA/B27/N2 supplements survived up to 12 days at 37° and over 14 days in 34° with over 90% total cell viability at day 14 and an increase in cell number over 100% of day 1 in culture, indicating *in vitro* differentiation of retinal cells to a rod photoreceptor fate (Figure 3.2). A main effect for media condition was evident, so that cells survival in NeuroA/B27/N2 media was improved over DMEM ($p<0.0001$). A main effect for temperature was also found where an increase in temperature (from 34˚C to 37˚C) was accompanied by a significant decrease in cell survival ($p<0.001$) (Three way ANOVA, $F(3,64)=159.4$, $p<.0001$). Further *in vitro* experiments were hence conducted using serum free Neurobasal-A growth media and incubation at 34°.

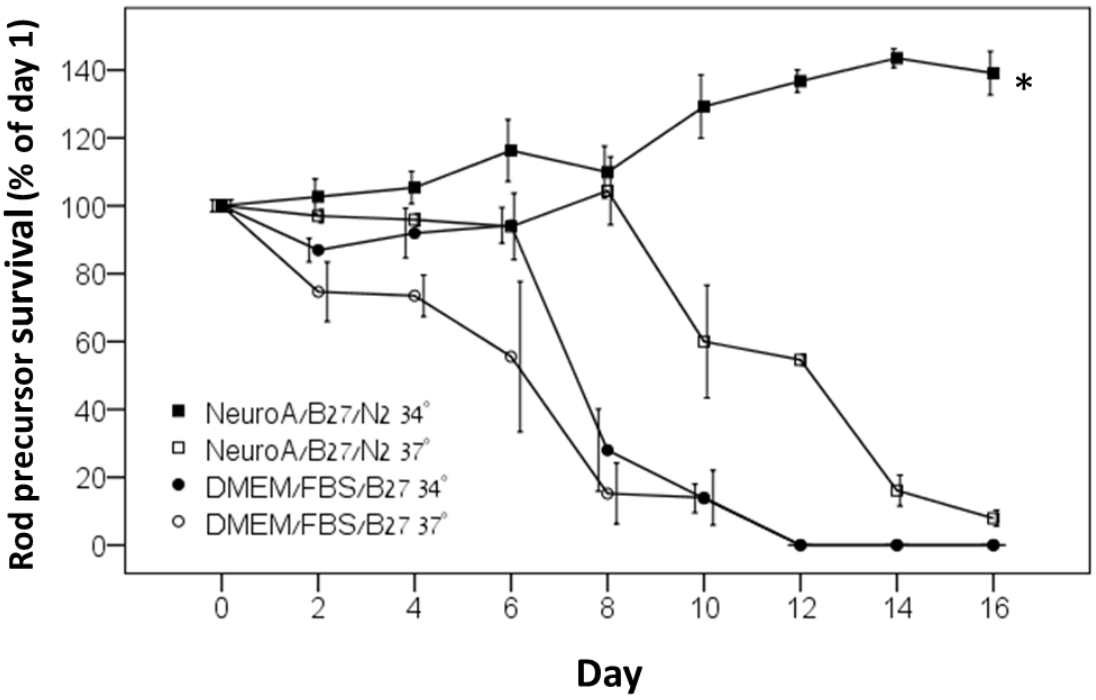

Figure 3.2: Effects of temperature and growth media on rod precursor survival *in vitro*

Retinae of PN0-3 Nrl.GFP mice were dissociated and incubated at either 34°c or 37°c in one of two culture media: a. NeuroA/B27/N2; b. DMEM/FBS/B27. Nrl.GFP positive rod precursors cultured in NeuroA/B27/N2 at 34°c survived throughout the culture period, whereas cell viability in other conditions progressively decreased. Cells cultured in NeuroA/B27/N2 exhibited better overall survival than did cells cultured in DMEM/FBS/B27 ($F(3,64)=159.4$, $p<.0001$). Three way ANOVA; media composition, temperature and day in culture as factors. Data points represent mean and SEM of GFP+ cells normalized to mean of GFP+ cells on day 1. Error bars represent mean ±1 SEM of 8 biological replicates (4 technical replicates for each biological replicate). *$p<0.05$.

3.4.1.2. Establishing supplementation requirements

The supplement N2 was traditionally used for neural stem cell (NSC) cultures[241], whereas B27 was described first for the maintenance of primary neurons in culture[242]. In prolonged assessment of retinal explant viability, the combination of these two supplements (but not each supplement alone) encouraged long term tissue viability[159]. A methodological comparison of media supplements in a culture of dissociated retinal cells revealed prolonged survival in cells cultured in NeuroA/B27/N2 media, compared to no supplementation or each supplement on its own ($p<0.0001$) (Two way ANOVA, $F(12,40)=6.2$, $p<0.0001$, Tukey's test for multiple comparisons) (Figure 3.3). On day 14 of culture, over 95% of cells were viable in the optimal media condition (NeuroA/B27/N2) as detected by trypan blue staining.

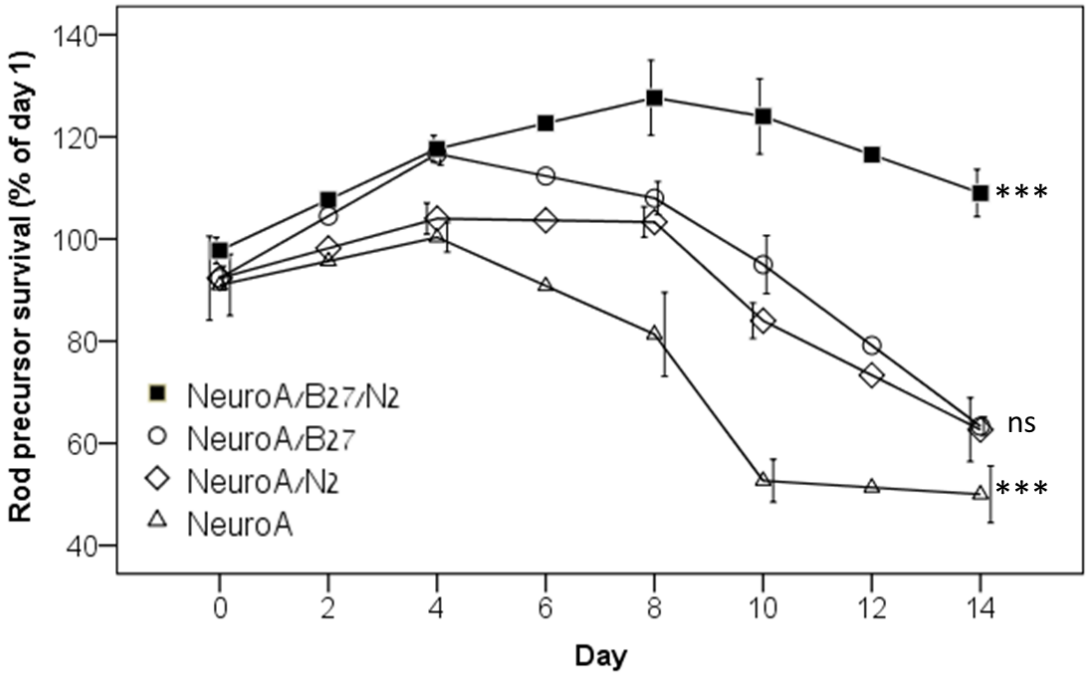

Figure 3.3: Effects of media supplementation on rod precursor survival *in vitro*

Retinae of PN0-3 Nrl.GFP mice were dissociated and incubated at 34°c in one of four media: NeuroA/B27/N2, NeuroA/B27, NeuroA/N2, NeuroA. Throughout the culture period a significant difference was observed in number of GFP+ cells in the different conditions ($F(12,40)=6.2$, $p<0.0001$). Survival of cells cultured in NeuroA with both supplements was significantly higher than other media conditions ($P<0.0001$), and no supplementation resulted in significantly lower survival ($p<0.0001$). Two way ANOVA; media composite and day in culture as factors. Tukey's post hoc test for multiple comparisons. Data points represent mean and SEM of GFP+ cells normalized to mean of GFP+ cells on day 1. Error bars represent mean ±1 SEM of 6 biological replicates (4 technical replicates for each biological replicate). *$p<0.05$.

3.4.1.3. Sustained survival and development of cells in vitro

In order to determine a window for *ex vivo* assessment of gene therapy and an optimal time point for cell transplantation, patterns of cell survival *in vitro* were investigated. Retinae of PN0-3 Nrl.GFP mice were dissociated and cultured in the optimised media conditions. In this culture system it was possible to maintain rod PhRP cells in culture for over 4 weeks (Figure 3.3A) with over 95% viability of cells at the end of the culture period as assessed by the trypan blue exclusion test. Increase in numbers of GFP+ cells in culture was observed, peaking at day 12, in which the number of GFP+ cells increased to approximately 146.2±17.9% SEM of first day of culture. This was maintained with no change up to day 14, followed by a decrease in cell numbers on day 16 ($p<0.001$). On day 31 mean cell number was 28.7%±6.4% of day 1. This is consistent with the rod development and patterns of GFP expression in the Nrl.GFP mouse (figure 3.3B-C). While decreasing in number, cells maintained consistent levels of GFP expression throughout the culture period and only following day 20 cells began clumping in the culture plate, corresponding with reduced cell numbers in culture (Figure 3.5A), however cells remained highly viable (>95%) on day 30 of culture (Figure 3.5B). Frequent media changes in the wells in this study most likely removed cell debris following cell death and non-viable cells, resulting in the decrease in the number of viable cells in culture and sustained survival of the remaining cells.

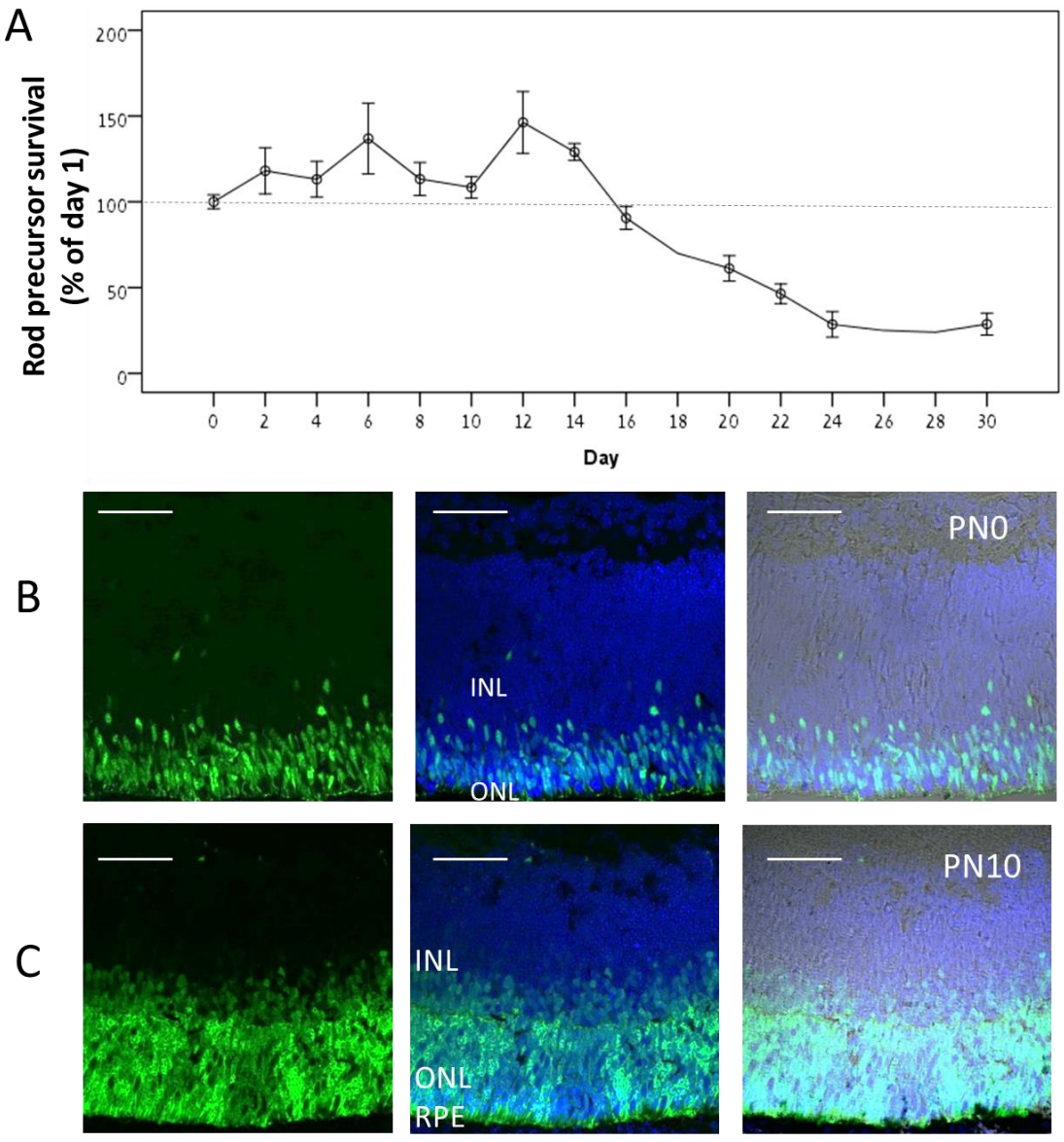

Figure 3.4: Prolonged survival and expansion of rod PhRPs *in vitro*

A. Pattern of cell survival during 31 days in culture. An expansion in GFP+ rod precursor cell numbers was observed in culture throughout the first 14 days with subsequent reduction in cell numbers. B-C. Similar increase in number of GFP+ cells is observed *in vivo* in the Nrl.GFP mouse following rod cell differentiation from PN day 0 (B) to PN day 10 (C). Scale bar, 50μm. Error bars represent mean ±1 SEM of 12 biological replicates (4 technical replicates for each biological replicate) INL; inner nuclear layer, ONL; outer nuclear layer, RPE; retinal pigment epithelium. PN; post natal.

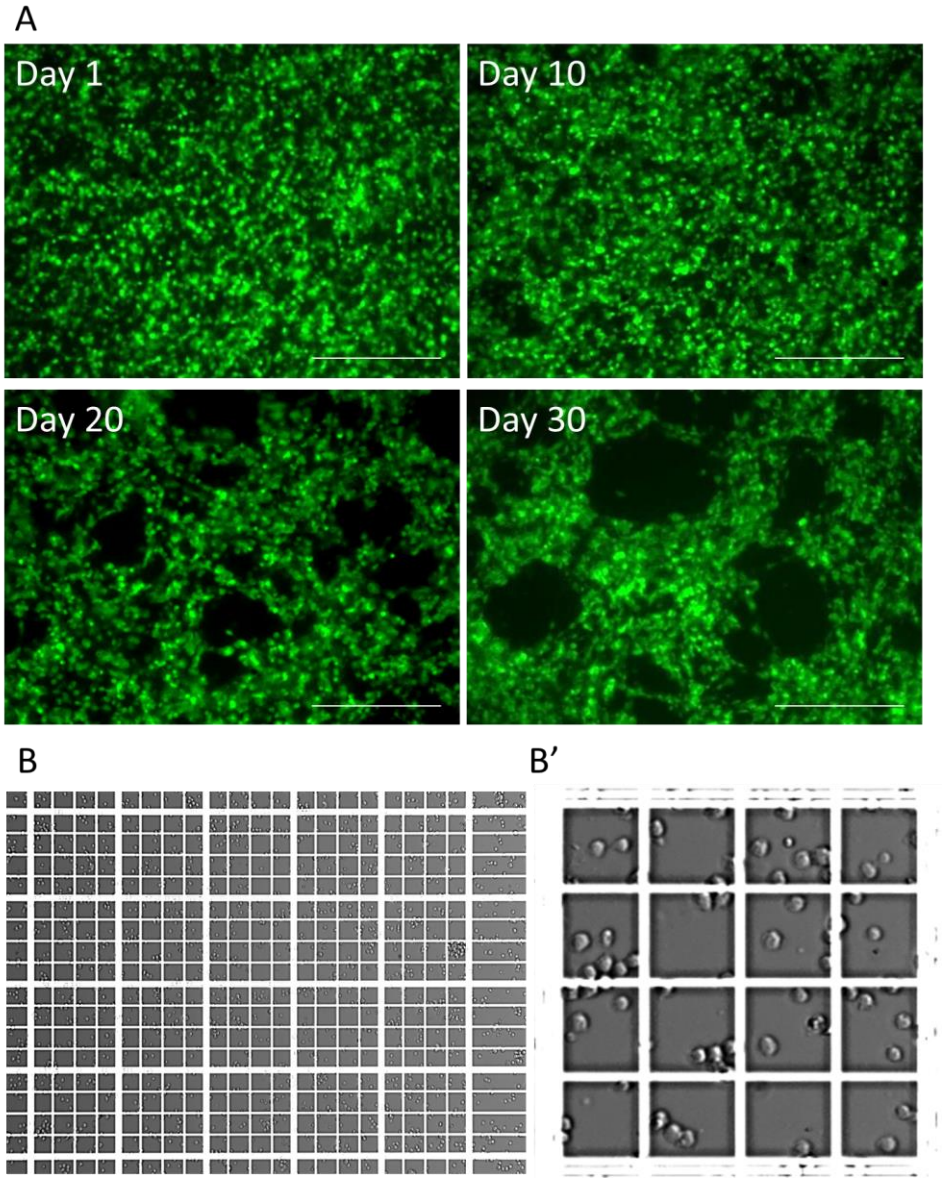

Figure 3.5: Cell appearance and viability in prolonged culture

A. Constant GFP levels and morphology were observed throughout culture period, with difference in cell arrangement *in vitro* following day 20. This corresponds to reduction in cell numbers in culture. Scale bar, 100µm. B. Over 95% of cells cultured in NeuroA/B27/N2 were viable on day 30 *in vitro* B’. Representative 1x1mm chamber of the hemocytometer, showing higher resolution of viable cells. These observations suggest that while cell numbers decrease, a portion of cultured rod precursor cells survive *in vitro* for 4 weeks.

3.4.2. Gene expression analysis

To investigate whether rod precursors maintain expression of genes required for OS function throughout the culture period, expression of rod-specific genes (rho, pde6b, Gnat1, cnga1) was quantified on days 7, 14 and 30 *in vitro* relative to freshly dissociated neonate (PN3) cells.

Cells *in vitro* on day 7 and 14 did not differ in rod-specific gene expression to freshly dissociate cells, absence of gene upregulation indicates that cells did not continue to mature *in vitro* and is consistent with the lack of OS formation in culture. However on day 30 of culture, downregulation of rho ($F(2,25)=10.28$, $p<0.001$) and Gnat1 ($F(2,25)=3.5$, $p<0.045$) was observed, and although not reaching significance, a similar trend was observed in regulation of PDE6b ($F(2,25)=3.3$, $p<0.051$) and Cnga1 genes ($F(2,25)=2.7$, $p<0.083$) (Figure 3.6). As cultured cells are ultimately intended for transplantation, their ability to mature and produce OS function *in vivo* would be critical. The downregulation of rod specific genes prior to transplantation would not allow for optimal cells function. Sustained gene expression in cells up to day 14 suggests that these rod precursors may maintain the ability to mature and function as adult rods.

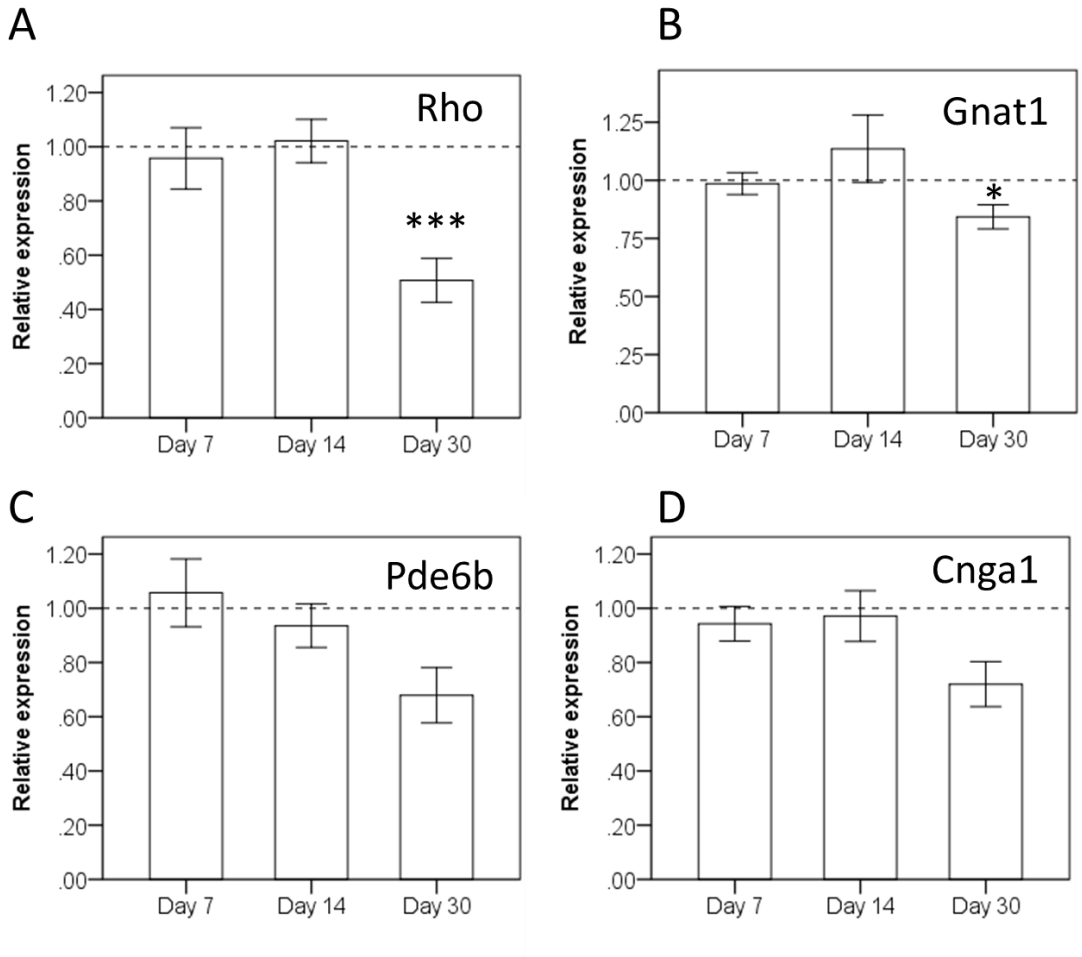

Figure 3.6: Gene expression in cells throughout prolonged culture

Gene expression analysis was performed to assess the expression of rod-specific genes in dissociated retinal cells in different time-points of the culture period. A-D. mRNA expression levels were maintained throughout the first 14 days of culture. On day 30 of culture downregulation of rho ($F(2,25)=10.28$, ***$p<0.001$)(A) and Gnat1 ($F(2,25)=3.5$, *$p<0.045$)(B) were observed. While not significant, a trend towards downregulation of PDE6b ($F(2,25)=3.3$, $p<0.051$)(C) and Cnga1 ($F(2,25)=2.7$, $p<0.083$)(D) were also observed. Gene expression is presented relative to mRNA expression in freshly dissociated retinae obtained from age matched Nrl.GFP mice (postnatal day 3) (Dashed line). One way ANOVA, Bonferroni test for multiple comparisons. n=7.

3.4.3. Magnetic-activated cell sorting (MACS) of rod precursors in prolonged culture

In order to achieve rod enrichment in culture, MACS separation of retinal cells was assessed in cultured cells. After 7 days of culture, PN0-3 Nrl.GFP cells were lifted and dissociated a second time to ensure a single cell suspension for cell sorting. Magnetic beads were attached to cells by CD73 antibody, a rod photoreceptor cell surface marker[45,243]. CD73-positive (CD73+), CD73-negative (CD73-) and unsorted cells were assessed by number of GFP+ cells in cell cohorts. GFP is specifically expressed in rod cells through the Nrl promoter and thus the enrichment of Nrl.GFP in CD73+ cohorts is evidence of rod enrichment.

In the unsorted culture, 42.15 ± 8.02% (mean % ±1 S,E.M) of all cells in culture were GFP+, following MACS, in the CD73+ sorted cell culture 86.33 ± 6.4% expressed GFP, whereas in CD73- sorted culture GFP was expressed in 23.8± 3.67% of all cells. Number of GFP+ cells was significantly increased in the CD73+ cohort, compared to unsorted cells ($t(4)=11.14$, $p<.0001$) and significantly decreased in the CD73- cohort ($t(4)=5.29$, $p<.005$) (Figure 3.7). These results were consistent with results of cell sorting in freshly dissociated retinae[126]. The efficiency of sorting was reproducible in the prolonged culture system with equivalent numbers of GFP+ cells in CD73+ cohorts sorted at day 1, 7 and 14 of culture ($F(2,8)=0.145$, ns).

This platform will allow for the study and transplantation of rod enriched cell suspensions following prolonged culture.

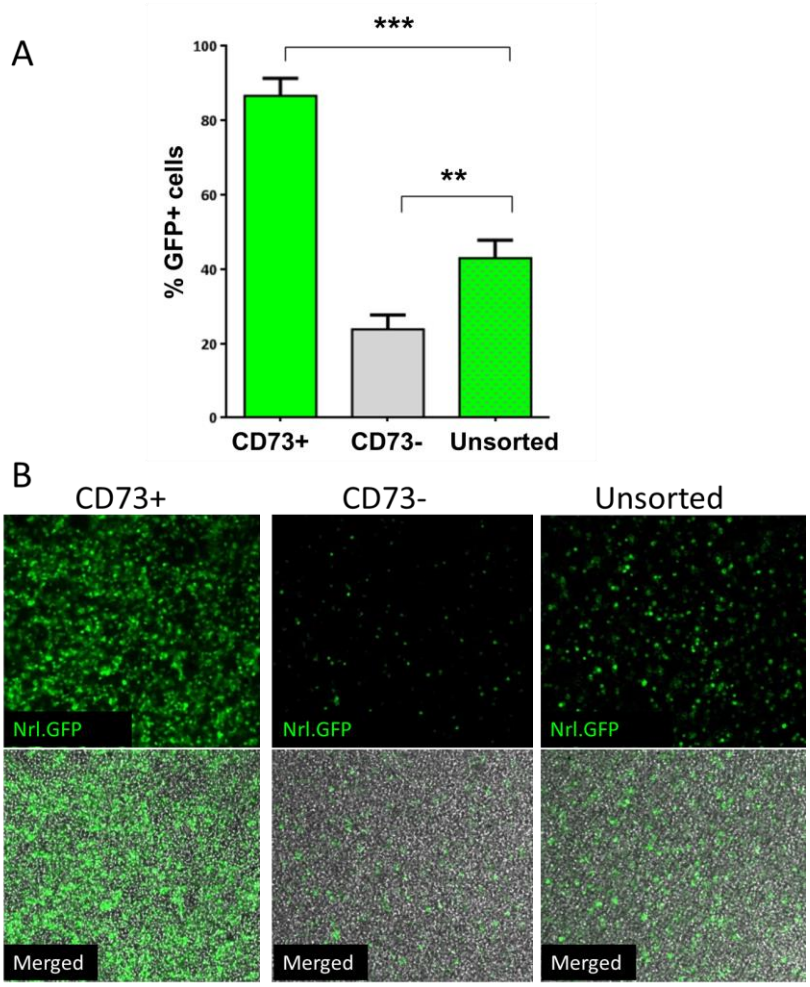

Figure 3.7: MACS separation of PhRPs in prolonged culture

A. Analysis of unsorted, CD73-negative, and CD73-positive cells from PN0-3 Nrl.GFP retinas reveals an increase in GFP-positive cells in CD73-positive (CD73+) sorted cells in comparison to unsorted cells, which have been labelled with magnetic beads and passed through the MACS column but had not undergone magnetic sorting ($t(4)=11.14$, $p<.0001$). A decrease in percentage of GFP-positive cells was observed in the CD73-negative (CD73-) cohort, compared to unsorted cells ($t(4)=5.29$, $p<.005$). **p< 0.01, ***p<0.001. B. Representative images of CD73+, CD73- and unsorted cells. Top row: Nrl.GFP+ rods; bottom row: merged image of Nrl.GFP+ cells and IMC image of all cells in the well. Scale bar, 50µm. MACS; Magnetic-activated cell sorting.

3.4.4. *In vivo* survival of rods following prolonged culture

PN0-3 dissociated Nrl.GFP retinae were cultured for a period of 14 days prior to transplantation and PN3 Nrl.GFP retinae were freshly dissociated prior to transplantation to provide a control. Cells were MACS sorted as above and immediately transplanted by subretinal injection to neonate WT mice (PN0). Cells were here assessed for *in vivo* survival following transplantation (rather than for maturation or connectivity as will be presented in Chapter 5 and 6).

Following transplantation, Nrl.GFP+ cells were observed residing in the host subretinal space and ONL 14 days post transplantation of freshly dissociated cells (Figure 3.9A) and cells which had been maintained in culture for 14 days (Figure 3.9B). Instances of GFP+ cells in the host ONL (Figure 3.9C-D) may indicate cell integration into the host retina, but may represent a fusion artefact as will be elaborated in the discussion.

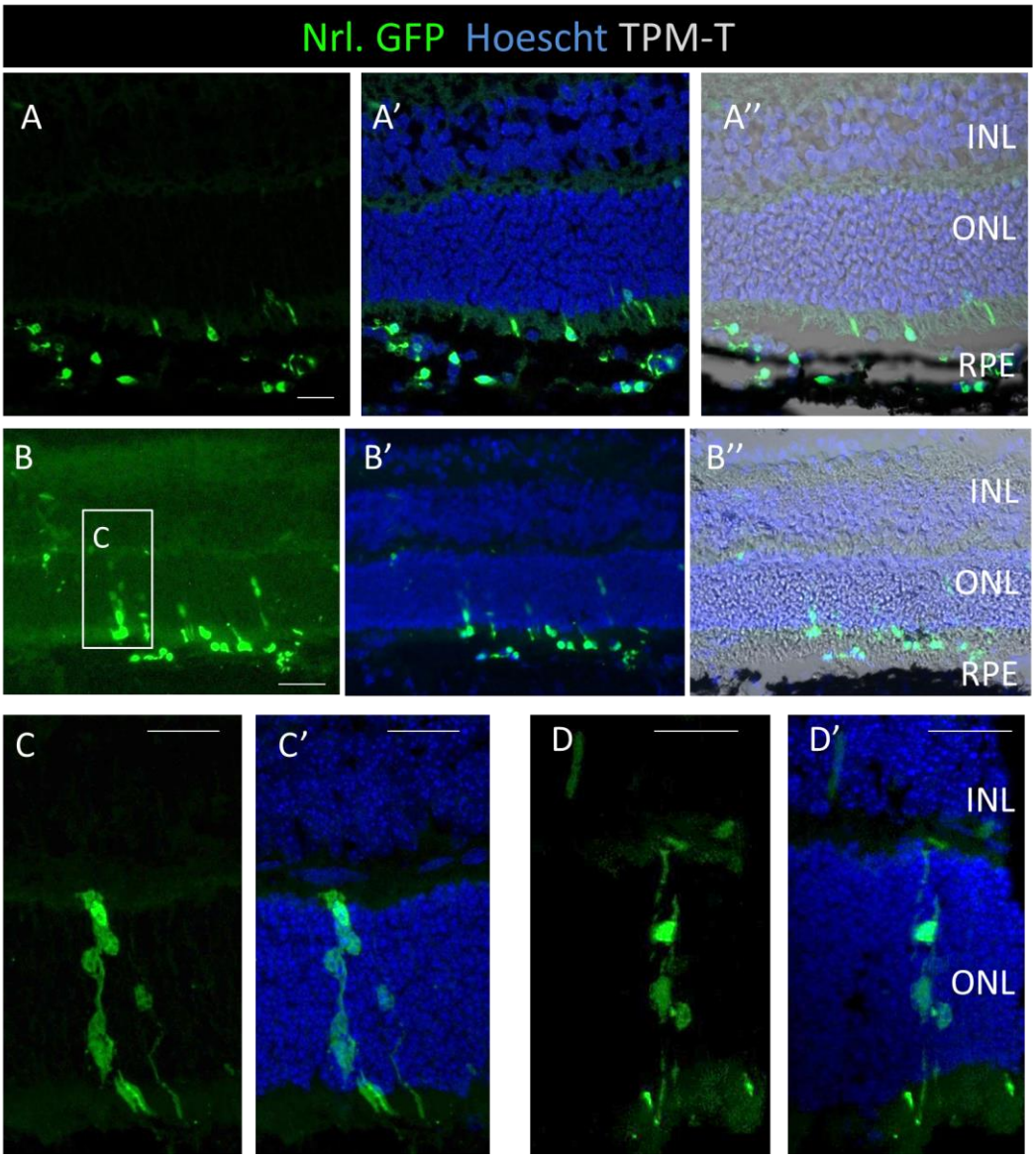

Figure 3.8: *In vivo* survival of cells following prolonged culture

Nrl.GFP rod precursor cells were transplanted into neonate WT mice, donor cells were transplanted either on the day of retinal dissociation or following 14 days of culture. A-A''. Freshly dissociated Nrl.GFP rod precursor cells survived in the subretinal space of neonate WT mice. B-B''. Nrl.GFP rod precursor cells which had been cultured for 14 days were observed to survive in the subretinal space similarly to freshly dissociated cells. C-D. GFP+ cells were also observed within the host ONL indication the possibility for rod cell integration in the neonate WT retina following prolonged culture. Scale bar, 10μm. INL, inner nuclear layer, ONL; outer nuclear layer, RPE; retinal pigment epithelium, TPM-T is the transmitted light transducing channel of the confocal microscope.

3.5. Discussion

Taken together, the data presents defining steps for maintenance and characterisation of survival of neonatal rod PhRPs in prolonged culture.

A system for *ex vivo* culture of rod PhRPs was assessed through repetitive imaging of dissociated photoreceptors with intrinsically fluorescent rod photoreceptors. Optimised media and temperature conditions were established and gene analysis confirmed the continuous expression of rod OS specific genes over the course of 14 days of culture. Rod PhRPs were successfully enriched in culture by use of magnetic assisted cell sorting via the rod cell surface marker CD73. Transplantation of cultured cells in the neonate retina provides a first account of rod photoreceptor survival and possible integration following subretinal transplantation.

Optimisation of conditions for cell culture of dissociated neonate retinae provides a reliable and reproducible system for *ex vivo* investigation of retinal cells. Cells maintain high viability throughout 14 days of culture, and with reduced viability thereafter for up to a month. The marked increase in rod precursor cells in culture over the first 14 days can be attributed to *ex vivo* generation of rods from retinal precursor cells. In the Nrl.GFP mouse GFP+ cells are post mitotic, Nrl.GFP is first expressed at embryonic day 12 and peaks at PN4-5 *in vivo*[244] . The increase in number of GFP+ cells throughout the culture period suggests that retinal cells continue to differentiate towards a rod photoreceptor fate up to day 12-14 *ex vivo*. This corresponds to rod cell birth in

the developing mouse retina, which occurs throughout a broad developmental window, peaking at PN0 and occurring up to day 11 [244-246], with 73% of cells produced postnatally differentiating as rods[247].

mRNA analysis of cultured cells at different time points *in vitro* indicated that expression of rod specific genes (Rho,Gnat1, PDe6b, Cnga1) was maintained at least throughout the first 14 days in culture. Maintained gene expression may suggest that cells in culture maintain their identity as rod precursors *ex vivo*, and may be used in transplantation studies and mature *in vivo*. Each of the considered genes encodes a protein which is immensely important in visual transduction; Rhodopsin (Rho) initiates the visual transduction cascade, leading to the activation of transducin (Gnat1) which stimulates the coupling of rhodopsin and cGMP-PDE. PDE6b is the ß subunit of cGMP-PDE; its activation leads to hydrolysis of cGMP and results in closure of cGMP-gated channels and hyperpolarization of the cell. Finally Cnga1 encodes a protein which forms a cGMP-gated cation channel in the cell plasma membrane, allowing depolarization of rods. The downregulation of Rhodopsin and Gnat1 on day 30 likely excludes cells in this late stage of culture from transplantation studies. Gene downregulation corresponds to the lack of outer segment (OS) development in cells *in vitro*, downregulation of proteins that are not essential for cell survival or function likely represents a mechanism for preservation of cell survival in these cultured cells. Taken together with observations of survival patterns, the period up to day 14 may be optimal for investigation of *ex vivo* gene therapy and collection of rod precursor cells for transplantation.

The finding that dissociated retina can be reliably sorted throughout the prolonged culture period to reproducibly enrich rod precursor cells without reducing cell viability, will allow for testing of gene delivery vectors specifically in a culture of rod cells, thus allowing for identification of cell specific expression *in vivo* in animals. Furthermore, it will allow for rod enrichment prior to transplantation without use of FACS, which has been associated with low viability of sorted stem cell-derived photoreceptors following transplantation[73].

Rod precursors which had been maintained in culture for 14 days and then enriched by MACS, survived in the neonatal subretinal space 14 days following subretinal transplantation. This demonstrates a first account of survival and possible integration of primary rod PhRPs after prolonged culture. The identification of transplanted cells in animal studies is often achieved by endogenous transgene expression, such as the expression of Nrl.GFP, and consequently GFP positive cells in the ONL of host animals are identified as donor cells. An under-recognised or under-reported phenomenon in the field of photoreceptor cell transplantation is the concept of cell fusion. In transplantation of stem cells, the process of cell-cell fusion has emerged as an unpredicted and possibly confounding factor; circulating haematopoietic stem cells (HSCs) have been shown to fuse with target cells including hepatocytes, cardiac myocytes, and oligodendrocytes[248-250], and macrophages derived from HSCs have been observed to fuse with hepatocytes[251]. Applying these observations to the retinal transplantation model, it is possible that GFP cells residing in the subretinal space fuse with overlaying host photoreceptors, and

these take up the green fluorescence, creating an artefact. Instead, abnormally shaped photoreceptor cells residing in the subretinal space, which have been observed following photoreceptor transplantation into severely degenerate mice[62,70], may be more relevant than previously acknowledged for the results of photoreceptor transplantation studies.

3.6. Conclusions

A reliable *in vitro* culture system was established for the prolonged culture of rod PhRP cells. Rod precursor cells survived in culture for up to 31 days, maintaining constant levels of viability and rod-specific gene expression up to day 14. Cell cultures were consistently enriched with rod PhRPs throughout this period and cells which had been cultured for 14 days survived in the subretinal space of neonate WT mice for 14 days. The ability to maintain rod precursors *ex vivo* for a prolonged period of time will allow a sufficient window of opportunity for investigation and comparison of *ex vivo* gene therapy techniques which require different periods of time for transgene expression (Chapter 4). Initial cell survival observed here in neonate WT mice will be further investigated and characterized in Chapter 5 by transplantation of *ex vivo* treated cells into mice with advanced retinal degeneration.

4. *Ex Vivo* Gene Delivery to Rod Precursors and Generation of Rhodopsin Vectors

4.1. Introduction

The rhodopsin gene (mouse *rho*, human *RHO*) encodes a G protein-coupled receptor that is highly expressed in rod photoreceptor outer segments (OS) and is central to visual transduction. The *RHO* encoded transmembrane protein constitutes ~90% of the protein content of mammalian rod OS disk membranes. Mutations in the rhodopsin gene account for close to 25% of cases of autosomal dominant retinitis pigmentosa (RP)[17] (adRP) and have also been found to be involved in autosomal recessive (arRP) and sporadic RP, though to a lesser extent[252-255]. Dominant mutations in the *RHO* gene can be caused by gain of gene function, loss of function or a combination of both. Loss of function is associated mainly with arRP, however it may be implied in adRP

when the single operational allele is not sufficient to maintain functional vision[194]. Gain of function of *RHO* has been associated with the P23H mutation in approximately 12% of adRP patients: in this form of disease, the mutant protein is over expressed and misfolded, leading to protein aggregation in the endoplasmic reticulum and subsequent apoptosis or opsin aggregation, resulting in cytotoxicity[42].

Therapeutic strategies which have been investigated in mouse models to rescue rod photoreceptors from degeneration include expression of the wild type gene to replace function of the mutant protein[139,154,256-258], or a two-step approach in which the mutant gene is first supressed, followed by its replacement with the WT gene[259-261]. The first strategy may be used for treatment of patients with different *RHO* mutations as it does not specifically target a single mutation. However, in both forms of treatment the protein would need to be delivered in a dose sufficient to replace this highly expressed protein but avoid overexpression and toxic effects.

A widely studied mouse model with disruption of the endogenous *rho* gene ($Rho^{-/-}$)[50] has provided a valuable tool for the study of RP. These mice do not elaborate rod OS and their rod cells degenerate, followed by degeneration of cones and complete ONL degeneration by approximately 3 months of age. This model has also been used for the investigation of rhodopsin replacement; Rescue and long term preservation of rods in the $Rho^{-/-}$ mouse has been achieved by crossing mice of this model with a mice expressing the human *RHO gene* [259]. In another study, *in vivo* Adeno-Associated Virus (AAV)2/5

mediated delivery of *RHO* to adult and neonate Rho$^{-/-}$ mice was reported to restore up to 40% of WT rho mRNA levels and provide histological and functional rescue[256]. The Rho$^{-/-}$ model has also been used in key transplantation studies as a host for rod precursor cell replacement[67,70,75] as will be further elaborated in the following chapter.

AAV vectors are established as an advantageous method for ocular gene therapy in clinical trials[146,262-264] and for delivery of genes to photoreceptor cells[265,266] in animals. Recombinant AAV-2 (rAAV-2) vectors were among the first to be developed and AAV pseudotypes have been created by packaging of the AAV2 vector sequence into viral capsids of different serotypes[267] to enhance cell specific tropism (see Section 1.6.2.2). A further direction to be considered for efficient and targeted gene delivery to photoreceptors is the selection of a promoter/enhancer element with photoreceptor-restricted transcriptional activity and appropriate size for AAV packaging.

AAV2/8 coupled with the human rhodopsin kinase promoter, also known as the G protein-coupled receptor kinase 1 (RHOK, also GRK1[268]) has shown high efficacy in transfection of photoreceptor cells following *in vivo* delivery to non-human primates[265]. AAV2/7 and AAV2/8 with a rhodopsin promoter have been shown to be more efficient than AAV2/9 and AAV2/5 in targeting mouse photoreceptors *in vivo* and following *ex vivo* delivery in photoreceptors differentiated from mouse retinal stem cells[194]. Optimisation of AAV vectors for photoreceptors in mice revealed increased efficiency of capsid mutant AAV2/2 in mouse photoreceptors using the human RHOK promoter. These results were

verified *in vitro* in a cone photoreceptor cell line and *in vivo* following intravitreal delivery[266].

The rhodopsin promoter is designed to target rod photoreceptors, but has been shown to allow unintentional transgene expression in both rod and cone photoreceptors[269,270]. In order to specifically and uniformly express the rhodopsin gene in photoreceptor cells, the 0.2kb human rhodopsin kinase promoter was here selected for investigation and comparison of *ex vivo* transduction by two AAV serotypes.

A restrictive factor for gene delivery using AAV is the limited packaging capacity of 4.7kb genomic DNA per viral particle[271] with substantially reduced efficiency of expression when packaging larger genes[188]. Non-viral methods for gene delivery have been suggested as an alternative for delivery of large genes to the retina[171-174]. However such methods have been reported to have low efficiency in transfecting retinal cells and providing therapeutic levels of gene expression *in vivo*.

Ex vivo treatment of cells prior to transplantation may provide a more suitable platform for the delivery of therapeutic genes into photoreceptor cells, avoiding the degradation mechanisms that face non-viral vectors *in vivo*. The RHO gene, which is a small gene of only 1047bp, does not challenge the packaging capacity of AAV and can thus be delivered with both viral and non-viral methods to study and compare the efficiency of *ex vivo* gene delivery.

Minicircle (MC) DNA is derived from a plasmid by removal of the plasmid bacterial backbone, thus designed to reduce size and avoid transcriptional

silencing of the delivered transgene, and so improving efficiency of expression in cells (see Section 1.6.3.2). The exclusion of the origin of replication together with the plasmid bacterial backbone prevents MCs from replicating, and in dividing cells transgene expression is lost when the cell divides. This may be an advantage when transient expression is required, but a disadvantage for gene delivery when sustained expression is sought. In post mitotic cells which are not dividing, sustained expression may be achieved. This method may therefore be appropriate for *ex vivo* gene therapy in a differentiated cell type such as photoreceptor precursors.

In recent trials, Liposome-mediated MC DNA delivery has shown expression *in vitro* in HEK293T cells for 14 days (with initial transfection efficiency of ~80% and thereafter a decrease to ~10% by day 14) and *in vivo* expression in normal and tumour livers for at least two months (last time point measured)[222]. In a study of MC gene therapy delivery for myocardial infarction, stable gene expression was measured in the heart 3 months following delivery, with over 50% higher levels of the target gene expression compared to plasmids.

The study of MC DNA delivery to cells of the neural retina has not yet been investigated. The possibility of retinal transfection by MC and the packaging of the *RHO* gene and RHOK promoter in a minicircle vector to achieve transgene expression in PhRPs will herein be investigated.

4.2. Aim

The aim was to develop an AAV vector and non-viral minicircle vector for efficient *ex vivo* delivery of the RHO gene to rho$^{-/-}$ PhRP cells. To achieve this aim the following objectives were pursued:

1. Selection of an appropriate AAV serotype and assessment of *in vitro* transduction of rod PhRP cells
2. Assessment of *in vitro* transfection of retinal cells using minicircle DNA
3. Cloning a plasmid carrying the rhodopsin gene
4. Generation of an AAV vector
5. Generation of a minicircle vector
6. Assessment of expression after AAV and minicircle gene delivery.

4.3. Methods

4.3.1. Animals

Retinae were dissociated from neonate mice PN0-3 and cultured for *in vitro* assessment as follows: WT mice were used for assessment of GFP expression *in vitro* and *in vivo*, Nrl.GFP mice were used for investigation of dose dependent toxicity of Doxorubicin and Rho$^{-/-.Nrl.GFP}$ were used for assessment of AAV and minicircle vector delivery of the rhodopsin construct. Subretinal transplantation of cells for investigation of host retina transduction following

administration of rAAV2/2 Y444F RHOK.GFP was performed in adult WT mice (age 6-8 weeks) n=9.

4.3.2. *In vitro* investigation of AAV vectors

Primary cells were dissociated from neonate retinae and plated in 24 well plates ($2x10^5$/well). After 24 hours virus was administered to cells at a multiplicity of infection (MOI) of approximately 10^5vg/cell. Media were changed every 48 hours thereafter and cells were imaged daily to detect GFP/DsRed expression.

For assessment of the effects of proteasome inhibition (PI) *in vitro*, Doxorubicin (Calbiochem, USA) was added to wells with the virus in 2ml of complete media at a concentration of 170nM, 1.7μM or 17μM.

4.3.3. Investigation of host retinal transduction following transplantation of AAV treated cells

To investigate host retinal transduction by free viral particles following transplantation of AAV treated cells, transduced cells were lifted from the well, and cleansed from free AAV particles in one of the following methods:

1) No rinse: Cells were transferred to a sterile centrifuge tube and spun at 70*g* for 5min, then concentrated to 10^5/μl in PBS for transplantation.

2) One rinse in PBS: Cells were transferred to a sterile centrifuge tube and spun at 70*g* for 5min, then re-suspended in 5ml PBS in a new sterile centrifuge

tube, spun at 70*g* and for 5min and concentrated to 10^5/µl in PBS for transplantation.

3) Two rinses in PBS: Cells were rinsed as described in the previous condition with an additional rinse step in PBS (5ml PBS, new sterile tube, centrifuge at 70*g*) and concentrated to 10^5/µl in PBS for transplantation.

All cells were then prepared for transplantation and subretinally transplanted as described in chapter 2, but at a concentration of 10^5cells/2µl - instead of $2x10^5$ cells/2µl - in order to reduce the number of cells residing in the eye and allow assessment of host retinal transduction in areas with no transplanted cells. Eyes were collected 9 days post transplantation and processed for confocal microscopy. In order to assess transduction of the host retina, images were obtained away from the transplantation site in retinal sections that did not include transplanted cells.

4.3.4. *In vitro* assessment of minicircle vectors

Primary cells were dissociated from neonate retinae and plated in 24 well plates ($2x10^5$/well) and HEK293T cells were seeded at 10^4/ well. 24 hours after seeding, cells were transfected as described in Chapter 2, with dose dependent administration of MC DNA: 0.05pg DNA/cell, 0.5pg DNA/cell, 5pg DNA/cell, 50pg DNA/cell. Following optimisation, cells were transfected with

approximately 50pg DNA/cell. Media were changed every 48 hours thereafter and cells were imaged daily to detect GFP/DsRed expression.

4.3.5. Gene expression analysis

Gene expression was determined by messenger RNA (mRNA) levels measured by quantitative PCR (qPCR) (detailed methods in chapter 2). mRNA analysis was assessed for the Rhodopsin (Rho) gene, by primers designed to detect both mouse *rho* and human *RHO*[230]*.*

RNA was extracted from retinal cells of PN3 Rho$^{-/-.Nrl.GFP}$ mice, which had been treated by delivery of the *RHO* gene with rAAV2 Y444F or MC gene therapy, or maintained in culture without gene therapy treatment (N=7 wells each). Results are expressed in terms of change in mRNA expression relative to similarly cultured cells from PN3 WT mice (N = 7 wells).RNA was extracted 7 days following gene therapy (Day 8 *in vitro*).

4.4. Results

4.4.1. AAV transduction of rod precursor cells *in vitro*

4.4.1.1. Selection of AAV serotype for in vitro transduction of rod precursor cells

In order to select an AAV serotype for *ex vivo* transduction of rod photoreceptor cells, two serotypes which have been established to transduce mouse and non-human primate photoreceptors *in vivo* were compared for expression of GFP in

dissociated WT rod precursors. Capsid mutant rAAV2/2 Y444F[200,201,266] was compared to rAAV2/8[194,265,266]. Both vectors expressed GFP driven by the human rhodopsin kinase (RHOK) promoter[268]. As described in the previous chapter, dissociated retinal cells from neonatal mice can be efficiently sorted by the rod specific CD73 cell surface marker, thus attaining a rod enriched cell culture. Transduction of CD73+ cultured cells (rod precursor enriched to approximately 86% of cells in culture) was thus compared to CD73- (rod precursor depleted to approximately 24% of cells in culture) cells for selection of a rod specific serotype. On day 9 post transfection, GFP expression was more efficient in rod enriched cohorts compared to rod depleted cohorts transfected with both rAAV2/2 Y444F RHOK.GFP ($t=19.4$, $p<0.001$) and rAAV2/8 RHOK.GFP ($t=12.7$, $p<0.001$). In the rod precursor enriched culture, transduction with rAAV2/2 Y444F achieved efficient GFP expression in 90.8%±1.8%SEM of cells, which was more efficient than GFP expression by rAAV2/8 reaching 81.9%±2.1%SEM ($t=3.29$, $*p<0.05$). No difference in efficiency was observed between the vectors in the rod precursor depleted culture ($t=0.21$, ns) (Figure 4.1). Accordingly, the capsid mutant rAAV2/2 Y444F serotype coupled with the RHOK promoter was selected for further investigation.

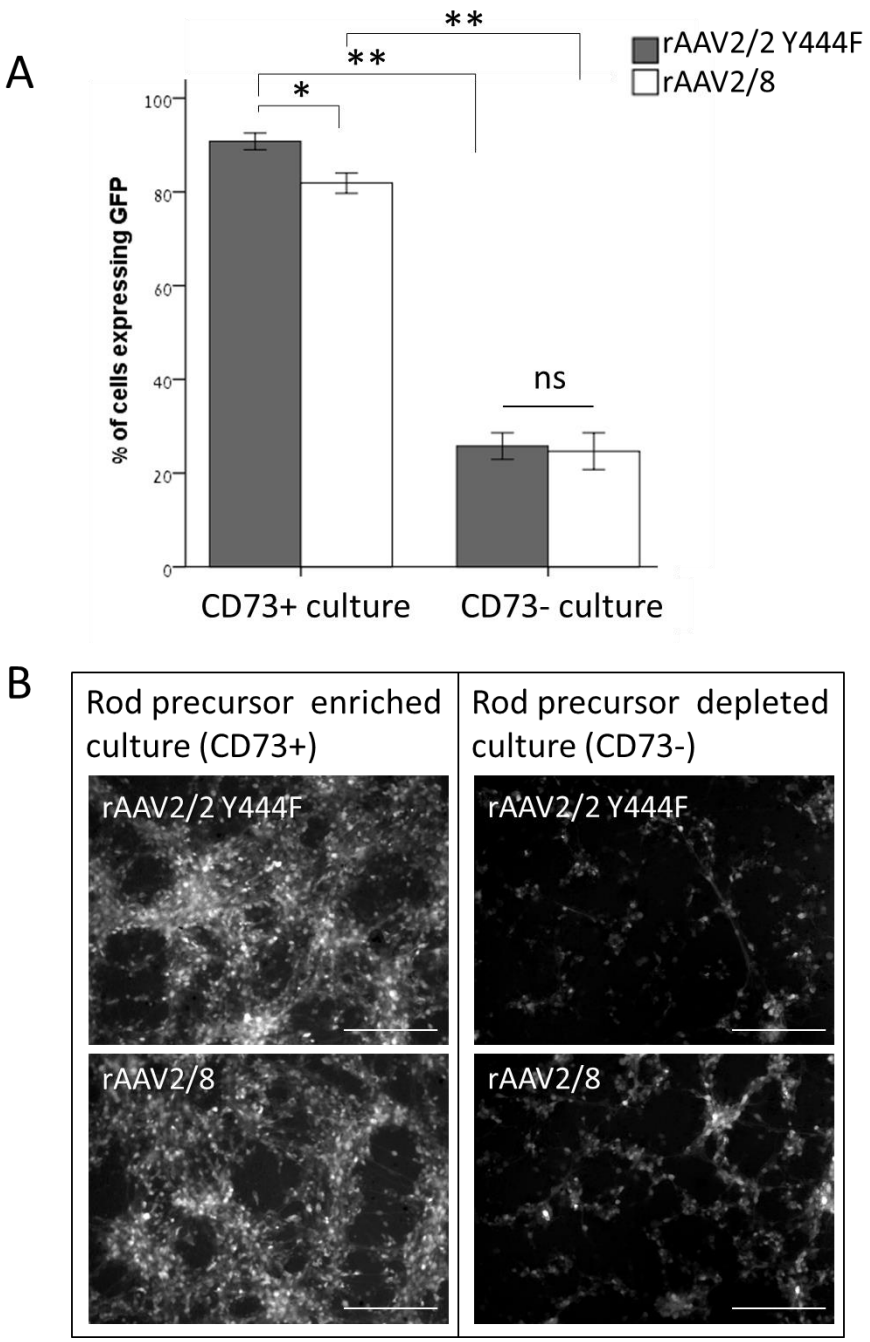

Figure 4.1: *In vivo* transduction efficiency of AAV serotypes in rod precursor enriched culture

A. Dissociated cells from neonatal WT mice were MACS sorted via the CD73 rod cell surface marker and CD73 positive (CD73+) and negative (CD73-) cohorts were transfected with rAAV2/2 Y444F RHOK.GFP or rAAV2/8 RHOK.GFP vectors. GFP expression was assessed 9 days post transfection. A. GFP was expressed more efficiently in rod precursor enriched cultures by

both rAAV2/2 Y444F RHOK.GFP (t=19.4, p<0.001) and rAAV2/8 RHOK.GFP (t=12.7, p<0.001). A significant difference was observed in GFP expression between the two vectors in the rod precursor enriched cohorts (CD73+) (paired t test, t=3.29, *p<0.05), but not in rod precursor depleted cohorts (t=0.21, ns). Values indicate the percentage of GFP-positive cells compared to the total number of cells in culture. Error bars represent mean ±1 SEM of 9 biological replicates (4 technical replicates for each biological replicate).
B. Representative Images of GFP expression from the two vectors in cultures enriched or depleted in rod precursor cells on day 9 post transfection. Scale bar, 100μm.

4.4.1.2. Investigating improved transduction by proteasome inhibition in retinal cells in vitro

Increased transduction by capsid mutant AAV vectors has been reported to be due to a decrease in ubiquitin tagged proteasome mediated degradation[199]. To investigate further efficiency in *ex vivo* transduction of retinal cells by a capsid mutant vector, the effect of the proteasome inhibitor (PI) Doxorubicin was assessed in dissociated neonate retinal cells (PN0-3).

PIs have been shown to increase AAV transduction *in vitro* and *in vivo* in a serotype-specific and cell-specific manner[198,272-275], therefore first a non-toxic dose of Doxorubicin was established in dissociated photoreceptor cultures from Nrl.GFP mice. Three doses of Doxorubicin were administered to cells. Cell viability was reduced in comparison to control cells in the high (p<0.0001) and medium (p<0.001) dose and only at a low dose (170nM) was this PI non-toxic

in cells (Figure 4.2). This dose was thus used to investigate improved transduction by rAAV2 Y444F in cultured retinal cells.

To see whether PI could further augment transduction, rAAV2/2 Y444F RHOK.GFP was delivered to dissociated neonate WT cells, alone or with the addition of Doxorubicin (170nM). 9 days following transfection, levels of expression did not differ between the two groups (t=0.54, ns) (Figure 4.3), indicating that this PI did not augment *ex vivo* transduction of cells by capsid mutant rAAV2. Due to the highly significant reduction in cell viability following administration of high doses of Doxorubicin and the absence of increased transduction efficiency, in further experiments Doxorubicin was not used in the delivery of capsid mutant rAAV2.

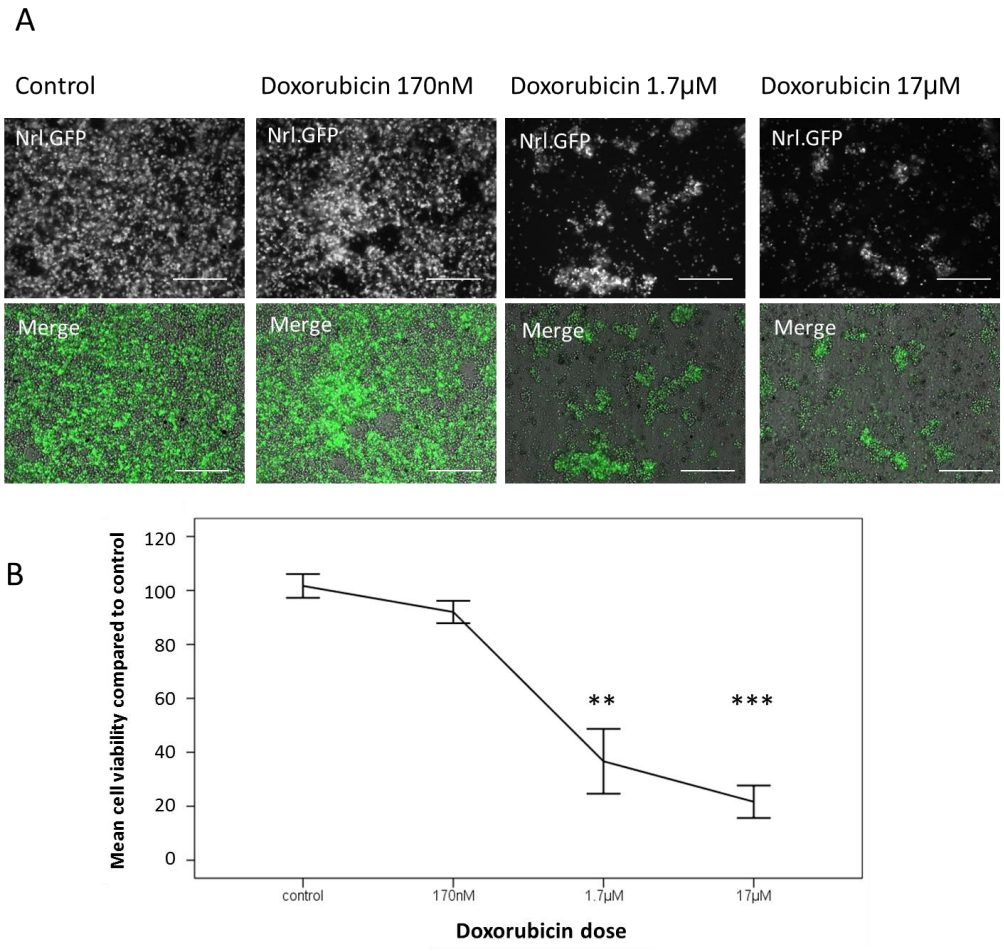

Figure 4.2: Establishing a non-toxic dose of proteasome inhibition in early neonatal PhRPs

Three doses of the PI doxorubicin (170nM, 1.7μM, 17μM) were administered to dissociated cells from neonate Nrl.GFP mice and cell survival was compared to similarly plated control cells to which no PI was added. A. 7 days post administration GFP expression was reduced in high concentrations of doxorubicin. Scale bar 100 μm. B. viability was assessed by use of trypan blue staining, revealing a significant difference between the four groups (one way ANOVA, $F_{3,8}=29.06$, $p<0.0001$). Post-hoc analysis with Bonferroni correction revealed a decrease in cell viability in the high dose (17μM) (***$p<0.0001$) and medium dose (1.7μM) (**$p<0.001$) and only at a low dose (170nM) this PI was non-toxic in cells (ns). Error bars represent mean ±1 SEM of 3 biological replicates (4 technical replicates each).

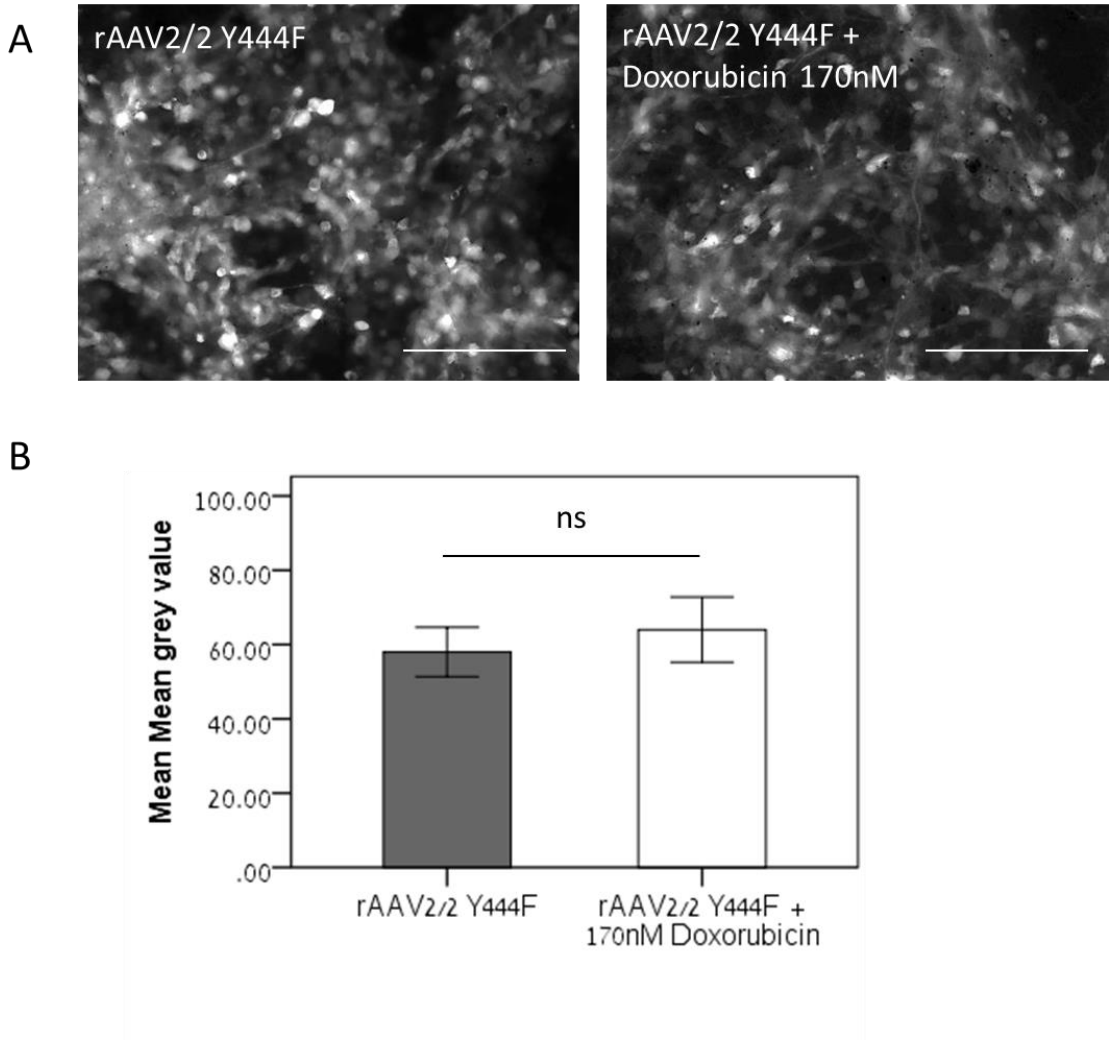

Figure 4.3: Effect of proteasome inhibition on rAAV2 Y444F transduction of dissociated retina

rAAV2/2 Y444F RHOK.GFP was delivered to dissociated early postnatal WT cells, alone or with the addition of Doxorubicin (170nM). A. Representative images of GFP expression in each group 9 days after transfection. Scale bar 50μm. B. Grey value analysis showed no difference in levels of GFP expression between the two groups (t=0.54, ns), indicating that proteasome inhibition by doxorubicin did not augment *ex vivo* transduction of cells by capsid mutant rAAV2. Error bars represent mean ±1 SEM of 5 biological replicates (4 technical replicates for each biological replicate).

4.4.1.3. Elimination of viral particle transduction in vivo following transplantation of ex vivo transduced cells

rAAV2/2 Y444F has been reported to transduce photoreceptor cells *in vivo* (among other retinal cell types, including ganglion cells and bipolar cells) when driven by a ubiquitous small chicken β-actin (smCBA) promoter[200]. Here, the photoreceptor specific promoter RHOK was used to assess transduction of rod cells: however, central for further application of *ex vivo* AAV-treated cells in cell replacement studies is the question whether the transplanted cell suspension includes free AAV particles or whether viral particles could be released from lysed cells post transplantation and potentially transduce the host retina.

To investigate this question, a cohort of MACS sorted (CD73+) neonate WT cells were treated with rAAV2/2 Y444F RHOK.GFP as above, and maintained in culture for 7 days. Cells were transplanted into the subretinal space of adult WT mice after either 1) No further rinse of cells, 2) one additional rinse, or 3) two additional rinse phases.

9 days following injection, expression of GFP was investigated in the host retina away from the transplantation site in sections so as not to include transplanted cells (Figure 4.4A). GFP was highly expressed in the ONL of host mice of the first group (no rinse) (Figure 4.4B), lower expression was observed in ONL of the second group (one rinse) (Figure 4.4C) and no GFP expression was observed in eyes from the third group (two rinses) (Figure 4.4D). Expression in all eyes was confined to the ONL, and no transduction of other retinal cell

layers was observed. Immunohistochemistry of transduced retina shows expression of the photoreceptor specific marker recoverin and the rod specific protein rhodopsin in GFP+ cells, further assuring the specificity of the RHOK promoter for photoreceptor transduction (Figure 4.5). For future transplantation experiments using AAV treated cells, two rinse phases where applied to prevent host retina transduction *in vivo*.

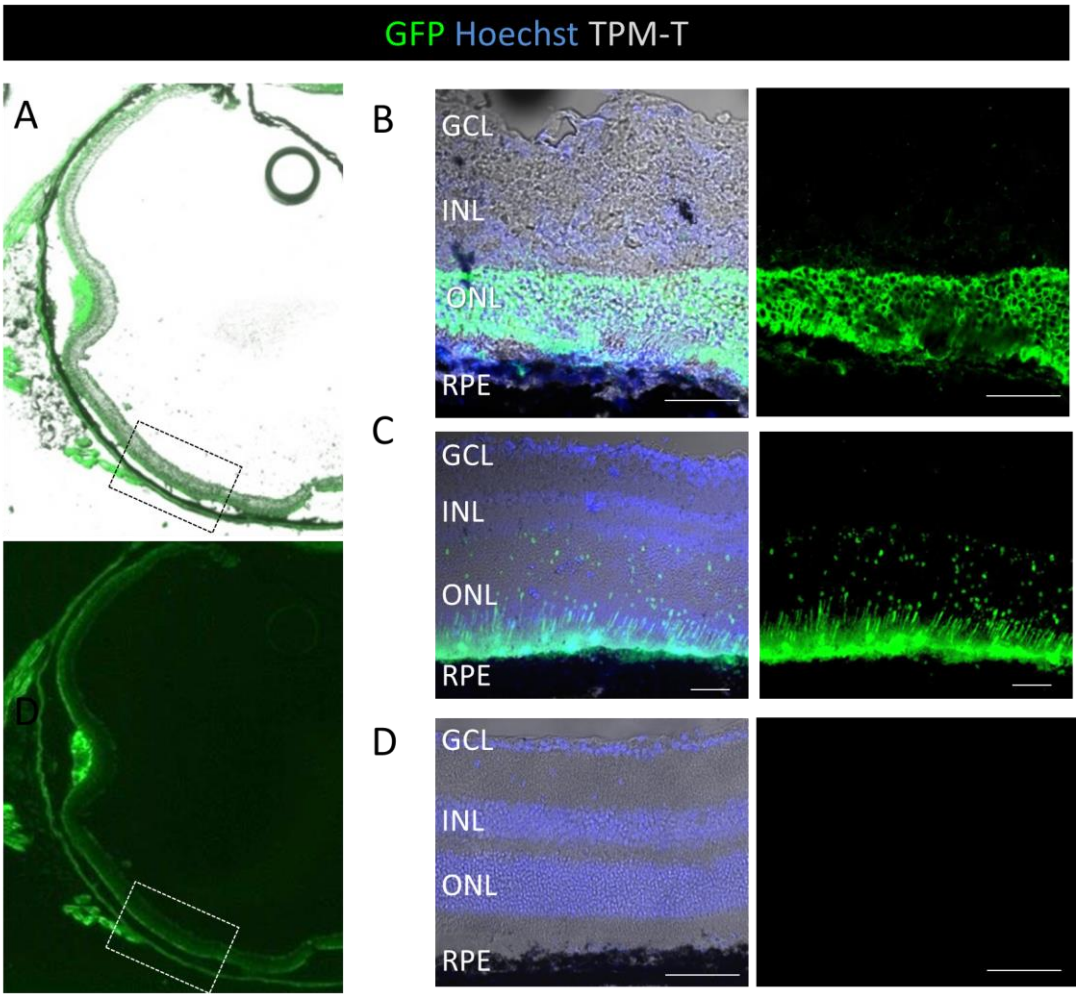

Figure 4.4: Limiting transduction of host retina by treated cells

Dissociated cells from neonate WT mice were transfected by RHOK.rAAV2 Y444F.GFP and subretinally transplanted into adult WT mice for assessment of host retinal transduction by treated cells. A-A'. Assessment was conducted in the host retina away from the transplantation site, in areas in which no transplanted cells were identified. The dashed frame represents such an area which is distinct to the subretinal mass of donor cells (white arrow). B. without rinsing cells prior to transplantation, high transduction of the host retina was observed, with specific expression of GFP in the ONL. C. Reduced GFP expression was observed following a single rinse phase and expression was also observed to be constricted to the ONL. D. following two rinse phases no transduction of the host retina was observed. This was consistent in all transplanted mice. Scale bar, 50μm. GCL; ganglion cell layer, INL, inner nuclear layer, ONL, outer nuclear layer, RPE, retinal pigment epithelium; TPM-T is the transmitted light transducing channel of the confocal microscope.

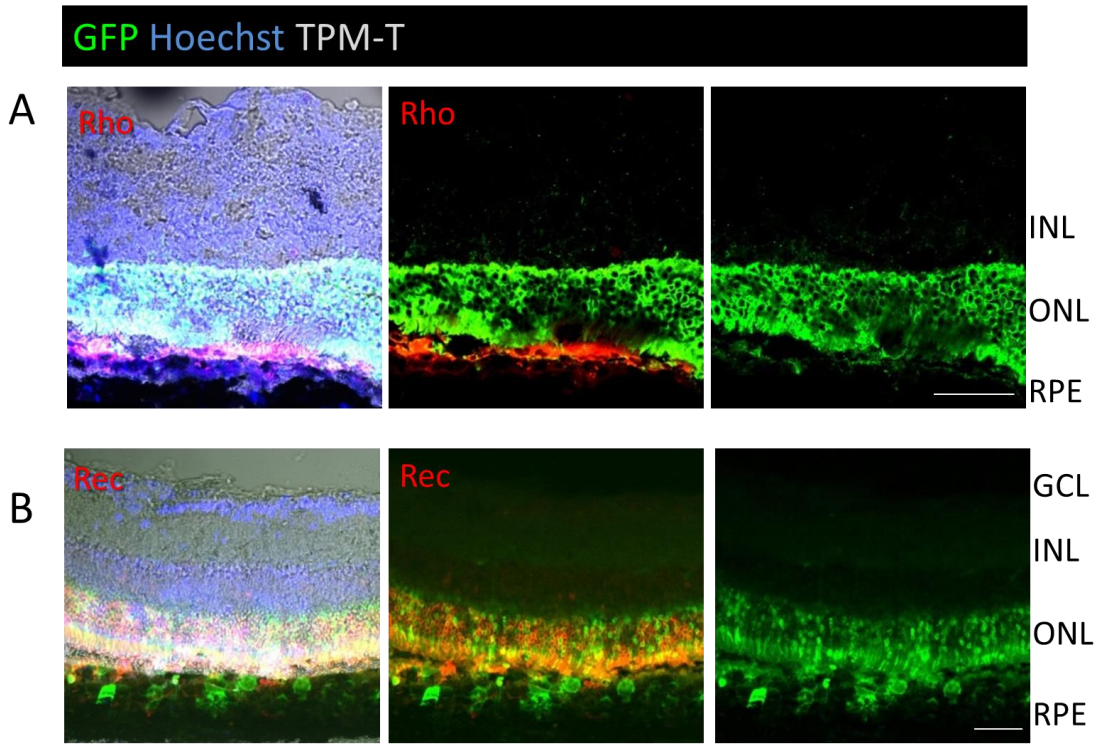

Figure 4.5: Immunohistochemistry of the transduced host ONL

The ONL of WT hosts following transplantation of RHOK.rAAV2 Y444F.GFP transduced cells with no rinse was assessed by immunohistochemistry. A. High expression of rhodopsin (rho) was observed in outer segments of transduced rod cells. B. The pan-photoreceptor protein recoverin (rec) was observed throughout the transduced ONL. Expression of these proteins is restricted to photoreceptor cells and shows the boundaries of GFP expression in adult WT ONL without transduction of the INL. Scale bar. 50μm. GCL; ganglion cell layer, INL, inner nuclear layer, ONL, outer nuclear layer, RPE, retinal pigment epithelium.

4.4.2. Optimization of minicircle transfection of primary retinal cells

Minicircles (MC) have not been used previously for transfection of retinal cells *in vivo* or *in vitro*, hence prior to production of a cell specific vector for gene therapy, a commercially available minicircle expressing GFP, driven by the ubiquitous cytomegalovirus (CMV) promoter (CMV.GFP.SV40polyA MC, System Biosciences) was assessed for transfection of PN0-3 WT dissociated retinal cells.

HEK293 cells were similarly transfected for comparison. Transfection of HEK293 cells was readily attained by minicircle DNA by use of Genejuice (Novagen), with initial expression detected at 24 hours and peak expression at 72 hours post transfection. However, with this method no expression was observed in dissociated retinal cells, regardless of dose of DNA administered to cells (Figure 4.6A).

In order to increase transfection of dissociated retinal cells, the polycationic liposomal formulation Nanojuice with addition of a transfection booster containing a high concentration of dendrimers (Novagen) was employed. Following initial optimization of ratios of core transfection reagent and transfection booster to reduce cell toxicity (as described by manufacturer) a ratio of 1µg DNA: 2µl NanoJuice: 2µl NanoJuice booster was selected for transfection of retinal cells. With this method, expression of GFP was attained only with the high dose of DNA (50pg DNA/cell) with peak expression 72 hours post transfection and sustained expression observed for 7 days thereafter (Figure 4.6B).

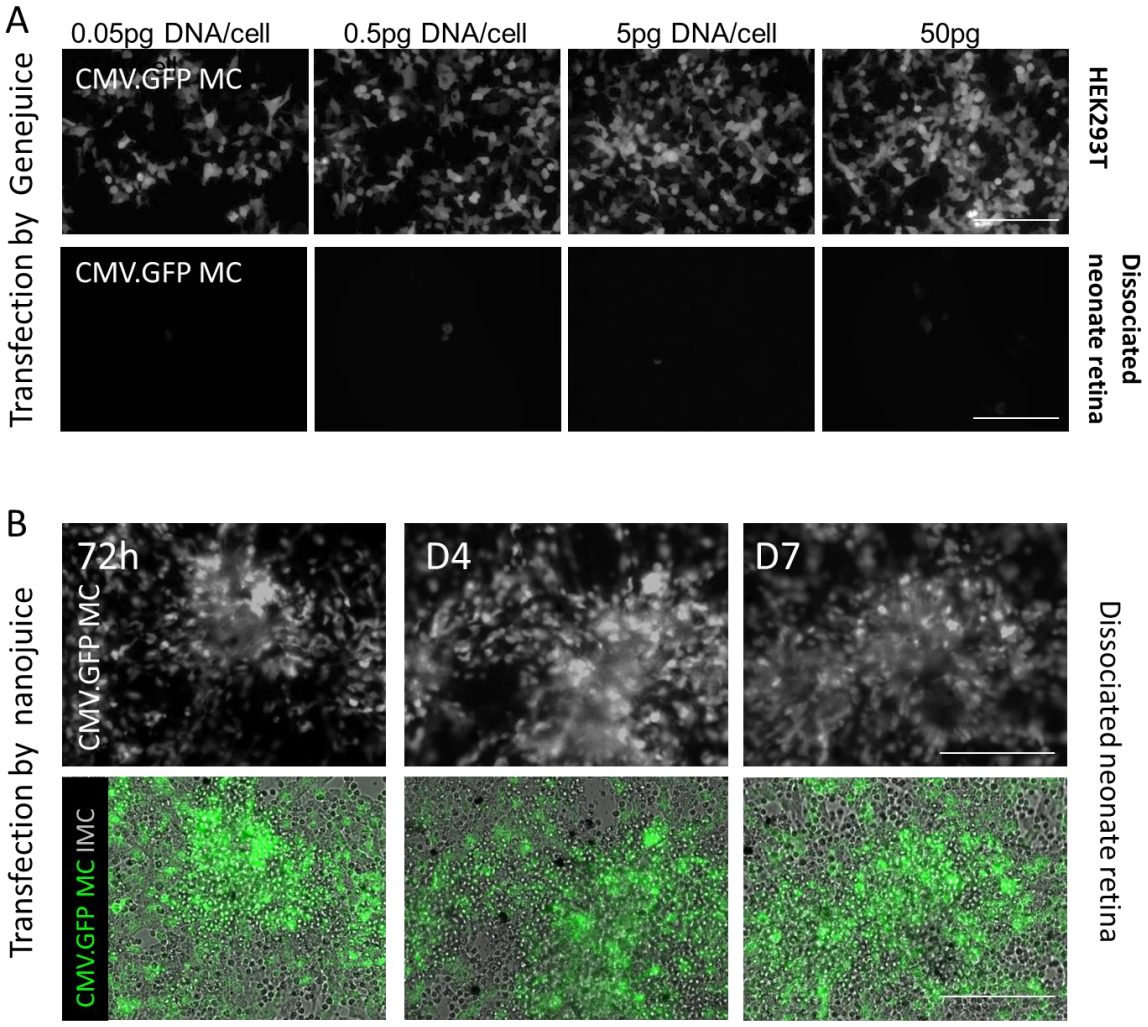

Figure 4.6: Optimisation of minicircle delivery to early neonate retina *in vitro*

Minicircle DNA was delivered in a dose dependent manner to HEK293 cells and dissociated neonate WT retina by use of liposomal transfection reagent.

A. 72 hours post transfection HEK293T cells expressed GFP in all dose conditions. No expression was observed in transfected neonate cells when compared to similarly plated untreated neonate cells. scale bar=50μm. B. GFP expression was observed 72 hours post CMV.GFP MC transfection of neonate dissociated retinal cells and was sustained for 7 days post transfection. Scale bar= 50μm. MC; minicircle.

4.4.2.1. Expression patterns of minicircle DNA in retinal cells

Expression patterns were analyzed by comparing GFP levels after transfection of WT neonatal retinal cells with CMV.GFP.SV40polyA MC or Puf6.1 cytomegalovirus enhanced chicken β-actin. GFP (CMV.CBA.GFP) plasmid. Onset of GFP expression by MC transfection was at 12 hours. Peak expression occurred at 72 hours, with approximately 30±7.1% of cells expressing GFP. Sustained expression was observed thereafter for 7 days with a reduction in expression to 5±2.3% of cells *in vitro* by day 14. Plasmid transfection was achieved in only 4 of 7 assessed wells, with low transfection of 3±2.4% of cells at 72 hours. These results represent increased expression of MC over plasmids in dissociated retinal cells.

4.4.3. Vector design

In order to produce a therapeutic gene delivery vector, a plasmid vector was first designed to include necessary elements for the delivery and identification of the RHO gene in PhRP cells.

For delivery of RHO to PhRP cells, elements that would need to be included in the expression cassette include a promoter, the WT RHO gene, and polyadenylation (polyA) sequence, which is important for nuclear export and stability of mRNA.

The human rhodopsin Kinase promoter (RHOK) (205bp) was selected, as this promoter was shown to successfully and reliably target photoreceptor cells in

mice[268]. In order to evaluate efficacy of transduction *in vivo*, as well as for the purpose of identification of transduced cells following transplantation, it is useful to include a reporter gene. The rhodopsin gene (1,047bp) was here proposed for delivery in $Rho^{-/-.Nrl.GFP}$ cells, GFP wavelength is 488nm, thus the reporter selected was the red fluorescent marker DsRed (678bp), produced from *Discosoma coral* which emits a wavelength of 555nm and can be easily distinguished from the target cells endogenous GFP signal. An internal ribosome entry site (IRES) sequence (580bp) (Clontech, USA) was included before the DsRed sequence in the vector to allow internal initiation of translation, that is translation of a second protein away from the 5' end of an mRNA molecule[276] and thus expression of two proteins (here: RHO and DsRed) from one mRNA strand.

The expected full construct length was therefore 2510bp (Figure 4.7A), designed to be appropriate for packaging in AAV together with a polyA sequence (274bp) and two ITRs (145bp each) (total of ~3kb for AAV packaging) (Figure 4.7B) complying with the packaging capacity of AAV (~4.7kb), as packaging capacity is reduced once this size is exceeded.

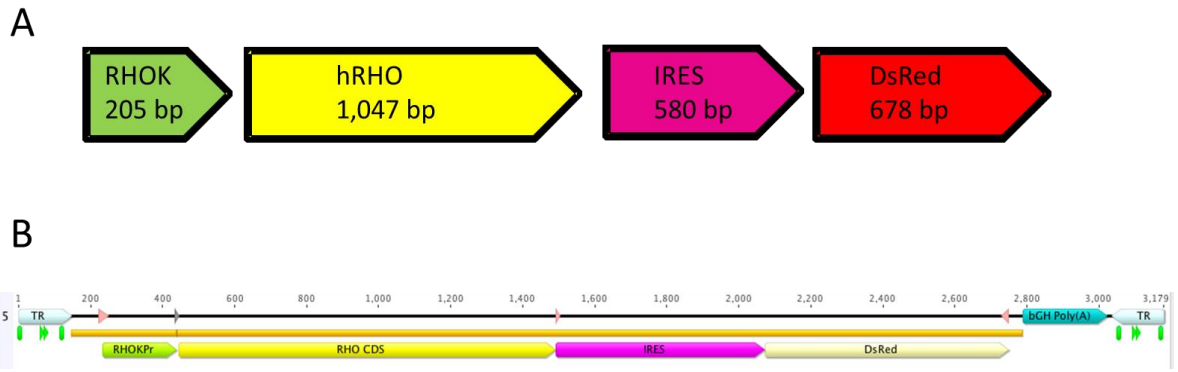

Figure 4.7: Vector design

A. The transgene construct containing a rhodopsin kinase promoter (RHOK), RHO gene, an internal ribosome entry site (IRES) and a DsRed fluorescent marker. B. the design of the corresponding plasmid containing a polyA sequence and an inverted terminal repeat (ITR) on either side.

4.4.4. Cloning the RHOK.RHO.IRES.DsRed plasmid

The RHOK promoter, RHO, IRES and DsRed DNA fragments were isolated and RHOK and Rho were joined by the PCR SPLICE technique[277] and then joined to IRES and DsRed to produce a full RHOK.RHO.IRES.DsRed construct (Figure 4.8A-C).

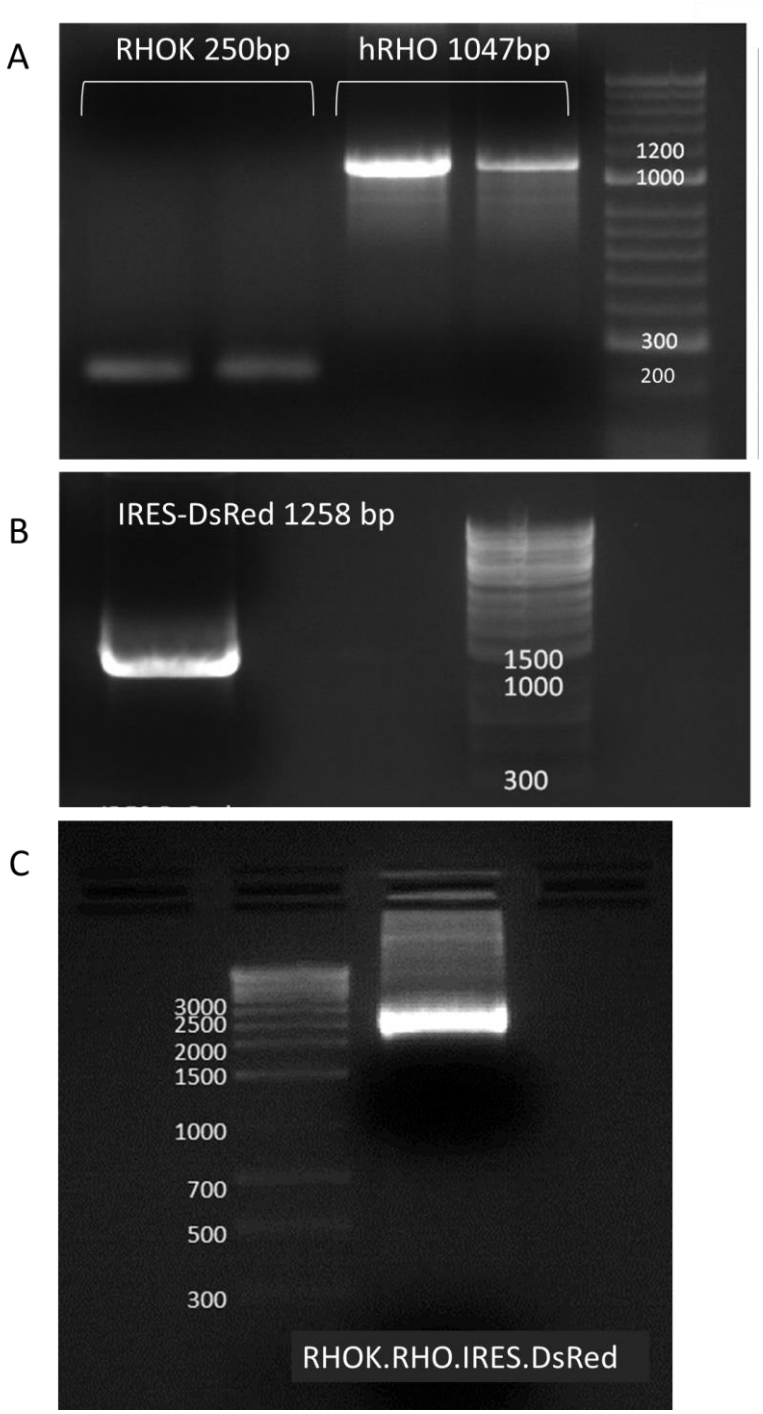

Figure 4.8: Isolation of construct fragments and PCR SPLICE of the RHOK.RHO.IRES.DsRed construct

A-B. Isolation of the RHOK promoter, human RHO and IRES-DsRed fragments by PCR. C. The construct was produced by joining the RHOK promoter to RHO and to IRES DsRed by SPLICE PCR.

The RHOK.RHO.IRES.DsRed construct was digested at Mfe1 and Not1 restriction sites, and inserted into an AAV plasmid (AAV-CAG) backbone containing AAV ITRs. To achieve this, the AAV plasmid was also digested by Mfe1 and Not1, resulting in separation of the plasmid backbone and ITRs from the CAG promoter (Figure 4.9A-B).

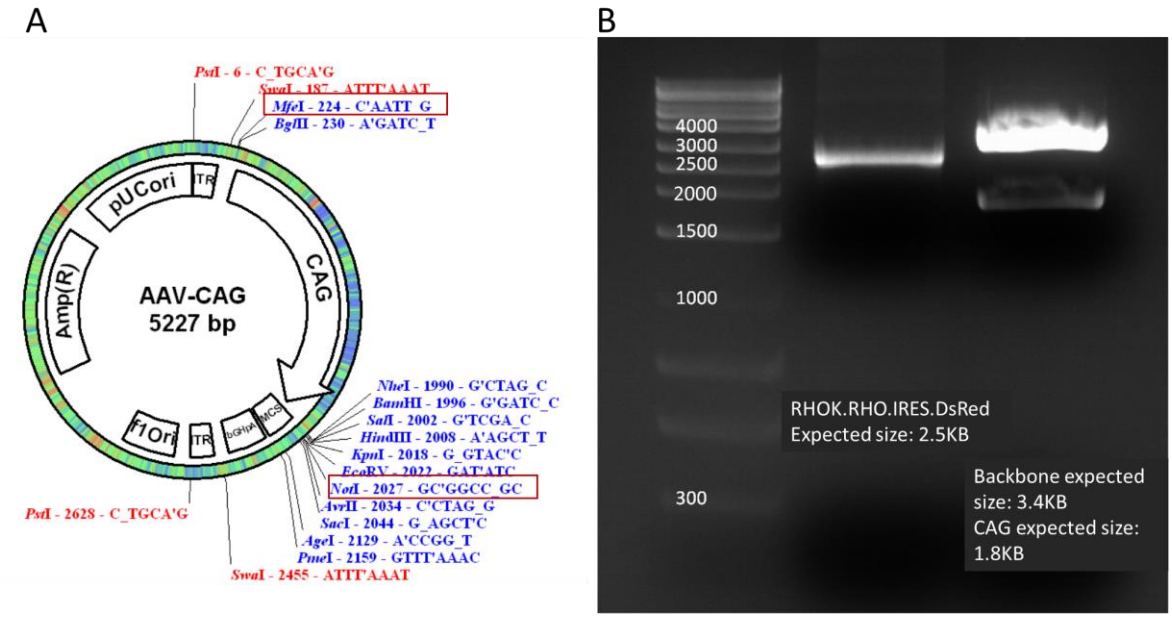

Figure 4.9: Mfe1 and Not1 digestion of the RHOK.RHO.IRES.DsRed construct and AAV plasmid

A. Schematic of the AAV (AAV-CAG) plasmid containing AAV ITRs and Mfe1 and Not1 restriction sites. B. The RHOK.RHO.IRES.DsRed construct and the AAV plasmid were digested at Mfe1 and Not1 restriction sites. Plasmid digestion resulted in separation of the plasmid backbone and ITRs (3.4kb) from the CAG promoter (1.8kb).

The plasmid backbone and the full construct were ligated and amplified in bacteria, followed by miniprep and subsequent megaprep to produce a high concentration of DNA for vector production (Figure 4.10A). The presence of the RHOK.RHO.IRES.DsRed construct in the resulting plasmid (schematic in Figure 4.10B) was confirmed by double digest using Mfe1 and Not1 (Figure 4.11c) and by sequencing.

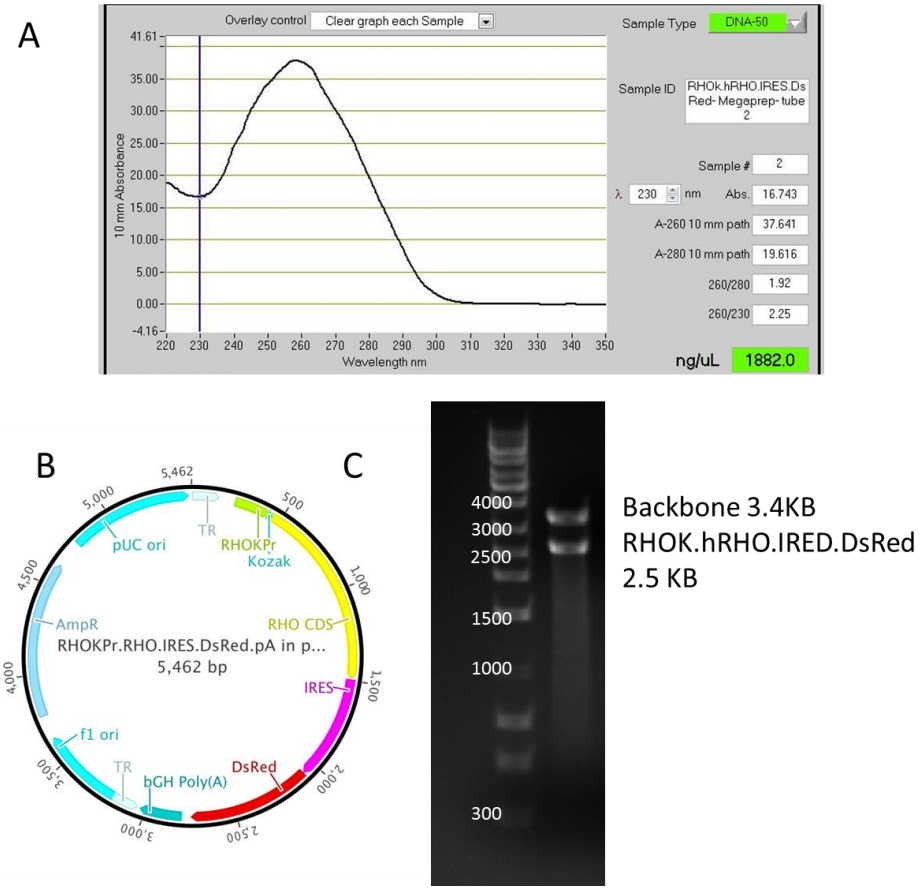

Figure 4.10: Production of RHOK.RHO.IRES.DsRed plasmid

A. Nanodrop image showing plasmid concentration and purity following cloning. B. Schematic of the RHOK.RHO.IRES.DsRed plasmid. C. following cloning the presence of the construct was confirmed by double digest using Mfe1 and Not1, separating the construct (2.5kb) from the plasmid backbone (3.4kb). The sequence was also confirmed by Sanger sequencing.

4.4.5. AAV vector generation

4.4.5.1. Verification of ITR integrity

The AAV ITR structures are critical for successful transduction. The ITRs are unstable in bacteria, and plasmids that lose their ITRs have a replication advantage during cloning. Thus verifying recovered plasmids for retention of ITRs is imperative prior to AAV production[278]. The high GC content of the ITRs sequence and their palindromic structure cause the formation of tight hairpin secondary structures which effect polymerase efficacy and limit the success of DNA sequencing in these regions. However, these regions contain XmaI sites, which can be used for diagnosis of ITR integrity. As expected, digestion of the RHOK.RHO.IRES.DsRed at XmaI restriction sites (Figure 4.11A) produced four DNA fragments, two large fragments on either side of the ITRs containing the expression cassette and bacterial backbone (Figure 4.11B) and two small fragments residing between each pair of restriction sites (Figure 4.11C), thus confirming the presence of intact ITRs in the plasmid.

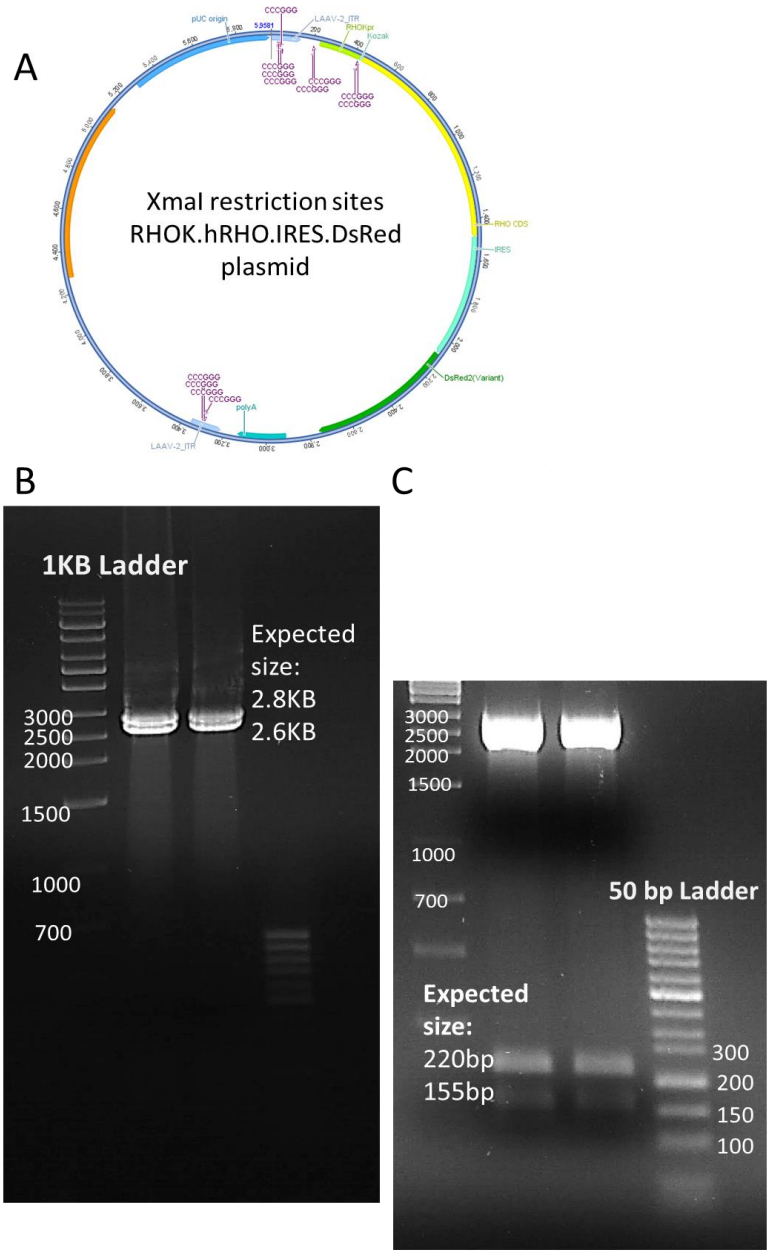

Figure 4.11: Verification of ITR integrity by XmaI digestion

A. XmaI restriction sites within the RHOK.RHO.IRES.DsRed plasmid sequence. Expected fragments with Xma1 digest: 2.8KB, 2.6KB, 220bp, 155bp. The difference in fragment size limited imagining on the same gel, B) a 1% agarose gel was used to visualise the 2.8KB and 2.6KB fragments and C) a 2% agarose gel was used to visualise the 220bp, 155bp, together confirming the presence of ITRs in the AAV plasmid.

4.4.5.2. Production of rAAV vector

As described above, the rAAV2/2 Y444F vector combined with the RHOK promoter was successful in targeting photoreceptor cells *in vitro*.

The production of rAAV2/2 Y444F RHOK.RHO.IRES.DsRed was achieved by packaging the RHOK.RHO.IRES.DsRed plasmid product in rAAV2/2 Y444F by use of the rAAV2/2 Y444F rep-cap plasmid and a helper plasmid. The rAAV2/2 Y444F rep-cap plasmid was previously generated in our lab (de-Silva et al., unpublished data) by inducing a mutation in the capsid protein from tyrosine to phenylalanine at position 444.

Virus production was achieved using standard AAV production protocol as described in Chapter 2.2. Virus titres determined by qPCR (Figure 4.12) were $5x10^{11}$ genome particles (gp)/ml.

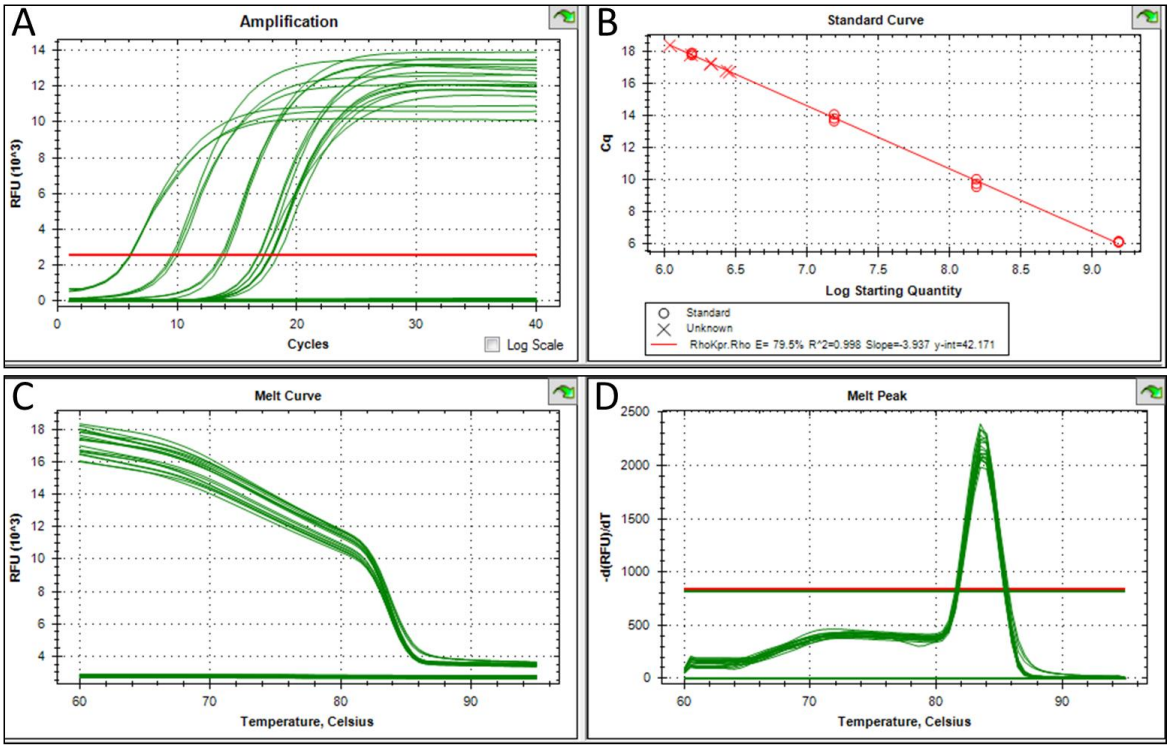

rAAV2/2 Y444F RHOK.Rho.IRES.DsRd titre: $5x10^{11}$ gp/ml.

Figure 4.12: qPCR for AAV titre following AAV production

A. Amplification curves with a clear exponential phase indicate suitable amplification of the tested samples. B. the standard curve indicated efficiency of primer binding at 79.5% representing low yet adequate binding, and R2 of 0.998 indicating good reproducibility between replicate samples. D. The melt curve shows a single peak indicating no surplus binding sites. gp; genome particles.

4.4.6. Production of Minicircle vector

Minicircle (MC) vector was generated from the RHOK.RHO.IRES.DsRed plasmid (5958bp) as described in Chapter 2.2.3. A MC product of 3200bp (Figure 4.13) with a DNA concentration of 1mg/ml was generated. DNA quality was assessed by plasmid factory. A summary of quality control measures is detailed in table 4.1.

The presence of the RHOK.RHO.IRES.DsRed construct in the resulting MC was confirmed by sequencing.

Test	Result	Analytical method
DNA concentration	1.0 mg/ml	UV absorption 260 nm
DNA purity	Peak at 258nm	UV scan (220-320nm)
RNA	Not visible	Gel electrophoresis
Bacterial chromosomal DNA	Not visible	Gel electrophoresis
Supercoiled minicircle homogeneity	99.3%	Capillary gel electrophoresis
Endotoxin (LPS)	<100 E.U/mg DNA	Short LAL assay (Limulus amebocyte lysate)

Table 4.1: Quality control of Minicircle DNA by PlasmidFactory

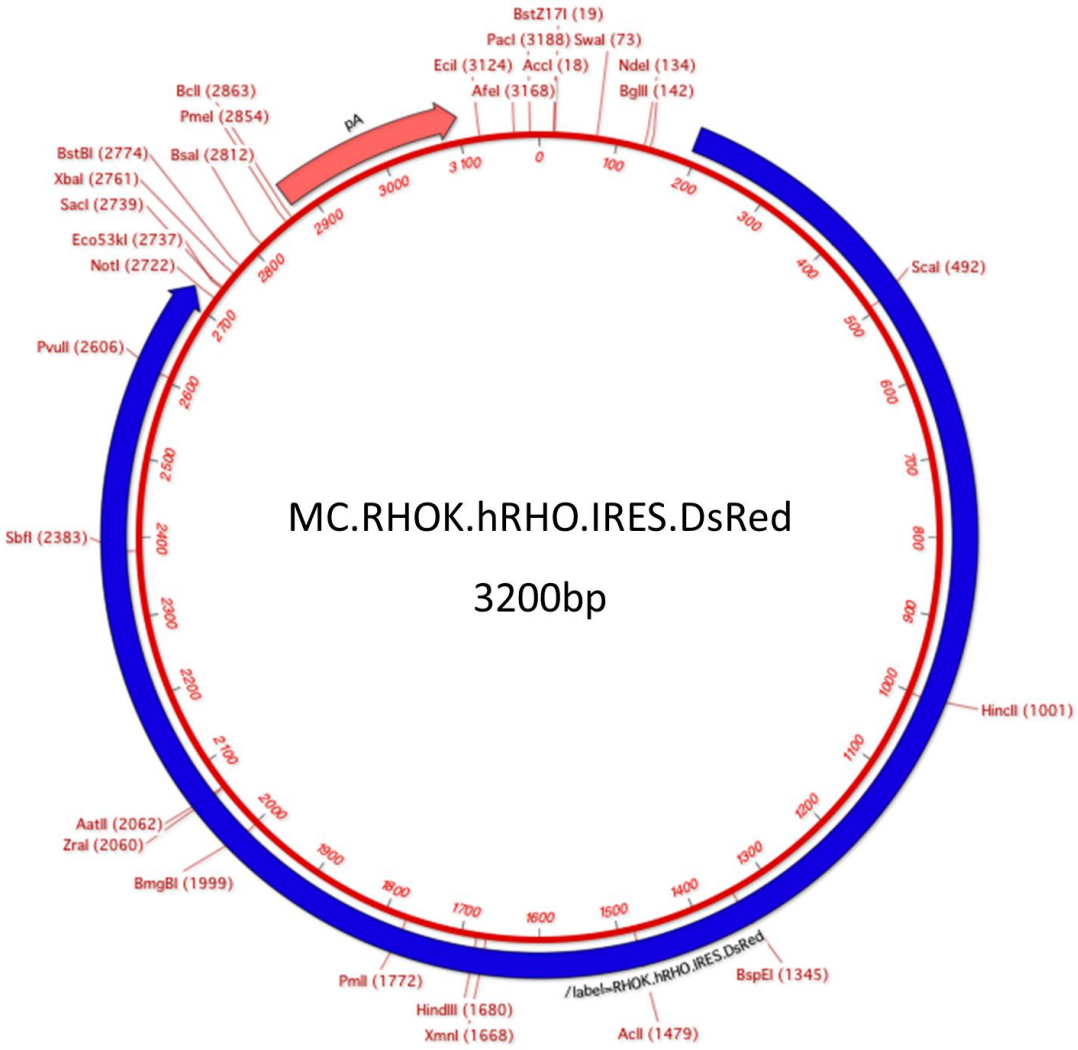

Figure 4.13: Schematic of RHOK.RHO.IRES.DsRed minicircle

4.4.7. *Ex vivo* gene delivery with rAAV2 Y444F and Minicircle DNA

rAAV2/2 Y444F and Minicircle vectors carrying the RHOK.RHO.IRES.DsRed expression cassette were delivered *ex vivo* to dissociated retinal cultures from neonate $Rho^{-/-.Nrl.GFP}$ mice (PN0-3). These mice have a null mutation in the rhodopsin gene and express GFP in rod cells. Assessment of gene therapy outcomes will only be realised following transplantation and maturation of treated rod precursor cells. Here, validation and comparison of the *in vitro* efficiency of vectors was sought.

4.4.7.1. Fluorescent reporter expression

In these two vectors the rhodopsin gene was delivered together with a red fluorescent reporter (DsRed), thus co-expression of the endogenous Nrl.GFP and the exogenous DsRed in treated $Rho^{-/-.Nrl.GFP}$ cells would indicate transduction/transfection of rod cells. Neonate cultures were sorted with MACS and rod precursor enriched cultures were assessed. DsRed expression was observed in cultured cells following gene delivery (Figure 4.14A-B) with prevalence of co-localisation of Nrl.GFP and DsRed in rod precursor cells in both groups (Figure 4.14C-D), validating successful vector production.

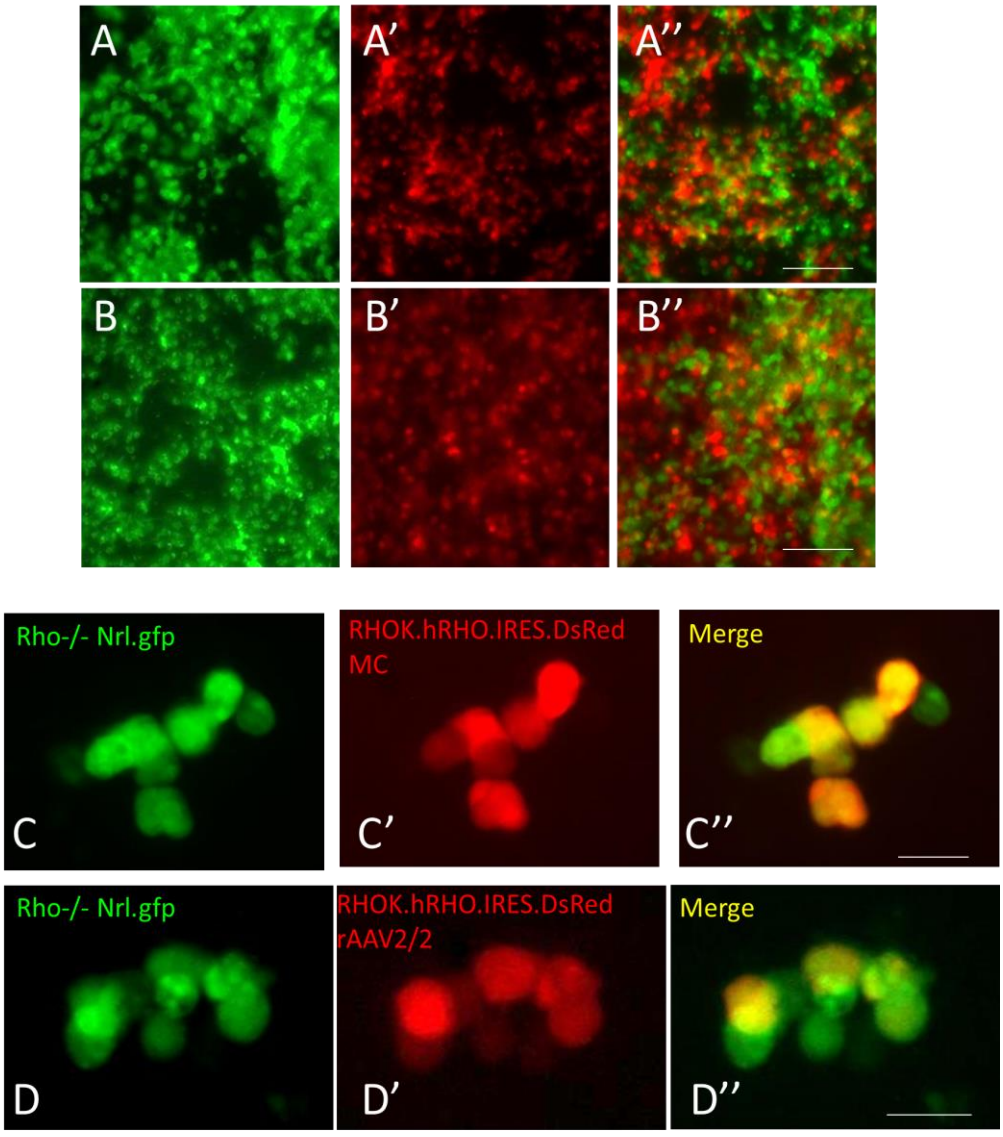

Figure 4.14: Expression of DsRed in cells treated by rAAV2 Y444F and MC DNA

A. DsRed transgene expression was detected in MC treated cells 3 days post transfection and B. in rAAV2 Y444F treated cells 7 days post transfection. C. Magnification of cells treated by MC showing expression Nrl.GFP, C'. DsRed and C''. Merged image showing co-localisation of cytoplasmic GFP and DsRed in the cells. D. Magnification of cells treated by rAAV2 Y444F showing expression Nrl.GFP and D'. DsRed. D''. Merged image showing co-localisation of cytoplasmic GFP and DsRed in the cells. Scale bar A-B, 100µm; Scale bar C-D,10µm.

Onset of DsRed expression was 3 days following AAV transfection and 12 hours following MC transfection, with corresponding peak DsRed expression levels of 80.4%±6.52% (AAV day 9) and 61%±7.02% SEM (MC day 4) of cells in rod precursor-enriched culture (unpaired t test, t=2.02 p=0.078, ns) (Figure 4.15). Sustained expression was achieved with both vectors up to day 14 *in vitro* (last time-point assessed). Importantly, this comparison was made by peak expression on different days *in vitro*, however AAV has been shown to peak *in vivo* only weeks following transduction[279]. *In vivo* patterns of MC expression are still under evaluation, thus assessment of vector efficiency for *ex vivo* gene therapy will be further investigated when compared in donor rod cells post transplantation.

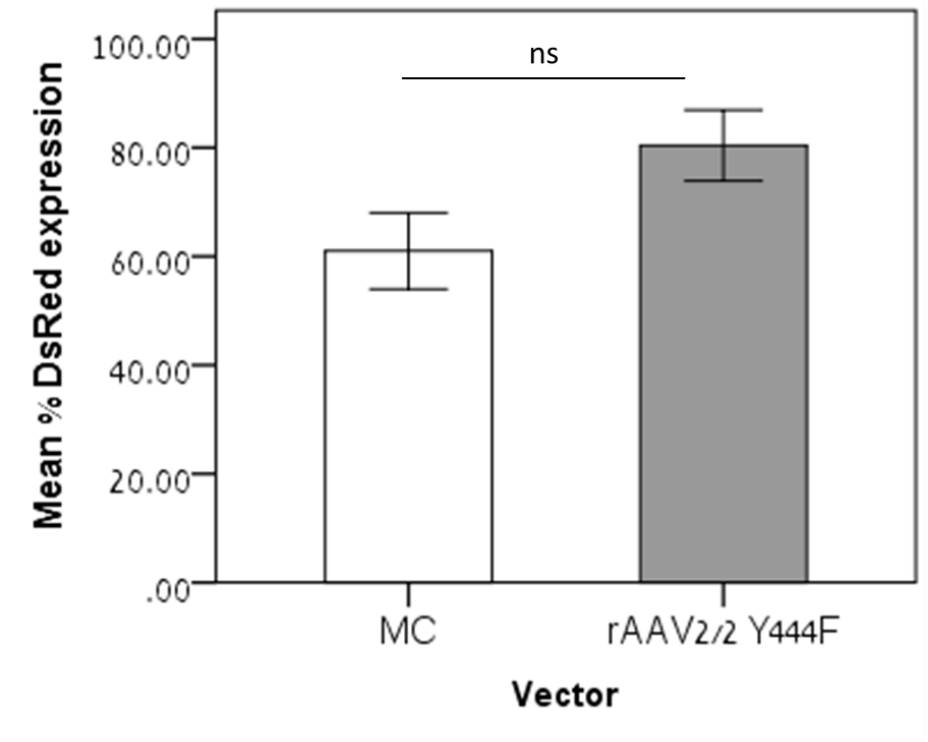

Figure 4.15: comparison of peak DsRed expression levels by gene therapy vectors

DsRed expression was detected in rod precursor-enriched culture 3 days following rAAV2 Y444F transfection, with peak expression on day 9. DsRed was detected 12 hours following MC treatment, reaching peak expression on day 4. There was no significant difference between these two vectors in the percent of cells expressing DsRed at the point of peak expression. (Unpaired t test, t=2.02 p=0.078, ns). Grey value analysis, n=7 (4 technical replicas per biological replica)

4.4.7.2. Gene expression analysis

To evaluate the *in vitro* efficiency of rhodopsin gene replacement by both vectors, and assure this gene is not over expressed in mice, which may lead to loss of function as in cases of autosomal dominant RP[176], mRNA expression

was assessed by qPCR. *In vitro* expression of rhodopsin in treated Rho$^{-/-.Nrl.GFP}$ cells at day 7 post transfection was normalized to similarly cultured WT cells (Figure 4.16). As expected, the rhodopsin gene was not detected in Rho$^{-/-}$ mice, however, upregulation of rhodopsin compared to untreated Rho$^{-/-}$ was detected in both MC treated cells ($p<0.001$) and rAAV2 Y444F cells ($p<0.001$). While expression following treatment differed from *rho* expression in WT eyes (both $p<0.001$), mRNA expression in cells treated with the MC vector reached 0.6±0.07SEM of WT *rho* levels and cells treated with the rAAV2 Y444F vector expressed 0.44±0.08 SEM of WT *rho*. Gene expression by the two vectors did not differ ($p=0.39$, ns) (One way ANOVA, $F(3,24)=53.4$, $p<0.001$, N=7 per group, Tukey's correction for multiple comparisons). Gene expression in the WT cells was further compared to rhodopsin expression in eyes obtained from PN13 WT mice, in order to evaluate expression in differentiated rods *in vivo*. PN13 *rho* expression was significantly upregulated compared to dissociated WT retinae ($t=6.18$, $p<0.001$). This was expected, as cells in culture did not develop outer segments (OS), which is the primary cell structure in which *rho* is expressed. Thus while levels of expression following gene therapy are expected to be augmented *in vivo*, these experiments provide proof of upregulation of the rhodopsin gene in rho$^{-/-}$ cells following *ex vivo* gene delivery with either rAAV2 and MC DNA, and importantly show that the level of gene expression is not upregulated compared to WT. This is important as *in vivo* rho replacement studies have shown that over expression of rhodopsin may lead to protein misfolding and may thereby be detrimental[42,154,280].

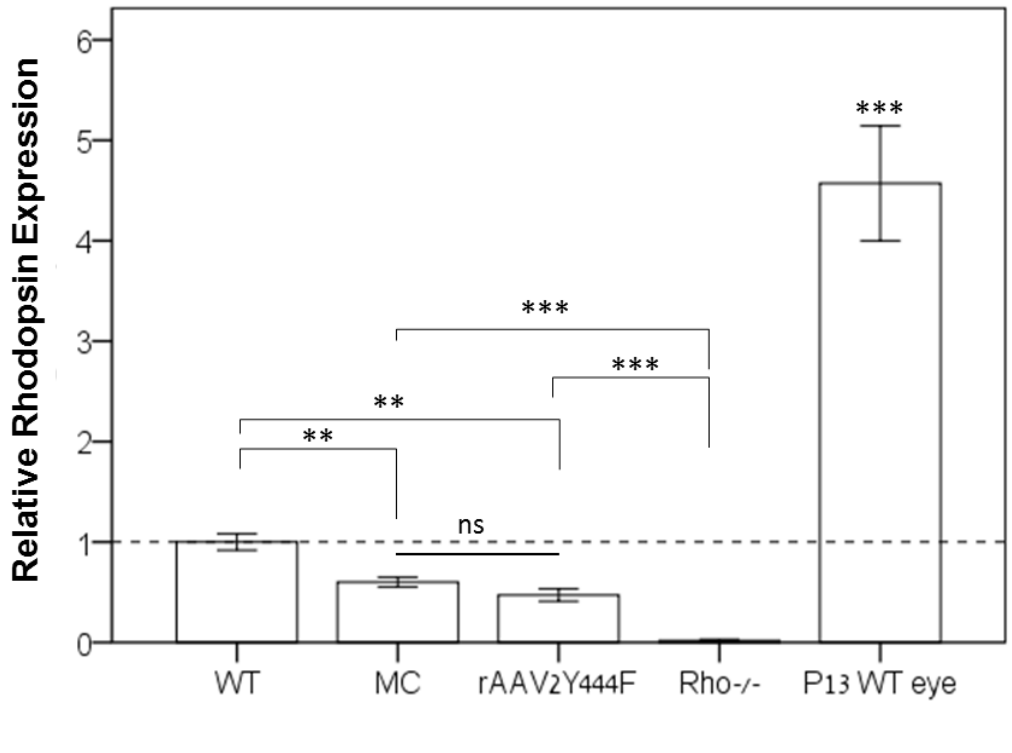

Figure 4.16: mRNA expression of the rhodopsin gene following *ex vivo* gene therapy

mRNA expression was assessed by qPCR. Compared to untreated Rho-/- cells, upregulation of the Rhodopsin gene was found in cells treated by MC (***p<0.001) and by rAAV2 Y444F (***p<0.001). Both genes did not reach the levels of WT expression (p<0.001 in both comparisons), with MC treated cells expressing approximately 60% of neonate WT rhodopsin and rAAV2 Y444F treated cells expressing approximately 44% of neonate WT rhodopsin levels. No difference was found between the two gene therapy treatment groups (p=0.39, ns). One way ANOVA, F(3,24)=53.4, p<0.001, Tukey's correction for multiple comparisons. *Rho* expression levels in the retinae of mice at postnatal day 13 was separately compared to neonate WT *rho* expression in cultured cells, and was found to be highly upregulated (t=6.18, ***p<0.001). n=7 in each group. These results indicate upregulation of the rhodopsin genes in rho-/- cells following treatment, and suggest that rod cell maturation is required in order to achieve therapeutically relevant levels of rhodopsin expression. Results are expressed relative to the expression of *rho* in dissociated WT retinal cells, represented by the dashed line.

4.5. Discussion

In this chapter, a viral AAV vector and non-viral minicircle (MC) DNA vector were developed and tested for *ex vivo* delivery of the rhodopsin gene to rod photoreceptor cells.

In optimization of *ex vivo* AAV delivery to rod photoreceptor cells, AAV serotypes were compared and the capsid mutant rAAV2/2 Y444F was shown to be more efficient for transduction of rod photoreceptor cells than AAV2/8 coupled with the photoreceptor-specific rhodopsin kinase (RHOK) promoter. Cells were transplanted into WT mice following *ex vivo* delivery of rAAV2 Y444F and procedures for cell preparation and rinsing were optimized to eliminate AAV transduction of host photoreceptor cells. Next, optimization of gene delivery by MC DNA was conducted in retinal cells by use of the ubiquitous CMV promoter, and transfection by MC was first successfully achieved in retinal cultures by use of a polycationic liposomal agent, providing support for further experimentation and development of non-viral vector with this technology.

A plasmid vector for delivery of the *RHO* gene and a DsRed fluorescent reporter was created driven by the RHOK promoter, followed by production of a rAAV2 Y444F vector and design of a MC vector from the same plasmid. The two vectors were compared *in vitro* in retinal cells from the $Rho^{-/-.Nrl.GFP}$ mouse, which carries a null *rho* mutation, and showed successful expression of the DsRed reporter gene in rod precursors with no difference in levels of peak

transgene expression in cells treated with the two methods. Gene expression analysis confirmed the restoration of approximately 40-60% of the WT levels of rhodopsin mRNA expression in retinal cells obtained from $Rho^{-/-.Nrl.GFP}$ mice, with no significant difference in expression between the two vectors.

In a preliminary experiment for optimization of the AAV vector, increased efficiency of the rAAV2 Y444F over the rAAV8 vector in rod enriched cultures was observed; however, both vectors were highly efficient for the *ex vivo* transfection of photoreceptor cells. Increased efficiency of the rAAV2 Y444F may be due to the capsid mutation rather than the serotype used, as the capsid mutant rAAV2 was compared to rAAV8 which did not include a capsid mutation. The capsid is essential for cellular tropism and efficiency of transgene expression, as it influences both extracellular events related to binding to specific receptors and intracellular events effecting AAV trafficking and uncoating[281,282]. While AAV8 has been reported to efficiently transduce photoreceptors without induction of a capsid mutation[161,265], use of a capsid mutant rAAV8 with a tyrosine Y733F mutation has been shown efficiently to transduce photoreceptor cells among other cell types *in vivo*[200,201], with photoreceptor transduction levels comparable to that observed with rAAV2 Y444F when driven by a ubiquitous chicken β-actin (CBA) promoter[200]. Thus further assessment of tropism by different capsid mutant AAV serotypes, driven by the RHOK promoter may be needed in order to select the ideal vector for *ex vivo* delivery of genes to photoreceptors.

The addition of the PI doxorubicin did not augment transduction by rAAV2 Y444F. This is consistent with the concept that these mutants evade proteasome degradation, allowing more transgene copies to enter the nucleus and enhance expression without further efficiency by a proteasome inhibitor. The continued use of rAAV2 Y444F without a PI was thus sought in order to prevent toxicity to cells *in vitro* or to host cells *in vivo* in future transplantation studies.

In vivo assessment of RHOK.rAAV2 Y444F.GFP transduction of the WT host retina revealed two important points. The first point is that the proper processing of cells *ex vivo* following AAV transfection is required to prevent transduction of the host retina with free AAV particles. This finding is extremely relevant to transplantation of cells derived from stem cells, as the *ex vivo* delivery of a fluorescent transgene may be beneficial for fluorescence activated cell sorting (FACS) or cell identification post transplantation. Transplantation of AAV transduced human stem cell-derived photoreceptors has been previously reported, with transduced cells identified in the relatively conserved ONL of mice[73]. In order to ensure that transduction of the host retina does not lead to false identification of host retinal cells, mistaken to be transplanted cells in such studies, methods must be used to process and rinse cells prior to transplantation. The second important consideration arising from these results is the specificity of rAAV2 Y444F vector *in vivo*. Transduction was only observed in the host ONL and co-localized with photoreceptor-specific markers; this is consistent with the vector being driven by the photoreceptor specific

RHOK promoter. Transduction was not observed in other cell types of the neural retina, representing a positive result in relation to the aims of this study.

Transfection of retinal cells by non-viral MC DNA was next assessed. This method of transfection has not been previously reported in primary photoreceptor cells, thus for initial testing, the ubiquitous strong cytomegalovirus (CMV) promoter was employed for assessment of retinal cell MC transfection.

While low levels of transfection (under 5%) were achieved using plasmid DNA, transfection was achieved in approximately 30% of retinal cells by MC DNA. Higher efficiency of transfection by MC compared to plasmid has been previously reported[183,202,203,214,222] and was here shown for the first time in dissociated retinal cells. Transgene expression following CBA.MC.GFP transfection lasted 7 days, and was subsequently reduced to maintain expression in approximately 5% of cells by day 14.

Following cloning of the RHOK.RHO.IRES.DsRed plasmid, and production of corresponding rAAV2 Y444F and MC vectors, the two gene therapy vectors were tested *in vitro*. High transfection efficiency was achieved in rod enriched cultures with both vectors, with comparable peak transgene expression. In rod enriched cultures, MC transfection was achieved in approximately 60% of cells and was sustained for 14 days. This is in contrast to the expression patterns observed by transgene delivery with a ubiquitous promoter in cultures with all retinal cell types and represents the first account of sustained MC expression in photoreceptor cells. The transient expression observed by use of a ubiquitous

promoter is consistent with the developmental stage of retinal cells of mice at postnatal day 0-3, which continue dividing *in vitro* (as observed in Chapter 3). In dividing cells, minicircle expression is transient, as minicircles lack an origin of replication and expression is lost with cell division[225]. It is possible that dividing cells were more readily transfected in this experiment. However, PhRPs are post mitotic thus do not lose transgene expression by division and may therefore benefit from sustained expression of MC molecules maintained in the episome.

Peak transgene expression was observed to be lower in MC treated cells compared to rAAV2 Y444F treated cells. However, this difference was not statistically significant due to relatively high variance within wells of treated cells.

Finally, gene expression analysis showed upregulation of the rhodopsin gene compared to untreated cells 7 days following gene-delivery to rod cells from $rho^{-/-}$ mice. This was similarly achieved with both vectors. Although gene expression was different than WT levels, approximately 60% and 40% of levels of native neonate rhodopsin were restored *in vitro* by MC and rAAV2 Y444F treatments, correspondingly. Importantly, levels of rhodopsin expression in the maturing retina are highly upregulated and rhodopsin is only fully expressed in the outer segment (OS) of adult rod cells. Cell maturation and OS formation is dependent on the retinal environment and growth factors secreted from the retinal pigmented epithelium (RPE)[283,284], and has not shown to occur *in vitro*. Therefore the success of reinstating an appropriate amount of rhodopsin to

these cells can only be fully assessed after transplantation of treated cells and *in vivo* rod maturation.

In the next chapter, transplantation of *ex vivo* treated cells will be examined to investigate whether *ex vivo* gene therapy could effectively restore rhodopsin expression in cells to allow transplanted cells to replace lost photoreceptor cells and restore visual function in $Rho^{-/-}$ mice with sever retinal degeneration.

4.6. Conclusions

In this chapter a highly efficient promoter and AAV serotype for *ex vivo* transduction of photoreceptor cells was identified and optimized for transplantation of *ex vivo* treated cells. A novel non-viral method of gene delivery to photoreceptor cells by minicircle DNA showed efficient and sustained transgene expression in rod precursor cells following treatment.

A viral rAAV2 Y444F vector and a non-viral MC vector were used to deliver the rhodopsin gene and a DsRed fluorescent marker to rod cells and sustained transgene expression and upregulation in mRNA expression of the rhodopsin gene were achieved *in vitro* in $rho^{-/-}$ rod PhRPs with both vectors.

Ex vivo delivery of the rhodopsin gene to PhRPs restored between 40-60% of neonate rhodopsin expression, however, restoration of this opsin function to rod photoreceptor cells and the feasibility of visual improvement by transplantation of treated cells can only be assessed after rod maturation. In the next chapter, $Rho^{-/-.Nrl.GFP}$ rod precursor cells, treated *ex vivo* with rAAV2 Y444F or MC DNA will be transplanted into the degenerate retina of adult $Rho^{-/-}$ mice, to assess the possibility of appropriate rod maturation, cell replacement and restoration of vision by these cells.

5. Transplantation of *Ex Vivo* Treated Rod Precursor Cells for Photoreceptor Regeneration

5.1. Introduction

Blindness in patients with retinitis pigmentosa (RP) is usually caused by complete degeneration of photoreceptors of the outer nuclear layer (ONL). Patient-specific induced pluripotent stem cells (iPSc) could provide an autologous source of cells to replace the lost ONL. However, the use of patient-derived iPSc would require that the disease-causing gene mutation be corrected before cells are transplanted. Transplantation of *ex vivo* genetically treated photoreceptors has not yet been reported.

In most cases of RP, rod cells are the first to degenerate, followed by degeneration of cones and complete loss of the ONL. In animal models of RP, gene therapy and neuroprotection have been suggested to impede photoreceptor cell degeneration or protect cone cells from degenerating in early stages of disease[139,154,158,256-261]. Cell replacement studies in mice have shown

improvement in visual function following replacement of photoreceptor cells in animals with partial[67,70,72,73,75] or complete[62] degeneration of the ONL.

In the previous chapter it has been shown that rAAV2 Y444F and non-viral minicircle (MC) delivery of the *RHO* gene to $Rho^{-/-.Nrl.GFP}$ cells restored a degree of rhodopsin to treated cells *in vitro.* Following from those data, the work presented in this chapter investigates transplantation of cells which have been treated *ex vivo* with viral and non-viral gene therapy. The extent of sustained expression following transplantation and the possibility for treated donor cells to mature, reconstruct the degenerate retina and restore visual function in host animals was investigated.

The Rhodopsin knockout mouse was selected as host animal for this investigation, and has been previously used in gene therapy studies (as described in the previous chapter) and in cell replacement studies as a host model of RP, because degeneration in this model is caused by the absence of the rhodopsin gene, which is highly implicated in the disease and causes loss of dysfunctional rods followed by loss of functioning cones by 3 months of age.

Previous research has shown that following transplantation of PhRPs to 4-week old $Rho^{-/-}$ hosts, which still maintained cone function, an improvement was obtained in the pupil light reflex (PLR) and in extracellular field potentials of the ganglion cell layer (GCL), when stimulated at a low light intensity designed to isolate rod responses[67]. An improvement in vision also followed transplantation of mouse iPSC-derived PhRPs to $Rho^{-/-}$ mice at 4-6 weeks of age, with an increase in electro retinal function, measured by electroretinography (EEG) 3

weeks following transplantation[75]. Later time points for transplantation were also investigated[70], showing a decrease in integration and OS formation of rod precursor cells when transplanted to Rho$^{-/-}$ mice at 6-10 week compared to 4 weeks of age, representing time points after and before severe ONL degeneration. Levels of cell integration and visual function, measured by optomotor testing (OMR) were found to increase after transplantation to 6-8 weeks old animals following disruption of glial scaring and the outer limiting membrane (OLM)[70].

The current work sought to investigate the transplantation of *ex vivo* treated cells at a stage in which no functioning rod or cone photoreceptors were present in the host, representing a relevant time point for transplantation in blind patients with RP. *Ex vivo* treated rod precursors were transplanted into adult Rho$^{-/-}$ mice at age 12-14 weeks, representing a stage of complete retinal degeneration and loss of cone function[50,51], therefore, a first level of investigation examined the feasibility of retinal reconstruction by transplanted donor cells.

The complete collapse of the ONL in late stages of degeneration leaves no host photoreceptor layer for cells to integrate into; instead, cells would need to form a new layer and revive synaptic and morphological connections with the host RPE and INL.

Reconstruction of the retina depends both on the degree of host degeneration and the ability of cells to form connections with the host retina which had undergone gliosis[70] and on the developmental stage of donor cells[67].

Rod photoreceptor cells have been shown to survive and reconnect with downstream retinal circuits in the retina when transplanted at a post mitotic rod precursor stage[62,67,89]. The relatively early stage of cell transplantation means that cells would need to continue maturation *in vivo* to assume an adult rod cell morphological phenotype and express rod specific proteins, such as rhodopsin to instigate the visual transduction cascade and restore visual function.

The light sensing function of photoreceptors normally depends on the outer segment (OS), which contains the enzymatic components of the visual cycle. $Rho^{-/-}$ mice have been previously reported to develop few short outer segments which are misaligned and do not contain the rhodopsin protein[285,286]. *Ex vivo* restoration of *RHO* to cells may allow for formation of this critical structure and correct localisation of the rhodopsin protein in the OS for restoration of functional properties to the host retina. Detection of the rhodopsin gene as well as other rod OS specific genes in the retina following transplantation would indicate that they have originated from treated donor rod precursors which have matured and developed OS structures *in vivo*. The retinal pigment epithelium (RPE) is critically important for rod maintenance in the adult retina, as the discs at the terminal ends of rod OS are continually shed and phagocytosed in the RPE. Hence in transplanted cells the ideal position for formation of OS structures would be in close proximity to the RPE.

The next stage of investigation sought to identify whether transplanted $Rho^{-/-.Nrl.GFP}$ rod precursors following *ex vivo* gene therapy could restore visual function.

Well established assays were applied to investigate different aspects of the visual system. The Pupil Light Reflex (PLR) assay[62,67,287-289] assessed the brainstem reflex triggered by visual input, to investigate whether light sensitivity was restored in the retina and whether relay of signals from the eye towards the brain had occurred. The mouse light/dark box test[62,290-292], measuring Behavioural Light Avoidance (BLA) was used to evaluate the effect of retinal reconstruction on visually guided behaviour. Optomotor response (OMR)[70,158,232,234,235] was measured to evaluate the visual response to a dynamic stimulus in the different experimental groups and in the treated compared to untreated eye. Finally, an Electroretinography (ERG)[50,51,75,293] assay was used in order to investigate the electric impulses in the eye under scotopic and photopic conditions.

In the healthy eye, retinal stimulation is activated by the rod and cone photoreceptors, with contribution by a third class of photoreceptors, the melanopsin-containing intrinsically-photosensitive retinal ganglion cells (ipRGCs)[294,295]; the latter being normally active in bright and prolonged light stimuli. Rod photoreceptors, in contrast, are especially attuned to dim light conditions and short flashes of light. Therefore in order to specifically target rod mediated visual function in the degenerate retina, PLR was elicited by a brief flash of light and behavioural testing was conducted under dim light conditions[62,72]. ERG testing was assessed under scotopic and photopic conditions, using both flash and flickering light stimulus, to assess the

contribution of the different classes of photoreceptors to visual responses in treated mice.

5.2. Aim

The aim was to restore expression of rhodopsin in *rho*$^{-/-}$ rod PhRP cells by *ex vivo* delivery of the wild type *RHO* gene and to transplant treated cells to replace lost photoreceptors and restore visual function in blind adult Rho$^{-/-}$ mice. A further aim was to compare efficiency of gene delivery using the mutant adeno associated virus rAAV2 Y444F, to gene delivery using a non-viral minicircle DNA vector.

In order to track treated *rho*$^{-/-}$ cells following transplantation, donor cells were obtained from Rho$^{-/-.Nrl.GFP}$ mice, which harbor the same rhodopsin mutation as host mice and additionally express GFP specifically in rod photoreceptors through the Nrl promoter.

The objectives related to these aims were as follows:

1. Assessment of the Rho$^{-/-}$ host mouse model and Rho$^{-/-.Nrl.GFP}$ donor cells
2. Cell preparation, *ex vivo* gene delivery and subretinal transplantation
3. Reconstruction of the ONL by *ex vivo* treated cells and assessment of sustained survival and maturation of cells.
4. Assessment of visual function restoration

5.3. Methods

5.3.1. Animals

12-14 week old $Rho^{-/-}$ mice received a unilateral (left) subretinal injection of rod precursor cells from $Rho^{-/-.Nrl.GFP}$ mice which were treated *ex vivo* by one of the following methods:

1. Minicircle (MC) treatment: Cells received *ex vivo* treatment with MC RHOK.RHO.IRES.DsRed vector
2. rAAV2 Y444F treatment: cells received *ex vivo* treatment with rAAV2 Y444F RHOK.RHO.IRES.DsRed vector
3. Sham treatment: $Rho^{-/-.Nrl.GFP}$ cells were similarly processed but not treated.

Untreated age-matched C57/BL6 (WT) mice and $Rho^{-/-}$ mice were assessed alongside treatment groups as controls.

A first cohort was assessed for cell survival and optimisation of PLR response assay 3-4 weeks following transplantation (n=9 animals in each treatment and control group) and a second cohort was assessed for cell survival, protein expression and restoration of functional vision 8-10 weeks following transplantation (n=7 animals in each treatment and control group).

Retinal morphology was assessed in 12 week old $Rho^{-/-}$ mice and 6 week old $Rho^{-/-.Nrl.GFP}$ mice for characterisation of retinal degeneration.

5.3.2. Behavioural and functional assessment

12-14 old $Rho^{-/-}$ mice were assessed prior to transplantation by pupil light response (PLR), behavioural light avoidance (BLA) and optomotor response (OMR) assays to determine baseline behaviour and to stratify groups prior to long term transplantation. 8-10 weeks following transplantation, assessment of PLR, BLA, OMR and ERG analysis was conducted to assess visual function and isolate rod from cone mediated vision. All methods are described in Chapter 2.

5.4. Results

5.4.1. Characterisation of the $Rho^{-/-}$ and $Rho^{-/-.Nrl.GFP}$ mouse models

5.4.1.1. Genotyping

The rhodopsin knockout mouse $Rho^{-/-}$ and $Rho^{-/-.Nrl.GFP}$ mouse were genotyped for presence of rhodopsin and GFP. The Nrl.GFP mouse which expresses both rhodopsin and GFP was assessed for comparison. As expected, presence of the rho gene was not detected in $Rho^{-/-}$ or $Rho^{-/-.Nrl.GFP}$, while GFP was present in $Rho^{-/-.Nrl.GFP}$ mice (Figure 5.1).

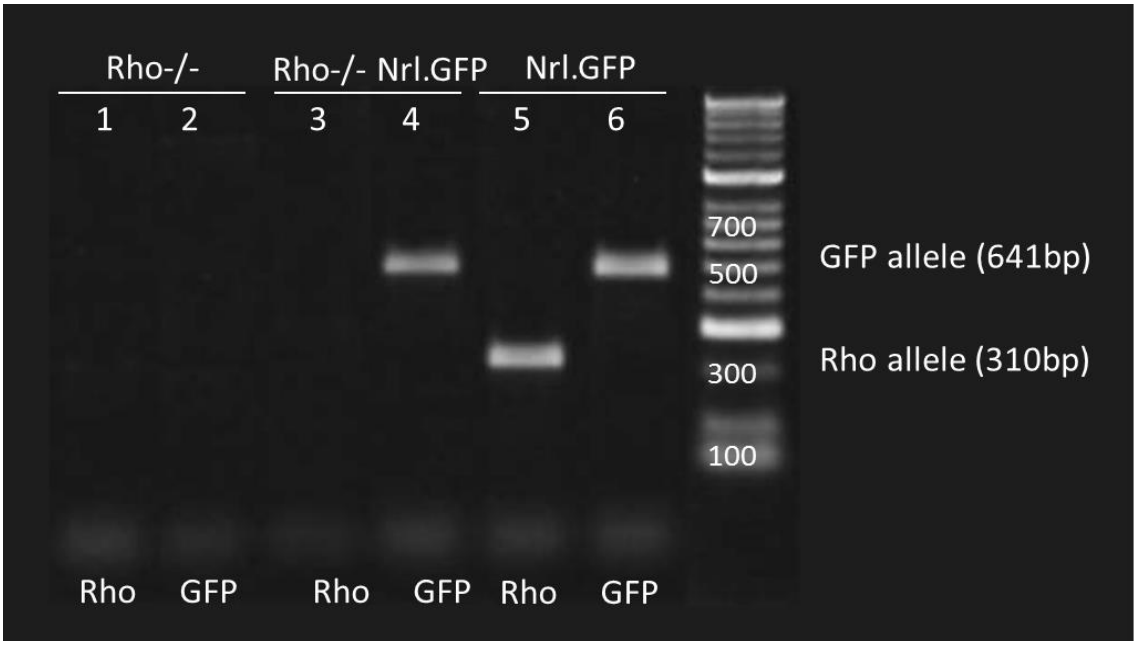

Figure 5.1: Genotyping of Rho$^{-/-}$ and Rho$^{-/-.Nrl.GFP}$ mice

Rho$^{-/-}$ (lanes 1-2), Rho$^{-/-.Nrl.GFP}$ (lanes 3-4) and Nrl.GFP (lanes 5-6) mice were genotyped for the presence of *rho* and *GFP*. As expected, neither of these alleles were detected in Rho$^{-/-}$ mice, while GFP, but not *rho* was detected in Rho$^{-/-.Nrl.GFP}$ mice. Nrl.GFP mice express both rho and GFP alleles and are presented for comparison.

5.4.1.2. Retinal histology

In the WT mouse at 12 weeks of age, the retina is structured in a laminated manner with photoreceptor cell bodies in the ONL elongating processes towards the RPE (Figure 5.2A) and rhodopsin abundantly expressed in the OS (Figure 5.2A'). In Rho$^{-/-}$ mice, by 12 weeks of age severe degeneration was observed with loss of the photoreceptors of the ONL and complete loss of OS structures (Figure 5.2B).

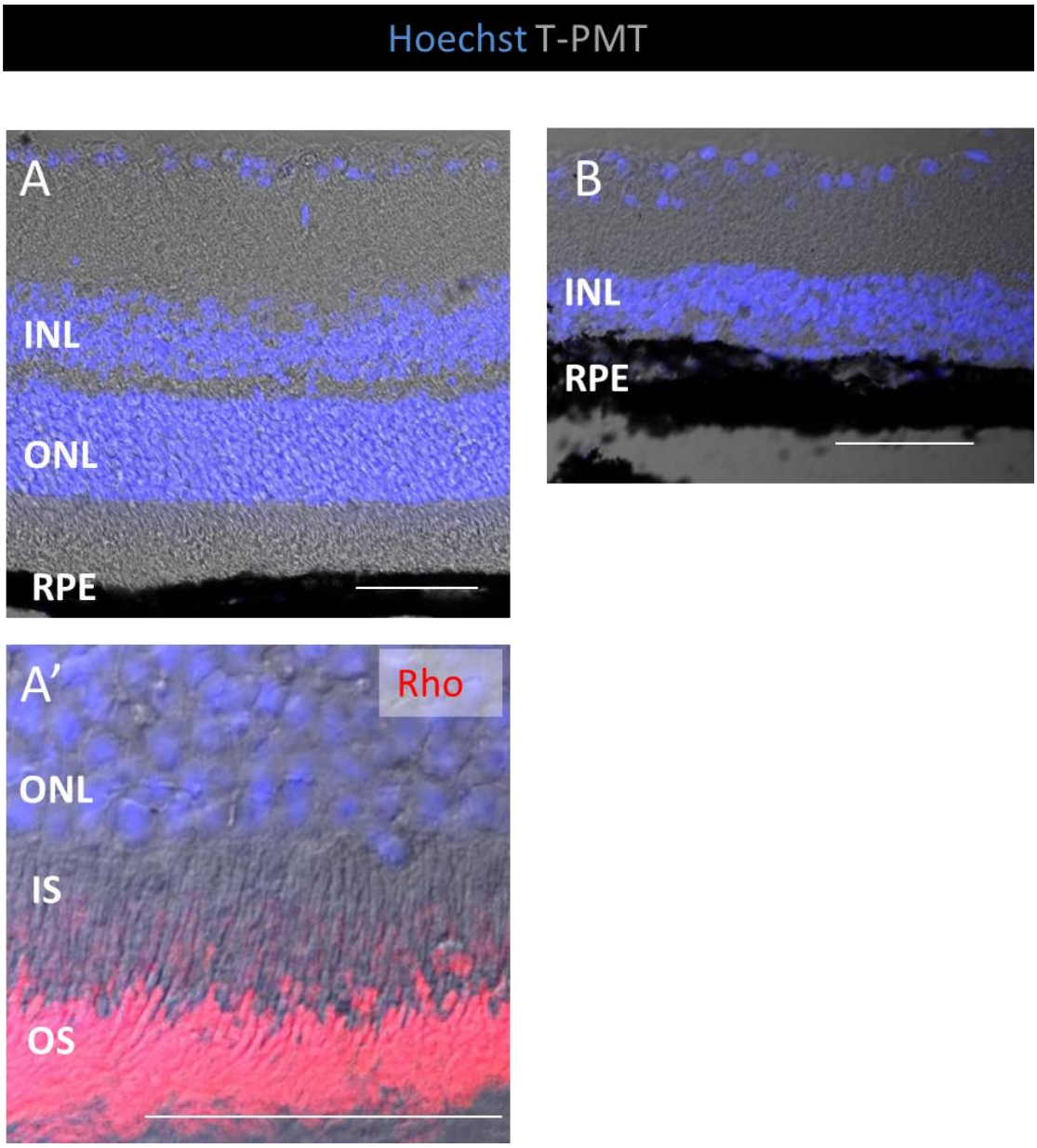

Figure 5.2: Histology of the Rho$^{-/-}$ retina

A. Histological section of 12 week old wild type retina. A'. Rhodopsin expression in the rod OS of the WT mouse. B. Histological section of 12 week old Rho$^{-/-}$ mouse retina showing severe degeneration of the ONL. INL; Inner nuclear layer, ONL; Outer nuclear layer, RPE; retinal pigment epithelium, IS; inner segments, OS; outer segments. Scale bar= 50µm.

Rod PhRPs were obtained from $Rho^{-/-.Nrl.GFP}$ mice as donor cells for transplantation studies prior to degeneration. In order to assess *in vivo* rod degeneration in this model, $Rho^{-/-.Nrl.GFP}$ mice were assessed at 6 weeks of age and compared to age matched Nrl.GFP mice without the rhodopsin mutation. In the Nrl.GFP mouse rod photoreceptors in the ONL are clearly marked by GFP and expression of rhodopsin is constricted to rod outer segments (OS) between the ONL and RPE (Figure 5.3A). In $Rho^{-/-.Nrl.GFP}$ mice however, although a thin layer of cells remains between the INL and RPE at 6 weeks of age, no GFP positive rod cells were observed and rhodopsin expression was not detected (Figure 5.3B) confirming *in vivo* rod loss.

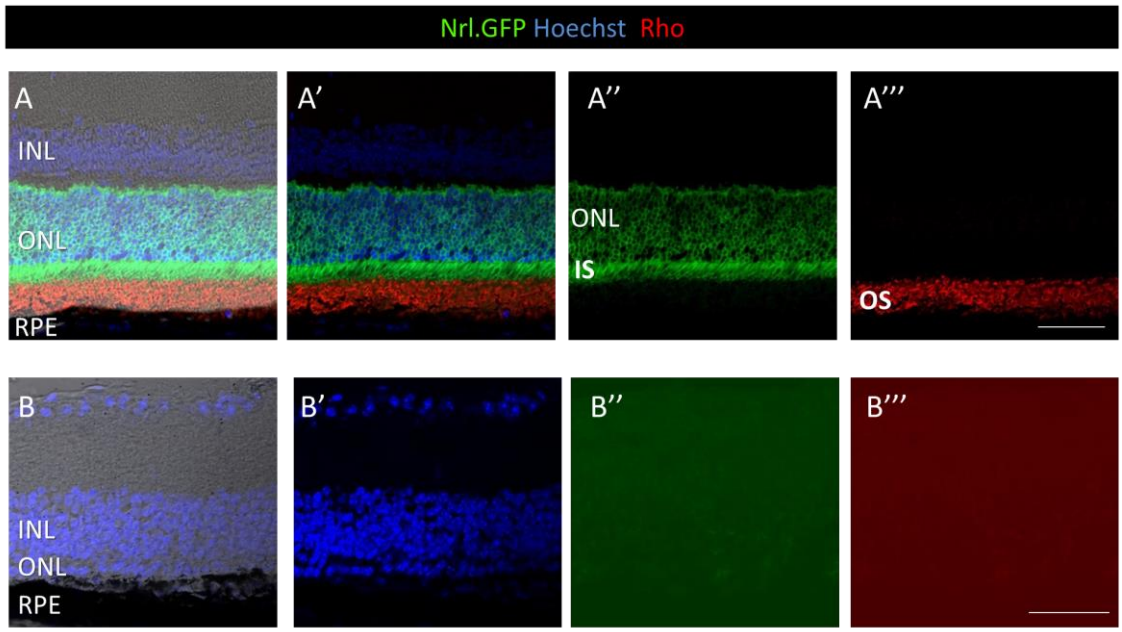

Figure 5.3: Histology of the Rho$^{-/-.Nrl.GFP}$ retina

A-A''. Histological section of 6 week old Nrl.GFP mouse. Fluorescent GFP signal is driven by the Nrl promoter and contained in the cytoplasm of cell bodies of the ONL and in IS but not in the OS. A'''. Immunohistochemistry labelling of OS by Rho antibody. B-B'. Histological section of 6 week old Rho$^{-/-.Nrl.GFP}$ retina' showing a thin layer of cells remaining between the INL and RPE. B''. GFP positive cells were not detected in the Rho$^{-/-.Nrl.GFP}$ retina, suggesting complete rod degeneration by this stage. B'''. No rhodopsin expression was observed in these mice. Retinal histology implies that by 6 weeks of age, untreated rods of the Rho$^{-/-.Nrl.GFP}$ degenerate completely *in vivo*. INL; Inner nuclear layer, ONL; Outer nuclear layer, RPE; retinal pigment epithelium, IS; inner segments, OS, outer segments. Scale bar= 50μm.

5.4.1.3. Assessment of baseline visual function in adult Rho-/- mice

Visual function was assessed in $Rho^{-/-}$ mice at 12-14 weeks to determine baseline levels of visual function in mice prior to transplantation of treated cells. $Rho^{-/-}$ (n=28) were tested, and results are presented alongside age matched wild type mice (n=8) as a positive control for testing conditions. Using the behavioural light avoidance assay, preference for light or dark was assessed, showing that $Rho^{-/-}$ mice spent 40.7±7.2% (mean % of time in light ±1 SEM) of the time in the dark compartment, indicating no tendency for light avoidance (Figure 5.4A). Measure of pupil light reflex (PLR) was assessed in $Rho^{-/-}$ mice, following a 0.1 sec light pulse of 10^{15} photons.cm^2.s and measured at 1.9 sec post stimulus[62]. Pupil area post stimulus was normalised in each mouse to the pupil area prior to light pulse. In tested $Rho^{-/-}$ mice pupils constricted to 91.8±2.6% of their baseline size prior to the light pulse, a negligible constriction compared to WT pupil constriction to 25.7±5.5% of original pupil area (mean % of pupil size ±1 SEM) (Figure 5.4B). Measurement was conducted at a relatively short latency following stimulus offset in order to evaluate rod photoreceptor function over other cell types that contribute to the PLR. The time point for measurement and light intensity selected will be further elaborated in experimental results in section 5.4.4.1. Finally, Optomotor response (OMR) was measured in an optokinetic drum in response to a rotating grating. WT mice displayed head tracking responses, corresponding to the directionality of grating rotation. In $Rho^{-/-}$ mice, the average response was between zero to one head tracks per trial (0.57±0.2) (mean number of head

tracks ±1 SEM) (Figure 5.4C), consistent with previously described head tracking behaviour of blind $Rho^{-/-}$ mice at 30 weeks of age[158]. Together with histological data presented in the previous section, these measures provide an extremely low if not absent baseline in terms of anatomy and visual function prior to transplantation.

Experimental groups for transplantation studies were stratified according to baseline behaviour to control for variance between treatment groups. Functional vision assays were optimised for assessment of vision following transplantation of treated rod PhRPs and will be presented in detail in comparison of experimental groups following treatments in section 5.4.4.

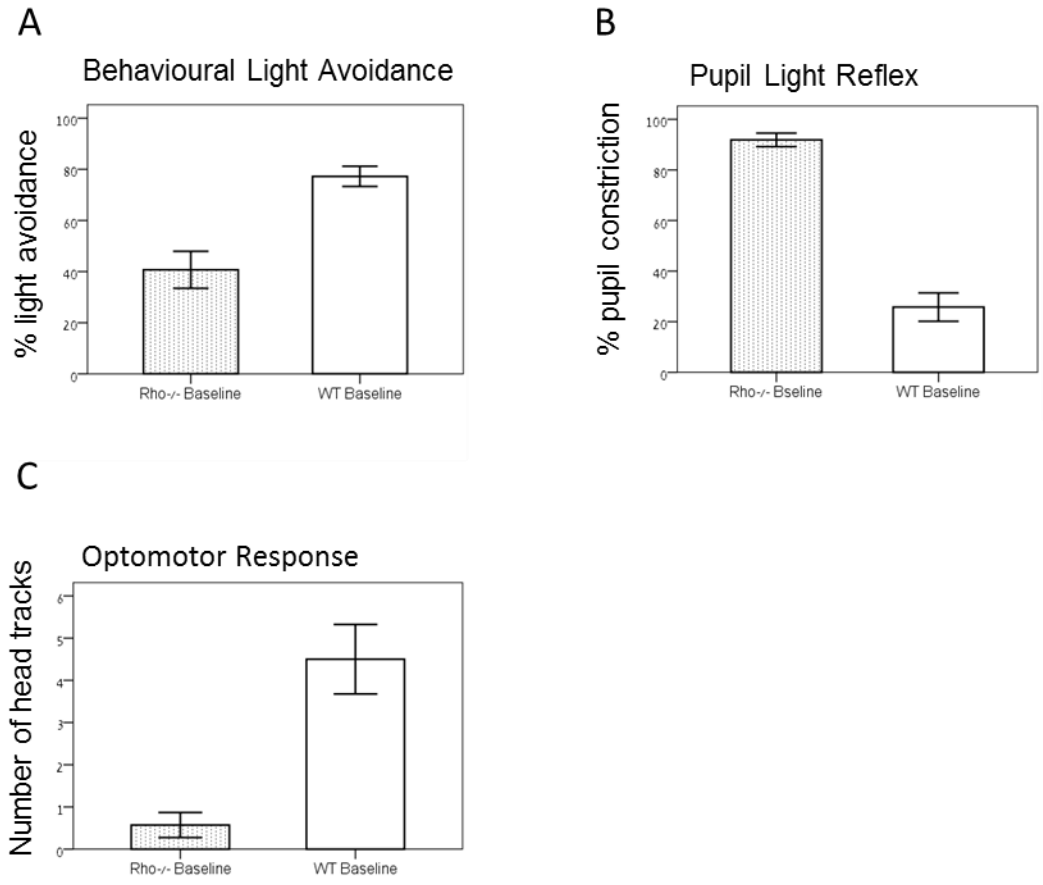

Figure 5.4: Baseline visual function of Rho$^{-/-}$ mice

Rho$^{-/-}$ mice were assessed for baseline visual function at 12-14 weeks of age. Responses of age matched WT mice are presented for reference.
A. Rho$^{-/-}$ mice did not show preference towards the dark compartment in the behavioural light avoidance assay. B. Following a light stimulus, pupil area in Rho$^{-/-}$ mice was reduced to 91.8±2.6% of their size prior to the light pulse. C. Mean number of head tracking responses in the optomotor response test was under 1 head track per trial (0.57±0.2). Baseline results of functional vision were used to stratify experimental groups prior to transplantation.

5.4.2. Preparation of cells and subretinal transplantation

Retinae were dissociated from $Rho^{-/-.Nrl.GFP}$ PN1-3 mice. Cell sorting was performed by magnetic activated cell sorting (MACS), using the CD73 rod cell surface marker to enrich cultured cells to 87.2±7.1% GFP+ rod precursor cells as described in chapter 3.

Rhodopsin gene therapy was delivered to $Rho^{-/-.Nrl.GFP}$ cells in culture by means of rAAV2 Y444F or by minicircle (MC) DNA vector carrying the *RHO* gene and a DsRed fluorescent reporter driven by the rhodopsin-kinase promoter (RHOK.RHO.IRES.DsRed) as described in Chapter 4. A third group of $Rho^{-/-.Nrl.GFP}$ cells received no treatment and was maintained in culture for sham transplantation. Treated cells were transplanted on day 3 of culture, after initial onset of expression was verified in both gene therapy groups by detection of DsRed expression. Rod-enriched cohorts were determined to be >95% viable by trypan blue exclusion stain (Figure 5.5).

Cell cohorts were rinsed and dissociated prior to transplantation and $2x10^5$ cells were subretinally injected to adult $Rho^{-/-}$ hosts.

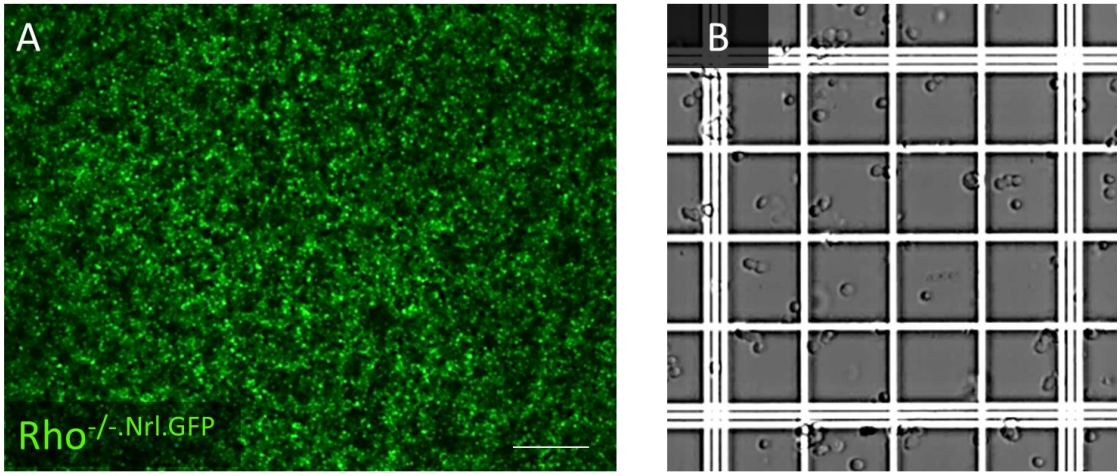

Figure 5.5: Rho$^{-/-.Nrl.GFP}$ retina prior to transplantation

A. Appearance of rod-enriched dissociated retinae from neonatal Rho$^{-/-.Nrl.GFP}$ mice. The cells harbor a null mutation in the rhodopsin gene and GFP is expressed specifically in rod PhRPs by the Nrl promoter. Scale bar, 100μm. B. Representative image of 1x1mm chamber of the hemocytometer showing over 95% cell viability by trypan blue exclusion stain.

5.4.3. Reconstruction of the adult Rho$^{-/-}$ ONL by treated Rho$^{-/-.Nrl.GFP}$ rods

Ten weeks following transplantation of Rho$^{-/-.Nrl.GF}$ rod PhRPs treated with MC DNA or rAAVY444F RHOK.RHO.IRES.DsRed, histological analysis showed a thick layer of cells had formed in the subretinal space of treated mice of both groups. The new layer was interposed between the INL and RPE of host mice to reform the ONL of adult Rho$^{-/-}$ mice. GFP signal in cells of the reconstructed layer confirms the cells' identity as transplanted donor Rho$^{-/-.Nrl.GFP}$ cells and expression of DsRed was detected in transplanted cells.

Figure 5.6 shows a representative image of an ONL reconstruction by cells treated with MC DNA and the corresponding scanning laser ophthalmoscope (SLO) image of the mouse retina obtained *in vivo* 10 weeks post transplantation showing widespread cell survival in the retina.

To evaluate morphology of transplanted cells, a layer of cells transplanted following rAAV2 Y444F treatment was compared to a histological section of an adult Nrl.GFP retina. In the WT retina, as presented in the Nrl.GFP mouse, rod photoreceptor cells extend clear inner and outer segments towards the RPE. While transplanted cells were properly localised in the subretinal space and the thickness of the newly formed cell layer was comparable to that of the WT retina, the grafted ONL was positioned adjacent to the RPE without a laminated segment structure (Figure 5.7).

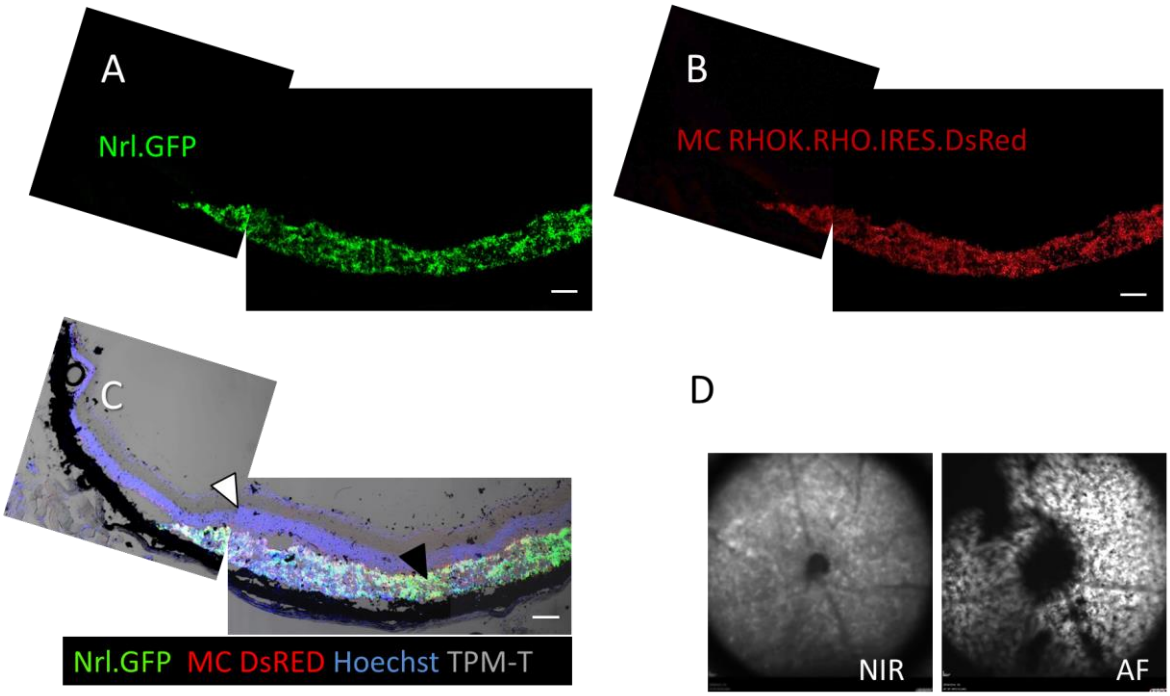

Figure 5.6: Reconstruction of the adult Rho-/- ONL by MC treated rod precursor cells

Three continuous confocal images of an adult $Rho^{-/-}$ retina transplanted with $Rho^{-/-.Nrl.GFP}$ cells following *ex vivo* gene therapy with MC RHOK.RHO.IRES.DsRed. A. GFP expression is endogenous to donor rods in the Rho-/-Nrl.GFP mouse and indicates reconstruction of the host ONL by transplanted rod precursors. B. DsRed is expressed *in vivo* in cells following treatment with MC. C. Merged image showing partial co localisation of Nrl.GFP and DsRed signals in transplanted cells. White arrow indicates the host INL and black arrow indicates the reconstructed cell layer in place of the lost ONL. D. Corresponding *in vivo* image of the retina obtained by scanning laser ophthalmoscopy (SLO) 10 weeks post transplantation. GFP positive cells are observed in AF mode as white dots or clusters (black areas represent areas of retina which were not seeded with transplanted cells, due to incomplete detachment of the retina around the optic nerve). MC; minicircle, INL; inner nuclear layer, ONL; outer nuclear layer, NIR; near infra-red, AF; autofluorescence. Scale bar 100µm

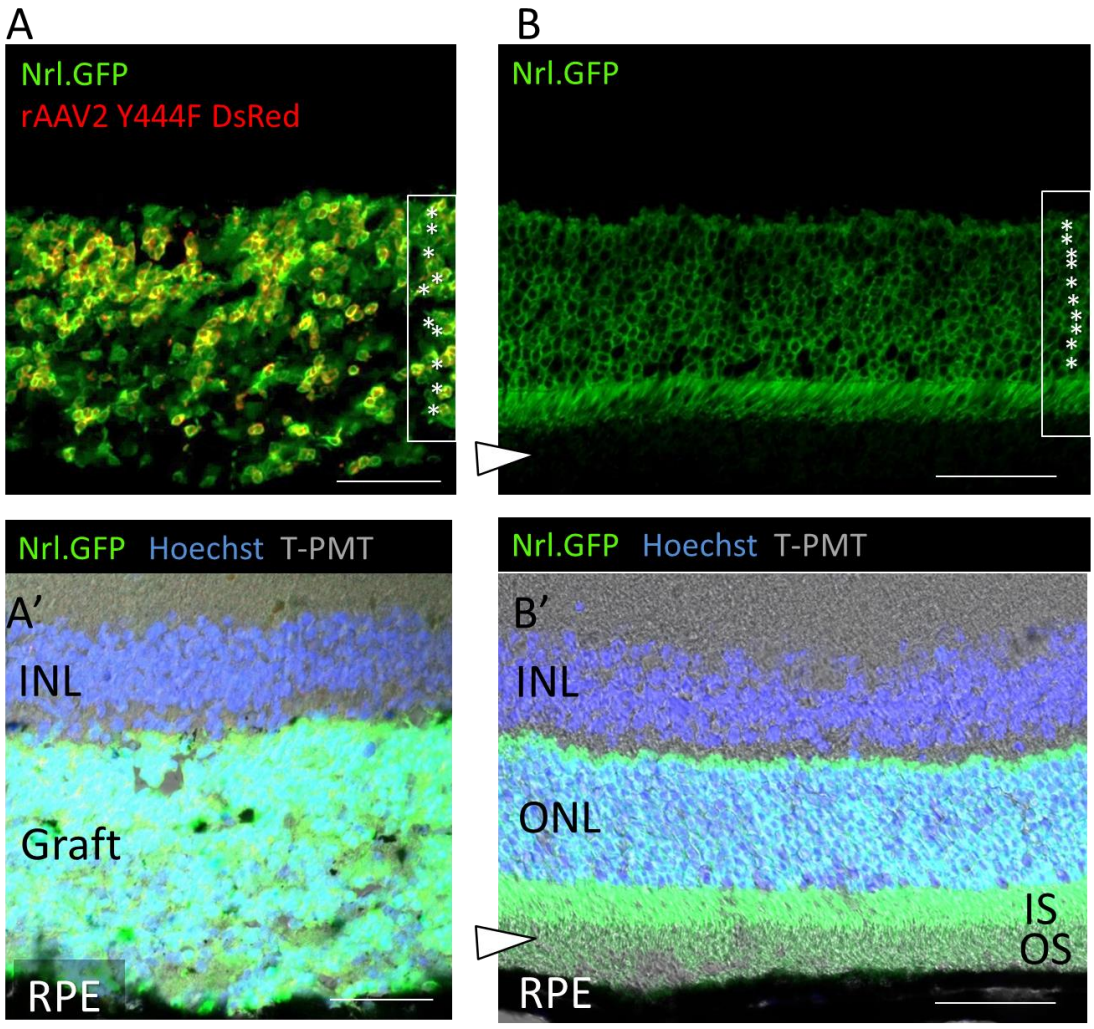

Figure 5.7: Reconstruction of the adult Rho-/- ONL by rAAV2 Y444F treated rod precursor cells

A-A'. Reconstructed layer of GFP/DsRed cells residing in the subretinal space of the adult $Rho^{-/-}$ host 10 weeks post transplantation of $Rho^{-/-.Nrl.GFP}$ rod precursor cells treated with rAAV2 Y444F. 10 cell bodies of one row of cells between the host INL and RPE are marked with white stars (*). B. The ONL of the WT mouse as shown in the adult Nrl.GFP retina, with a corresponding row of cell bodies marked. B'. Rod cell bodies in the Nrl.GFP retina form distinct IS and OS between the ONL and RPE (white arrows). Grafted cells residing in the subretinal space did not extend a clear layer of segments towards the RPE (A'). INL; inner nuclear layer, ONL; outer nuclear layer, RPE; retinal pigment epithelium, IS; inner segments, OS; outer segments. Scale bar 50µm.

5.4.3.1. Comparison of cell survival in treatment groups

10 weeks post transplantation a thick layer of GFP positive cells was observed in mice of both treatment groups and co localisation of the delivered DsRed fluorescent reporter was observed with the GFP signal in cells following *ex vivo* MC treatment (Figure 5.8A) and rAAV2 Y444F treatment (Figure 5.8B)

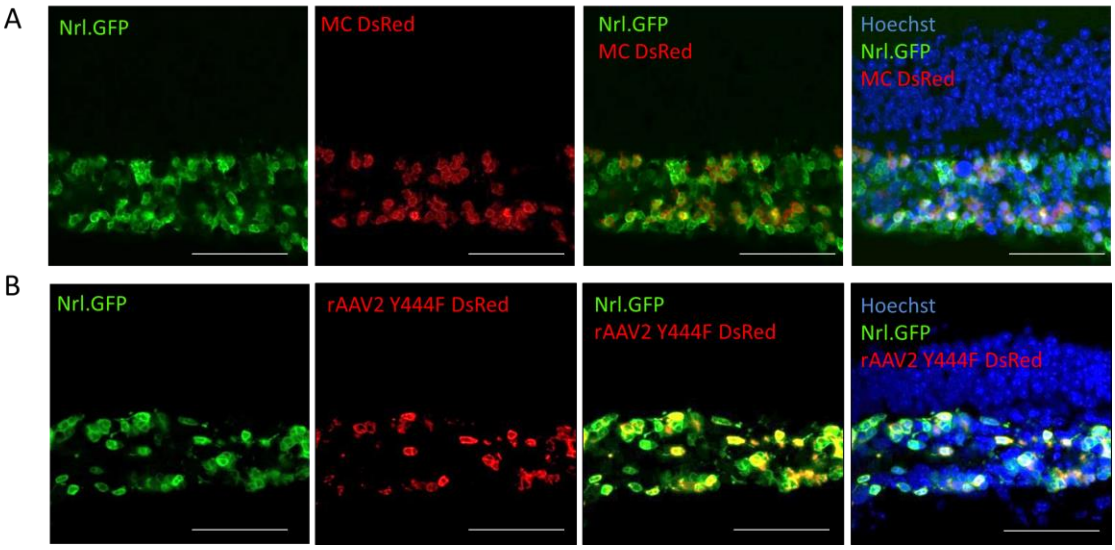

Figure 5.8: Co-localisation of Nrl.GFP and DsRed reporter gene in treated cells

GFP signal was highly expressed in transplanted cells of both treatment groups with DsRed expression constricted to transplanted cells. The co-localisation of GFP and DsRed proteins indicates survival of cells which have been successfully transfected by the MC vector (A) or transduced by rAAV2 Y444F vector (B). Scale bar 50µm.

Surviving cells in the subretinal space of treated mice were quantified by GFP expression. The percent of DsRed positive cells was calculated in surviving cells and compared in groups of adult $Rho^{-/-}$ mice 4 weeks and 10 weeks post transplantation (n=5 specimens per group) (Figure 5.9). Four weeks post transplantation 7.6±9.2% (mean ±1 SEM) of MC treated cells survived of which 54.4±6.2% of cells were DsRed positive. In the AAV treatment group 7.2±1.3% of cells survived of which 87.9±6.3% were DsRed positive. In the Sham treatment group 0.31±0.07% of cells survived at 4 weeks with no DsRed detected. At this stage a significant difference between the three groups was observed in number of GFP expressing cells (One way ANOVA, $F(2,12)=18.96$, $p<0.0001$) and DsRed expressing cells (One way ANOVA, $F(2,12)=26.05$, $p<0.0001$). Post hoc analysis revealed a difference in cell survival between sham and MC treatment ($p<0.0001$) and between sham and AAV treatment ($p=0.001$), but not between the two groups (ns). A difference in the percent of DsRed positive cells was observed between the two groups at this timepoint ($p=0.002$) with higher expression of DsRed in cells following AAV treatment.

10 weeks following transplantation, 4.95±0.39% of cells in the MC treatment group were still present in the subretinal space, with 63.3±9.5% DsRed expression, indicating that cells which were not transfected by the *RHO* vector were more likely to degenerate. In the AAV treatment group 3.26±0.65% of cells survived at 10 weeks maintaining DsRed expression in 86.3±4.5% of cells. 0.05±0.008% of cells of the Sham transplantation group survived ten weeks following transplantation. A difference was observed between the three

treatment groups in number of surviving cells (One way ANOVA, $F(2,12)=31.49$, $p<0.0001$) and DsRed expression (One way ANOVA, $F(2,12)=53.3$, $p<0.0001$). Both MC and AAV gene therapy groups were significantly different from sham transplantation (both $p<0.0001$) but no difference was observed between the two treatment groups in number of surviving cells ($p=0.058$, ns) or percent of DsRed expressing cells ($p=0.063$, ns).

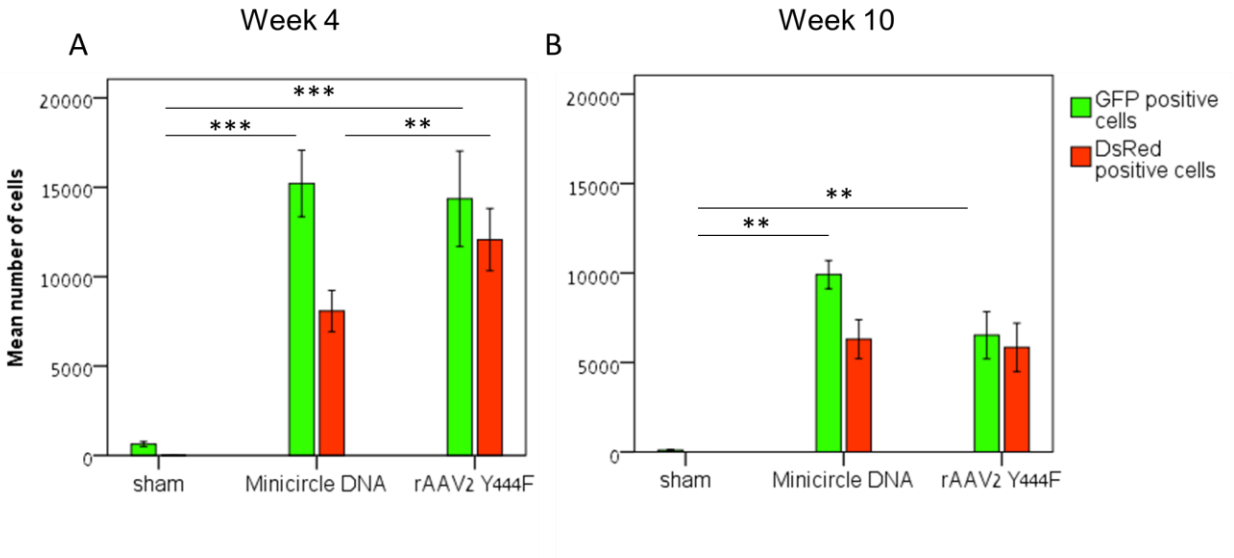

Figure 5.9: Quantification of GFP and DsRed expression in transplanted cells

A. Four weeks following transplantation a significant difference in cell survival was observed between the three treatment groups in number of GFP positive cells ($F(2,12)=18.96$, $p<0.0001$) and DsRed expressing cells ($F(2,12)=26.05$, $p<0.0001$). In both MC and rAAV2 Y444F treatment groups, cells survived significantly more than in the Sham treatment group ($p<0.0001$ in both). A difference in the percent of DsRed expressing cell was found between the gene therapy groups, with a higher percentage of DsRed expression in cells following rAAV2 Y444F treatment ($p=0.002$). B. Ten weeks following transplantation, number of surviving cells was smaller in all groups, however a significant difference was maintained in cell survival ($F(2,12)= 31.49$, $p<0.0001$) with cells surviving in significantly higher numbers in treatment groups compared to sham (both $p<0.0001$). No difference in cell survival or DsRed expression was observed between the MC and rAAV2 Y444F treatment groups at this time point. N=5 per group, One way ANOVA, Bonferroni correction for multiple comparisons.

5.4.3.2. Protein expression and maturation of transplanted cells

Immunohistochemistry was used to assess expression of rhodopsin in transplanted $Rho^{-/-.Nrl.GFP}$ rod precursor cells transplanted following *ex vivo* rhodopsin gene therapy. Immunoreactivity against Rhodopsin was found in donor cells of the MC treated group (Figure 5.10) and rAAV2 Y444F group (Figure 5.11). Both donor cells and host animals are homozygous for the null rhodopsin mutation, thus expression of the rho protein indicates production of rhodopsin in outer segment disks following replacement of the defective gene by WT *RHO.* Cells developed morphologically abnormal outer segments, with rhodopsin expression localised in the shortened outer segment structures of treated cells. Grafted cells did not align in a parallel directionality towards the RPE and OS were formed pointing in different directions.

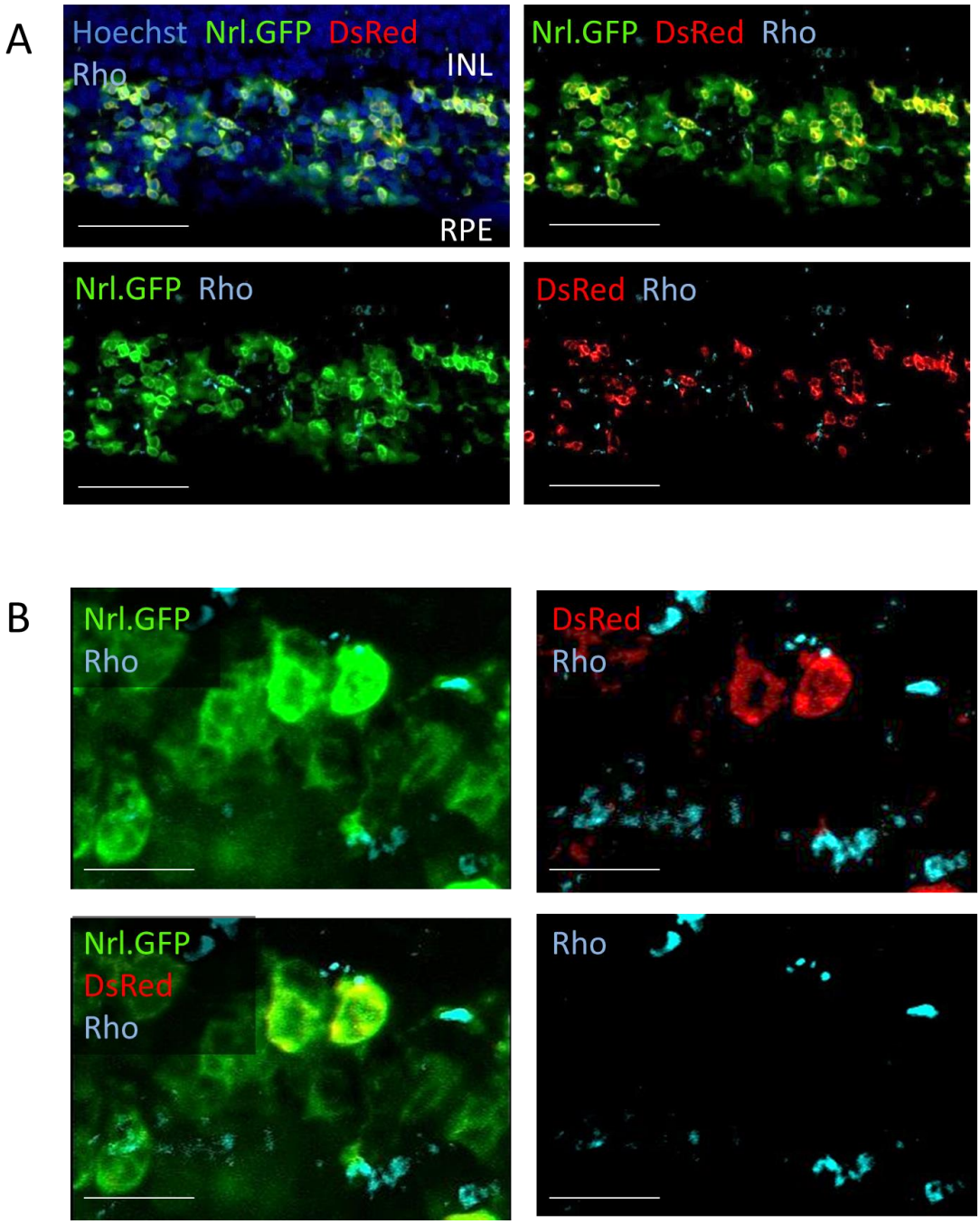

Figure 5.10: Rhodopsin expression in donor cells following MC *ex vivo* gene therapy

A. Rho expression was found in MC treated GFP/DsRed positive donor cells residing in the subretinal space of Rho-/- mice following transplantation. Scale bar, 50 µm. B. Cells extended slender inner segments with short outer segment structures expressing rhodopsin. Scale bar, 10 µm.

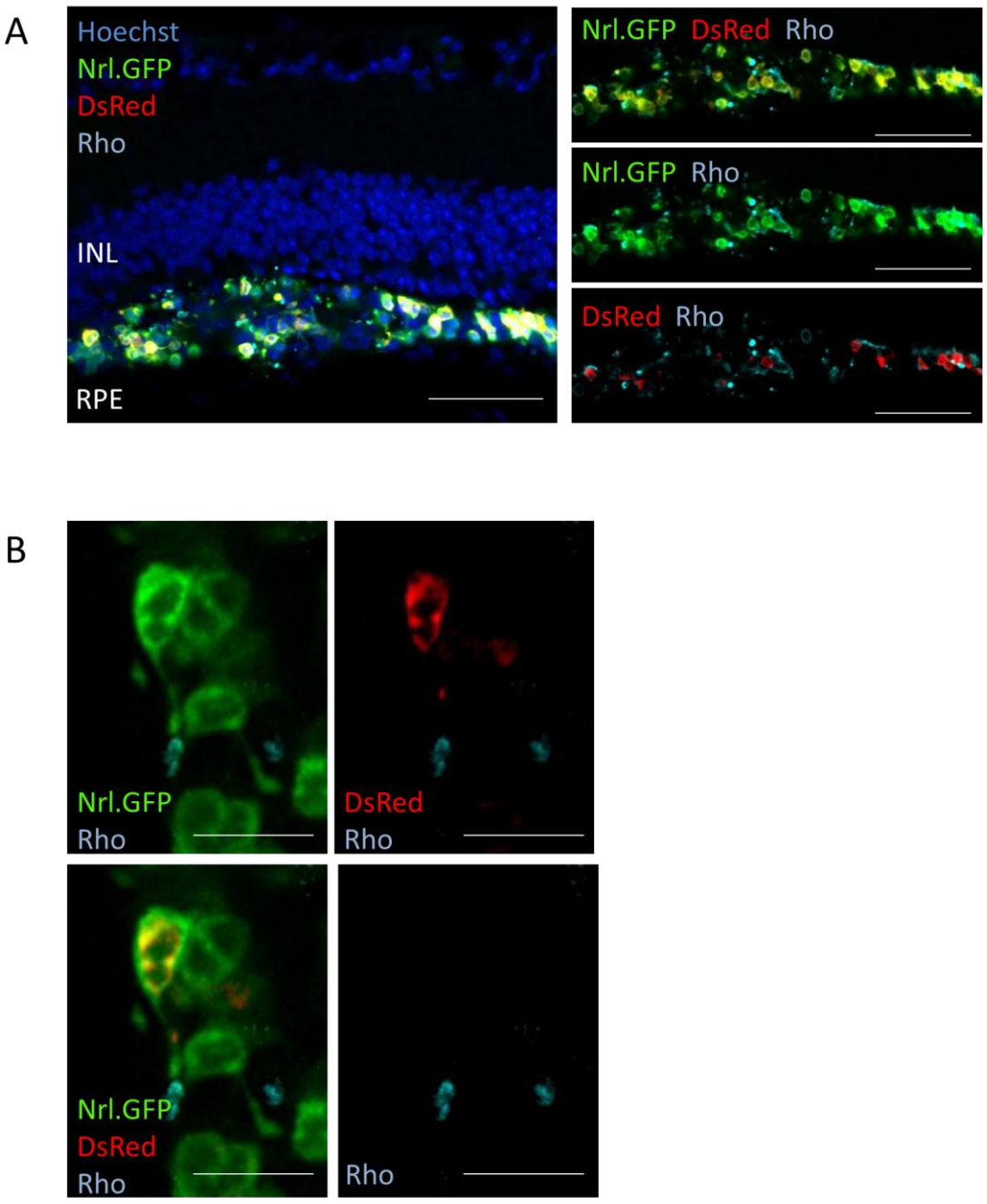

Figure 5.11: Rhodopsin expression in donor cells following rAAV2 Y444F *ex vivo* gene therapy

A. Rho expression in rAAV2 Y444F treated GFP/DsRed positive donor cells residing in the subretinal space of Rho-/- mice following transplantation. Scale bar, 50 µm. B. cells extended inner segments with short outer segment structures expressing rhodopsin. Scale bar, 10 µm.

To assess maturation of rod cells 10 weeks following transplantation, the presence of the rod specific OS proteins Phosphodiesterase 6B (PDE6b) and Retinal Outer Segment Membrane Protein 1 (ROM1) were assayed and the pan-photoreceptor marker recoverin was analysed as a control for protein localisation. Treated cells expressed both OS proteins and recoverin (Figure 5.12). The appearance of OS protein localisation in transplanted cells confirmed previous observation of newly grafted cells being morphologically distinct from WT rod cells with shorter OS and misaligned OS direction. Recoverin was appropriately localised in the cell cytoplasm and co expressed with cytoplasmic GFP, confirming cell identity as photoreceptors.

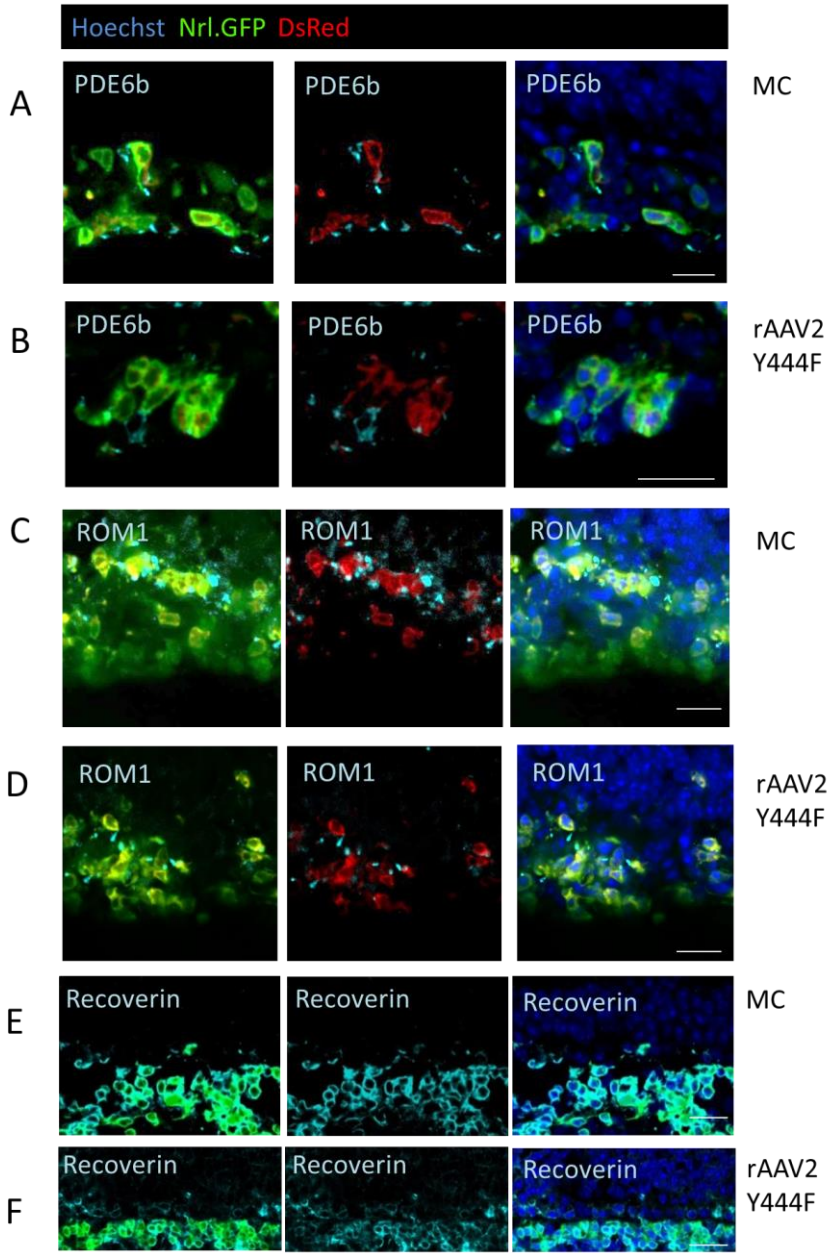

Figure 5.12: Expression of rod specific markers by transplanted treated cells

A-D. Phosphodiesterase 6B (PDE6b) and Retinal Outer Segment Membrane Protein 1 (ROM1) were expressed in OS structures of cells treated by MC and rAAV2 Y444F gene therapy, providing evidence of rod cell maturation in grafted cells expressing intrinsic GFP and the DsRed fluorescent marker. E-F. The pan-photoreceptor marker recoverin was expressed in the cell cytoplasm, co-localising with cytoplasmic Nrl.GFP, confirming cell identity as photoreceptors and providing a control for localisation of OS proteins. Scale bar 10µm.

5.4.3.3. Connectivity between graft and host

In order for cells to restore visual function, donor rod photoreceptors need to form connections with the host INL and retinal circuits downstream.

The terminal of rod photoreceptors is identified by localisation of the synaptic vesicle membrane protein Synaptophysin. Immunohistochemistry with anti-synaptophysin showed presence of this protein in the border region between host INL and grafted cells (Figure 5.13A-B). The pattern of staining indicated that donor treated rods had formed synaptic terminals in close proximity to the host inner retina.

As transplanted cells did not integrate into a pre-existing ONL in the severely degenerate retina of the $Rho^{-/-}$ mouse but formed a new layer of cells, Glial fibrillary acidic protein (GFAP) was assayed to identify Müller glia and determine whether formation of a glial barrier occurred between the host retina and transplanted cells. In both groups, glial processes were extended into grafted cells without clear formation of a horizontal glial barrier (Figure 5.13C-D). The presence of a glial barrier would impede interaction of the donor cell layer with the host retina, however, the finding that in some regions of the retina glial processes extended vertically into the donor cell layer may support the absence of a total glial barrier between donor and host cells. Müller cells are required for function of photoreceptors thus integration and support of the donor cells by host glia would be important for integration of the newly formed ONL.

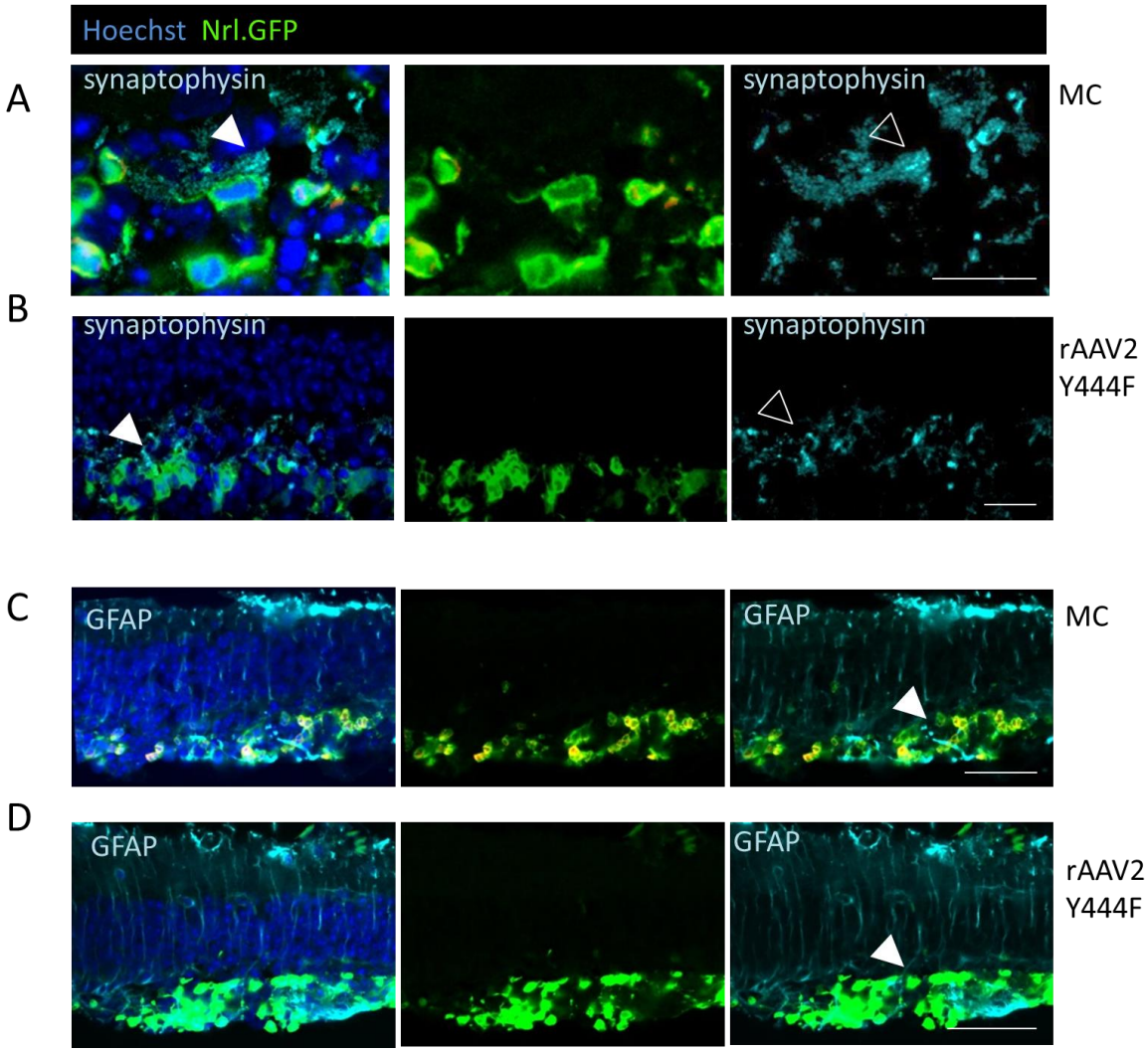

Figure 5.13: Graft host connectivity

A-B. Synaptophysin was appropriately localised between the host INL and donor cell mass in both treatment groups (white arrows), and was also found between rod cells of the graft (black arrow). Scale bar 10μm. C-D. Host Müller cells are identified by glial fibrillary acid protein (GFAP). Müller cell processes extended from the host INL into the graft (white arrows) without formation of a clear horizontal glial barrier. This finding is favourable in regards to morphology of the retina post transplantation, as an absence of a complete glial barrier would support maintenance of the newly formed ONL. Scale bar 50μm.

5.4.4. Restoration of visual function

Experiments were designed to determine whether visual function was restored in adult $Rho^{-/-}$ with end stage retinal degeneration following transplantation of $Rho^{-/-.Nrl.GFP}$ rod precursors which were treated *ex vivo* for replacement of the rhodopsin gene. Visual function was assessed before and after surgery in the same animals to provide evidence of functional restoration in animals as well as reliable differences between treatment groups, following stratification of experimental groups by baseline results.

5.4.4.1. Restoration of pupil light reflex in treated animals

Preliminary experiments were conducted in animals three weeks following transplantation of MC, AAV2 Y444F or sham treated cells (n=9 per group) to determine optimal settings for detection of rod specific PLR. The objective was to assess rod specific function over other cell types that contribute to the PLR, such as RGC[296] or specifically ipRGCs[5,295], thus the PLR magnitude was calculated at a relatively short latency after light stimulus in order to assess the down slope of the constriction phase rather than full pupil constriction. This approach has been validated in the study of mice and humans with retinal disease[62,287]. The timepoint selected was 1 second post stimulus, which represents early pupil constriction driven by rod cells (reducing the direct effects from melanopsin expressing ganglion cells). In order to select a light intensity that would favour assessment of rod photoreceptors, intensity

response curves were generated across three light intensities (10^{14}, 10^{15}, 10^{16} Photons/cm^2/s) in each animal. The dimmest stimulus resulted in almost no pupil constriction in all groups, whereas the strongest stimulus resulted in strong constriction in almost all mice, indicating involvement of other cell types. At the median light intensity, an improvement over baseline was found in both MC (Paired t test, t=5.7 p<0.0001) and AAV2 Y444F (Paired t test, t=2.8 **p<0.01) treatment groups, but not in the sham transplantation group (Paired t test, t=1.35, p=0.17, ns). The possibility to detect restoration of pupil light reflex in treated animals, but not sham transplanted animals indicates an improved effect of gene therapy over any effect of sham surgery with rhodopsin deficient cells, or of a general neuroprotective effect of cell transplantation. Furthermore, the specific light intensity used (approximately 200lux) was determined to specifically identify the PLR resulting from rod cells and was therefore further used to evaluate changes in retinal sensitivity and compare groups following transplantation.

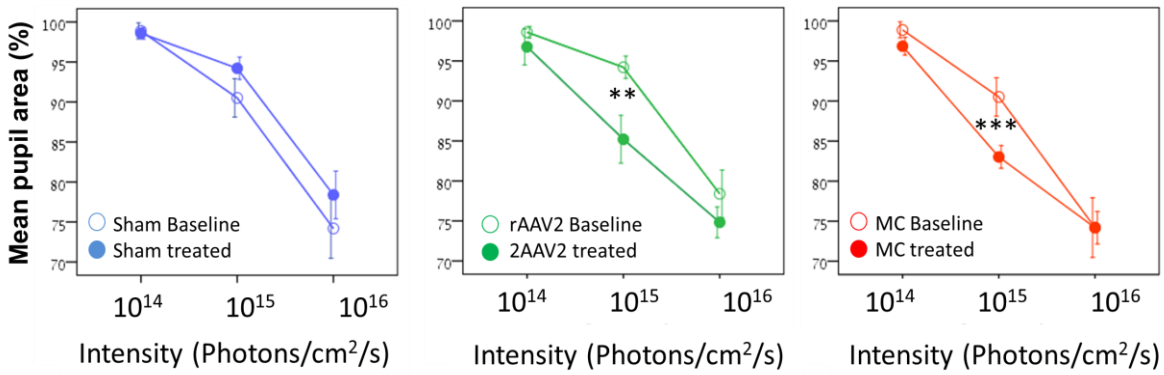

Figure 5.14: Restoration of pupil light reflex in treated animals 3 weeks following transplantation

Irradiance response curve, showing paired analysis of mean pupil area prior to transplantation (baseline) and three weeks following treatment. A significant improvement in the pupil light reflex (PLR) was detected at the median light intensity in animals in the rAAV2 Y444F group (Paired t test, t=2.8 **p<0.01, N=9) and Minicircle group (Paired t test, t=5.7 ***p<0.0001, N=9). The PLR did not improve following sham transplantation (Paired t test, t=1.35, p=0.17, ns, N=18).

8 weeks following transplantation the three groups were compared by normalizing mean pupil area following light stimulus to mean area prior to stimulus (Figure 5.15). Groups differed in their pupil light response following transplantation (One way ANOVA, $F(2,18)=14.78$, $p<0.001$) with an improvement over sham transplantation in both MC($p<0.0001$) and rAAV2 Y444F($p<0.05$) treated cells. Improvement in PLR was greater in the MC treated group compared to rAAV2 Y444F treatment in these mice ($p<0.05$).

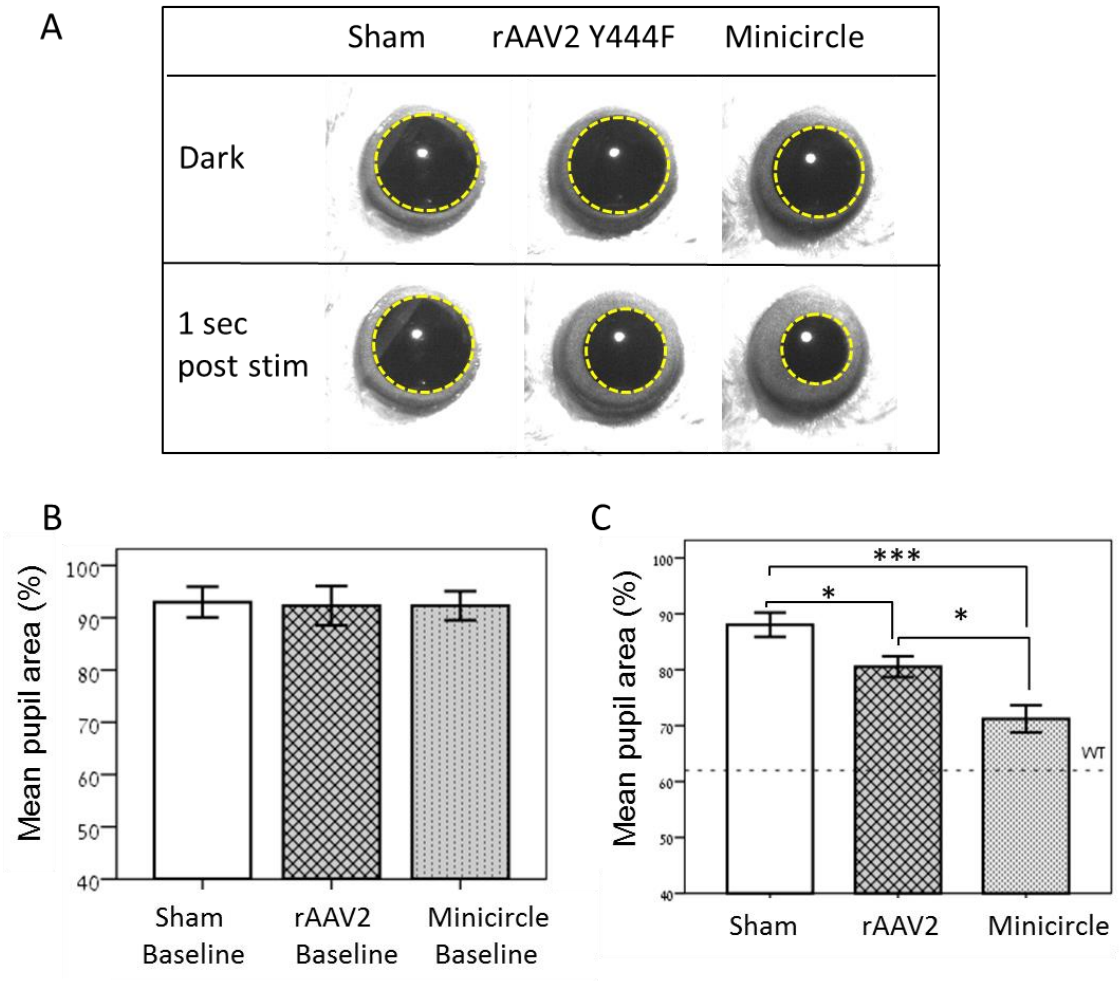

Figure 5.15: Comparison of pupil light reflex in treatment groups

A. Representative images of pupil light reflex (PLR) prior to stimulus and 1 sec post stimulus at a light intensity of 10^{15} photons/cm^2/s in treatment groups eight weeks post transplantation. B. Baseline measurements prior to transplantation show no differences between mice in the different experimental groups prior to transplantation. C. The three treatment groups differed in mean pupil area ($F(2,18)=14.78$, $p< 0.001$) with PLR significantly improved in the rAAV2 Y444F group (*p=0.043) and minicircle group (***p<0.0001). The minicircle treatment group improved more than the rAAV2 Y444F group (*p=0.019). Dashed line represents mean wild type (WT) PLR. One way ANOVA, Bonferroni correction for multiple comparisons, N=7 per group.

5.4.4.2. Restoration of behavioural light avoidance

Mice are nocturnal animals, and exhibit behavioural light avoidance (BLA), meaning they have a tendency to avoid light exposure in open environments[297]. This was measured experimentally by assaying the amount of time mice spent in lit or dark compartments of the BLA arena.

BLA was tested in MC, rAAV2 Y444F and sham treated mice 9 weeks following subretinal transplantation. Age matched wild type and untreated $Rho^{-/-}$ mice were tested for validation of the test protocol and reference behaviour at baseline (age 12-14 weeks) and following treatment (age 21-23 weeks). The amount of time each group spent in the light and dark chambers was calculated and the average % of time spent in the dark compartment was evaluated as a measure of BLA.

At age 12-14 weeks WT mice spent 76.25±3.9% (mean ± 1 SEM) of the test period in the dark compartment and at age 21-23 weeks spent 78.63±2.9% of the test period in the dark compartment. Untreated $Rho^{-/-}$ mice avoided light 40.71±7.2% of the test period at 12-14 weeks and 50.29±3.5% at age 21-13 weeks. Mean responses of untreated WT and Rho-/- mice are indicated by the top and bottom dashed lines in Figure 5.16 respectively.

Experimental groups were stratified by baseline behaviour prior to transplantation so that there were no differences between mean behaviour of mice in the three treatment groups (Figure 5.16A). Following treatment, sham treated mice avoided light significantly less that mice in the MC treatment group

($p<0.05$) and rAAV2 Y444F group ($p<0.05$) (One way ANOVA, $F(2,18)=4.97$, $p<0.05$). No difference was observed between groups. An improvement over baseline behavior was also observed in both MC treated group ($p<0.01$) and rAAV2 Y444F group ($p<0.05$). A difference from baseline was not observed in the sham transplantation group (ns).

The number of transitions between the compartments of the test arena is used as a measure of anxiety in mice during this test[297,298], This was measured in order to assess whether differences in anxiety levels contribute to the difference observed between groups. The number of transitions between the lit and dark compartments did not differ between groups (One way ANOVA, $F(2,18)=0.53$, ns), indicating that the results described above are not likely to be caused by differences in anxiety levels between treatment groups.

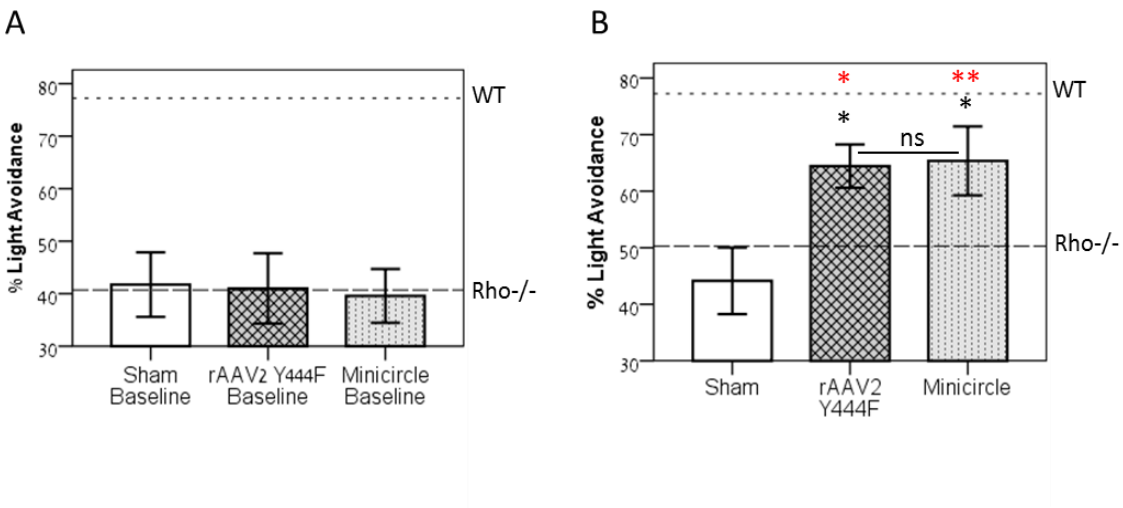

Figure 5.16: Behavioral light avoidance

A. Experimental groups were stratified by baseline behaviour prior to transplantation so that there was no difference in light avoidance in the three groups (One way AVOVA, F(2,18=0.05 ,ns). B. 9 weeks after transplantation the three groups differed in the amount of time spent in the dark compartment (F(2, 18)=4.97, p<0.05) so that mice in the sham transplantation group avoided light less than mice which were transplanted with cells following rhodopsin gene therapy delivered by minicircles (*p=0.036) and rAAV2 Y444F (*p=0.047). There was no difference in the behaviour of the two gene therapy groups (ns). One way ANOVA, Bonferroni correction for multiple comparisons, N=7 in each group. When comparing baseline behaviour to light avoidance behaviour following transplantation, a significant increase in light avoidance was observed in $Rho^{-/-}$ mice transplanted with cells treated by minicircle gene therapy (t=3.23, **p=0.007) and rAAV2 Y444F gene therapy (t=3.03, *p=0.013), but not in the sham transplantation group (ns) indicated by red significance stars. The top dashed reference line represents the mean light avoidance response of age matched WT mice and the bottom reference line represents the mean light avoidance response of age matched untreated $Rho^{-/-}$ mice. NS; not significant. Error bars represent ± 1 SEM.

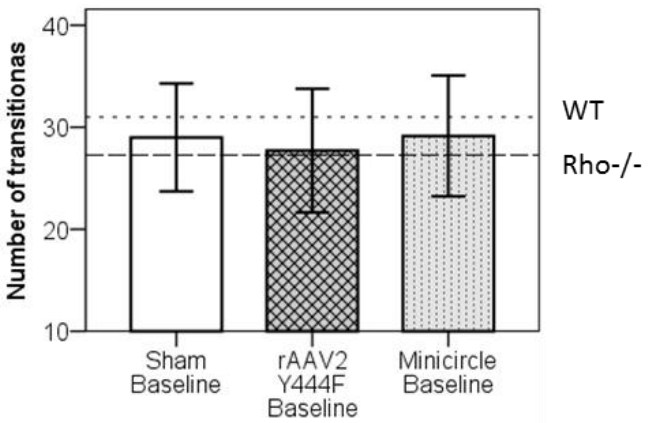

Figure 5.17: Anxiety related behaviour

Anxiety may modify the behaviour of mice and account for differences in result of the behavioural light avoidance test. To control for this variable anxiety related behaviour was measured specifically using the number of transitions between the compartments of the test arena. The numbers of transitions between the lit and dark compartments did not differ between groups following transplantation ($F(2,18)=0.53$, ns). One way ANOVA, $p<0.05$, $N=7$ in each group. The top dashed reference line represents the mean light avoidance response of age matched WT mice and the bottom reference line represents the mean light avoidance response of age matched untreated $Rho^{-/-}$ mice. NS; not significant. Error bars represent ± 1 SEM.

5.4.4.3. Restoration of optomotor response

Optomotor response (OMR) was tested to evaluate whether treated animals could respond to a dynamic stimulus. As mice received a unilateral transplantation of treated cells, the OMR was used to specifically evaluate

paired treated and untreated eyes in mice in response to a 1 cycle/degree rotating grating.

Groups were stratified by baseline behaviour so that there were no differences between groups and at baseline no head tracking behaviour was observed in any of the mice; mean responses were between zero and 1 head tracks per trial, which more likely represents a margin of error in this test rather than a behavioural response. Importantly, no preference for direction of head tracking was observed in animals at baseline so that head tracks were not more likely to occur in a clockwise or anti-clockwise direction (Figure 5.18A).

9 weeks following transplantation head tracking behaviour in response to the rotating grating was found in mice of both treatment groups (Figure 5.18B), with significantly more head tracks elicited by the treated eye compared to untreated eye in rAAV2 Y444F treated mice (paired t test, $t=4.5$, $p<0.01$) and MC treated mice (paired t test, $t=4.05$, $p<0.01$), but not in sham transplanted mice (paired t test, $t=0.47$, ns). Head tracking in the treated eye differed between the three groups (One way ANOVA, $F(2,18)= 8.77$, $p<0.01$), with an increased number of head tracks by animals in both gene therapy groups (both $p<0.01$). No difference was observed in number of head tracks per trial between MC and rAAV2 Y444F treated mice.

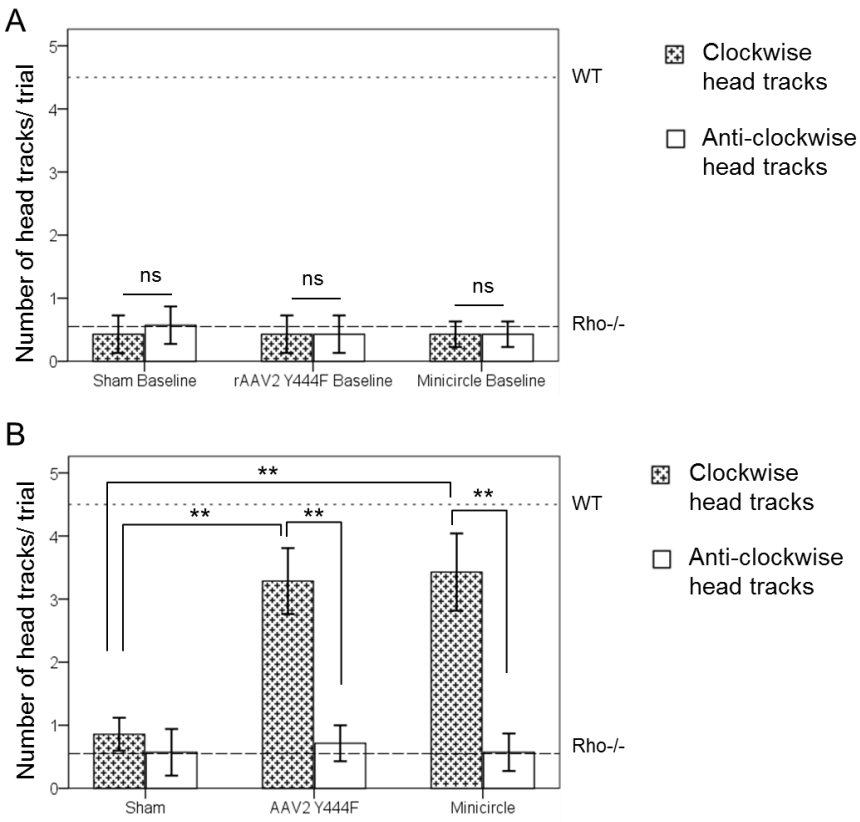

Figure 5.18: Optomotor response

The Optomotor head tracking response is elicited by the rotation of a grating, so that a clockwise rotation elicits a head track from the left eye and an anti-clockwise rotation elicits a response driven by the right eye. Comparison of mean number of clockwise and anticlockwise head tracks provides a measure of difference between paired eyes. A. Directionality bias was not observed in untreated mice (paired t test, all ns). B. Following unilateral transplantation to the left eye, mice of the rAAV2 Y444F group tracked the grating more when moving in the clockwise direction (driven by the treated eye) compared to anticlockwise direction (paired t test, t=4.5, **p=0.004) a similar difference was observed in the Minicircle group (paired t test, t=4.05, **p=0.007). Mice in the sham transplantation group did not differ in the number of clockwise or anticlockwise head tracks (paired t test, t=0.47, ns). Mean number of head tracks elicited by the treated eye was different between the three treatment groups (One way ANOVA, $F(2,18)= 8.77$, $p<0.01$), so that animals in the sham treatment groups tracked the grating less than mice in the AAV group (**p=0.007) and minicircle group (**p=0.005). One way ANOVA, Bonferroni correction for multiple comparisons, N=7 in each group. NS; not significant. Error bars represent ± 1 SEM.

5.4.4.4. Electroretinography

Analysis was conducted to compare MC and rAAV2 Y444F treatments with sham treatment and uninjected age matched Rho$^{-/-}$ mice. The protocol was applied also to age matched WT mice and results are shown for reference.

In order to detect rod mediated function, the amplitude of a and b wave responses to a flash of light were first measured under scotopic conditions following 12 hours of dark adaptation. Light intensity was gradually increased, with a delay between steps for rod sensitivity restoration. Under scotopic conditions, no difference was detected between the a-wave response in the treated eye of experimental groups and corresponding eye of untreated Rho$^{-/-}$ mice in the different light intensities (Two way ANOVA, F=1, p=0.4, ns). Similarly, no detectable difference was observed in b-wave amplitudes between the groups (F=0.47, p=0.7, ns) (Figure 5.19A). The absence of improvement in scotopic ERG response was expected, as mice lose scotopic b-wave ERG by 10 weeks[50,51,285], and following transplantation at 12-14 weeks, a very large number of rod cells would be required to restore this response. However, the question of cone photoreceptor involvement in the results described above required further investigation of cone mediated function in these mice, as a difference in cone function may imply that cells are effecting transplantation by means of cone neuroprotection, rather than rod regeneration. Following light adaptation, mice of the different treatment groups showed no difference in response to increasing intensity of light flashes under photopic conditions in

amplitude of a-wave (F=0.65, p=0.59, ns) or b-wave (F=0.73, p=0.53 ,ns) response (Figure 5.19B).

In order to further characterise the response of treatment groups, under scotopic condition, the amplitude of b-wave was measured in response to a flickering light stimulus in varying light intensities (1-10 cd.s.m^2) and frequencies (6-30Hz). As rod cells require a period of time for restoration of function following a flash of light, the response to the flicker stimulus would selectively represent cone sensitivity. No difference was found between the experimental groups in this experiment (all ns) in response to a flicker amplitude of 6Hz at a light intensity of 1 cd.s.m^2 (F=1.54, p=0.23) or 10 cd.s.m^2 (F=1.9,p=0.22) and flickering light of 20Hz (F=3.26 p=0.1) and 30 Hz (F=0.47, p=0.72) at 10 cd.s.m^2. (Figure 5.20A). Representative responses to the light flicker in the different groups are shown in Figure 5.20B.

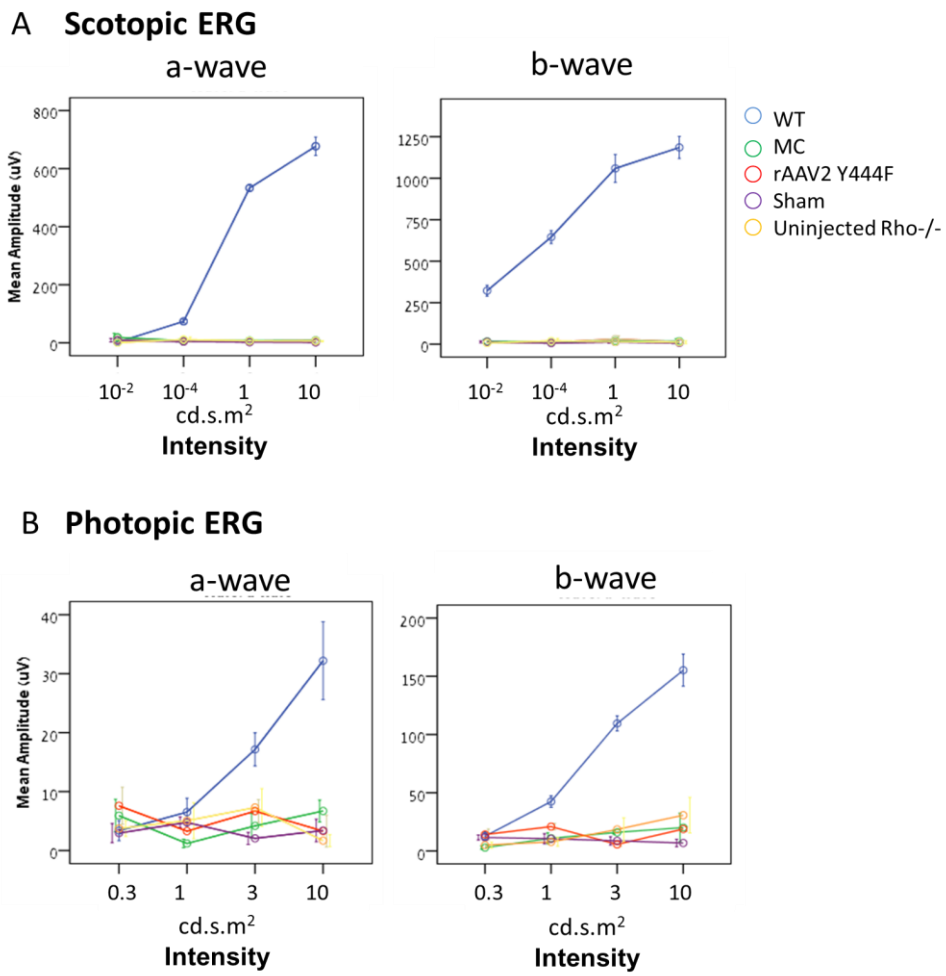

Figure 5.19: Electroretinography response to flash stimulus

A. Following dark adaptation, scotopic ERG recordings, aimed to assess rod photoreceptor function, showed no difference in a-wave responses in mice treated with MC, rAAV2 Y444F, sham transplantation or untreated Rho-/- mice ($F(6,43)=1$, $p=0.4$, ns). Similarly, no detectable difference was observed in b-wave amplitudes between these groups ($F(6,43)=0.47$, $p=0.7$, ns). B. Following light adaptation, a and b-wave amplitudes were measured in the experimental groups to assess cone photoreceptor sensitivity to an increasing light stimulus. Measures of a-wave amplitude in all groups were under 10μ, representing a margin of error in this test rather than a true response. There was no detectable difference between groups in this test in a-wave amplitude ($F(6,43)=0.65$, $p=0.59$, ns) or b-wave amplitude ($F(6,43)=0.73$, $p=0.53$,ns). Two way ANOVA, response amplitude and light intensity as factors. N=7 per group. Error bars represent mean ±1 SEM. Blue lines represent the response of age matched WT mice and are presented for reference.

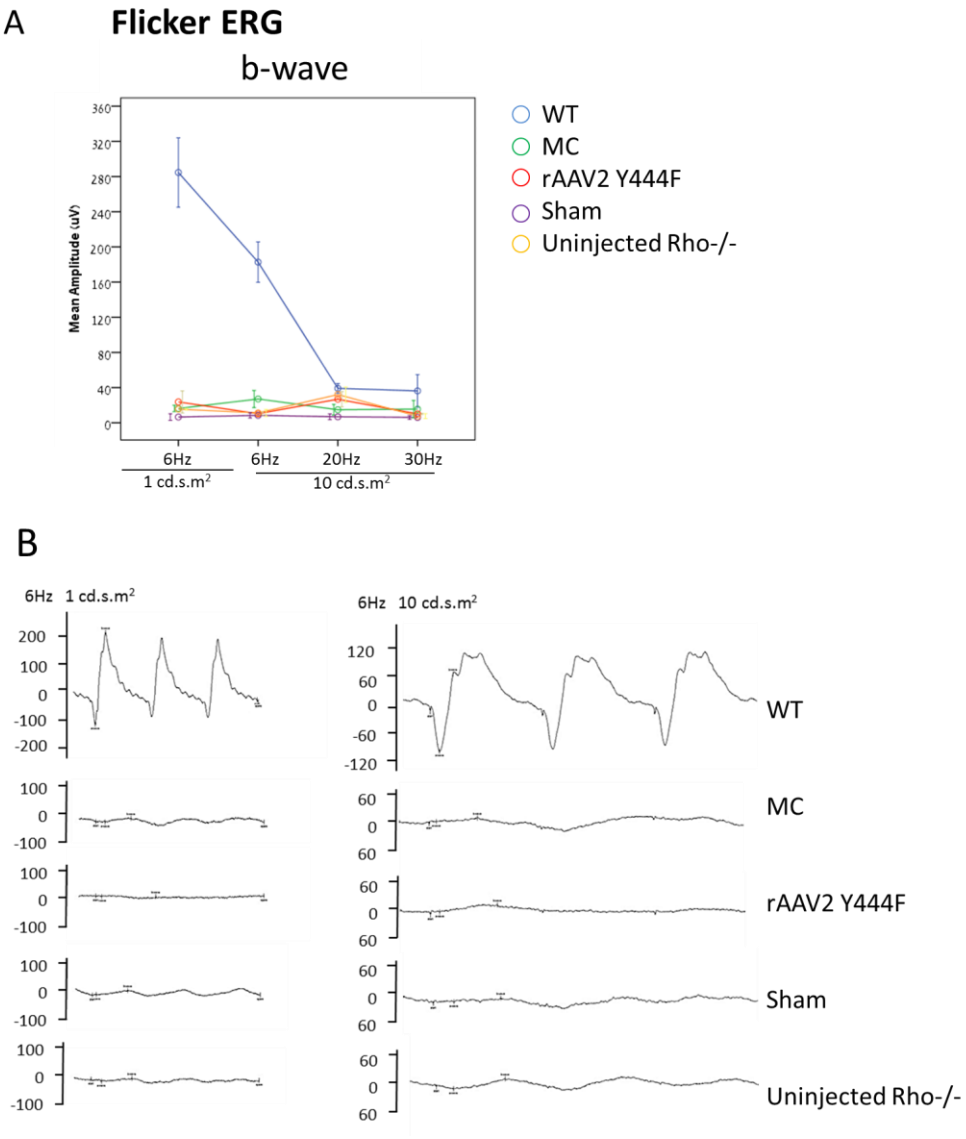

Figure 5.20: Electroretinography response to flicker stimulus

A. The b-wave response did not differ between groups in response to a flicker amplitude of 6Hz at a ligh intensity of 1 cd.s.m^2 (F=1.54, p=0.23 ,ns) or 10 cd.s.m^2 (F=1.9,p=0.22 ,ns) and flickering light of 20Hz (F=3.26 p=0.1,ns) and 30 Hz (F=0.47, p=0.72 ,ns) at 10 cd.s.m^2. One way ANOVA, N=7 per group. Error bars represent mean ±1 SEM. Blue lines represent the response of age matched WT mice and are presented for reference. B. representative b-waves elicited by the different experimental groups following a flickering light stimulus of 6Hz with a light intensity of 1 or 10 cd.s.m^2 showing the patterns of b-wave and in WT mice and in the experimental groups.

5.5. Discussion

Taken together, these data show that *rho-/-* cells which had been supplemented with the *RHO* gene *ex vivo* by both viral and non-viral methods survive and reconstruct the degenerate retina of the Rho-/- mouse. Transplanted cells express the rhodopsin gene, as well as other mature photoreceptor markers and while they do not assume normal cell morphology, they are able to restore functional and behavioural visual responses in treated animals. This data present the first evidence of retinal reconstruction and visual rescue by transplantation of genetically corrected photoreceptor cells. These data also provide the first account of highly efficient and sustained expression in photoreceptor cells by use of MC DNA.

3 months old $Rho^{-/-}$ mice were assessed prior to transplantation and were observed to display severe degeneration of the ONL. The groups were measured for functional and behavioural vision to show small pupil constriction in response to light in the PLR assay, no preference for light avoidance in the BLA test and no response in most animals to a dynamic stimulus during the OMR test. The low variability in animal responses in these three tests allowed successful stratification of three comparable groups to reduce the variability in experimental groups prior to transplantation.

Cells of $Rho^{-/-.Nrl.GFP}$ mice were dissociated, enriched in rod precursor cells and treated by AAV2 Y444F or MC DNA RHOK.RHO.IRES.DsRed with high cell viability prior to transplantation.

Ten weeks following transplantation, donor cells of both experimental groups repopulated the subretinal space of $Rho^{-/-}$, forming a distinct cell layer expressing both intrinsic GFP, which is driven in rod cells by the Nrl promoter and DsRed which was included as a marker gene in the gene therapy vectors. Both markers were localised in the cell cytoplasm and high levels of co-expression were detected in cells, indicating correct localisation of the delivered fluorescent marker in rod cells and sustained gene expression at this time-point.

Quantification of GFP and DsRed expression in cells was obtained and compared four weeks post transplantation and ten weeks post transplantation. In both time points the number of GFP positive surviving cells in the two gene therapy treatment groups was highly raised in comparison to the sham treated cells, but no differences in cell survival were observed between groups. In all groups less GFP positive cells were present in the subretinal space ten weeks following transplantation, reflecting loss of photoreceptor cells in the absence of immune suppression as time progressed[227]. However Dsred expression followed a different pattern; four weeks following transplantation, DsRed expression was higher in rAAV2 Y444F treated cells then in MC treated cells. This difference is consistent with DsRed expression levels observed in cells *in vitro* in chapter 4 and corroborates previous observations of more efficient expression of genes in the retina by viral vectors compared to non-viral vectors *in vivo*[168].

Ten weeks following transplantation, levels of DsRed expression were not significantly different between the gene therapy treatment groups. While percentage of DsRed expressing cells remained consistent in the AAV treatment group, expression levels in the MC treated group were elevated. This most likely does not reflect higher MC expression in this transplantation cohort, but may indicate that the cells degenerating in this group were cells which did not express the therapeutic gene. While photoreceptor cells transduced by AAV have been previously reported to survive *in vivo* following transplantation[73], this provides the first account of sustained gene expression in cells following MC DNA gene delivery.

Following detection of the DsRed fluorescent reporter gene in cells, the next level of assessment was to evaluate the restoration of the rhodopsin gene in treated cells. In both treatment groups, cells developed slender inner segments that could be detected by GFP, and the rhodopsin gene was expressed at these cell terminals, marking the outer segments (OS) of cells. Rhodopsin expression in cells with the rhodopsin null mutation in both treatment groups is necessarily attributed to the effect of gene therapy, as both donor cells and host animals do not express rhodopsin. Restoration of rhodopsin to cells suggests that rod precursor cells matured following treatment and could be functionally active. Correspondingly, other OS proteins were also detected in transplanted cells, outside of the cell cytoplasm, and expression of the pan-photoreceptor marker recoverin was highly observed in the cytoplasm of cells. Importantly, the OS which formed in donor cells did not assume normal cell

morphology or orientation towards the RPE. It has been previously shown that photoreceptor cells derived from healthy mice do not develop normal morphology post transplantation in the severely degenerate retina, but are still able to improve functional vision[62]. Moreover, photoreceptor cells that lack a fully formed outer segment were recently shown to support useful vision in mice[74], challenging the notion that normal photoreceptor structure is required in order to improve vision by cell transplantation.

Connectivity between the graft and host was next assessed, providing support for synapse formation and lack of complete glial barrier between the transplanted cells and host inner retina. Müller glia were detected to extend processes across the donor-host boundary, possibly structurally supporting the grafted cells and sustaining survival. It has been previously shown that glial scaring increases with age in mice with retinal degeneration, and this may impair cell survival following transplantation[70], however connectivity has been shown in transplantation into the severely degenerate retina with both single cell suspension[62] and 3D retinal organoids[89].

In order further to assess the connectivity of cells to the retina and downstream pathways in the brain, measures of functional vision were obtained. Results were compared between gene therapy treatment groups and animals transplanted with sham untreated $Rho^{-/-.Nrl.GFP}$ cells. The sham transplantation controls for the effects of surgery and cellular tropic effects without the additional effect of rhodopsin supplementation by gene therapy.

In order to study whether treated donor cells could lead to improvement of light-derived response or visual function, different aspects of the visual system were examined.

The pupil light reflex (PLR) assesses whether light impulses transmitted to the retina can travel to the brainstem via central targets, to feed into appropriate neural pathways and produce an arc reflex and consensual constriction of the contralateral eye. Three weeks following transplantation, the PLR of both groups improved over baseline. This improvement was further observed eight weeks following transplantation, with increased pupil constriction in both groups compared to sham transplantation. A greater degree of pupil constriction was observed in mice following MC treatment compared to rAAV2 Y444F treatment.

The difference between groups may imply greater efficiency of MC treatment in deriving this response, but may also be attributed to the different expression patterns of viral and non-viral vectors. AAV vectors have been shown to reach peak expression *in vivo* only weeks following subretinal transplantation[279,299], the full effect of rAAV2 Y444F gene therapy may require a longer time period for examination. The time-point selected for comparison of groups took into account the relatively long period of time required for gene expression by AAV gene therapy, together with previous observations that transplanted cells progressively degenerate *in vivo* post transplantation in absence of immune suppression[227] and that healthy photoreceptors were shown to degenerate within 3 months[62]. A time point of 8-10 weeks following transplantation was selected for comparison of groups, in order to maintain cells *in vivo* long

enough for robust gene expression by AAV, but not long enough for cells to degenerate.

The Behavioural light avoidance test (BLA) measures whether light can be detected to derive behavioural response in mice. Being nocturnal animals, mice tend to avoid bright environments and prefer to be in the dark. The tendency for light avoidance, together with the opposing tendencies for anxiety and exploratory behaviour were the basis of this test. While mice of all groups explored the arena with a similar amount of transitions between compartments, the two gene therapy groups spent a greater amount of time in the dark compartment compared to sham treated mice. There was no difference in the response of animals treated by MC or rAAV2 Y444F in this test. Both gene therapy groups displayed greater light avoidance following transplantation compared to baseline measurements obtained prior to transplantation, indicating restoration of visually guided behaviour following transplantation of treated cells. No improvement was obtained by the sham transplantation, further corroborating the specific effect of rhodopsin supplementation gene therapy on restoration of visual function.

The optomotor response was used to assess image forming vision and examine whether a dynamic stimulus could be detected by mice. Furthermore, as the optomotor head tracking response is contingent on the optokinetic nystagmus[233,235] in eyes, the directionality of head tracking indicates the eye from which the head track is derived[234]. While no preference for head track directionality was found in WT, untreated $Rho^{-/-}$ or sham transplanted mice, in

mice of the gene therapy groups, the treated eye elicited a markedly greater OMR response than the untreated eye. The degree of improvement in the OMR response was similar in both gene therapy groups and they were both higher that the sham transplanted mice. This test shows the specificity of restored visual function in the treated eyes in both treatment groups and that both treatments improved vision for detection of the difference between a static and dynamic stimulus at a visual acuity of 0.1 cycles/ degree.

An important consideration in design of these tests was the selective assessment of vision resulting from transplanted rod photoreceptor cells. The three classes of light sensing cells that may be involved are the rod and cone photoreceptors and the newly discovered class of photoreceptors, the intrinsically photosensitive retinal ganglion cell (ipRGC)[294] which are located in the inner nuclear layer and may still be present and contribute to vision in mice following degeneration of the ONL.

Functional experiments were thus designed to avoid contribution of ipRGCs or remaining host cone photoreceptors and isolate the specific response of donor rod cells.

In the PLR protocol a brief flash of light (100 ms) was administered as the stimulus, as ipRGC have been reported to integrate light signals over a period of time[300]. The time selected for analysis was 1 second following the offset of the light stimulus. A time point between 0-2 sec has been previously validated to isolate the response of classical photoreceptors over ipRGC[62,287], and thus a

relatively early period within this time frame was selected for detection of early phase pupil constriction following dark adaptation, which would selectively represent the sensitivity of donor rod photoreceptors.

In the BLA and OMR tests, the light stimulus was constant throughout the test period; in principle, the period of testing would allow for sufficient time for involvement of ipRGCs in the visual response. To overcome this problem, a LED array emitting a green light centred at 510 nm was used. This is closer to the wavelength of maximal rod sensitivity rather than that of ipRGCs (480nm). Additionally, a dim level of light was used (approximately 10 lux at the centre of each arena) which is closer to the scotopic level of light and therefore more adapted to rod response over that of cones or ipRGCs.

Electro retinal function was measured by electroretinography (ERG) and showed no improvement of rod function under scotopic conditions following treatment with rAAV2 Y444F or MC over sham transplantation or age matched untreated $Rho^{-/-}$ mice. A positive result in relation to this study was that no differences were found between groups in response to a continuous bright stimulus or in light stimuli following light adaptation. The lack of response in photopic conditions indicates the loss of detectable cone cell function in animals of all groups and provides evidence that the responses observed in previous testing can be reliably attributed to transplanted treated rods and not to neuroprotection of host cones. Importantly, the absence of an ERG response is not indicative of absent circuit formation by transplanted cells. Since the ERG is a vector response resulting from the summation of

synchronous electrical changes arising from many individual cells, a very large number of radially-aligned photoreceptors is needed to achieve an a-b wave. In humans, RP patients lose their ERG response early on, at a time when they still maintain excellent visual acuity, and so being without an ERG does not equate to having no vision[301] . The relatively low number of transplanted cells may more reliably allow assessment of vision by the functional and behavioural methods previously described in this chapter.

5.6. Conclusions

Taken together, the results presented in this chapter show that transplantation of rho$^{-/-}$ rod precursor cells following *ex vivo* gene supplementation of rhodopsin can reconstruct the ONL of adult Rho$^{-/-}$ mice and restore visual function in these blind mice. The results obtained by viral gene therapy via rAAV2 Y444F were similar to those obtained with non-viral gene therapy via minicircle (MC) DNA and represent the first successful transplantation of *ex vivo* gene-corrected photoreceptors in a disease specific model of RP.

Rod cells survived *in vivo* 10 weeks following transplantation, forming a new layer between the host INL and RPE, in place of the lost ONL and expressed the rhodopsin gene, which was absent in cells prior to *ex vivo* gene therapy. The newly formed layer of cells developed outer segments (OS) which were morphologically distinct from WT OS but expressed rod specific markers.

Reconstruction of the degenerate retina by treated cells led to the restoration of visual function and visually guided behaviour as shown by the PLR, BLA and OMR assays, in mice that were blind at baseline. Mice did not show improvements in scotopic or photopic ERG function, providing a measure to exclude the involvement of a tropic effect on host cones and specifically attributing the improvement of visual function to transplanted rod cells.

These results provide the first account of retinal reconstruction and restoration of visual function by photoreceptor cells following *ex vivo* gene therapy. MCs have not been previously used for treatment of photoreceptors, hence sustained expression and the similar results obtained by rAAV2 Y444F and MC treatments provide a robust novel method for non-viral gene delivery to photoreceptor cells.

Taken together these results show successful transplantation of genetically corrected rod precursors in a model of retinal disease and afford a foundation for the development of *ex vivo* gene therapy in human photoreceptor precursors.

6. Transplantation of Photoreceptors Derived from Human Pluripotent Stem Cells

6.1. Introduction

Retinitis pigmentosa (RP) is one of the leading causes of untreatable blindness. It is characterized by degeneration of rod photoreceptors followed by gradual loss of cones[16]. Mammalian photoreceptor cells do not have the capacity to regenerate and once they are lost, light is no longer perceived. At present, there is no treatment to regenerate lost photoreceptors in humans, and retinal degeneration accounts for most untreatable forms of visual impairment and blindness in the developed world.

Pre-clinical studies in animals have shown that transplantation of post mitotic photoreceptor precursor cells could provide a promising therapeutic strategy to replace lost photoreceptors. Improvement of visual function following

photoreceptor cell transplantation in animal models with a varied range of retinal dysfunction has been described[62,70-73]. In the previous chapters, the *ex vivo* treatment and transplantation of genetically defective photoreceptors was presented, to demonstrate restoration of visual function in a disease-specific model of RP.

However, for clinical application, post mitotic human photoreceptors do not represent an obtainable source of cells for cell replacement, as they develop only in the second trimester of pregnancy[108,109]. In order to obtain an expandable source of cells for transplantation, in vitro differentiation of human pluripotent stem cells (PSC) may be directed to obtain retinal tissue, and specifically photoreceptor precursors for the treatment of RP.

In the early embryo, pluripotent embryonic stem cells (ESC) can differentiate into all types of somatic cells. Every nucleated cell in the body (excluding gametes and some immunological cells) contains the same genomic DNA, and different cell types gain their unique characteristics by sequential regulation of distinct genes during development. These epigenetic changes to chromosomal DNA regulate access of transcription factors to specific genes, providing appropriate molecular switches required for cell division, growth and finally specific cell function[77]. Adult somatic cells can be reprogrammed to regain stem-cell like pluripotency through over-expression of defined transcription factors.

In a milestone study by Takahashi and Yamanaka in 2006[108], mouse somatic cells were first reprogrammed to create induced pluripotent stem cells (iPSC)

by over-expression of four transcription factors, namely octamer-binding transcription factor-3/4 (OCT3/4), SRY-related high-mobility-group (HMG)-box protein-2 (SOX2), c-MYC and Kruppel-like factor-4 (KLF4), followed by generation of iPSCs from human adult fibroblast cells using the same four transcription factors[302]. Since these first experiments, variations in cell reprogramming protocols have been largely explored, mostly with the aim of reducing the induction of potentially oncogenic factors, specifically c-Myc and KLF4 into the genome[303-310]. Retro- and lentiviruses have been the main delivery method chosen to overexpress reprogramming factors to induce pluripotency in somatic cells, but as previously mentioned; these methods have a drawback of integrating foreign DNA into the reprogrammed cell genome, thus presenting a threat of unpredictable effects of random DNA integration. Therefore methods to reduce or avoid viral integration have been sought by replacing viral vectors with non-integrating plasmids[307,311], episomal vectors[307,312], excisional techniques[313,314], direct delivery of reprogramming protein[315], minicircle DNA[224] and miRNA reprogramming[316] , to name a few.

ESC and iPSC have been studied extensively in the field of retinal regeneration[45,71,73,75,80,82,88-91,96,99,101,104,105,109,112-117,119,150,153,317-333]. *In vitro* retinal differentiation from ESC or iPSC largely imitates developmental landmarks of *in vivo* differentiation in health and disease[45,121,122].

In the developing human embryo at 4-5 weeks, the optic vesicle evaginates from the diencephalon of the neural tube and folds to form the optic cup. After disconnection of the lens vesicle, two layers of tissue form separately: the RPE

progenitor outer layer which expresses PAX6 and the basic-helix-loop-helix-zipper transcription factor gene MITF[334], and the neural retina progenitor layer which expresses PAX6 and the transcription factor gene RX[335]. Later in development, photoreceptor precursors express the homeobox gene CRX and eventually mature to express the pan-photoreceptor marker Recoverin[335]. The neural retina progenitor layer differentiates into the seven principal neural retinal cell subtypes, namely ganglion cells, horizontal cells, amacrine cells, cone photoreceptors (opsin+), bipolar cells, rod photoreceptors (Rhodopsin+/NRL+) and Müller glia, in a sequential fashion[116].

In order to mimic natural development, *in-vitro* differentiation of retinal cells from ESC and iPSC require orchestration of sequential induction steps, amongst which are the inhibition of BMP and Wnt signaling[336-340], the initiation of IGF-1 in eye field development[341] and Notch inhibition in photoreceptor development[342].

Accordingly, differentiation protocols were established for animal as well as human ESC, employing extrinsic chemical signalling pathways to direct cell fate into retinal progenitor cells (Pax6+/Rx+) by Wnt and Nodal inhibition[343], or differentiation towards photoreceptors by addition of retinoic acid and taurine to formerly established culture media[105,117]. Additional protocols emerged inducing photoreceptor-precursor differentiation by recombinant noggin (a BMP inhibitor), IGF-1 and Dickkopf-1 (Dkk-1) (an antagonist of the Wnt/β-catenin signalling pathway)[113]. Following work with ESC, related protocols were

directed to differentiate retinal cells from iPSC, generating both photoreceptor and RPE phenotypes[45,75,114,319,320,325,332,333].

In the past decade, progress has been made in differentiation of pluripotent cells towards retinal neural linages, including photoreceptor cells [104,113,117,323], retinal ganglion cells [106,344], bipolar cells and amacrine cells[120]. Photoreceptors derived from animal ESC or iPSC[117] [73,112-114,117,323,345] and human ESC or iPSC[73,104,105,116,302,306,325,345] have been generated as candidates for disease modeling and photoreceptor cell replacement therapy.

Studies suggested that pluripotent stem cell-derived photoreceptors may engraft in a remaining host ONL after transplantation[73,75,87,114] and express rod photoreceptor markers[73,75,87,114,346,347], but this was not achieved in end stage degeneration in the absence of a host ONL, as would be most clinically relevant.

Furthermore, previous studies generated a mixed population of retinal cells and thus either transplanted varied retinal cells, without selection for photoreceptors[73] or alternatively required further purification steps, such as transduction of photoreceptor cells by a fluorescent marker, followed by fluorescence activated cell sorting (FACS), which critically impaired cell survival[114] and is undesirable for human therapy. The surface antigen CD73, has been used as a marker to enrich murine photoreceptor precursors by magnetic-activated cell sorting (MACS) [125,126,240,348], though extrapolation to human cells remains unproven.

The first clinical trials using human pluripotent stem cells to treat vision loss commenced in 2011[349]. Human ESC-derived RPE cells were transplanted into patients suffering from macular degeneration. Medium- to long-term safety, graft survival, and possible biological activity of hESC-RPE in individuals with age related macular degeneration (AMD) and Stargardt disease were recently reported using these hESC-derived cells[328,329]. Similarly, a clinical study using human iPSC-derived RPE cells to treat wet-AMD patients was initiated in 2014. The goal of these various clinical trials was primarily to assess safety, but in the long term also to prevent the loss of photoreceptors. However, photoreceptor cell replacement for blindness initiated by photoreceptor loss in forms of RP is not yet underway and there is a critical need for an efficient methodology to generate clinical grade photoreceptor precursor cells and assess the possibility for such cells to restore function in the completely degenerate retina.

A clinically-adaptable method of providing homogeneous populations of human photoreceptor precursors was recently developed by our collaborators at the biotechnology company Ocata Therapeutics Inc., using a completely serum-free and feeder-free direct differentiation system aimed at differentiation of a population of clinical grade photoreceptor precursors from both ESC and iPSC cell lines. This synchronized differentiation process generates photoreceptor precursors homogeneously expressing photoreceptor-precursor specific genes in over 90% of cells, and able to further mature in vitro and form photoreceptor-like cells (Unpublished data. The methods used by Ocata Therapeutics for cell differentiation and the results obtained are presented in detail in the Appendix).

ESC and iPSC-derived photoreceptor precursor cells developed by Ocata therapeutics were cryopreserved and sent to our lab. In this chapter, the transplantation of these human photoreceptor precursors into the completely degenerate retina in a mouse model of RP is investigated.

Rd1 mice were used as a host model of rapid and progressive RP with end-stage retinal degeneration. In these mice, retinal degeneration is caused by a null mutation in the rod photoreceptor cyclic GMP (cGMP) phosphodiesterase β subunit (pde6b) gene[53,54]. Most rod photoreceptor cells are lost by 3 weeks of age[350], followed by progressive rod and cone photoreceptor degeneration over the first 8 weeks of life[61] with absence of a functional ONL by 6-10 weeks of age[62,89].

6.2. Aim

The aim of the work reported in this chapter was to assess whether human ESC and iPSC-derived photoreceptor precursors could survive following transplantation and mature in the subretinal space of mice with end-stage outer nuclear layer (ONL) degeneration and whether these human cells are able to interact with residual retinal host circuitry to restore visual function in blind mice.

The objectives relating to these aims were as follows

1. Recovery of cryopreserved human cells and cell labelling prior to transplantation

2. Assessment of human ESC and iPSC-derived photoreceptor cell survival following subretinal transplantation in immune suppressed mice

3. Assessment of human ESC and iPSC-derived photoreceptor cell maturation in vivo

4. Assessment of visual function restoration in adult rd1 mice

6.3. Methods

6.1.1 Animals

Wild type (WT) C57BL/6 mice were provided by the Biomedical Sciences Division, University of Oxford. C3H/HeNHsd-Pde6b^{rd1} (*rd1*) mice were purchased from Harlan Laboratories (Hillcrest, UK) and genotyped to verify the rd1 mutation. Mice were all female and were 10-12 weeks old at the time of subretinal injection.

6.1.2 Immune suppression

Mice were immune suppressed by addition of cyclosporine A (50 mg/kg/day) and 5% fruit cordial to the drinking water[227] for 2 days prior to and 3 weeks following transplantation.

6.1.3 Cell recovery and transfection

Stem cells derived photoreceptor precursors (PhRP) were cryopreserved and maintained in liquid nitrogen. 72 hours prior to transplantation cells were thawed, transferred to 10cm Ultralow binding plates (Corning®) and cultured in NDM at 37 °C to form PhRP neural spheres. After 24 hours in culture cells were transduced via recombinant adeno associated virus (rAAV) serotype 2 expressing GFP specifically in photoreceptor cells via the rhodopsin kinase (RHOK) promoter at a multiplicity of infection (MOI) of approximately 10^5vg/cell.

After 48 hours PhRP neural spheres were dissociated with Accutase (Innovative Cell Technologies, Inc.) and filtered through a 40 µm cell strainer (BD FalconTM). Cells were re-suspended to a final concentration of 10^5 cells/µl balanced salt buffer for injection.

6.1.4 Subretinal transplantation

Subretinal transplantations were performed as detailed in Chapter 2. 2µl of diluted cells (approximately 2×10^5 cells) were transplanted in each injection, or buffer (PBS) was delivered unilaterally into the subretinal space of the right eye.

6.1.5 Behavioural and functional assessment

Mice were assessed 3 weeks following transplantation by use of the Optomotor Response test (OMR) and Behavioral Light Avoidance test (BLA) as described in chapter 2.

6.4. Results

6.1.6 Recovery and labelling of human photoreceptor precursors

6.1.6.1 Recovery and culture of H9-ESC and HA-IPSC photoreceptor precursor cells (PhRP).

Photoreceptor precursor cells (PhRP) derived from H9-ESC and HA-IPSC cell lines were received following cryopreservation and were maintained in liquid nitrogen in preparation for transplantation. Cells were thawed and recovered as described in Chapter 2 to form neural spheres in vitro 48 hours following thawing (Figure 6.1), and were recovered to retrieve >95% viable cells following cell dissociation, comparable to cell numbers quantified prior to cryopreservation (3-6 million cells/ vial). Distinct cell spheres were consistently recovered from both ESC and iPSC derived cryopreserved cells (Figure 6.1A-B), however a difference in cell size and morphology was apparent (Figure 6.1C-D). These differences represent variability of cell lines in vitro, but did not affect cell viability following dissociation of spheres.

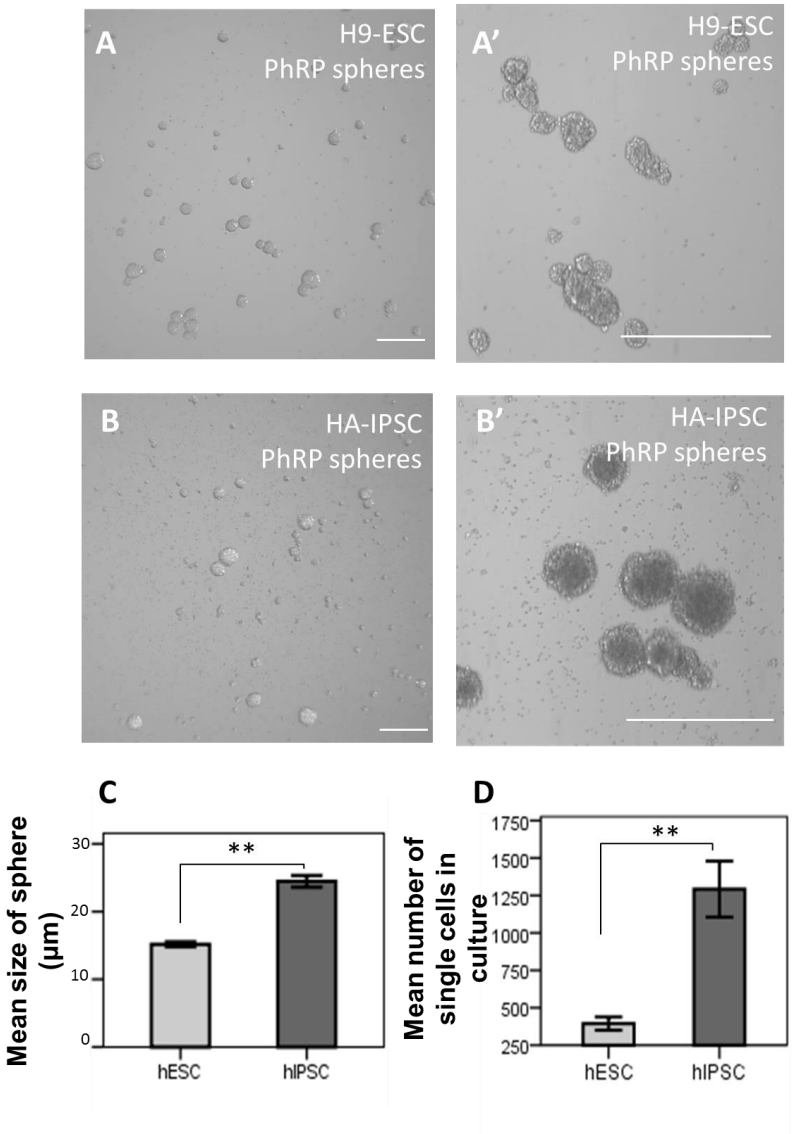

Figure 6.1: Recovery of human ESC and iPSC derived PhRP neural spheres

A-A'. H9-ESC derived neural spheres in culture. B-B'. HA-IPSC derived neural spheres in culture. Scale bar, 100µm. C. Mean size of H9-ESC derived neural spheres was significantly smaller than that of HA-IPSC derived neural spheres ($t=11.3$, $p<0.001$). D. Mean number of single cells, which were not included in a sphere was also significantly smaller per field of view (300µm) in H9-ESC culture compared to HA-IPSC ($t=4.67$, $p<0.001$). Error bars represent mean ± 1 S.E.M of 3 biological replicas (4 technical replicas each). ESC, Embryonic stem cells; iPSC, induced pluripotent stem cells; PhRP, photoreceptor precursor.

In order to discern transplanted human cells following transplantation, photoreceptor precursor (PhRP) neural spheres were transduced by a recombinant serotype 2 adeno associated virus (rAAV2/2) expressing GFP under the photoreceptor specific rhodopsin kinase promoter (RHOK). GFP expression was achieved in vitro 7 days post transduction in 70-90% of both H9-ESC (Figure 6.2A) and HA-IPSC (Figure 6.2B).

To reduce culture time prior to transplantation, and validate the contained transduction of donor cells by AAV, PhRP derived from H9-ESC (ESC-PhRP) cells were subretinally transplanted to WT mice and rd1 mice (n=4 per group) 48 hours post transduction, before GFP was expressed in cells. 7 days post transplantation; cells express GFP in vivo and were observed in the subretinal space of adult wild type mice (Figure 6.3A) and rd1 mice (Figure 6.3B) without transduction of the host inner nuclear layer (INL). Hence for further transplantations, PhRP spheres were transfected with GFP 24 hours after thawing and transplanted 48 hours thereafter.

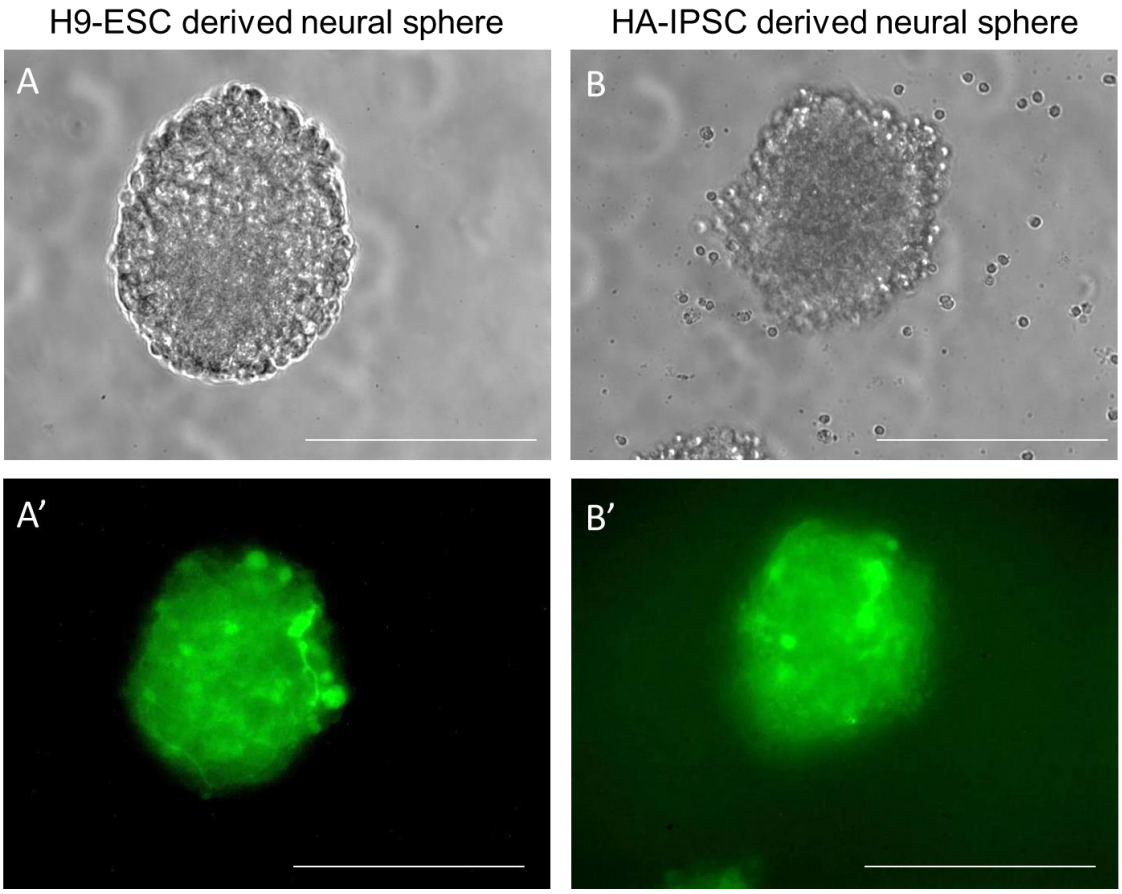

Figure 6.2: in vitro GFP transduction of human ESC and iPSC

A. H9-ESC PhRP sphere and B. HA-iPSC spheres. GFP was induced specifically in photoreceptor cells by AAV serotype 2 driving GFP by a rhodopsin kinase promoter. GFP expression was achieved in vitro 7 days post transduction of PhRPs derived from both H9-ESC (A') and HA-iPSC (B').

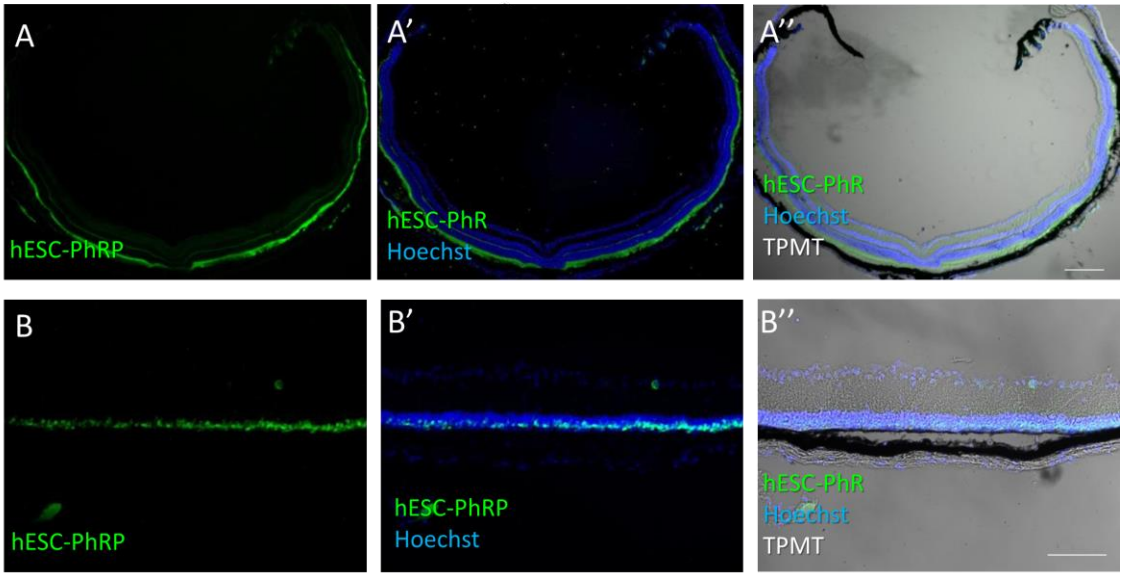

Figure 6.3: in vivo GFP expression in transplanted ESC-PhRP

Human cells were transplanted 48 hours post GFP and assessed 7 days post transplantation for validation of specific donor cell transduction and in vivo onset of GFP expression. A. GFP expressing cells were observed in the subretinal space of wild type mice, without transduction of the host inner nuclear layer (INL). B. following transplantation to *rd1* mice a distinct layer of GFP+ cells was observed between the INL and retinal pigment epithelium (RPE). Scale bar, 100µm.

6.1.7 Human PSC-derived PhRPs survived in severely degenerated subretinal space of *rd1* mice

The *rd1* mouse was used as model of progressive RP. In this model most photoreceptors are lost by 3-4 weeks of age [350], followed by progressive degeneration and loss of the ONL, by 6-10 weeks of age[62,89]. Human pluripotent stem cell (PSC)-derived PhRPs were transplanted into the subretinal space of *rd1* mice aged 10-12 weeks, at the end-stage of ONL

degeneration (Figure 6.4 compares *rd1* and WT retinal structure at 10 weeks). To prevent immune-rejection of human cells, immunosuppression with cyclosporine A was administered to host rd1 mice[96,227], starting 2 days prior to transplantation and continuing throughout the experiment.

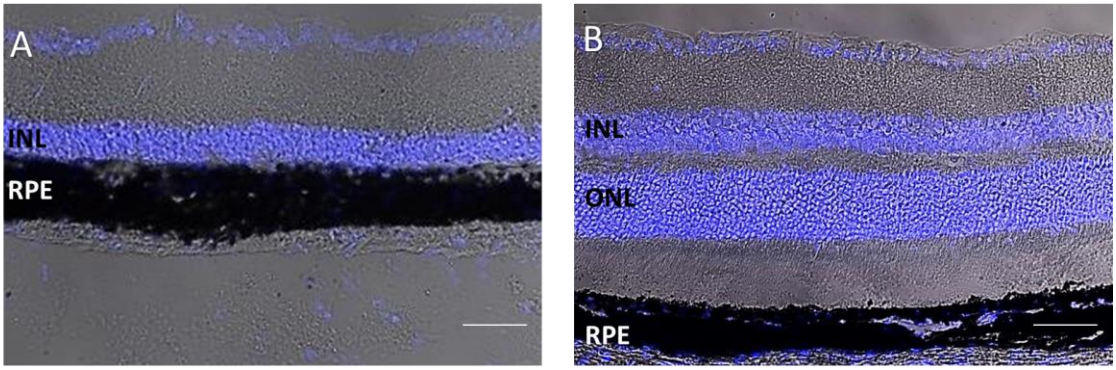

Figure 6.4: The rd1 retina at 10 weeks of age

A. The retina of an *rd*1 mouse at 10 weeks, compared to B. The retina of a wild type mouse at 10 weeks. In the rd1 mouse the ONL is completely lost by 10 weeks of age and there is no remaining layer of cells between the INL and RPE. Scale bar, 100µm. INL, inner nuclear layer; ONL, outer nuclear layer; RPE, retinal pigment epithelium.

A first group of *rd1* mice received transplantation of H9 ESC-derived photoreceptor precursor cells (ESC-PhRPs), a second group received transplantation of HA iPSC-derived iPSC-PhRPs photoreceptor precursor cells (iPSC-PhRPs) and a third group received a sham transplantation of PBS (n=8 per group, unilateral injections). To control for cell survival and differentiation, a further group of rd1 mice (n=5) received transplantation of undifferentiated H9

ESC-derived retinal neural precursor cells (RNPCs). All cells were transduced by rAAV2/2 Y444F.GFP prior to transplantation. To further control transduction of the host retina by a free AAV particles, the buffer used to wash AAV off the PhRPs before transplantation was kept and injected bilaterally into the subretinal space of another group of *rd1* mice (n=2).

Three weeks post transplantation, a distinct and robust layer of fluorescent cells was observed in vivo by scanning laser ophthalmoscopy (SLO) in animals injected with ESC-PhRPs (Figure 6.5A) and iPSC-PhRPs (Figure 6.5B), but not in the transduction control group (Figure 6.5C), confirming that observed GFP+ cells were indeed donor-derived and not a result of transduction of host retina.

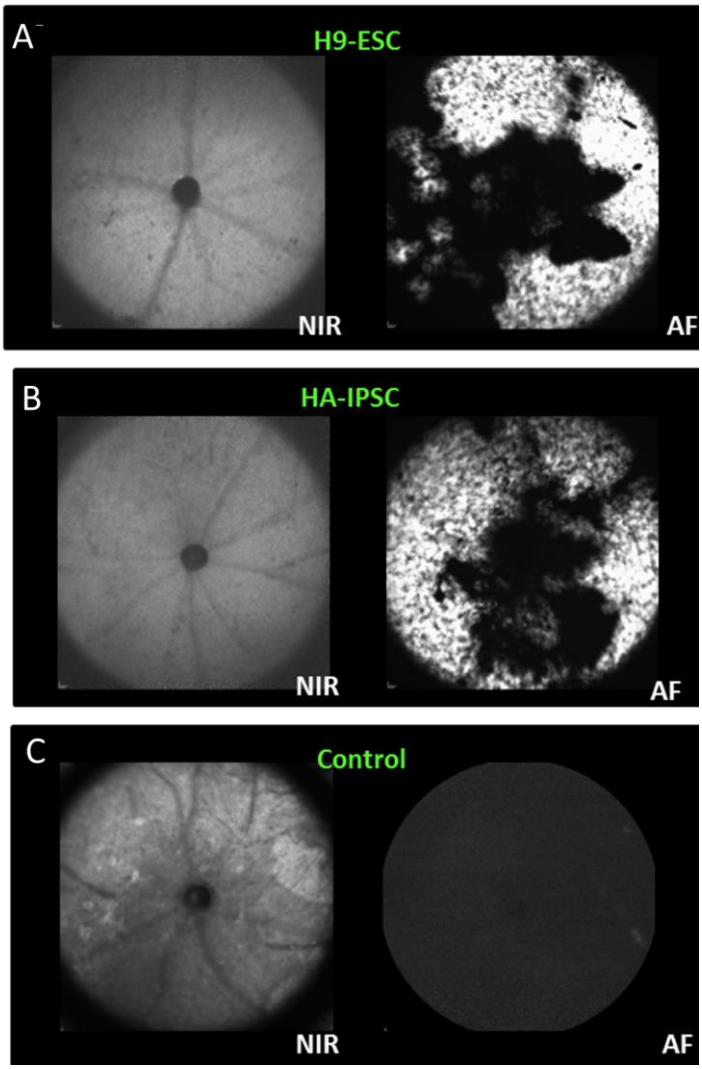

Figure 6.5: Transplanted ESC-PhRPs and iPSC-PhRPs Survive in the Subretinal Space of *rd1* Mice.

Scanning laser ophthalmoscopy (SLO) was performed in vivo three weeks post transplantation to assess the extent of surviving donor cells; GFP positive cells are observed in AF mode as white dots or clusters (black areas represent areas of retina which were not seeded with transplanted cells, due to incomplete detachment of the retina around the optic nerve head). Representative NIR and AF fundus images of *rd1* mice show a strong presence of GFP+ cells in the two treatment groups: A. ESC-PhRPs and B. iPSC-PhRPs. C. The buffer used to wash AAV off PhRP cells prior to transplantation was kept and injected bilaterally into the subretinal space of *rd*1 mice (n=2). No GFP was observed in AF imaging of this control group, indicating that GFP observed in vivo in treated animals was indeed a marker for transplanted human PhRP cells. NIR= near-infrared; AF= autofluorescence.

In the same mice, histology revealed human cells residing in the subretinal space of animals in both ESC-PhRP and iPSC-PhRP treated groups three weeks post-transplantation (Figure 6.6). On average 6.45 ± 1.1% (mean ±1 S.E.M) of transplanted ESC-PhRPs and 5.7 ± 1% of iPSC-PhRPs survived per animal, (n=8 specimens each). Similar to a previous report[62], transplanted PSC-PhRPs in this study developed processes to interact with host circuitry, but were distinct from host cells (Figure 6.6C) and did not adopt the normal morphology and orientation as described when retinae with a residual ONL were treated with mouse rod precursors[67,72,351,352] or human photoreceptor cells[73]. Under 0.001% of GFP-RNPCs, which were transplanted as a control for cell survival, were observed in the subretinal space of *rd1* mice, and were only evident in eyes of 2 of 5 transplanted animals.

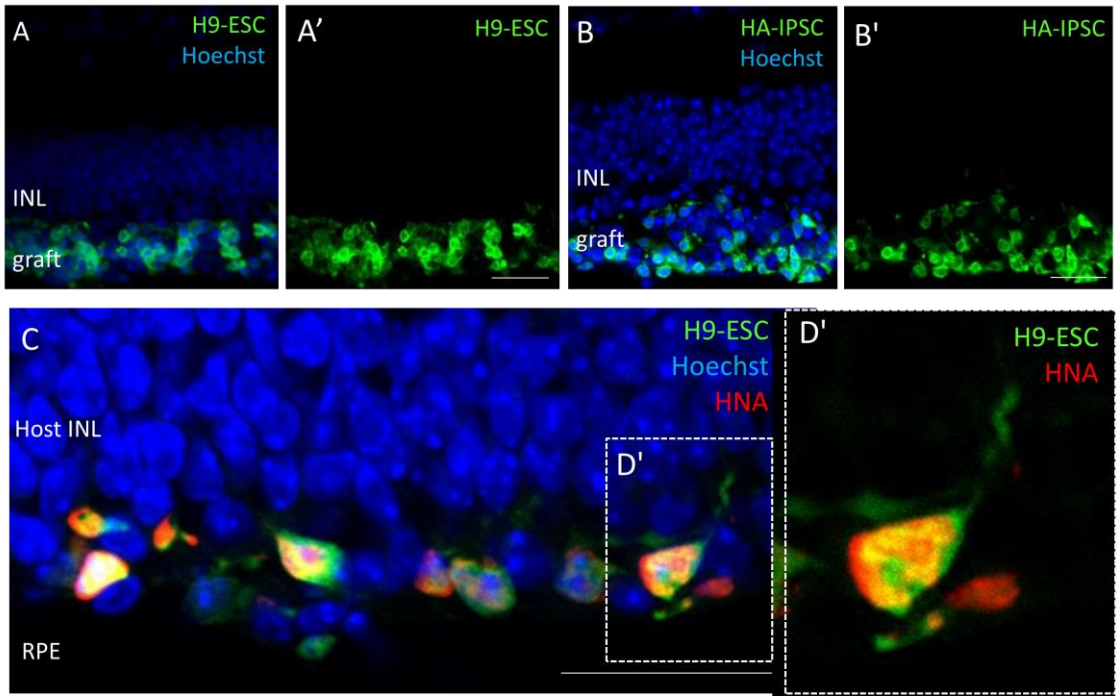

Figure 6.6: Transplanted ESC-PhRPs and iPSC-PhRPs reconstruct the ONL of adult rd1 mice

A-B. Histological assessment 3 weeks post transplantation revealed ESC-PhRP (A-A') and iPSC-PhRP (B-B') derived cell layers (Green) between the RPE and INL of the *rd1* retina, replacing and reconstructing the absent outer nuclear layer (ONL). D. Retinal sections were stained with human nuclear antigen (HNA) revealing expression and correct localisation of this human nuclear marker in GFP expressing cells. D'. Magnified image of transplanted H9-ESC derived cells stained with HNA, showing that human cells developed processes, but did not adopt normal photoreceptor morphology or laminated inner and outer segment structures pointing towards the RPE. Scale bar, 25µm. RPE, retinal pigment epithelium; INL, inner nuclear layer; HNA, human nuclear antigen.

6.1.8 Transplanted human PSC-derived PhRPs mature in vivo

Three weeks post transplantation, ESC-PhRPs and iPSC-PhRPs examined by immunohistochemistry, expressed mature photoreceptor proteins, including the pan-photoreceptor marker recoverin (Figure 6.7A and 6.7B, respectively).

The rod-specific cGMP phosphodiesterase β6 (PDE6β) was observed in the outer processes of transplanted cells (Figure 6.8A-B); a deficit in this phototransduction-enzyme is the underlying cause of retinal degeneration in the *rd1* mouse, confirming its expression by donor rods. The rod-specific protein rhodopsin was also expressed by human cells (Figure 6.8C-D). Localisation of rhodopsin and PDE6β proteins was correctly confined to the developing outer segments (OS) of cells, demonstrating OS formation and maturation of human rod cells in the degenerate rd1 subretinal niche.

The cone-specific protein cone arrestin (Fig. 5g-h) was also expressed in transplanted cells of both treatment groups. These observations indicate differentiation of human PhRPs towards rod and cone photoreceptor-like cells.

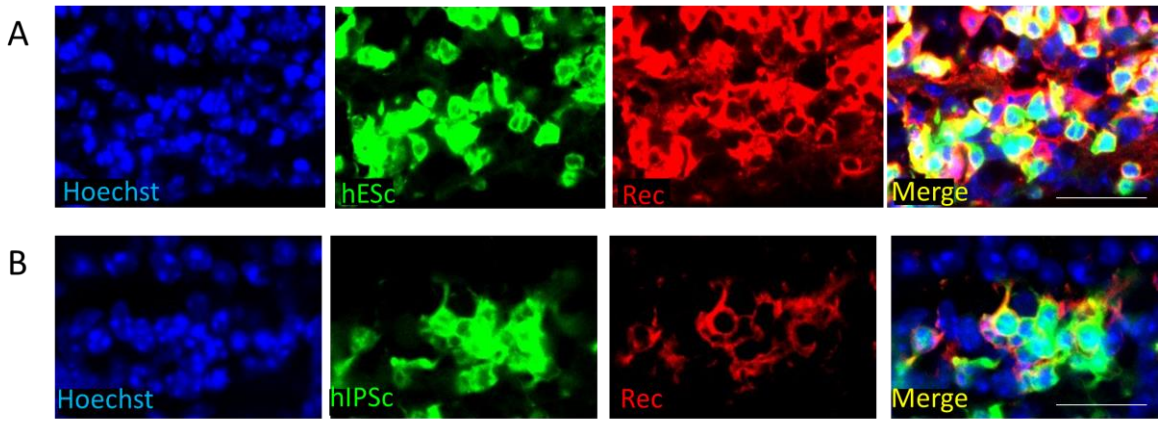

Figure 6.7: Expression of the pan-photoreceptor marker recoverin in transplanted human cells

The pan-photoreceptor marker recoverin was observed in the cytoplasm of transplanted cells within the graft in animals treated with both ESC-PhRPs (A) and iPSC-PhRPs. (B). Scale bar, 25μm.

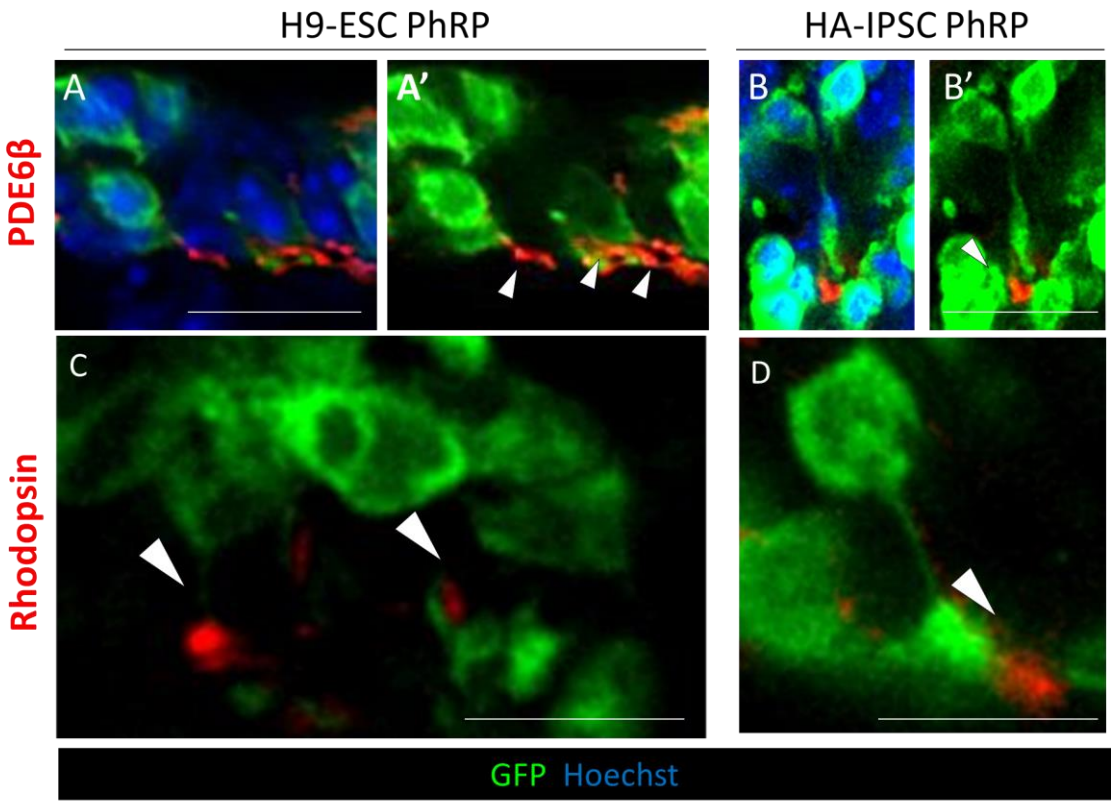

Figure 6.8: Expression of mature rod photoreceptor markers in transplanted human cells

Immunofluorescence staining 3 weeks post transplantation shows expression of mature rod photoreceptor markers localised in the developing outer segment (OS) of transplanted human PhRPs (Green). In all images cells are located in the subretinal space and oriented so that the host inner nuclear layer (INL) is located at the top of the image and the retinal pigment epithelium (RPE) at the bottom. A-B. The rod specific enzyme phosphodiesterase β6 (PDE6b), which is necessary in phototransduction and is absent in *rd1* mice due to mutation is reinstated in the retina and located in the outer processes of transplanted ESC-PhRPs (A-A') and iPSC-PhRPs (B-B'). The rod specific protein rhodopsin which is normally located in outer segment membrane disk was observed in outer segments of ESC-PhRPs (C) and iPSC-PhRPs (D). Scale bar 20μm.

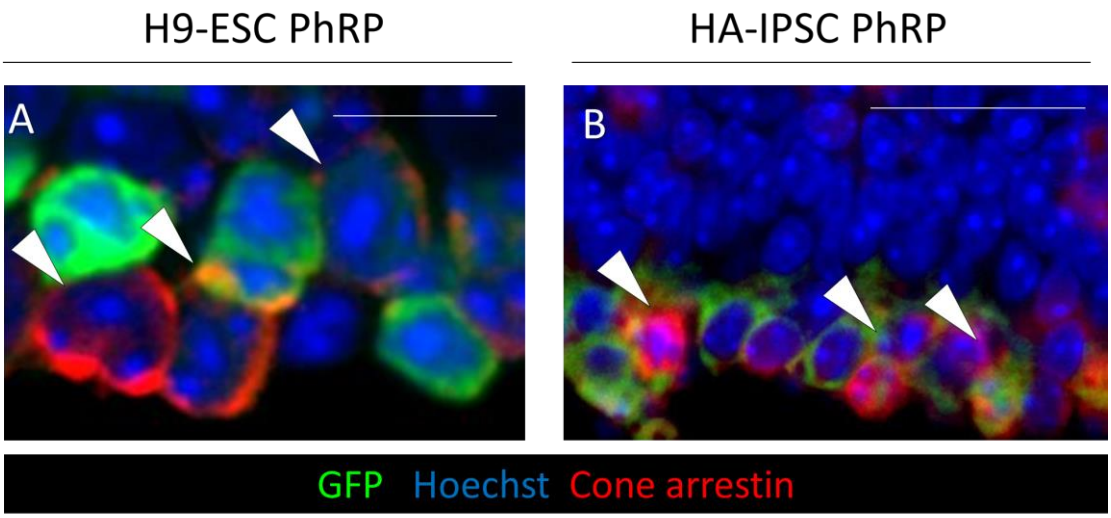

Figure 6.9: Expression of the cone photoreceptor marker cone arrestin in transplanted human cells

Immunofluorescence staining 3 weeks post transplantation. In all images cells are located in the subretinal space and oriented so that the host inner nuclear layer (INL) is located at the top of the image and the retinal pigment epithelium (RPE) at the bottom. The cone specific marker cone-arrestin was observed in maturing ESC-PhRPs (A) and iPSC-PhRPs (B). Co-localisation with cytoplasmic GFP in cells within the graft indicates differentiation of cone photoreceptors from human PhRP.

6.1.8.1 Transplanted human iPSC-derived PhRPs form connections with the host retina

As described in the previous chapter, the development of photoreceptor signalling mechanism can be identified by the synaptic vesicle glycoprotein, synaptophysin, which is normally expressed in photoreceptor synaptic terminals in contact with bipolar cells. Three weeks post transplantation synaptophsin

protein was present between the human graft and the host retina (Fig. 6.10), indicative of an interaction between donor cells and host bipolar cells.

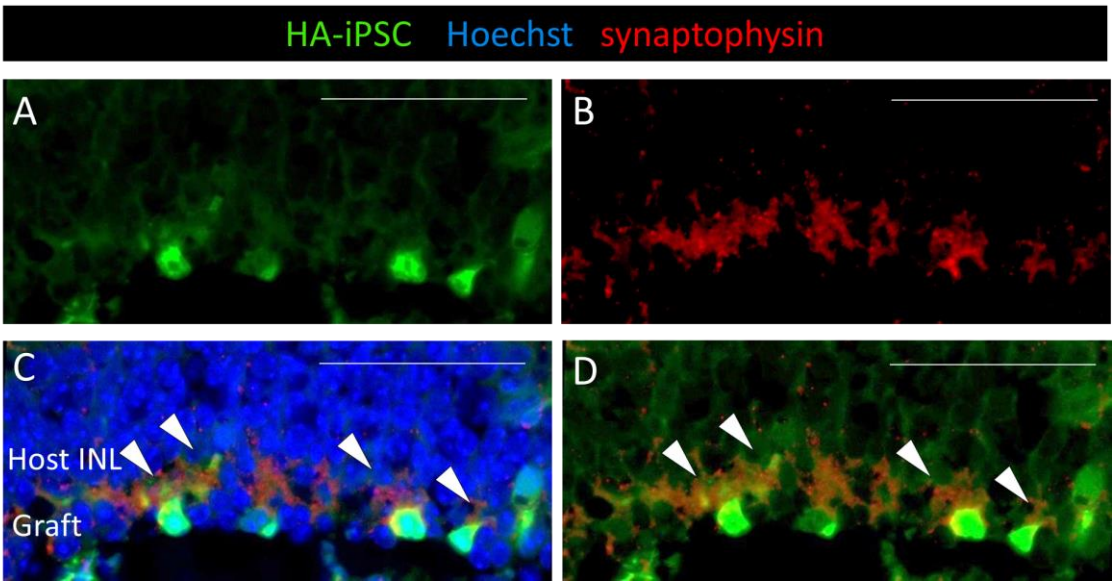

Figure 6.10: Synapse formation between graft and host

Expression of Synaptophysin, a synaptic marker, was present between the host INL and the GFP+ graft. Synaptophysin is localised between the host and graft and is expressed in transplanted cells (white arrows) indicating synaptic transmission between human iPSC-derived grafted cells and the host rd1 retina. Scale bar, 20µm. INL, inner nuclear layer.

Gliosis is a limiting factor in CNS regeneration and has been proposed to represent a cellular attempt to protect remaining tissue from further damage[353]. In the retina gliosis predominantly involves Müller glia cells, which upregulate the glial fibrillary acidic protein (GFAP) of the Müller cell processes at the edge

of the neural retina[354]. The presence of a glial scar in the retina may stand as a physical barrier to cell integration[355]. Host Müller glia (GFAP positive) were found to form a glial barrier at some areas of the retina, however glial processes were also found to extend into the engrafted human PhRPs (Figure 6.11), supporting a degree of integration between the host and graft layers without a significant glial barrier forming between them.

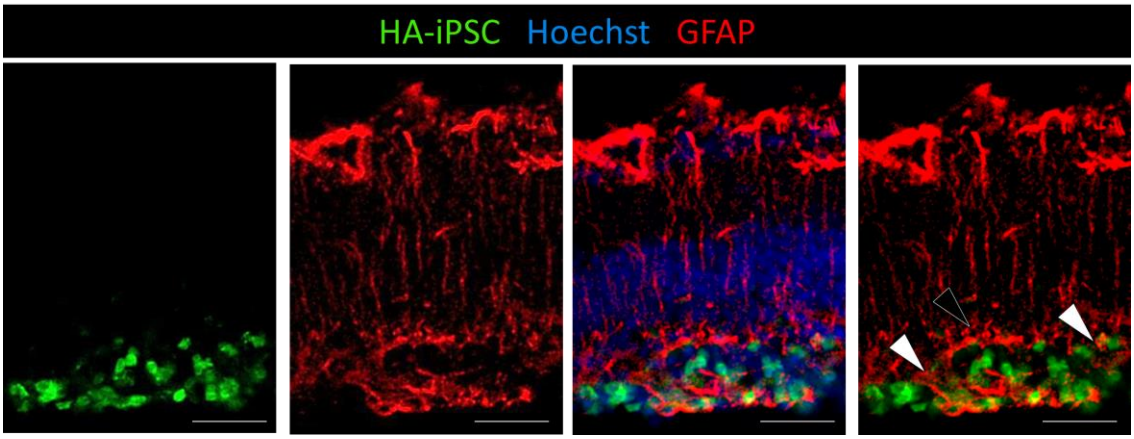

Figure 6.11: Absence of a complete glial barrier between host and graft

Glial fibrillary acidic protein (GFAP), a protein expressed by inner retinal astrocytes and Müller glia, is expressed by the glial cells of the host retina (red). Gliosis in the degenerate retina may occur to protect the retina from further damage, and a horizontal glial scar at the edge of the host ONL was observed in some areas of the retina (black arrow). However, glial processes were also observed to extend into the graft (green), without formation of a complete glial barrier between host and graft (white arrows). Scale bar, 20μm.

6.1.9 Recovery of basic visual function in animals with end-stage retinal degeneration.

In order further to assess transplanted cell maturation and integration into host circuitry, changes in basic behavioural function were assessed in treated *rd1* mice. Behavioural testing was conducted after dark adaptation and using a dim green 510-nm illumination, which is closest to the wave length detected by rod cells. This light intensity was selected in order to target transplanted rod cells while eliminating the contribution of potentially functional host cone cells or ipRGCs.

6.1.9.1 Restoration of the optomotor response in rd1mice treated with human PSC-derived PhRP

We assessed the presence of an optomotor response (OMR) to a rotating grating, by adapting a previous protocol[158]. The test animal is placed in the centre of a rotating striped drum. An OMR is recorded when the animal turns its head to track the rotating grating. Tracking in each direction is independently driven by one eye[233]; so that an OMR elicited by rotation in a clockwise direction is driven by the left eye, and a response to anti-clockwise rotation is driven by the right eye (the treated eye in this study) (see schematic representation in Chapter 2). An increase in the number of direction-dependent head tracks was found when comparing head tracks driven by treated eyes compared to untreated eyes of animals transplanted with ESC-PhRPs (Paired t

test, t=2.86, p<0.05) and iPSC-PhRPs (Paired t test, t=5.02, p<0.01), but not in the shame treatment group (paired t test, t=0.31, ns). A difference was found between the three treatment groups in the number of treated eye-derived head tracks (One way ANOVA, F=7.8, p<0.01), with post hoc analysis revealing improvements in ESC-PhRP (p<0.05) and iPSC-PhRP (p<0.01) groups compared to sham treatment, but no difference between the two PhRP treatments (ns) (Fig. 6.12).

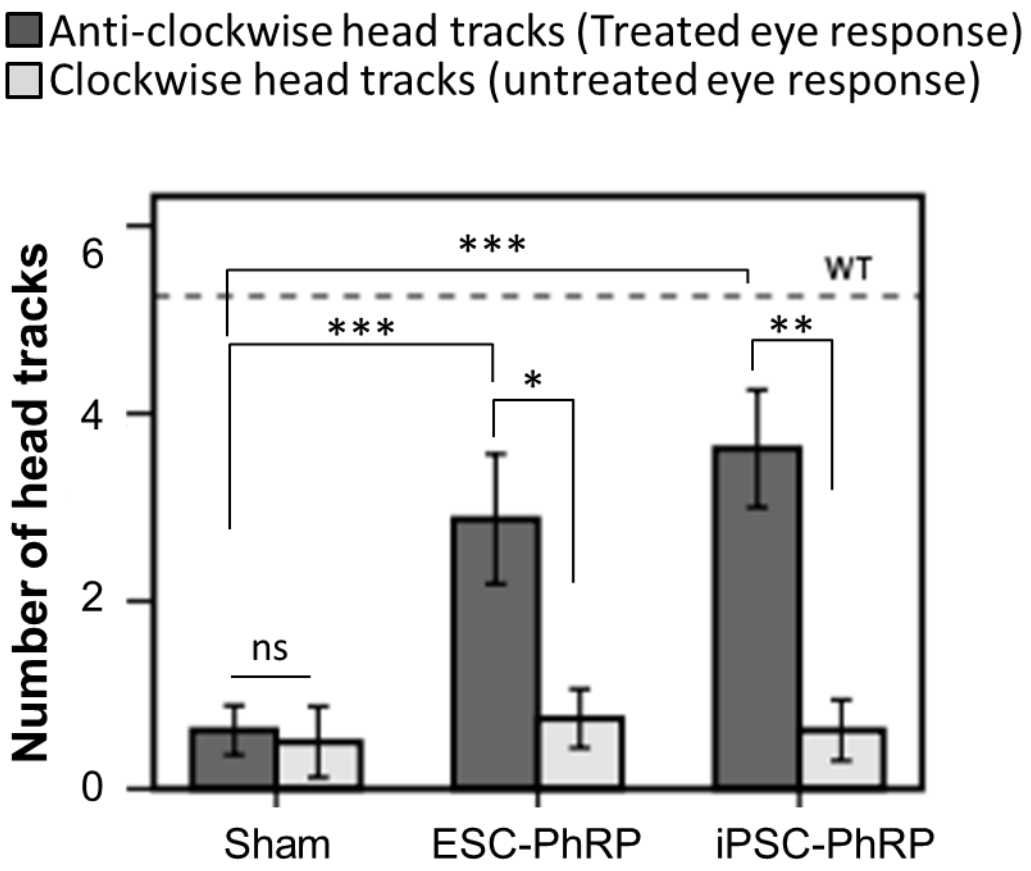

Figure 6.12: Restoration of the optomotor response in rd1 treated with human PSC- PhRP

Three weeks post-transplantation, an increase in the number of anti-clockwise head tracks was observed by PSC-PhRP treated mice in the optomotor response (OMR) test, indicating an improvement in OMR driven by treated eyes (dark grey) compared to paired untreated eyes (light grey) after transplantation of ESC-PhRPs (paired sample t-test, $t=2.86$, $p=0.024$) and iPSC-PhRPs (paired sample t-test, $t=5.02$, $p=0.002$). In the sham treated group there were no differences in OMR driven by treated and untreated eyes (paired sample t test, $t=0.31$, ns). Furthermore, OMR response was improved in PhRP treatment groups compared to sham treatment (one way-ANOVA, $F=7.8$, $p=0.003$), with an increase in the response in both ESC-PhRP ($p<0.05$) and iPSC-PhRP ($p<0.005$) treated animals (Bonferroni test for multiple comparisons). Bars represent mean ±1 SEM. N=8 in each group. ESC, embryonic stem cells; iPSC, induced pluripotent stem cells; PSC, pluripotent stem cells; PhRP, photoreceptor precursors.

To investigate further the results obtained by the OMR test, behavioural performance was correlated to the number of positively identified human cells in each animal (Table 6.1), and showed a positive correlation between the number of GFP+ surviving cells and performance in OMR for both ESC-PhRP (R^2= 0.626, F=10.0, p=0.19; Figure 6.13A) and iPSC-PhRP (R^2= 0.518, F= 6.45, p=0.044; Figure 6.13B) treated animals.

Animal	Treatment	Surviving cells	OMR	BLA
1	H9-ESC	11302	1	11.80
2	H9-ESC	4296	0	25.62
3	H9-ESC	7050	3	19.45
4	H9-ESC	20230	5	71.18
5	H9-ESC	7240	2	33.18
6	H9-ESC	16549	2	59.15
7	H9-ESC	19281	5	65.57
8	H9-ESC	17431	5	50.52
9	HA-iPSC	3289	2	30.47
10	HA-iPSC	5649	2	22.28
11	HA-iPSC	10947	4	70.15
12	HA-iPSC	9835	4	51.70
13	HA-iPSC	11542	2	57.80
14	HA-iPSC	14002	5	59.77
15	HA-iPSC	19018	7	57.82
16	HA-iPSC	16992	3	72.85

Table 6.1: Number of surviving cells, and results of optomotor response (OMR) and behavioural light avoidance (BLA) in individual animals

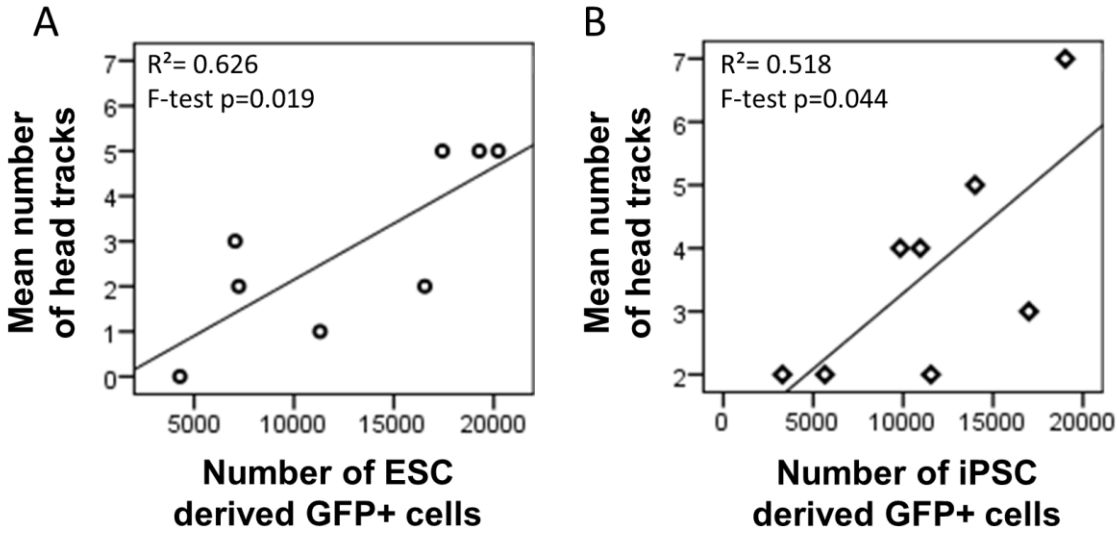

Figure 6.13: Recovery of OMR responses in *rd1* mice following transplantation of human PhRPs correlates to the number of engrafted cells

A positive correlation was found between number of head tracks and number of surviving GFP+ cells in rd1 mice treated with A. ESC-PhRPs (R^2=0.729, F=16.13, p<0.01) and B. iPSC-PhRPs (R^2=0.612, F=9.46, p<0.05). N=8 in each group.

6.1.9.2 Restoration of the light avoidance response in rd1 mice is dependent upon a high number of surviving cells

To qualify further the observed behaviour, the behavioural light avoidance assay (BLA), was conducted as previously described [62]. Mice were free to transition between light and dark compartments of a test arena, and the percent of time spent avoiding light was quantified. As mice are nocturnal animals, they tend to avoid bright environments[297]; however, this is dependent on the perception of light, thus the tendency to avoid light in the BLA arena can be taken as a measure of visually guided behaviour. In this test, rd1 mice in the three treatment groups did not differ in their tendency to avoid light (ANOVA, $F=1.4$, $p=0.26$, ns; Figure. 6.14A). Measures of anxiety-related behaviour were examined in order to assess whether a difference in anxiety between the groups may contribute to the result. The number of times mice transitioned between compartments was quantified as a first measure of anxiety related behaviour, and revealed no difference between the three experimental groups (one way-ANOVA, $F=0.9$, $p=0.42$, ns) (Figure 6.14B). The distance travelled while in the lit compartment was quantified to assess exploratory behaviour, with no difference observed in the different treatment groups (one way-ANOVA, $F=0.13$, $p=0.88$, ns) (Figure 6.14C).

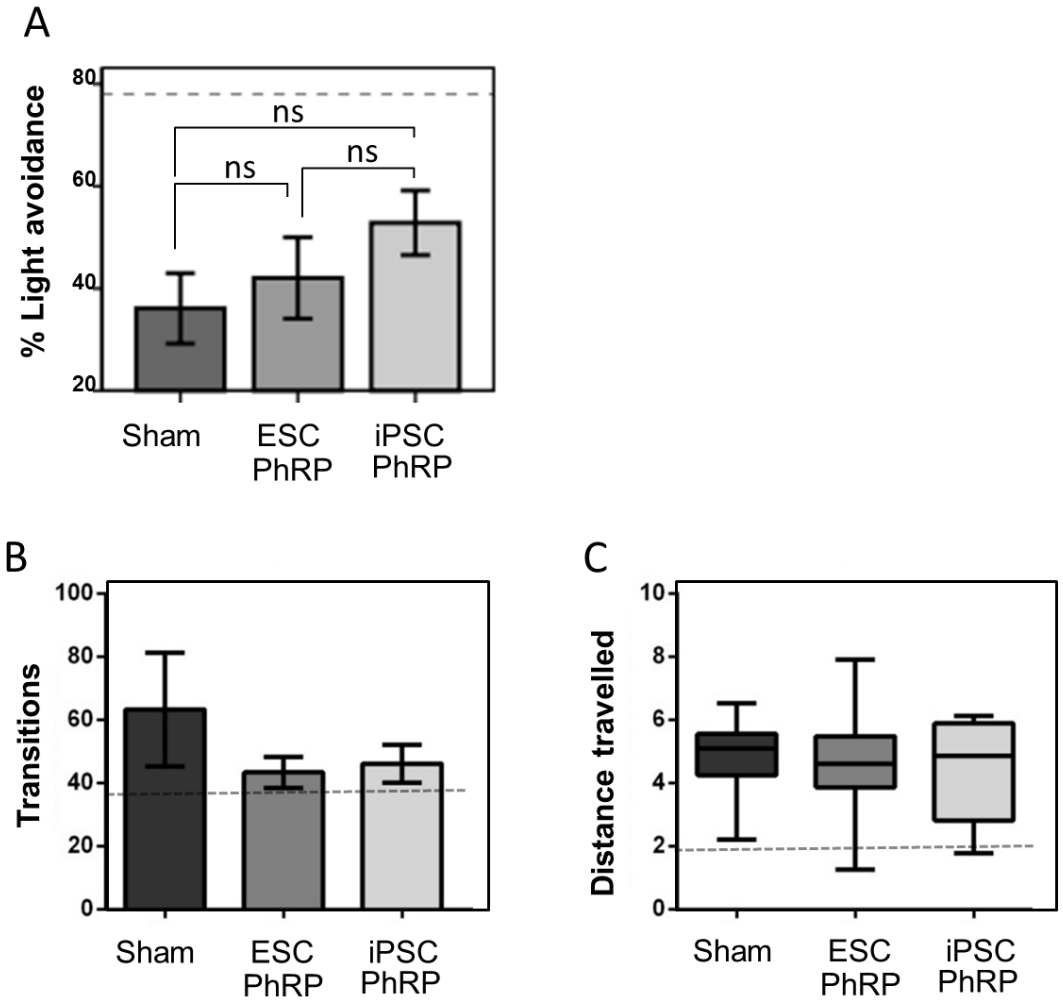

Figure 6.14: Quantification of behavioural light avoidance

A. There were no differences between the three groups in mean light avoidance responses (F=1.43, p=0.26, ns). Anxiety related behaviour was quantified to assess whether a difference in anxiety and exploration of the test arena contributed to behaviour in this test. Transitions between chambers and distance travelled within the lit chamber were assessed during the experiments as behavioural measures of anxiety in *rd*1 mice. B. There were no differences between the three groups in mean number of transitions between the light and dark chambers (F=0.9, p=0.42, ns). C. The mean distance travelled while in the lit chamber did not differ between groups (F=0.13, p=0.88, ns) throughout the test. The dashed line represents the mean response of age-matched wild-type mice. Bars represent mean ±1 SEM. One way ANOVA, N=8 in each group.

Although no significant differences were found between groups in behavioural light avoidance, a trend was observed, in which some mice in the PSC-PhRP treated groups responded more than sham transplanted mice. In order to assess the reason for variation in the results, light avoidance behaviour was qualified to the number of engrafted cells in each animal.

As with the OMR, we found that number of engrafted cells in individual animals strongly correlated with light avoidance behaviour in both ESC-PhRP (R^2= 0.73, F=16.1, p< 0.01; Figure 6.15A) and iPSC-PhRP (R^2= 0.61, F=9.46, p<0.05; Figure 6.15B) treated animals (n=8 per group) (individual results are displayed in Table 6.1).

Since light avoidance behaviour is driven by the light-intensity, which might have a threshold effect to the number of light-sensitive cells, a further sub-analysis was performed, including only mice with above-median number of surviving cells (top 50%) in the treated groups. In this case, though it should be qualified that numbers were small in this sub-analysis, a difference was observed between treatment groups (Kruskal-Wallis test, X^2=6.0, p=0.041) with an increase in light avoidance in both ESC-PhRP (n=4, p<0.05) and iPSC-PhRP (n=4, p<0.05) treated animals (Dunn's test for multiple comparisons) (Figure 6.15C).

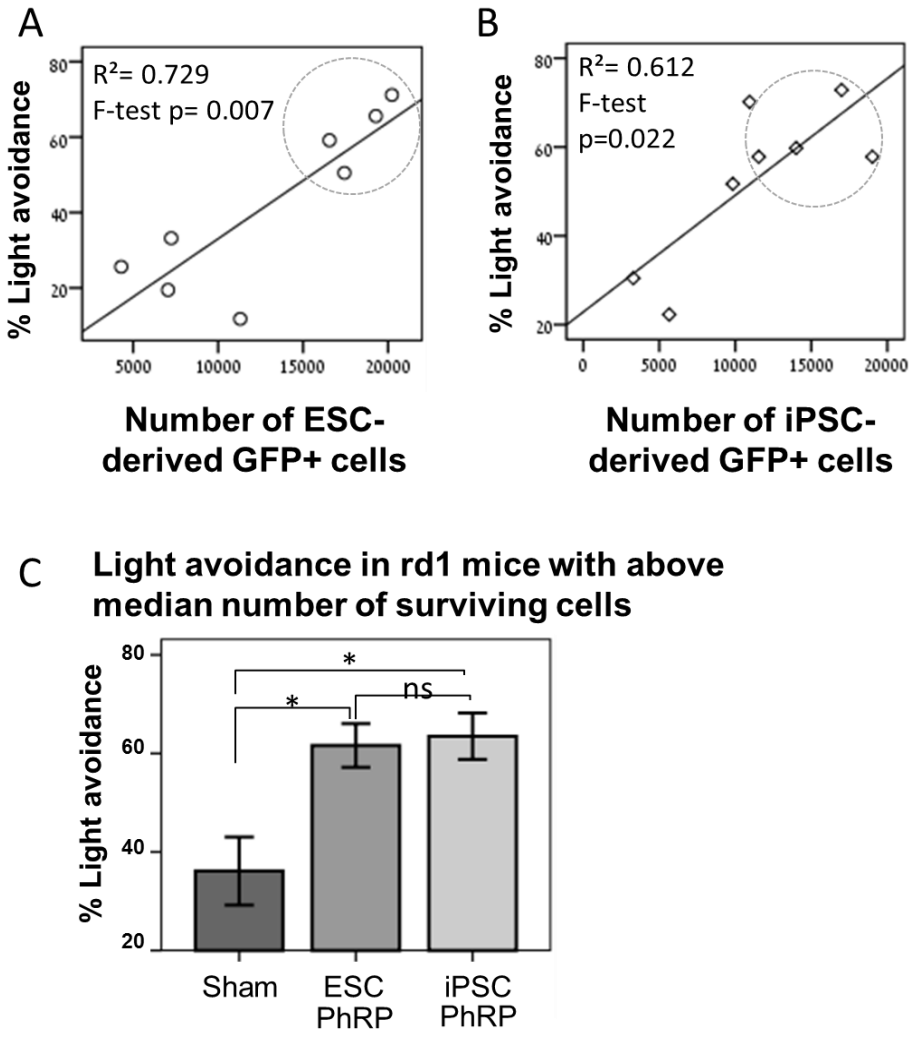

Figure 6.15: Recovery of BLA responses in *rd1* mice following transplantation of human PhRPs correlates to the number of engrafted cells

A. a positive correlation was observed between number of GFP+ surviving cells and behavioural light avoidance in individual animals of treated with ESC-PhRP (R^2= 0.729, F=16.13, p< 0.01). B. a similar correlation was observed in the iPSC-PhRP treated group (R^2= 0.612, F=9.46, p<0.05). C. Comparing only animals with above-median numbers of GFP+ cells (encircled in A and B) a difference emerged between the three groups (X^2=6 (df2), p<0.05) showing improvement in ESC-PhRP treated (n=4, p<0.05) and iPSC-PhRP treated (n=4, p<0.05) subgroups compared to sham treatment, but no difference between the two PSC-PhRP treated groups. Non-parametric Kruskal-Wallis test (Dunn's test for multiple comparisons), p<0.05. The dashed line represents the mean response of age-matched wild-type mice. Bars represent mean ±1 S.E.M.

6.5. Discussion

Collectively, the data presented show that photoreceptor precursors (PhRPs) can be derived from human ESC and iPSC lines to produce a source of cells for photoreceptor cell replacements in a model of end stage RP. Transplanted PhRP cells survived in the completely degenerate retina of immune suppressed mice with end-stage retinal degeneration and formed a new layer, replacing the degenerated ONL and became immuno-positive for phototransduction proteins, adopting a morphology consistent with generating a primitive outer segment. The restoration of basic behavioral light responses correlated with the number of engrafted cells in the subretinal space, using both ESC and iPSC-derived PhRP.

The completely serum-free and feeder-free direct differentiation system developed by Ocata Therapeutics efficiently supported the development of functional PhRPs from human ESC and iPSCs without differences in the efficiency of the two types of cells.

Human iPSC which were used in this chapter for transplantation were generated by a non-integrative mRNA approach, so addressing the major limitation of clinical application of iPSCs generated from integrative delivery system; the permanent genetic modification resulting from the integration of viral vectors. Furthermore, since iPS cells could potentially be produced from a patient’s own cells, PhRPs and photoreceptors from such human iPSC lines

would be histocompatible with the patient, which makes patient specific cell therapy possible.

By synchronizing the differentiation process, this simplified system for PhRP generation may be used to reproducibly generate highly enriched retinal PhRPs, at a stage appropriate for transplantation and in vivo maturation from a range of human PSC lines. This system may be amenable to the development of an in vitro GMP-compliant retinal cell manufacturing protocol for future preclinical and human studies. In particular, this differentiation method allows generation of PhRPs at different development stages, which could be used to target various retinal degeneration diseases at different progression stages.

In addition to efficacy, safety is an ultimate concern in transplantation of derivatives from PSCs. Current approaches generate a mixture of retinal neurons requiring further purification steps to obtain pure photoreceptor precursors. The methods used by Ocata Therapeutics initiated direct differentiation of human ESC and iPSC, leading to stepwise differentiation into EFPs, RNPCs, PhRPs and photoreceptor-like cells that homogeneously express cell-specific genes without further sorting. This method generated a near homogenous population of PhRP (>90%) expressing markers specific for photoreceptor cell fate with less than 10% of cells expressing the cell proliferation marker Ki67. On further culture these cells were able to generate a population of cells in which over 95% of cells express photoreceptor specific markers.

The homogeneous population used in this study is comparable to the population of cells attained following FACS sorting in previous studies using human ESC-derived PhRP[73], where cell sorting yielded a cell suspension in which 90% of cells could subsequently be histologically labeled as rod or cone photoreceptors. Correspondingly, in another study[75], after transplantation of mouse iPSC, the proliferation marker Ki67 was still detected in cells three weeks following transplantation, although rigorous MACS cell purification was applied for depletion of the pluripotency marker SSEA1, and no tumor formation was detected.

The human PSC-derived PhRPs used in this chapter were not further sorted after cell differentiation, and matured to restore a degree of vision to blind mice with no adverse effect three weeks post transplantation. These results provide support the use of this synchronized differentiation approach for production of human PhRP for transplantation, however further research would be required to assess the safety of these cells prior to application in a clinical setting.

A central question in the translation of PSCs to clinical trials is the feasibility of manufacturing cells in a safe and stable manner for clinical trials. Human rod photoreceptor differentiation requires long *in-vitro* culture periods, and may take roughly 80 days to differentiate photoreceptor-precursors from iPSC[113,116] and in the order of 100-120 days to produce mature photoreceptors[45,105,119]. This is a costly, time consuming and delicate procedure that must be closely monitored throughout all stages to ensure viability and safety of the final cell product. As an alternative, after initial culture, large-stocks could be cryopreserved and

delivered in frozen aliquots for short term additional culture and generation of newly differentiated cells to produce storable neural retina generated from human PSC for use in research and clinical trials.

The recovery of cryopreserved human PSC with high viability and successful transplantation and maturation of the cells described in this chapter provides support for use of recovered cryopreserved PhRP in clinical settings.

The potential of safely storing PSC would provide the possibility of maintaining personalized human leukocyte antigen (HLA)-haplotype matched cell lines in iPSC banks[356-358] similar to banks formerly suggested for ESC[359]. Such banks could reduce the financial resources and time required to produce clinically suitable patient-specific or immune-matched cells, by maintaining differentiated and purified tissue for immunologically-personalized transplantation. However, it should be noted that recovery of human iPSC after cryopreservation is still underway and thawed cells have been reported to demonstrate compromised cloning efficacy and reduced cell survival[360] and consequently a number of groups have been working to improve cell survival and efficacy after cryopreservation using Rho-kinase (ROCK) inhibitors[356,361,362].

In this chapter, cryopreserved human ESC and iPSC derived PhRPs were recovered with high viability and subretinally transplanted in the *rd1* mouse model of end-stage RP. We transplanted PhRPs in this fast degeneration model at 10-12 weeks of age, a time point in which there is no remaining ONL [62,89]. Robust cell survival and in vivo expression of photoreceptor markers by transplanted cells suggest that the severely damaged retina is a permissive

space for human cell maturation. Survival and maturation in the completely degenerate retina has been achieved by transplantation of mouse primary cells in suspension[62] or mouse PSC-derived 3D retinal sheets [89], but has not been shown before using human derived cells.

In the current work it was shown that transplanted human cells formed a distinct layer in the *rd1* subretinal space, resembling in some ways the configuration of the subretinal electronic retina[13,14] in human clinical trials for end-stage RP. The lack of precise differentiation into vertical photoreceptor profiles with long outer segments is in keeping with observations from transplantation experiments in the *rd1* mouse host and may result from the inability for transplanted suspension-cells to become radially orientated to the RPE in the compressed outer nuclear environment in end stage degeneration[62,346,347]. This would most likely reduce the light sensitivity of these cells; however, the number of surviving cells observed with SLO and histologically in some animals would largely compensate for reduced sensitivity of individual cells. Similar to the subretinal electronic retina, electrical current changes within the transplanted cells may influence bipolar and horizontal cells even without conventional synapses, if the cells are in close enough apposition. The positive results with the subretinal implant which has 1,500 pixels[13] demonstrate future potential of a cell therapy approach, which could implant millions of cells[127]. While some light sensitivity has been previously shown to be possible without the elaboration of outer segments in transplanted human cells[73] and photoreceptors with profound structural damage have been shown to support

vision in mice[74], the abnormal cell morphology and lack of radially orientated cells in our study led us to consider an alternative explanation of neuroprotection of residual host cones.

Neuroprotection and photoreceptor rescue by transplanted RPE cells has been shown in the *rd1* mouse [330]; however, this was achieved in 2 weeks old mice, a stage in which there were still remaining photoreceptors in the ONL, making rescue by neurotrophic factors more likely. At 10-12 weeks of age, a small number of cones exist in the peripheral area of retina[363]; however, the number of remaining photoreceptor cells in *rd1* mice would not be sufficient to account for visual restoration. Nonetheless, if the existing cones are in a dormant or unhealthy status, PSC-PhRPs may restore their functionality by neuroprotection or another unknown mechanism. To account for this possibility, behavioral tests were conducted following dark adaptation and under dim light; designed to target transplanted rod photoreceptor sensitivity rather than transplanted cones or residual cones in host animals. Additional support for the restoration of phototransduction by donor cells comes from the observation that markers expressed by transplanted cells are consistent with light-sensitivity and donor-host connectivity.

An improvement was found in the optomotor response of treated animals and was of a similar magnitude using either ESC or iPSC derived cells; corroborating in vitro observations of similar differentiation efficacy in these cell lines (Appendix). Both the OMR response and light avoidance behavior

correlated with the numbers of surviving donor cells, which is more in keeping with a direct response from these cells as opposed to random events.

A variation in the number of surviving cells could represent variation in transplantation or delivery of immune suppression to different animals; however, it is also possible that the subretinal space was a more permissive environment for cell survival in animals which shared a preexisting inherent trait such as slower cone degeneration. Survival of non-functional cones in end-stage RP patients has been previously documented [364]. Hence further exploration of this question could be important in identifying optimal time points for transplantation in humans.

6.6. Conclusions

Taken together, the data presented in this chapter show that human pluripotent stem cells (PSC)-derived photoreceptor precursors (PhRP) can be successfully transplanted to survive and mature in the subretinal space of mice with end-stage retinal degeneration and reconstruct the host retina to restore a degree of visual function in mice. Similar results were obtained by transplantation of ESC-derived PhRP or iPSC-derived PhRP, providing novel evidence that these cells may possess the potential for photoreceptor replacement therapy in blind patients with end-stage retinal degeneration.

In the previous chapters, a model for disease-specific gene therapy in mouse rod photoreceptor precursor cells and successful cell replacement by *ex vivo* genetically treated photoreceptor precursors was described in a model of retinitis pigmentosa (RP). The data presented in this chapter affords proof for cell replacement using healthy human PSC-derived PhRP, and provides a defining step for further pre-clinical studies of cell replacement using patient-specific iPSC for personalized *ex vivo* gene therapy.

7. General Discussion

7.1. Overview

Taken together, the data presented in this thesis show regeneration of the retina and restoration of a degree of visual function following transplantation of *ex vivo* corrected mouse rod photoreceptor precursor cells and healthy human ESC and iPSC-derived photoreceptor precursors, in models of end stage photoreceptor degeneration in retinitis pigmentosa (RP).

Additionally, sustained gene expression by use of minicircle DNA was here first successfully attained in photoreceptor cells, providing therapeutic levels comparable to gene delivery achieved in these experiments by a capsid mutant adeno associated virus (AAV).

Two major experimental avenues were pursued in this thesis; the first was the development of viral and non-viral gene therapy vectors for rhodopsin supplementation and regeneration of the photoreceptor layer of $Rho^{-/-}$ mice by *ex vivo* treated donor $rho^{-/-}$ rod photoreceptor precursors. The second experimental avenue was the regeneration of the *rd1* retina by use of human stem cell-derived photoreceptors.

With regard to the first experimental avenue, a cell culture system was developed, supporting sustained *ex vivo* viability of rod photoreceptor

precursors for up to a month and maintaining cells in a developmental stage appropriate for rod precursor cell enrichment and transplantation up to day 14. This system was reliably employed throughout experiments in this thesis and may be used in future research for investigation of gene therapy or neuroprotection in retinal cells.

Using the prolonged culture system, an efficient rAAV serotype for *ex vivo* transfection of rod cells was identified and minicircle DNA was established as a novel non-viral method for transfection of retinal cells, showing superior transgene expression compared to plasmid delivery. By use of the photoreceptor-specific RHOK promoter, rAAV2 Y444F and minicircle DNA gene therapy vectors were successfully developed for augmentation of the human rhodopsin gene. Peak expression levels of these two vectors were similar *in vitro*, reinstating roughly 40-60% of neonatal WT rhodopsin expression in $rho^{-/-}$ cells.

Following transplantation into $Rho^{-/-}$ mice at a stage of advanced retinal degeneration e*x vivo* treated cells formed a new ONL in the correct anatomical location, to replace the absent layer in host mice. The data show that a light sensitive layer of cells may be reconstructed by treated donor rods; grafted cells developed OS and expressed the rhodopsin protein *in vivo* two months following transplantation. The expression of rhodopsin by $rho^{-/-}$ cells in the $Rho^{-/-}$ retina indicates the production of this critical phototransduction protein as a result of *ex vivo* gene therapy. Donor cells matured *in vivo* to express OS-specific and photoreceptor markers. Although abnormal morphology was

observed in cells, synaptic integration between the graft and host restored the transmission of light-evoked signals to the brain so that a degree of visual function was reinstated in previously blind hosts. These data constitute the first account of successful cell replacement using *ex vivo* treated retinal cells in a disease-specific RP model and represent a step on the path to the development of a method for restoration of vision in advanced stages of RP by patient-specific iPSC-derived photoreceptors.

The future application of cell replacement using human stem cells at a clinically relevant time-point of advanced ONL degeneration would be contingent upon the possibility for human photoreceptors to survive and mature in the degenerate subretinal niche. This had not been previously explored and represents the second experimental avenue of research in this thesis.

Collaboration was formed with the biotechnology company Ocata Therapeutics, where healthy human ESC and iPSC-derived photoreceptor precursors (PhRP) were differentiated (Appendix) for use in this transplantation study. Establishing a commercial connection is an important component with any academic based research programme, where the ultimate goal is to develop a treatment for patients.

Human pluripotent stem cell (PSC)-derived PhRP were found to survive and form a new ONL in the subretinal space three weeks following transplantation to immune suppressed *rd1* mice, a mouse model for rapid ONL degeneration. Human cells matured *in vivo* to express phototransduction proteins and form primitive outer segments. Connectivity with the host retina was observed and

transplanted photoreceptors reinstated a degree of visual function in animals, which increased in relation to the number of surviving human cells in the host retina.

7.2. Ex vivo gene correction

In advanced stages of RP where significant loss of photoreceptors has occurred, cell replacement therapy may be required for restoration of vision. Patient-specific iPSC may provide an immunologically-advantageous source of cells for transplantation; however, since patient iPSC harbor the genetic mutation responsible for photoreceptor degeneration, ex vivo correction of the mutation would be required in order to provide healthy autologous cells for transplantation.

7.2.1. Viral and no-viral gene therapy to photoreceptor cells

The experiments presented in this thesis demonstrate the application of rAAV2 Y444F and minicircle (MC) gene therapy for augmentation of the rhodopsin gene in $rho^{-/-}$ photoreceptor precursor cells prior to transplantation in adult $Rho^{-/-}$ mice, representing a disease-specific model for *ex vivo* gene therapy and cell replacement.

AAV-mediated gene augmentation has been established as an effective strategy for gene therapy of inherited retinal dystrophies; a number of clinical trials involving AAV mediated RPE65 augmentation provided visual

improvement in patients with Leber's congenital amaurosis (LCA)[262,263,365,366]. Recently, AAV-mediated delivery of the CHM gene has been shown to improve photoreceptor function in patients with the x-linked recessive disease choroideremia[146].

The study of *in vitro* viral gene augmentation in patient specific cells is gaining interest in the field of ocular gene therapy. AAV8 mediated gene delivery has been used in patient iPSC, for rescue of RPE phenotype by delivery of the Membrane Frizzle-related Protein (MFRP) *in vitro* to RPE cells from a patient with MFRP-associated RP[150]. Recently, successful gene transfer to CEP290-associated LCA patient iPSC-derived photoreceptor precursors was achieved using lentiviral-mediated gene augmentation, restoring cellular phenotypes[122]. These studies provide important evidence for the restoration of cellular phenotype in retinal and specifically photoreceptor cells with an inherited genetic mutation.

Ex vivo AAV-mediated gene augmentation in photoreceptor precursor cells, showing sustained gene expression following cell transplantation, was presented in this thesis for the first time. The specific delivery of the transgene to photoreceptor cells using the photoreceptor-specific RHOK promoter produced robust transgene expression in rho$^{-/-}$ cells, which were subsequently able to produce rhodopsin and improve visual function in mice.

AAV-mediated transfer of the rhodopsin gene was achievable due to the small size of this gene (1047bp). However, mutations associated with genes larger than 4.7kb, such as the CEP290 gene mentioned above (~8kb[122]), are less

amenable for efficient AAV delivery, requiring an alternative safe and efficient method for gene transfer.

Delivery of the rhodopsin transgene by minicircle (MC) DNA, which is not limited in packaging capacity, was shown to achieve sustained expression in cells *in vitro* and *in vivo*. These experiments represent the first report of gene delivery to retinal cells using the non-viral minicircle DNA method.

Expression levels *in vitro* by MC delivery of rhodopsin and functional improvement attained following transplantation of minicircle treated cell were similar to those attained by rAAV2 Y444F. This was a somewhat unforeseen outcome, as in a majority of studies the efficiency of non-viral gene delivery to photoreceptor cells *in vivo* has been reported to be lower than that of viral delivery methods[168,170,176].

While electroporation has shown limited ability in increasing the efficiency of *in vivo* delivery of genetic material to the adult neurosensory retina[172,173], it has shown relatively high efficiency in the facilitation of transfection of newborn photoreceptor precursor cells[367,368]. Although the clinical relevance of *in vivo* neonatal cell transfection may be low, it corroborates the robust *ex vivo* transfection of neonatal cells reported here with MC DNA, indicating neonatal cells may be more amenable to non-viral transfection than adult photoreceptors.

More importantly, the unique properties of MC make them optimal for gene transfer and may explain the efficient transfection achieved by MC compared to previously studied non-viral vectors. MC do not contain a bacterial backbone

and thus eliminate bacterial immunogenic unmethylated CpG motifs[212] which are involved in silencing of episomal transgene expression[209]. The elimination of the bacterial backbone also reduces the size of the DNA to be transferred into cells[213], increasing their bioavailability. Relevant to the results obtained with MC DNA are recent reports of sustained and efficient gene expression in the neonatal retina, and to a lesser extent in the adult retina, by use of compact DNA nanoparticles[177-179]. Further experimentation comparing these small and efficient non-viral vectors may be useful for further application in retinal gene therapy.

7.2.2. Dosing and gene augmentation

Studies in knockout animal models, or in animals with null mutations, have largely attempted to maximize transgene expression by gene augmentation. However, overexpression of certain genes has been shown to have detrimental effects. In Transgenic mice bred to over express *rho*, overexpression by 23% was sufficient to lead to photoreceptor degeneration[280]. Similarly, AAV5-mediated overexpression of *RHO* in mature WT photoreceptors by subretinal injection increasingly reduced visual function in treated animals over 1-3 months post injection[154]. This is consistent with overexpression of *RHO* which has been associated with the P23H mutation in approximately 12% of adRP patients[42].

In a recent in vitro study, lenti-virus gene augmentation was assessed in CEP290-associated LCA patient iPSC-derived photoreceptor precursors[122].

While rescue of photoreceptor phenotype was achieved with a low dose, overexpression of this protein caused increased cell death in a dose dependent manner; showing adverse cellular toxicity associated with CEP290 overexpression in photoreceptor precursor cells *in vitro*.

In the experiments in this thesis, AAV-mediated gene delivery to photoreceptors was achieved by delivery of up to 10^5 rAAV2 Y444F viral genomes (vg) per cell. This dose was designed to be comparable to previous reports, showing efficient AAV9 and AAV5 *in vitro* delivery to photoreceptors differentiated from mouse retinal stem cells[194], and is comparable to the doses of rAAV2 used in recent clinical trials of retinal gene therapy, which ranged between approximately 6×10^9 vg/eye and 10^{12} vg/eye[146,263,366,369].

Toxicity was not observed in cells following rAAV2 Y444F-mediated rhodopsin delivery, indicating safety as well as efficiency of this method. Further investigation of dose-dependent outcomes of *ex vivo* photoreceptor transduction may increase the efficiency of gene expression using this viral vector, and identify the most efficient dose while minimising pathogenic potential.

The dose used for the delivery of minicircle DNA was not supported by previous findings regarding the retina, as this method had not been previously reported for the transfection of retinal cells. Therefore the dose established for gene delivery represented a DNA dose which could be effectively used to express the transgene in combination with the polycationic liposomal transfection technique, without inducing retinal cellular toxicity *in vitro* (50pg DNA/cell).

Efficient and sustained expression was achieved by this dose. However, further investigation of the maximal limits of minicircle-mediated rhodopsin gene therapy may afford a better understanding of the mechanisms of this vector and further increase therapeutic levels of minicircle-mediated rhodopsin gene augmentation.

The methods described in this thesis provide safe and efficient methods for *ex vivo* delivery of the rhodopsin gene to photoreceptor precursors prior to transplantation. Viral and non-viral augmentation of the WT *RHO* gene may be further investigated for clinical applications to replace a missing gene or effectively dilute a negative effect of the mutant protein in diseases in which the specific genetic mutation is not identified.

In consideration of treatment for patient-specific iPSC with a known genetic mutation, a further strategy for application of gene correction to cells, which eliminates dose-dependent ectopic gene expression, is the use of specific gene targeting by application of emerging genome editing techniques.

7.2.3. Future directions: Gene editing in patient-specific iPSC

In patients with genetic mutations, in which the locus of mutation has been identified, the native gene regulatory elements can be specifically utilized for treatment using genome editing strategies. For recessive diseases, in which a single gene is implied, correction of a single mutated allele may be sufficient to achieve a therapeutic effect[121].

Recent advances in genome editing techniques, including transcription activator-like effector nucleases (TALENs) and CRISPR (clustered regularly interspaced short palindromic repeats)/Cas9 system, allow the targeted correction of patient-specific cells *in vitro*, and have provided support for extremely efficient endogenous gene correction[370-372]. The CRISPR/Cas9 system can be used to specifically edit human genes, using pre-designed 20 nucleotide small guide RNA (sgRNA) coupled with Cas9 nuclease[373,374]. Gene editing is achieved by a double strand break to the genomic DNA and subsequent homology-directed repair. Importantly, the corrected gene remains under the normal endogenous promoter, thus avoiding expression in inappropriate cell types or incorrect levels of expression[86], which may occur with viral and non-viral gene replacement.

TALEN has been reported to specifically target loci in pluripotent iPSC genes[370], and using the CRISPR/Cas9 system, five separate genetic loci in ESC could be simultaneously mutated[372]. These methods may be applied for gene correction in genetic mutations associated with RP in iPSC-derived photoreceptor precursor cells, or may potentially be used even earlier for gene correction in patient-specific iPSC prior to cell differentiation.

7.3. Cell replacement

7.3.1. Transplantation in severely degenerated retina

The host mice used in this thesis represent severe degeneration models of RP. The Rho$^{-/-}$ mouse, which had been characterized for progressive photoreceptor degeneration, and the *rd1* mouse which is a rapid model of retinal degeneration, both progressively lose photoreceptor cells, and were used in this study after degeneration had occurred in order to model the anatomy in end stage RP in humans. Transplantation of cells in the Rho-/- mouse at 12-14 weeks of age and into the rd1 mouse at 10-12 weeks of age assured that there were no functioning host photoreceptor cells remaining in mice to influence transplantation outcomes or be subjected to neuroprotection following transplantation.

The strategy employed in this thesis, of photoreceptor transplantation into the completely degenerate retina differs from recent studies, which predominantly used mice with an intact or partially degenerate ONL for transplantation[67-70,72,73,75,87,114,125,126,153,227,348,351]. The strategy of transplantation into the completely degenerate retina has recently been employed in the transplantation of mouse photoreceptor precursors[62] and mouse iPSC derived 3D retinal sheets[89]. The work presented in this thesis shows the reconstruction of the ONL in the Rho$^{-/-}$ mouse, following progressive degeneration using *ex vivo* genetically corrected rho$^{-/-}$ rod photoreceptor precursors, and the first transplantation of human ESC and iPSC-derived photoreceptor precursor cells

in the completely degenerate retina of the *rd1* mouse by use of immune suppression.

7.3.2. Donor cell morphology

Data presented in this thesis show the reconstruction of the ONL in mice with advanced retinal degeneration by genetically treated rho$^{-/-}$ mouse rod precursors and human PhRP. The formation of outer segment (OS) structures expressing phototransduction enzymes represents a final stage in photoreceptor differentiation.

The morphology and gene expression of cells presented in transplantation studies in this thesis support the maturation of adult photoreceptors from donor cells. However, cell morphology was largely abnormal in transplanted cells, including shortened and misaligned OS and the absence of long inner fiber formation. Abnormal morphology of treated rho$^{-/-}$ mouse photoreceptors following transplantation (Chapter 5) may represent the inherent morphology of rho$^{-/-}$ rod photoreceptors which have been shown to possess shortened outer segments. It is possible that rhodopsin augmentation by gene therapy did not completely rescue the cellular phenotype in these cells. Likewise, transplanted human PSC-derived PhRP (Chapter 6) developed primitive OS *in vivo* following transplantation and restored light sensitivity in blind mice; however this was assessed three weeks following transplantation, while *in vitro* differentiation of human PhRP to photoreceptor-like cells required at least 2 week (Appendix).

The abnormal morphology observed in human photoreceptors may thus represent an early stage of photoreceptor maturation and additional assessment at later time points may determine the full potential of cell maturation.

Taking these caveats into account, the restoration of vision generated by human and mouse transplanted cells in this thesis and the resemblance in the profile of morphologically abnormal photoreceptors, together with a previous report of abnormal cell morphology following transplantation of healthy mouse rod precursor cells in *rd1* mice[62], support the assertion that the abnormal morphology observed in donor cells reflects an expected outcome following cell transplantation in the absence of supporting host ONL cells.

7.3.3. Visual function

Visual function was used as a critical measure to assess the outcome of transplantation studies. The assessment of visually guided behavior and function in mice before and after transplantation (Chapter 5) allowed experimental group stratification to reduce variability in results, and, importantly, provided a means to measure different aspects of visual function in the same mice before and after transplantation, instead of assessment only after transplantation as had been previously described[67,72,73,75].

Functional and behavioural experiments were specifically designed to isolate rod-mediated function and avoid contribution of potentially residual cone cells

or isRGCs. A short light stimulus was used in the PLR assay and response was measured at a relatively short time after stimulus offset in order to minimize contribution of isRGC to the response. Behavioural light avoidance (BLA) and optomotor response (OMR) experiments were conducted by use of a dim green light 510 nm, which is close to the peak sensitivity of rhodopsin (approximately 500 nm) and sufficiently distant from the peak sensitivity of ipRCGs which express melanopsin as their chromophore (480 nm), hence avoiding stimulation of the latter. Electroretinography (ERG) was conducted under photopic and scotopic conditions, in order to specifically assess the contribution of rod and cone photoreceptors to responses in mice (all described in Chapter 2).

Following transplantation of ex vivo treated rod precursors, 20-24 week old $Rho^{-/-}$ mice improved in all measures of vision assessed, with the exception of ERG. The absence of rod-ERG does not signify the absence of vision, and may represent instead an insufficient number of radially aligned photoreceptors in order to retrieve such a response, as has been observed in RP patients who maintain vision in absence of an ERG response[301]. Improvement in ERG b-wave was previously achieved in a transplantation study using the $Rho^{-/-}$ mouse, but these mice received transplantation at a considerably earlier stage of degeneration (4–6 week old) and ERG improvement was only observed in animals with high numbers of integrated cells (6 of 10 animals). By selectively assessing photopic cone-ERG responses in mice in this thesis, which can be more reliably achieved with bright light or flickering stimulus, cone mediated function was undetected in transplanted mice, providing support for the

absence of functioning cones in the host retina, which may affect the outcomes of other measures of visual function.

The absence of improvement in mice transplanted with untreated rho$^{-/-}$ rod precursors (sham treatment), and the significant difference in response of mice transplanted with *ex vivo* treated cells compared to sham, further supports that the improvement observed was derived from regeneration of the photoreceptor layer by treated donor cells. Equivalent outcomes achieved by photoreceptor cells following the two different gene therapy treatments are consistent with the comparable upregulation in rhodopsin observed in these cells *in vitro*.

Following transplantation of human ESC and iPSC-derived PhRP, an improvement in visual function was observed in *rd1* mice in the sensitivity of the treated eye, but not of the untreated eye, in the OMR test. Furthermore this was markedly improved over the sham transplantation group, indicating restoration of image forming vision. The improvement in OMR linearly increased as a function of the number of surviving cells detected in the treated eyes. A similar correlation was found in the BLA test, where improvement increased with the number of transplanted cells. In this test, only mice with a high number of surviving cells avoided light.

As measures of vision were designed to detect rod function, which is absent in *rd1* mice, these behavioral outcomes, together with maturation of human photoreceptors *in vivo,* indicate that improvement in behavior is related to the number of functioning transplanted cells and validate differences in the

sensitivity of the various behavioral and functional measures in detection of functional vision.

7.3.4. Future directions: Photoreceptor cell replacement in RP

The data provide a basis for the development of clinical applications of human stem cells-derived photoreceptor precursors for cell replacement therapy in advanced retinitis pigmentosa (RP), and afford a model for effective viral and non-viral ex vivo gene correction of patient-specific cells prior to transplantation.

These results provide initial indication of safety and efficiency using human PSC-derived PhRP, and may lead to future application of homogeneously differentiated ESC and iPSC-derived PhRP in clinical trials, similar to a clinical trial recently initiated for transplantation of ESC and iPSC derived RPE cells in patients with macular degeneration and Stargardt disease[328,329]. However, it is important to consider that the immune systems of rodent models and primates differ considerably and further safety measures, such as assessment of cell purity and assessment of immune suppression prior to clinical testing, would be essential before transplantation of cells derived from ESC and iPSC in patients.

In future studies, iPSC-derived PhRP from patients with RP could be differentiated to model and treat the genetic cause of disease and be used in pre-clinical transplantation studies to investigate reconstruction of the ONL by genetically corrected human photoreceptor precursors. The non-viral minicircle method for gene therapy has shown sustained and efficient gene transfer and could be employed for gene delivery to treat mutations in which the defective

gene is too large for packaging in AAV. By use of patient-specific cells, safety and efficiency of gene transfer and restoration of cellular phenotype and function to patient-specific cells could provide a means for obtaining a source of cells for transplantation in clinical trials in the same patients.

Recent advances in development of 3D light sensitive multi-layered retinal sheets from human ESC[87] and iPSC[88] may provide a renewable source for harvesting photoreceptor precursors within a retinal matrix with RPE bound to the outer segment discs, and transplanting retinal sheets in place of single cells as was described in this thesis. Importantly, ESC and iPSC retinal sheets produce a multi-layered tissue, containing rod and cone photoreceptor precursors, inter-neurons and ganglion cells, thus the efficiency of transplantation would need to be further investigated, as the transplantation of inner nuclear layers may interfere with transplanted photoreceptors connecting to the host retina.

Another possibility for efficient transplantation of photoreceptors is the differentiation and transplantation of cells in a sheet formation by use of biodegradable polymer scaffold. This innovative method employed injection of the engineered retinal tissue on a scrollable scaffold[80,91], reducing trauma during injection, and has been reported to promote cell integration and survival of retinal progenitor cells in areas of the damaged retina[91]. This method may prove to be applicable for the expansion and transplantation of differentiated human PSC-derived retinal cells in a clinical setting.

A remaining task for the future is the determination of whether ESC or iPSC would be most appropriate for transplantation in patients. While outcomes in this thesis did not show different results by these two cell types, the advantages and disadvantages of each must be considered. The great advantages of iPSC cells as renewable sources for transplantation must be considered together with the perils of immune suppression in combination with the possible introduction of cells that may still maintain the ability to proliferate *in vivo*, which would expose patients to the risk of tumorigenesis[123]. Outcomes of clinical trials using ESC-derived RPE[328,329] and the impending results of clinical trials which have been initiated in 2014 for iPSC-derived RPE transplantation will provide measures of safety for the clinical application of human ESC and iPSC for ocular cell replacement.

7.4. Conclusion

Collectively, the data presented in this thesis demonstrate the regeneration of the retina and restoration of visual function in advanced retinal degeneration, by use of *ex vivo* virally and non-virally genetically-treated mouse rod photoreceptor precursors and healthy human ESC and iPSC-derived photoreceptors.

A reliable cell culture system was developed for sustained survival of mouse rod photoreceptor precursor *ex vivo* and an optimized capsid mutant AAV vector and a non-viral minicircle DNA vector were produced for *ex vivo* delivery of WT rhodopsin to rod photoreceptor precursor cells with a null rhodopsin mutation. *Ex vivo* treated rod precursors were transplanted in adult mice with the same mutation and regenerated a layer of photoreceptors in these mice. Rhodopsin expression was reinstated in *ex vivo*-treated photoreceptors following maturation, and was achieved with comparable efficiency using AAV and minicircle-mediated gene therapy. Reconstruction of the ONL by transplanted light sensitive cells resulted in the rescue of retinal degeneration and restoration of visual function to mice, to the extent that visually guided behavior improved in treated animals.

These results provide the first account of reversal of end stage degeneration by use of *ex vivo* genetically modified retinal cells and provide a novel method for non-viral gene delivery to the retina.

Furthermore, human ESC and iPSC-derived photoreceptor precursors, transplanted in *rd1* mice with rapid and progressive ONL degeneration, matured in the subretinal space and reconstructed the ONL, to restore a degree of visual function in previously blind mice. The efficiency of ESC and iPSC derived photoreceptors was similar, providing a first account of visual improvement in the completely degenerate retina following transplantation of homogeneously differentiated human PSC-derived photoreceptor precursors.

These data provide a basis for photoreceptor cell replacement strategies using stem cells for RP and other retinal degenerations and for ex vivo gene correction in patient-specific iPSC prior to transplantation. Photoreceptor transplantation may in the future provide a feasible option for regeneration of the retina and restoration of vision in patients with advanced photoreceptor degeneration.

8. References

1. Sung, C.-H. & Chuang, J.-Z. The cell biology of vision. *The Journal of Cell Biology* **190**, 953-963 (2010).

2. Kolb, H. The architecture of functional neural circuits in the vertebrate retina. The Proctor Lecture. *Investigative ophthalmology & visual science* **35**, 2385-2404 (1994).

3. Bretillon, L.*, et al.* Needs in omega 3 and ocular pathologies. *OCL* **18**, 279-283 (2011).

4. Foster, R.G.*, et al.* Circadian photoreception in the retinally degenerate mouse (rd/rd). *Journal of comparative physiology. A, Sensory, neural, and behavioral physiology* **169**, 39-50 (1991).

5. Freedman, M.S.*, et al.* Regulation of mammalian circadian behavior by non-rod, non-cone, ocular photoreceptors. *Science (New York, N.Y.)* **284**, 502-504 (1999).

6. Curcio, C.A., Medeiros, N.E. & Millican, C.L. Photoreceptor loss in age-related macular degeneration. *Investigative ophthalmology & visual science* **37**, 1236-1249 (1996).

7. Arshavsky, V.Y., Lamb, T.D. & Pugh, E.N., Jr. G proteins and phototransduction. *Annual review of physiology* **64**, 153-187 (2002).

8. MacLaren, R.E. Re-establishment of visual circuitry after optic nerve regeneration. *Eye (London, England)* **13 (Pt 3a)**, 277-284 (1999).

9. Maclaren, R.E. & Taylor, J.S. Regeneration in the developing optic nerve: correlating observations in the opossum to other mammalian systems. *Progress in neurobiology* **53**, 381-398 (1997).

10. Stone, J.L., Barlow, W.E., Humayun, M.S., de Juan, E., Jr. & Milam, A.H. Morphometric analysis of macular photoreceptors and ganglion cells in retinas with retinitis pigmentosa. *Archives of ophthalmology* **110**, 1634-1639 (1992).

11. Vidal-Sanz, M., Bray, G.M., Villegas-Perez, M.P., Thanos, S. & Aguayo, A.J. Axonal regeneration and synapse formation in the superior colliculus by retinal ganglion cells

in the adult rat. *The Journal of neuroscience : the official journal of the Society for Neuroscience* **7**, 2894-2909 (1987).

12. Whiteley, S.J., Sauve, Y., Aviles-Trigueros, M., Vidal-Sanz, M. & Lund, R.D. Extent and duration of recovered pupillary light reflex following retinal ganglion cell axon regeneration through peripheral nerve grafts directed to the pretectum in adult rats. *Experimental neurology* **154**, 560-572 (1998).

13. Stingl, K*., et al.* Artificial vision with wirelessly powered subretinal electronic implant alpha-IMS. *Proceedings. Biological sciences / The Royal Society* **280**, 20130077 (2013).

14. Zrenner, E*., et al.* Subretinal electronic chips allow blind patients to read letters and combine them to words. *Proceedings of the Royal Society B: Biological Sciences* **278**, 1489-1497 (2011).

15. Li, Z.Y., Possin, D.E. & Milam, A.H. Histopathology of bone spicule pigmentation in retinitis pigmentosa. *Ophthalmology* **102**, 805-816 (1995).

16. Hartong, D.T., Berson, E.L. & Dryja, T.P. Retinitis pigmentosa. *Lancet* **368**, 1795-1809 (2006).

17. Daiger, S.P., Bowne, S.J. & Sullivan, L.S. Perspective on genes and mutations causing retinitis pigmentosa. *Archives of ophthalmology* **125**, 151-158 (2007).

18. Haim, M. Epidemiology of retinitis pigmentosa in Denmark. *Acta ophthalmologica Scandinavica. Supplement*, 1-34 (2002).

19. Ammann, F., Klein, D. & Franceschetti, A. Genetic and epidemiological investigations on pigmentary degeneration of the retina and allied disorders in Switzerland. *Journal of the Neurological Sciences* **2**, 183-196 (1965).

20. Chang, S., Vaccarella, L., Olatunji, S., Cebulla, C. & Christoforidis, J. Diagnostic Challenges in Retinitis Pigmentosa: Genotypic Multiplicity and Phenotypic Variability. *Current Genomics* **12**, 267-275 (2011).

21. Chizzolini, M*., et al.* Good Epidemiologic Practice in Retinitis Pigmentosa: From Phenotyping to Biobanking. *Current Genomics* **12**, 260-266 (2011).

22. Collin, R.W.J*., et al.* Mutations in C2ORF71 Cause Autosomal-Recessive Retinitis Pigmentosa. *The American Journal of Human Genetics* **86**, 783-788 (2010).

23. Sahel, J.A*., et al.* Rod-cone interdependence: implications for therapy of photoreceptor cell diseases. *Progress in brain research* **131**, 649-661 (2001).

24. Akeo, K., Saga, M., Hiida, Y., Oguchi, Y. & Okisaka, S. Progression of visual field loss in patients with retinitis pigmentosa of sporadic and autosomal recessive types. *Ophthalmic research* **30**, 11-22 (1998).

25. Bunker, C.H., Berson, E.L., Bromley, W.C., Hayes, R.P. & Roderick, T.H. Prevalence of Retinitis Pigmentosa in Maine. *American Journal of Ophthalmology* **97**, 357-365 (1984).

26. Grondahl, J. Estimation of prognosis and prevalence of retinitis pigmentosa and Usher syndrome in Norway. *Clinical Genetics* **31**, 255-264 (1987).

27. Novak-Lauš, K., Kukulj, S., Zorić-Geber, M. & Bastaić, O. Primary tapetoretinal dystrophies as the cause of blindness and impaired vision in the republic of Croatia. *Acta Clinica Croatica* **41**, 23-27 (2002).

28. Hamel, C. Retinitis pigmentosa. *Orphanet journal of rare diseases* **1**, 40 (2006).

29. Pomares, E.*, et al.* Comprehensive SNP-chip for retinitis pigmentosa-Leber congenital amaurosis diagnosis: new mutations and detection of mutational founder effects. *European journal of human genetics : EJHG* **18**, 118-124 (2010).

30. Sergouniotis, P.I.*, et al.* A survey of DNA variation of C2ORF71 in probands with progressive autosomal recessive retinal degeneration and controls. *Investigative ophthalmology & visual science* **52**, 1880-1886 (2011).

31. Waseem, N.H.*, et al.* Mutations in the gene coding for the pre-mRNA splicing factor, PRPF31, in patients with autosomal dominant retinitis pigmentosa. *Investigative Ophthalmology and Visual Science* **48**, 1330-1334 (2007).

32. Mansergh, F.C.*, et al.* Retinitis Pigmentosa and Progressive Sensorineural Hearing Loss Caused by a C12258A Mutation in the Mitochondrial MTTS2 Gene. *The American Journal of Human Genetics* **64**, 971-985 (1999).

33. Kajiwara, K., Berson, E.L. & Dryja, T.P. Digenic retinitis pigmentosa due to mutations at the unlinked peripherin/RDS and ROM1 loci. *Science (New York, N.Y.)* **264**, 1604-1608 (1994).

34. Katsanis, N.*, et al.* Triallelic inheritance in Bardet-Biedl syndrome, a Mendelian recessive disorder. *Science (New York, N.Y.)* **293**, 2256-2259 (2001).

35. Zeviani, M.*, et al.* Deletions of mitochondrial DNA in Kearns-Sayre syndrome. *Neurology* **38**, 1339-1346 (1988).

36. Lestienne, P. & Ponsot, G. Kearns-Sayre syndrome with muscle mitochondrial DNA deletion. *Lancet* **1**, 885 (1988).

37. Dryja, T.P.*, et al.* Mutations within the rhodopsin gene in patients with autosomal dominant retinitis pigmentosa. *The New England journal of medicine* **323**, 1302-1307 (1990).

38. Dryja, T.P.*, et al.* A point mutation of the rhodopsin gene in one form of retinitis pigmentosa. *Nature* **343**, 364-366 (1990).

39. Hargrave, P.A. & McDowell, J.H. Rhodopsin and phototransduction: a model system for G protein-linked receptors. *FASEB journal : official publication of the Federation of American Societies for Experimental Biology* **6**, 2323-2331 (1992).

40. Bessant, D.A., Ali, R.R. & Bhattacharya, S.S. Molecular genetics and prospects for therapy of the inherited retinal dystrophies. *Current opinion in genetics & development* **11**, 307-316 (2001).

41. Shintani, K., Shechtman, D.L. & Gurwood, A.S. Review and update: Current treatment trends for patients with retinitis pigmentosa. *Optometry - Journal of the American Optometric Association* **80**, 384-401 (2009).

42. Mendes, H.F., van der Spuy, J., Chapple, J.P. & Cheetham, M.E. Mechanisms of cell death in rhodopsin retinitis pigmentosa: implications for therapy. *Trends in Molecular Medicine* **11**, 177-185 (2005).

43. Sung, C.H., Davenport, C.M. & Nathans, J. Rhodopsin mutations responsible for autosomal dominant retinitis pigmentosa: Clustering of functional classes along the polypeptide chain. *Journal of Biological Chemistry* **268**, 26645-26649 (1993).

44. Iannaccone, A.*, et al.* Retinitis pigmentosa associated with rhodopsin mutations: Correlation between phenotypic variability and molecular effects. *Vision research* **46**, 4556-4567 (2006).

45. Jin, Z.B.*, et al.* Modeling retinal degeneration using patient-specific induced pluripotent stem cells. *PloS one* **6**, e17084 (2011).

46. Packer, A.M., Roska, B. & Hausser, M. Targeting neurons and photons for optogenetics. *Nature neuroscience* **16**, 805-815 (2013).

47. Garg, S.J. & Federman, J. Optogenetics, visual prosthesis and electrostimulation for retinal dystrophies. *Current opinion in ophthalmology* **24**, 407-414 (2013).

48. Loudin, J.D*., et al.* Optoelectronic retinal prosthesis: system design and performance. *Journal of neural engineering* **4**, S72-84 (2007).

49. da Cruz, L*., et al.* The Argus II epiretinal prosthesis system allows letter and word reading and long-term function in patients with profound vision loss. *The British journal of ophthalmology* **97**, 632-636 (2013).

50. Humphries, M.M*., et al.* Retinopathy induced in mice by targeted disruption of the rhodopsin gene. *Nature genetics* **15**, 216-219 (1997).

51. Jaissle, G.B*., et al.* Evaluation of the rhodopsin knockout mouse as a model of pure cone function. *Investigative ophthalmology & visual science* **42**, 506-513 (2001).

52. Morrow, E.M., Furukawa, T. & Cepko, C.L. Vertebrate photoreceptor cell development and disease. *Trends in cell biology* **8**, 353-358 (1998).

53. Bowes, C*., et al.* Retinal degeneration in the rd mouse is caused by a defect in the beta subunit of rod cGMP-phosphodiesterase. *Nature* **347**, 677-680 (1990).

54. Farber, D.B. From mice to men: the cyclic GMP phosphodiesterase gene in vision and disease. The Proctor Lecture. *Investigative ophthalmology & visual science* **36**, 263-275 (1995).

55. Hafezi, F., Grimm, C., Simmen, B., Wenzel, A. & Reme, C. Molecular ophthalmology: an update on animal models for retinal degenerations and dystrophies. *The British journal of ophthalmology* **84**, 922-927 (2000).

56. McLaughlin, M.E., Sandberg, M.A., Berson, E.L. & Dryja, T.P. Recessive mutations in the gene encoding the beta-subunit of rod phosphodiesterase in patients with retinitis pigmentosa. *Nature genetics* **4**, 130-134 (1993).

57. Carter-Dawson, L.D., LaVail, M.M. & Sidman, R.L. Differential effect of the rd mutation on rods and cones in the mouse retina. *Investigative ophthalmology & visual science* **17**, 489-498 (1978).

58. Sanyal, S. & Bal, A.K. Comparative light and electron microscopic study of retinal histogenesis in normal and rd mutant mice. *Zeitschrift fur Anatomie und Entwicklungsgeschichte* **142**, 219-238 (1973).

59. Jimenez, A.J., Garcia-Fernandez, J.M., Gonzalez, B. & Foster, R.G. The spatio-temporal pattern of photoreceptor degeneration in the aged rd/rd mouse retina. *Cell and tissue research* **284**, 193-202 (1996).

60. Gouras, P. & Tanabe, T. Ultrastructure of adult rd mouse retina. *Graefe's archive for clinical and experimental ophthalmology = Albrecht von Graefes Archiv fur klinische und experimentelle Ophthalmologie* **241**, 410-417 (2003).

61. Chang, B.*, et al.* Two mouse retinal degenerations caused by missense mutations in the beta-subunit of rod cGMP phosphodiesterase gene. *Vision research* **47**, 624-633 (2007).

62. Singh, M.S.*, et al.* Reversal of end-stage retinal degeneration and restoration of visual function by photoreceptor transplantation. *Proceedings of the National Academy of Sciences of the United States of America* **110**, 1101-1106 (2013).

63. Royo, P.E. & Quay, W.B. Retinal transplantation from fetal to maternal mammalian eye. *Growth* **23**, 313-336 (1959).

64. Turner, J.E. & Blair, J.R. Newborn rat retinal cells transplanted into a retinal lesion site in adult host eyes. *Brain research* **391**, 91-104 (1986).

65. Reh, T.A. & Levine, E.M. Multipotential stem cells and progenitors in the vertebrate retina. *Journal of neurobiology* **36**, 206-220 (1998).

66. Chacko, D.M., Rogers, J.A., Turner, J.E. & Ahmad, I. Survival and differentiation of cultured retinal progenitors transplanted in the subretinal space of the rat. *Biochemical and biophysical research communications* **268**, 842-846 (2000).

67. MacLaren, R.E.*, et al.* Retinal repair by transplantation of photoreceptor precursors. *Nature* **444**, 203-207 (2006).

68. Bartsch, U.*, et al.* Retinal cells integrate into the outer nuclear layer and differentiate into mature photoreceptors after subretinal transplantation into adult mice. *Experimental eye research* **86**, 691-700 (2008).

69. Eberle, D.*, et al.* Outer segment formation of transplanted photoreceptor precursor cells. *PloS one* **7**, e46305 (2012).

70. Barber, A.C.*, et al.* Repair of the degenerate retina by photoreceptor transplantation. *Proceedings of the National Academy of Sciences of the United States of America* **110**, 354-359 (2013).

71. Luo, J.*, et al.* Human retinal progenitor cell transplantation preserves vision. *The Journal of biological chemistry* **289**, 6362-6371 (2014).

72. Pearson, R.A.*, et al.* Restoration of vision after transplantation of photoreceptors. *Nature* **485**, 99-103 (2012).

73. Lamba, D.A., Gust, J. & Reh, T.A. Transplantation of human embryonic stem cell-derived photoreceptors restores some visual function in Crx-deficient mice. *Cell stem cell* **4**, 73-79 (2009).

74. Thompson, S.*, et al.* Photoreceptor cells with profound structural deficits can support useful vision in mice. *Investigative ophthalmology & visual science* **55**, 1859-1866 (2014).

75. Tucker, B.A.*, et al.* Transplantation of adult mouse iPS cell-derived photoreceptor precursors restores retinal structure and function in degenerative mice. *PloS one* **6**, e18992 (2011).

76. Gosens, I., den Hollander, A.I., Cremers, F.P. & Roepman, R. Composition and function of the Crumbs protein complex in the mammalian retina. *Experimental eye research* **86**, 713-726 (2008).

77. Comyn, O., Lee, E. & MacLaren, R.E. Induced pluripotent stem cell therapies for retinal disease. *Current opinion in neurology* **23**, 4-9 (2010).

78. Singh, M.S. & MacLaren, R.E. Stem cells as a therapeutic tool for the blind: biology and future prospects. *Proceedings. Biological sciences / The Royal Society* **278**, 3009-3016 (2011).

79. Pearson, R.A.*, et al.* Targeted disruption of outer limiting membrane junctional proteins (Crb1 and ZO-1) increases integration of transplanted photoreceptor precursors into the adult wild-type and degenerating retina. *Cell transplantation* **19**, 487-503 (2010).

80. Yao, J., Tao, S.L. & Young, M.J. Synthetic Polymer Scaffolds for Stem Cell Transplantation in Retinal Tissue Engineering. *Polymers* **3**, 899-914 (2011).

81. Ghosh, F., Johansson, K. & Ehinger, B. Long-term full-thickness embryonic rabbit retinal transplants. *Investigative ophthalmology & visual science* **40**, 133-142 (1999).

82. Khodair, M.A., Zarbin, M.A. & Townes-Anderson, E. Synaptic plasticity in mammalian photoreceptors prepared as sheets for retinal transplantation. *Investigative ophthalmology & visual science* **44**, 4976-4988 (2003).

83. Huang, J.C., Ishida, M., Hersh, P., Sugino, I.K. & Zarbin, M.A. Preparation and transplantation of photoreceptor sheets. *Current eye research* **17**, 573-585 (1998).

84. Seiler, M.J. & Aramant, R.B. Intact sheets of fetal retina transplanted to restore damaged rat retinas. *Investigative ophthalmology & visual science* **39**, 2121-2131 (1998).

85. Zhang, Y., Klassen, H.J., Tucker, B.A., Perez, M.T. & Young, M.J. CNS progenitor cells promote a permissive environment for neurite outgrowth via a matrix metalloproteinase-2-dependent mechanism. *The Journal of neuroscience : the official journal of the Society for Neuroscience* **27**, 4499-4506 (2007).

86. Tucker, B.A., Mullins, R.F. & Stone, E.M. Stem cells for investigation and treatment of inherited retinal disease. *Human molecular genetics* **23**, R9-r16 (2014).

87. Gonzalez-Cordero, A.*, et al.* Photoreceptor precursors derived from three-dimensional embryonic stem cell cultures integrate and mature within adult degenerate retina. *Nature biotechnology* **31**, 741-747 (2013).

88. Zhong, X.*, et al.* Generation of three-dimensional retinal tissue with functional photoreceptors from human iPSCs. *Nature communications* **5**, 4047 (2014).

89. Assawachananont, J.*, et al.* Transplantation of embryonic and induced pluripotent stem cell-derived 3D retinal sheets into retinal degenerative mice. *Stem cell reports* **2**, 662-674 (2014).

90. Tomita, M.*, et al.* Biodegradable polymer composite grafts promote the survival and differentiation of retinal progenitor cells. *Stem cells (Dayton, Ohio)* **23**, 1579-1588 (2005).

91. Redenti, S.*, et al.* Engineering retinal progenitor cell and scrollable poly(glycerol-sebacate) composites for expansion and subretinal transplantation. *Biomaterials* **30**, 3405-3414 (2009).

92. Huang, Y., Enzmann, V. & Ildstad, S.T. Stem cell-based therapeutic applications in retinal degenerative diseases. *Stem cell reviews* **7**, 434-445 (2011).

93. Pearson, R.A. Advances in repairing the degenerate retina by rod photoreceptor transplantation. *Biotechnology advances* **32**, 485-491 (2014).

94. Ong, J.M. & da Cruz, L. A review and update on the current status of stem cell therapy and the retina. *British medical bulletin* **102**, 133-146 (2012).

95. Brandl, C., Grassmann, F., Riolfi, J. & Weber, B.H. Tapping Stem Cells to Target AMD: Challenges and Prospects. *Journal of clinical medicine* **4**, 282-303 (2015).

96. Huang, R.*, et al.* Functional and morphological analysis of the subretinal injection of human retinal progenitor cells under Cyclosporin A treatment. *Molecular vision* **20**, 1271-1280 (2014).

97. Sakaguchi, D.S*., et al.* Transplantation of Neural Progenitor Cells into the Developing Retina of the Brazilian Opossum: An in vivo System for Studying Stem/Progenitor Cell Plasticity. *Developmental Neuroscience* **26**, 336-345 (2004).

98. Sakaguchi, D.S., Van Hoffelen, S.J. & Young, M.J. Differentiation and Morphological Integration of Neural Progenitor Cells Transplanted into the Developing Mammalian Eye. *Annals of the New York Academy of Sciences* **995**, 127-139 (2003).

99. Young, M.J., Ray, J., Whiteley, S.J.O., Klassen, H. & Gage, F.H. Neuronal Differentiation and Morphological Integration of Hippocampal Progenitor Cells Transplanted to the Retina of Immature and Mature Dystrophic Rats. *Molecular and Cellular Neuroscience* **16**, 197-205 (2000).

100. Mellough, C.B., Cui, Q. & Harvey, A.R. Treatment of adult neural progenitor cells prior to transplantation affects graft survival and integration in a neonatal and adult rat model of selective retinal ganglion cell depletion. *Restorative neurology and neuroscience* **25**, 177-190 (2007).

101. Klassen, H*., et al.* Neural precursors isolated from the developing cat brain show retinal integration following transplantation to the retina of the dystrophic cat. *Veterinary ophthalmology* **10**, 245-253 (2007).

102. Sakaguchi, D.S*., et al.* Neural progenitor cell transplants into the developing and mature central nervous system. *Ann N Y Acad Sci* **1049**, 118-134 (2005).

103. Kicic, A*., et al.* Differentiation of marrow stromal cells into photoreceptors in the rat eye. *The Journal of neuroscience : the official journal of the Society for Neuroscience* **23**, 7742-7749 (2003).

104. Mellough, C.B., Sernagor, E., Moreno-Gimeno, I., Steel, D.H. & Lako, M. Efficient stage-specific differentiation of human pluripotent stem cells toward retinal photoreceptor cells. *Stem cells (Dayton, Ohio)* **30**, 673-686 (2012).

105. Osakada, F*., et al.* Toward the generation of rod and cone photoreceptors from mouse, monkey and human embryonic stem cells. *Nature biotechnology* **26**, 215-224 (2008).

106. Parameswaran, S*., et al.* Induced pluripotent stem cells generate both retinal ganglion cells and photoreceptors: therapeutic implications in degenerative changes in glaucoma and age-related macular degeneration. *Stem cells (Dayton, Ohio)* **28**, 695-703 (2010).

107. Michalakis, S*., et al.* Restoration of cone vision in the CNGA3-/- mouse model of congenital complete lack of cone photoreceptor function. *Molecular therapy : the journal of the American Society of Gene Therapy* **18**, 2057-2063 (2010).

108. Takahashi, K. & Yamanaka, S. Induction of pluripotent stem cells from mouse embryonic and adult fibroblast cultures by defined factors. *Cell* **126**, 663-676 (2006).

109. Schmitt, S*., et al.* Molecular characterization of human retinal progenitor cells. *Investigative ophthalmology & visual science* **50**, 5901-5908 (2009).

110. Mullins, R.F*., et al.* Autosomal recessive retinitis pigmentosa due to ABCA4 mutations: clinical, pathologic, and molecular characterization. *Investigative ophthalmology & visual science* **53**, 1883-1894 (2012).

111. Gurdon, J.B. Adult frogs derived from the nuclei of single somatic cells. *Developmental biology* **4**, 256-273 (1962).

112. La Torre, A., Lamba, D.A., Jayabalu, A. & Reh, T.A. Production and transplantation of retinal cells from human and mouse embryonic stem cells. *Methods Mol Biol* **884**, 229-246 (2012).

113. Lamba, D.A., Karl, M.O., Ware, C.B. & Reh, T.A. Efficient generation of retinal progenitor cells from human embryonic stem cells. *Proceedings of the National Academy of Sciences of the United States of America* **103**, 12769-12774 (2006).

114. Lamba, D.A*., et al.* Generation, purification and transplantation of photoreceptors derived from human induced pluripotent stem cells. *PloS one* **5**, e8763 (2010).

115. Tucker, B.A., Anfinson, K.R., Mullins, R.F., Stone, E.M. & Young, M.J. Use of a synthetic xeno-free culture substrate for induced pluripotent stem cell induction and retinal differentiation. *Stem cells translational medicine* **2**, 16-24 (2013).

116. Meyer, J.S*., et al.* Modeling early retinal development with human embryonic and induced pluripotent stem cells. *Proceedings of the National Academy of Sciences of the United States of America* **106**, 16698-16703 (2009).

117. Osakada, F., Ikeda, H., Sasai, Y. & Takahashi, M. Stepwise differentiation of pluripotent stem cells into retinal cells. *Nature protocols* **4**, 811-824 (2009).

118. Osakada, F*., et al.* In vitro differentiation of retinal cells from human pluripotent stem cells by small-molecule induction. *Journal of cell science* **122**, 3169-3179 (2009).

119. Nakano, T*., et al.* Self-formation of optic cups and storable stratified neural retina from human ESCs. *Cell stem cell* **10**, 771-785 (2012).

120. Meyer, J.S.*, et al.* Optic vesicle-like structures derived from human pluripotent stem cells facilitate a customized approach to retinal disease treatment. *Stem cells (Dayton, Ohio)* **29**, 1206-1218 (2011).

121. Tucker, B.A.*, et al.* Patient-specific iPSC-derived photoreceptor precursor cells as a means to investigate retinitis pigmentosa. *eLife* **2**, e00824 (2013).

122. Burnight, E.R.*, et al.* CEP290 gene transfer rescues Leber congenital amaurosis cellular phenotype. *Gene therapy* **21**, 662-672 (2014).

123. Fairchild, P.J. The challenge of immunogenicity in the quest for induced pluripotency. *Nature reviews. Immunology* **10**, 868-875 (2010).

124. Fairchild, P.J. Taming the lion: the challenge of immunity in regenerative medicine. *Regenerative medicine* **10**, 227-229 (2015).

125. Eberle, D., Santos-Ferreira, T., Grahl, S. & Ader, M. Subretinal transplantation of MACS purified photoreceptor precursor cells into the adult mouse retina. *Journal of visualized experiments : JoVE*, e50932 (2014).

126. Eberle, D., Schubert, S., Postel, K., Corbeil, D. & Ader, M. Increased integration of transplanted CD73-positive photoreceptor precursors into adult mouse retina. *Investigative ophthalmology & visual science* **52**, 6462-6471 (2011).

127. Cramer, A.O. & MacLaren, R.E. Translating induced pluripotent stem cells from bench to bedside: application to retinal diseases. *Current gene therapy* **13**, 139-151 (2013).

128. Tolmachova, T.*, et al.* Functional expression of Rab escort protein 1 following AAV2-mediated gene delivery in the retina of choroideremia mice and human cells ex vivo. *Journal of molecular medicine (Berlin, Germany)* **91**, 825-837 (2013).

129. Simons, D.L., Boye, S.L., Hauswirth, W.W. & Wu, S.M. Gene therapy prevents photoreceptor death and preserves retinal function in a Bardet-Biedl syndrome mouse model. *Proceedings of the National Academy of Sciences of the United States of America* **108**, 6276-6281 (2011).

130. Li, X.*, et al.* Gene Therapy Rescues Cone Structure and Function in the 3-Month-Old rd12 Mouse: A Model for Midcourse RPE65 Leber Congenital Amaurosis. *Investigative ophthalmology & visual science* **52**, 7-15 (2011).

131. Bennicelli, J.*, et al.* Reversal of Blindness in Animal Models of Leber Congenital Amaurosis Using Optimized AAV2-mediated Gene Transfer. *Molecular therapy : the journal of the American Society of Gene Therapy* **16**, 458-465 (2008).

132. Tolmachova, T.*, et al.* CHM/REP1 cDNA delivery by lentiviral vectors provides functional expression of the transgene in the retinal pigment epithelium of choroideremia mice. *The journal of gene medicine* **14**, 158-168 (2012).

133. Dai, X.*, et al.* AAV-Mediated Lysophosphatidylcholine Acyltransferase 1 (Lpcat1) Gene Replacement Therapy Rescues Retinal Degeneration in rd11 Mice. *Investigative ophthalmology & visual science* **55**, 1724-1734 (2014).

134. Seo, S.*, et al.* Subretinal Gene Therapy of Mice With Bardet-Biedl Syndrome Type 1. *Investigative ophthalmology & visual science* **54**, 6118-6132 (2013).

135. Lopes, V.S.*, et al.* Retinal gene therapy with a large MYO7A cDNA using adeno-associated virus. *Gene therapy* **20**, 824-833 (2013).

136. Boye, S.L.*, et al.* AAV-Mediated Gene Therapy in the Guanylate Cyclase (RetGC1/RetGC2) Double Knockout Mouse Model of Leber Congenital Amaurosis. *Human Gene Therapy* **24**, 189-202 (2013).

137. Koch, S.*, et al.* Gene therapy restores vision and delays degeneration in the CNGB1(-/-) mouse model of retinitis pigmentosa. *Human molecular genetics* **21**, 4486-4496 (2012).

138. Beltran, W.A.*, et al.* Gene therapy rescues photoreceptor blindness in dogs and paves the way for treating human X-linked retinitis pigmentosa. *Proceedings of the National Academy of Sciences of the United States of America* **109**, 2132-2137 (2012).

139. Gorbatyuk, M.S.*, et al.* Functional Rescue of P23H Rhodopsin Photoreceptors by Gene Delivery. *Advances in Experimental Medicine and Biology* **723**, 191-197 (2012).

140. Michalakis, S.*, et al.* Gene therapy restores missing cone-mediated vision in the CNGA3-/- mouse model of achromatopsia. *Adv Exp Med Biol* **723**, 183-189 (2012).

141. Liu, Q.*, et al.* Expression of Wild-Type Rp1 Protein in Rp1 Knock-in Mice Rescues the Retinal Degeneration Phenotype. *PloS one* **7**, e43251 (2012).

142. Mihelec, M.*, et al.* Long-Term Preservation of Cones and Improvement in Visual Function Following Gene Therapy in a Mouse Model of Leber Congenital Amaurosis Caused by Guanylate Cyclase-1 Deficiency. *Human Gene Therapy* **22**, 1179-1190 (2011).

143. Mowat, F.M.*, et al.* RPE65 gene therapy slows cone loss in Rpe65-deficient dogs. *Gene therapy* **20**, 545-555 (2013).

144. Acland, G.M.*, et al.* Gene therapy restores vision in a canine model of childhood blindness. *Nature genetics* **28**, 92-95 (2001).

145. Jacobson, S.G.*, et al.* Gene therapy for leber congenital amaurosis caused by RPE65 mutations: safety and efficacy in 15 children and adults followed up to 3 years. *Archives of ophthalmology* **130**, 9-24 (2012).

146. MacLaren, R.E.*, et al.* Retinal gene therapy in patients with choroideremia: initial findings from a phase 1/2 clinical trial. *Lancet* **383**, 1129-1137 (2014).

147. Wiley, L.A.*, et al.* Patient-specific induced pluripotent stem cells (iPSCs) for the study and treatment of retinal degenerative diseases. *Prog Retin Eye Res* **44**, 15-35 (2015).

148. Tucker, B.A.*, et al.* Exome sequencing and analysis of induced pluripotent stem cells identify the cilia-related gene male germ cell-associated kinase (MAK) as a cause of retinitis pigmentosa. *Proceedings of the National Academy of Sciences of the United States of America* **108**, E569-576 (2011).

149. Yoshida, T.*, et al.* The use of induced pluripotent stem cells to reveal pathogenic gene mutations and explore treatments for retinitis pigmentosa. *Molecular brain* **7**, 45 (2014).

150. Li, Y.*, et al.* Gene therapy in patient-specific stem cell lines and a preclinical model of retinitis pigmentosa with membrane frizzled-related protein defects. *Molecular therapy : the journal of the American Society of Gene Therapy* **22**, 1688-1697 (2014).

151. Schwarz, N.*, et al.* Translational read-through of the RP2 Arg120stop mutation in patient iPSC-derived retinal pigment epithelium cells. *Human molecular genetics* **24**, 972-986 (2015).

152. Homma, K.*, et al.* Developing rods transplanted into the degenerating retina of Crx-knockout mice exhibit neural activity similar to native photoreceptors. *Stem cells (Dayton, Ohio)* **31**, 1149-1159 (2013).

153. West, E.L.*, et al.* Defining the integration capacity of embryonic stem cell-derived photoreceptor precursors. *Stem cells (Dayton, Ohio)* **30**, 1424-1435 (2012).

154. Mao, H.*, et al.* AAV delivery of wild-type rhodopsin preserves retinal function in a mouse model of autosomal dominant retinitis pigmentosa. *Hum Gene Ther* **22**, 567-575 (2011).

155. Pang, J.J.*, et al.* Gene therapy restores vision-dependent behavior as well as retinal structure and function in a mouse model of RPE65 Leber congenital amaurosis.

Molecular therapy : the journal of the American Society of Gene Therapy **13**, 565-572 (2006).

156. Yang, Y.*, et al.* Functional cone rescue by RdCVF protein in a dominant model of retinitis pigmentosa. *Molecular therapy : the journal of the American Society of Gene Therapy* **17**, 787-795 (2009).

157. Johnson, T.V. & Martin, K.R. Development and characterization of an adult retinal explant organotypic tissue culture system as an in vitro intraocular stem cell transplantation model. *Investigative ophthalmology & visual science* **49**, 3503-3512 (2008).

158. Lipinski, D.*, et al.* CNTF gene therapy confers lifelong neuroprotection in a mouse model of human retinitis pigmentosa. . *Mol Therapy*, in press (2015).

159. Lipinski, D.M., Singh, M.S. & MacLaren, R.E. Assessment of cone survival in response to CNTF, GDNF, and VEGF165b in a novel ex vivo model of end-stage retinitis pigmentosa. *Investigative ophthalmology & visual science* **52**, 7340-7346 (2011).

160. Hanna, J.*, et al.* Treatment of sickle cell anemia mouse model with iPS cells generated from autologous skin. *Science (New York, N.Y.)* **318**, 1920-1923 (2007).

161. McClements, M.E. & MacLaren, R.E. Gene therapy for retinal disease. *Translational research : the journal of laboratory and clinical medicine* **161**, 10.1016/j.trsl.2012.1012.1007 (2013).

162. Nonnenmacher, M. & Weber, T. Intracellular transport of recombinant adeno-associated virus vectors. *Gene therapy* **19**, 649-658 (2012).

163. Lipinski, D.M.*, et al.* Vesicular stomatitis virus glycoprotein- and Venezuelan equine encephalitis virus-derived glycoprotein-pseudotyped lentivirus vectors differentially transduce corneal endothelium, trabecular meshwork, and human photoreceptors. *Hum Gene Ther* **25**, 50-62 (2014).

164. Reichel, M.B.*, et al.* Immune responses limit adenovirally mediated gene expression in the adult mouse eye. *Gene therapy* **5**, 1038-1046 (1998).

165. Spencer, B., Agarwala, S., Miskulin, M., Smith, M. & Brandt, C.R. Herpes simplex virus-mediated gene delivery to the rodent visual system. *Investigative ophthalmology & visual science* **41**, 1392-1401 (2000).

166. Charbel Issa, P.*, et al.* Optimization of in vivo confocal autofluorescence imaging of the ocular fundus in mice and its application to models of human retinal degeneration. *Investigative ophthalmology & visual science* **53**, 1066-1075 (2012).

167. Trapani, I., Puppo, A. & Auricchio, A. Vector platforms for gene therapy of inherited retinopathies. *Prog Retin Eye Res* **43**, 108-128 (2014).

168. Charbel Issa, P. & MacLaren, R.E. Non-viral retinal gene therapy: a review. *Clinical & experimental ophthalmology* **40**, 39-47 (2012).

169. Tamboli, V., Mishra, G.P. & Mitrat, A.K. Polymeric vectors for ocular gene delivery. *Therapeutic delivery* **2**, 523-536 (2011).

170. Wang, W., Li, W., Ma, N. & Steinhoff, G. Non-viral gene delivery methods. *Current pharmaceutical biotechnology* **14**, 46-60 (2013).

171. Farjo, R., Skaggs, J., Quiambao, A.B., Cooper, M.J. & Naash, M.I. Efficient non-viral ocular gene transfer with compacted DNA nanoparticles. *PloS one* **1**, e38 (2006).

172. Kachi, S*., et al.* Nonviral ocular gene transfer. *Gene therapy* **12**, 843-851 (2005).

173. Johnson, C.J*., et al.* Technical brief: subretinal injection and electroporation into adult mouse eyes. *Molecular vision* **14**, 2211-2226 (2008).

174. Andrieu-Soler, C*., et al.* Enhanced oligonucleotide delivery to mouse retinal cells using iontophoresis. *Molecular vision* **12**, 1098-1107 (2006).

175. Souied, E.H*., et al.* Non-invasive gene transfer by iontophoresis for therapy of an inherited retinal degeneration. *Experimental eye research* **87**, 168-175 (2008).

176. Lipinski, D.M., Thake, M. & MacLaren, R.E. Clinical applications of retinal gene therapy. *Prog Retin Eye Res* **32**, 22-47 (2013).

177. Cai, X*., et al.* Gene delivery to mitotic and postmitotic photoreceptors via compacted DNA nanoparticles results in improved phenotype in a mouse model of retinitis pigmentosa. *The FASEB Journal* **24**, 1178-1191 (2010).

178. Cai, X*., et al.* A partial structural and functional rescue of a retinitis pigmentosa model with compacted DNA nanoparticles. *PloS one* **4**, e5290 (2009).

179. Conley, S.M. & Naash, M.I. Nanoparticles for retinal gene therapy. *Prog Retin Eye Res* **29**, 376-397 (2010).

180. Ding, X.Q*., et al.* Ocular delivery of compacted DNA-nanoparticles does not elicit toxicity in the mouse retina. *PloS one* **4**, e7410 (2009).

181. Mayrhofer, P., Schleef, M. & Jechlinger, W. Use of minicircle plasmids for gene therapy. *Methods Mol Biol* **542**, 87-104 (2009).

182. Gracey Maniar, L.E*., et al.* Minicircle DNA Vectors Achieve Sustained Expression Reflected by Active Chromatin and Transcriptional Level. *Molecular Therapy* **21**, 131-138 (2013).

183. Gaspar, V*., et al.* Minicircle DNA vectors for gene therapy: advances and applications. *Expert opinion on biological therapy* **15**, 353-379 (2015).

184. Berns, K.I. & Giraud, C. Biology of adeno-associated virus. *Current topics in microbiology and immunology* **218**, 1-23 (1996).

185. Daya, S. & Berns, K.I. Gene therapy using adeno-associated virus vectors. *Clinical microbiology reviews* **21**, 583-593 (2008).

186. Rolling, F. Recombinant AAV-mediated gene transfer to the retina: gene therapy perspectives. *Gene therapy* **11 Suppl 1**, S26-32 (2004).

187. McLaughlin, S.K., Collis, P., Hermonat, P.L. & Muzyczka, N. Adeno-associated virus general transduction vectors: analysis of proviral structures. *Journal of virology* **62**, 1963-1973 (1988).

188. Wu, Z., Yang, H. & Colosi, P. Effect of Genome Size on AAV Vector Packaging. *Molecular Therapy* **18**, 80-86 (2010).

189. Kotin, R.M., Linden, R.M. & Berns, K.I. Characterization of a preferred site on human chromosome 19q for integration of adeno-associated virus DNA by non-homologous recombination. *The EMBO journal* **11**, 5071-5078 (1992).

190. Schnepp, B.C., Clark, K.R., Klemanski, D.L., Pacak, C.A. & Johnson, P.R. Genetic fate of recombinant adeno-associated virus vector genomes in muscle. *Journal of virology* **77**, 3495-3504 (2003).

191. Miller, D.G., Petek, L.M. & Russell, D.W. Adeno-associated virus vectors integrate at chromosome breakage sites. *Nature genetics* **36**, 767-773 (2004).

192. Ferrari, F.K., Samulski, T., Shenk, T. & Samulski, R.J. Second-strand synthesis is a rate-limiting step for efficient transduction by recombinant adeno-associated virus vectors. *Journal of virology* **70**, 3227-3234 (1996).

193. Auricchio, A. Pseudotyped AAV vectors for constitutive and regulated gene expression in the eye. *Vision research* **43**, 913-918 (2003).

194. Allocca, M*., et al.* Novel adeno-associated virus serotypes efficiently transduce murine photoreceptors. *Journal of virology* **81**, 11372-11380 (2007).

195. Summerford, C. & Samulski, R.J. Membrane-associated heparan sulfate proteoglycan is a receptor for adeno-associated virus type 2 virions. *Journal of virology* **72**, 1438-1445 (1998).

196. Bartlett, J.S., Wilcher, R. & Samulski, R.J. Infectious entry pathway of adeno-associated virus and adeno-associated virus vectors. *Journal of virology* **74**, 2777-2785 (2000).

197. Sonntag, F., Bleker, S., Leuchs, B., Fischer, R. & Kleinschmidt, J.A. Adeno-associated virus type 2 capsids with externalized VP1/VP2 trafficking domains are generated prior to passage through the cytoplasm and are maintained until uncoating occurs in the nucleus. *Journal of virology* **80**, 11040-11054 (2006).

198. Yan, Z.*, et al.* Ubiquitination of both adeno-associated virus type 2 and 5 capsid proteins affects the transduction efficiency of recombinant vectors. *Journal of virology* **76**, 2043-2053 (2002).

199. Zhong, L.*, et al.* Next generation of adeno-associated virus 2 vectors: point mutations in tyrosines lead to high-efficiency transduction at lower doses. *Proceedings of the National Academy of Sciences of the United States of America* **105**, 7827-7832 (2008).

200. Petrs-Silva, H.*, et al.* High-efficiency transduction of the mouse retina by tyrosine-mutant AAV serotype vectors. *Molecular therapy : the journal of the American Society of Gene Therapy* **17**, 463-471 (2009).

201. Petrs-Silva, H.*, et al.* Novel properties of tyrosine-mutant AAV2 vectors in the mouse retina. *Molecular therapy : the journal of the American Society of Gene Therapy* **19**, 293-301 (2011).

202. Chen, Z.Y., He, C.Y., Ehrhardt, A. & Kay, M.A. Minicircle DNA vectors devoid of bacterial DNA result in persistent and high-level transgene expression in vivo. *Molecular therapy : the journal of the American Society of Gene Therapy* **8**, 495-500 (2003).

203. Darquet, A.M.*, et al.* Minicircle: an improved DNA molecule for in vitro and in vivo gene transfer. *Gene therapy* **6**, 209-218 (1999).

204. Chang, C.W., Christensen, L.V., Lee, M. & Kim, S.W. Efficient expression of vascular endothelial growth factor using minicircle DNA for angiogenic gene therapy. *Journal of controlled release : official journal of the Controlled Release Society* **125**, 155-163 (2008).

205. Huang, M.*, et al.* Novel minicircle vector for gene therapy in murine myocardial infarction. *Circulation* **120**, S230-237 (2009).

206. Osborn, M.J.*, et al.* Minicircle DNA-based gene therapy coupled with immune modulation permits long-term expression of alpha-L-iduronidase in mice with mucopolysaccharidosis type I. *Molecular therapy : the journal of the American Society of Gene Therapy* **19**, 450-460 (2011).

207. Wu, J.*, et al.* Minicircle-IFNgamma induces antiproliferative and antitumoral effects in human nasopharyngeal carcinoma. *Clinical cancer research : an official journal of the American Association for Cancer Research* **12**, 4702-4713 (2006).

208. Stenler, S.*, et al.* Gene transfer to mouse heart and skeletal muscles using a minicircle expressing human vascular endothelial growth factor. *Journal of cardiovascular pharmacology* **53**, 18-23 (2009).

209. Chen, Z.Y., He, C.Y., Meuse, L. & Kay, M.A. Silencing of episomal transgene expression by plasmid bacterial DNA elements in vivo. *Gene therapy* **11**, 856-864 (2004).

210. Chen, Z.Y.*, et al.* Linear DNAs concatemerize in vivo and result in sustained transgene expression in mouse liver. *Molecular therapy : the journal of the American Society of Gene Therapy* **3**, 403-410 (2001).

211. Yin, H.*, et al.* Non-viral vectors for gene-based therapy. *Nat Rev Genet* **15**, 541-555 (2014).

212. Jechlinger, W. Optimization and delivery of plasmid DNA for vaccination. *Expert review of vaccines* **5**, 803-825 (2006).

213. Kobelt, D.*, et al.* Performance of high quality minicircle DNA for in vitro and in vivo gene transfer. *Molecular biotechnology* **53**, 80-89 (2013).

214. Chen, Z.Y., He, C.Y. & Kay, M.A. Improved production and purification of minicircle DNA vector free of plasmid bacterial sequences and capable of persistent transgene expression in vivo. *Hum Gene Ther* **16**, 126-131 (2005).

215. Kay, M.A., He, C.-Y. & Chen, Z.-Y. A Simple And Rapid Minicircle DNA Vector Manufacturing System. *Nature biotechnology* **28**, 1287-1289 (2010).

216. Klinman, D.M. Immunotherapeutic uses of CpG oligodeoxynucleotides. *Nature reviews. Immunology* **4**, 249-258 (2004).

217. Krieg, A.M.*, et al.* CpG motifs in bacterial DNA trigger direct B-cell activation. *Nature* **374**, 546-549 (1995).

218. Kreiss, P.*, et al.* Plasmid DNA size does not affect the physicochemical properties of lipoplexes but modulates gene transfer efficiency. *Nucleic acids research* **27**, 3792-3798 (1999).

219. Yin, W., Xiang, P. & Li, Q. Investigations of the effect of DNA size in transient transfection assay using dual luciferase system. *Analytical biochemistry* **346**, 289-294 (2005).

220. Remaut, K., Sanders, N.N., Fayazpour, F., Demeester, J. & De Smedt, S.C. Influence of plasmid DNA topology on the transfection properties of DOTAP/DOPE lipoplexes. *Journal of controlled release : official journal of the Controlled Release Society* **115**, 335-343 (2006).

221. Alam, T.*, et al.* Correction of Diabetic Hyperglycemia and Amelioration of Metabolic Anomalies by Minicircle DNA Mediated Glucose-Dependent Hepatic Insulin Production. *PloS one* **8**, e67515 (2013).

222. Chang, T.Y.*, et al.* Durable expression of minicircle DNA-liposome-delivered androgen receptor cDNA in mice with hepatocellular carcinoma. *BioMed research international* **2014**, 156356 (2014).

223. Madeira, C.*, et al.* Nonviral gene delivery to neural stem cells with minicircles by microporation. *Biomacromolecules* **14**, 1379-1387 (2013).

224. Narsinh, K.H.*, et al.* Generation of Adult Human Induced Pluripotent Stem Cells Using Non-Viral Minicircle DNA Vectors. *Nature protocols* **6**, 78-88 (2011).

225. Argyros, O.*, et al.* Development of S/MAR minicircles for enhanced and persistent transgene expression in the mouse liver. *Journal of molecular medicine (Berlin, Germany)* **89**, 515-529 (2011).

226. Sharma, N.*, et al.* Efficient sleeping beauty DNA transposition from DNA minicircles. *Molecular therapy. Nucleic acids* **2**, e74 (2013).

227. West, E.L.*, et al.* Long-term survival of photoreceptors transplanted into the adult murine neural retina requires immune modulation. *Stem cells (Dayton, Ohio)* **28**, 1997-2007 (2010).

228. Beck, S.C.*, et al.* In vivo analysis of cone survival in mice. *Investigative ophthalmology & visual science* **51**, 493-497 (2010).

229. Megason, S., Amsterdam, A., Hopkins, N. & Lin, S. Uses of GFP in transgenic vertebrates. *Methods of biochemical analysis* **47**, 285-303 (2006).

230. O'Reilly, M*., et al.* A transgenic mouse model for gene therapy of rhodopsin-linked Retinitis Pigmentosa. *Vision research* **48**, 386-391 (2008).

231. Mitchiner, J.C., Pinto, L.H. & Vanable, J.W., Jr. Visually evoked eye movements in the mouse (Mus musculus). *Vision research* **16**, 1169-1171 (1976).

232. Thaung, C., Arnold, K., Jackson, I.J. & Coffey, P.J. Presence of visual head tracking differentiates normal sighted from retinal degenerate mice. *Neuroscience letters* **325**, 21-24 (2002).

233. Harvey, R.J., De'Sperati, C. & Strata, P. The early phase of horizontal optokinetic responses in the pigmented rat and the effects of lesions of the visual cortex. *Vision research* **37**, 1615-1625 (1997).

234. Douglas, R.M*., et al.* Independent visual threshold measurements in the two eyes of freely moving rats and mice using a virtual-reality optokinetic system. *Visual neuroscience* **22**, 677-684 (2005).

235. Grusser-Cornehls, U. & Bohm, P. Horizontal optokinetic ocular nystagmus in wildtype (B6CBA+/+) and weaver mutant mice. *Experimental brain research* **72**, 29-36 (1988).

236. Semo, M*., et al.* Dissecting a role for melanopsin in behavioural light aversion reveals a response independent of conventional photoreception. *PloS one* **5**, e15009 (2010).

237. Peachey, N.S., Goto, Y., al-Ubaidi, M.R. & Naash, M.I. Properties of the mouse cone-mediated electroretinogram during light adaptation. *Neuroscience letters* **162**, 9-11 (1993).

238. Pang, J.J*., et al.* Comparative analysis of in vivo and in vitro AAV vector transduction in the neonatal mouse retina: effects of serotype and site of administration. *Vision research* **48**, 377-385 (2008).

239. Fontaine, V., Kinkl, N., Sahel, J., Dreyfus, H. & Hicks, D. Survival of purified rat photoreceptors in vitro is stimulated directly by fibroblast growth factor-2. *The Journal of neuroscience : the official journal of the Society for Neuroscience* **18**, 9662-9672 (1998).

240. Koso, H*., et al.* CD73, a novel cell surface antigen that characterizes retinal photoreceptor precursor cells. *Investigative ophthalmology & visual science* **50**, 5411-5418 (2009).

241. Palmer, T.D., Takahashi, J. & Gage, F.H. The adult rat hippocampus contains primordial neural stem cells. *Molecular and cellular neurosciences* **8**, 389-404 (1997).

242. Svendsen, C.N., Fawcett, J.W., Bentlage, C. & Dunnett, S.B. Increased survival of rat EGF-generated CNS precursor cells using B27 supplemented medium. *Experimental brain research* **102**, 407-414 (1995).

243. Kaplan, H.J. & Fernandez de Castro, J.P. Retinal regeneration and stem cell therapy in retinitis pigmentosa. *Taiwan Journal of Ophthalmology* **2**, 41-44 (2012).

244. Akimoto, M.*, et al.* Targeting of GFP to newborn rods by Nrl promoter and temporal expression profiling of flow-sorted photoreceptors. *Proceedings of the National Academy of Sciences of the United States of America* **103**, 3890-3895 (2006).

245. Livesey, F.J. & Cepko, C.L. Vertebrate neural cell-fate determination: lessons from the retina. *Nature reviews. Neuroscience* **2**, 109-118 (2001).

246. Cepko, C.L., Austin, C.P., Yang, X., Alexiades, M. & Ezzeddine, D. Cell fate determination in the vertebrate retina. *Proceedings of the National Academy of Sciences of the United States of America* **93**, 589-595 (1996).

247. Young, R.W. Cell differentiation in the retina of the mouse. *The Anatomical record* **212**, 199-205 (1985).

248. Wagers, A.J. & Weissman, I.L. Plasticity of adult stem cells. *Cell* **116**, 639-648 (2004).

249. Camargo, F.D., Chambers, S.M. & Goodell, M.A. Stem cell plasticity: from transdifferentiation to macrophage fusion. *Cell proliferation* **37**, 55-65 (2004).

250. Hershenov, D. & Koch-Hershenov, R.J. Fission and confusion. *Christian bioethics* **12**, 237-254 (2006).

251. Daley, G.Q. Alchemy in the liver: fact or fusion? *Nature medicine* **10**, 671-672 (2004).

252. Wilson, J.H. & Wensel, T.G. The nature of dominant mutations of rhodopsin and implications for gene therapy. *Molecular neurobiology* **28**, 149-158 (2003).

253. Rosenfeld, P.J.*, et al.* A null mutation in the rhodopsin gene causes rod photoreceptor dysfunction and autosomal recessive retinitis pigmentosa. *Nature genetics* **1**, 209-213 (1992).

254. Kumaramanickavel, G.*, et al.* Missense rhodopsin mutation in a family with recessive RP. *Nature genetics* **8**, 10-11 (1994).

255. Reig, C.*, et al.* Identification of a novel rhodopsin mutation (Met-44-Thr) in a simplex case of retinitis pigmentosa. *Human genetics* **94**, 283-286 (1994).

256. Palfi, A.*, et al.* Adeno-associated virus-mediated rhodopsin replacement provides therapeutic benefit in mice with a targeted disruption of the rhodopsin gene. *Hum Gene Ther* **21**, 311-323 (2010).

257. Pawlyk, B.S.*, et al.* Gene replacement therapy rescues photoreceptor degeneration in a murine model of Leber congenital amaurosis lacking RPGRIP. *Investigative ophthalmology & visual science* **46**, 3039-3045 (2005).

258. Sarra, G.M.*, et al.* Gene replacement therapy in the retinal degeneration slow (rds) mouse: the effect on retinal degeneration following partial transduction of the retina. *Human molecular genetics* **10**, 2353-2361 (2001).

259. McNally, N.*, et al.* Structural and functional rescue of murine rod photoreceptors by human rhodopsin transgene. *Human molecular genetics* **8**, 1309-1312 (1999).

260. O'Reilly, M.*, et al.* RNA interference-mediated suppression and replacement of human rhodopsin in vivo. *American journal of human genetics* **81**, 127-135 (2007).

261. Millington-Ward, S.*, et al.* Suppression and Replacement Gene Therapy for Autosomal Dominant Disease in a Murine Model of Dominant Retinitis Pigmentosa. *Molecular therapy : the journal of the American Society of Gene Therapy* **19**, 642-649 (2011).

262. Bainbridge, J.W.*, et al.* Effect of gene therapy on visual function in Leber's congenital amaurosis. *The New England journal of medicine* **358**, 2231-2239 (2008).

263. Hauswirth, W.W.*, et al.* Treatment of leber congenital amaurosis due to RPE65 mutations by ocular subretinal injection of adeno-associated virus gene vector: short-term results of a phase I trial. *Hum Gene Ther* **19**, 979-990 (2008).

264. Campochiaro, P.A.*, et al.* Adenoviral vector-delivered pigment epithelium-derived factor for neovascular age-related macular degeneration: results of a phase I clinical trial. *Hum Gene Ther* **17**, 167-176 (2006).

265. Vandenberghe, L.H.*, et al. Dosage Thresholds for AAV2 and AAV8 Photoreceptor Gene Therapy in Monkey*, (2011).

266. Kay, C.N.*, et al.* Targeting Photoreceptors via Intravitreal Delivery Using Novel, Capsid-Mutated AAV Vectors. *PloS one* **8**, e62097 (2013).

267. Rabinowitz, J.E.*, et al.* Cross-packaging of a single adeno-associated virus (AAV) type 2 vector genome into multiple AAV serotypes enables transduction with broad specificity. *Journal of virology* **76**, 791-801 (2002).

268. Khani, S.C*., et al.* AAV-mediated expression targeting of rod and cone photoreceptors with a human rhodopsin kinase promoter. *Investigative ophthalmology & visual science* **48**, 3954-3961 (2007).

269. Glushakova, L.G*., et al.* Does recombinant adeno-associated virus-vectored proximal region of mouse rhodopsin promoter support only rod-type specific expression in vivo? *Molecular vision* **12**, 298-309 (2006).

270. Woodford, B.J., Chen, J. & Simon, M.I. Expression of rhodopsin promoter transgene product in both rods and cones. *Experimental eye research* **58**, 631-635 (1994).

271. Srivastava, A., Lusby, E.W. & Berns, K.I. Nucleotide sequence and organization of the adeno-associated virus 2 genome. *Journal of virology* **45**, 555-564 (1983).

272. Zhang, T., Hu, J., Ding, W. & Wang, X. Doxorubicin augments rAAV-2 transduction in rat neuronal cells. *Neurochemistry international* **55**, 521-528 (2009).

273. Duan, D., Yue, Y., Yan, Z., Yang, J. & Engelhardt, J.F. Endosomal processing limits gene transfer to polarized airway epithelia by adeno-associated virus. *The Journal of clinical investigation* **105**, 1573-1587 (2000).

274. Douar, A.M., Poulard, K., Stockholm, D. & Danos, O. Intracellular trafficking of adeno-associated virus vectors: routing to the late endosomal compartment and proteasome degradation. *Journal of virology* **75**, 1824-1833 (2001).

275. Yan, Z*., et al.* Distinct classes of proteasome-modulating agents cooperatively augment recombinant adeno-associated virus type 2 and type 5-mediated transduction from the apical surfaces of human airway epithelia. *Journal of virology* **78**, 2863-2874 (2004).

276. Filbin, M.E. & Kieft, J.S. Toward a structural understanding of IRES RNA function. *Current opinion in structural biology* **19**, 267-276 (2009).

277. Davies, W.L., Carvalho, L.S. & Hunt, D.M. SPLICE: a technique for generating in vitro spliced coding sequences from genomic DNA. *BioTechniques* **43**, 785-789 (2007).

278. Gray, S.J*., et al.* Production of recombinant adeno-associated viral vectors and use in in vitro and in vivo administration. *Current protocols in neuroscience / editorial board, Jacqueline N. Crawley ... [et al.]* **Chapter 4**, Unit 4.17 (2011).

279. Sarra, G.M*., et al.* Kinetics of transgene expression in mouse retina following sub-retinal injection of recombinant adeno-associated virus. *Vision research* **42**, 541-549 (2002).

280. Tan, E.*, et al.* The relationship between opsin overexpression and photoreceptor degeneration. *Investigative ophthalmology & visual science* **42**, 589-600 (2001).

281. Surace, E.M. & Auricchio, A. Adeno-associated viral vectors for retinal gene transfer. *Prog Retin Eye Res* **22**, 705-719 (2003).

282. Yang, G.S.*, et al.* Virus-mediated transduction of murine retina with adeno-associated virus: effects of viral capsid and genome size. *Journal of virology* **76**, 7651-7660 (2002).

283. Jablonski, M.M., Tombran-Tink, J., Mrazek, D.A. & Iannaccone, A. Pigment epithelium-derived factor supports normal development of photoreceptor neurons and opsin expression after retinal pigment epithelium removal. *The Journal of neuroscience : the official journal of the Society for Neuroscience* **20**, 7149-7157 (2000).

284. Liljekvist-Larsson, I., Torngren, M., Abrahamson, M. & Johansson, K. Growth of the postnatal rat retina in vitro: quantitative RT-PCR analyses of mRNA expression for photoreceptor proteins. *Molecular vision* **9**, 657-664 (2003).

285. Lem, J.*, et al.* Morphological, physiological, and biochemical changes in rhodopsin knockout mice. *Proceedings of the National Academy of Sciences of the United States of America* **96**, 736-741 (1999).

286. Rakshit, T. & Park, P.S. Impact of reduced rhodopsin expression on the structure of rod outer segment disc membranes. *Biochemistry* **54**, 2885-2894 (2015).

287. Aleman, T.S.*, et al.* Impairment of the transient pupillary light reflex in Rpe65(-/-) mice and humans with leber congenital amaurosis. *Investigative ophthalmology & visual science* **45**, 1259-1271 (2004).

288. Radel, J.D., Das, S. & Lund, R.D. Development of Light-activated Pupilloconstriction in Rats as Mediated by Normal and Transplanted Retinae. *The European journal of neuroscience* **4**, 603-615 (1992).

289. Hussain, R.Z.*, et al.* Direct and consensual murine pupillary reflex metrics: establishing normative values. *Autonomic neuroscience : basic & clinical* **151**, 164-167 (2009).

290. Thompson, S.*, et al.* Light aversion in mice depends on nonimage-forming irradiance detection. *Behavioral neuroscience* **124**, 821-827 (2010).

291. Bourin, M. & Hascoet, M. The mouse light/dark box test. *European journal of pharmacology* **463**, 55-65 (2003).

292. Takao, K. & Miyakawa, T. Light/dark transition test for mice. *Journal of visualized experiments : JoVE*, 104 (2006).

293. Wert, K.J., Davis, R.J., Sancho-Pelluz, J., Nishina, P.M. & Tsang, S.H. Gene therapy provides long-term visual function in a pre-clinical model of retinitis pigmentosa. *Human molecular genetics* **22**, 558-567 (2013).

294. Lucas, R.J., Douglas, R.H. & Foster, R.G. Characterization of an ocular photopigment capable of driving pupillary constriction in mice. *Nature neuroscience* **4**, 621-626 (2001).

295. Hattar, S.*, et al.* Melanopsin and rod-cone photoreceptive systems account for all major accessory visual functions in mice. *Nature* **424**, 76-81 (2003).

296. Young, M.J. & Lund, R.D. The retinal ganglion cells that drive the pupilloconstrictor response in rats. *Brain research* **787**, 191-202 (1998).

297. Misslin, R., Belzung, C. & Vogel, E. Behavioural validation of a light/dark choice procedure for testing anti-anxiety agents. *Behavioural processes* **18**, 119-132 (1989).

298. Crawley, J. & Goodwin, F.K. Preliminary report of a simple animal behavior model for the anxiolytic effects of benzodiazepines. *Pharmacology, biochemistry, and behavior* **13**, 167-170 (1980).

299. Schultz, B.R. & Chamberlain, J.S. Recombinant Adeno-associated Virus Transduction and Integration. *Molecular therapy : the journal of the American Society of Gene Therapy* **16**, 1189-1199 (2008).

300. Gooley, J.J.*, et al.* Melanopsin and rod-cone photoreceptors play different roles in mediating pupillary light responses during exposure to continuous light in humans. *The Journal of neuroscience : the official journal of the Society for Neuroscience* **32**, 14242-14253 (2012).

301. Sandberg, M.A., Weigel-DiFranco, C., Rosner, B. & Berson, E.L. The relationship between visual field size and electroretinogram amplitude in retinitis pigmentosa. *Investigative ophthalmology & visual science* **37**, 1693-1698 (1996).

302. Takahashi, K.*, et al.* Induction of pluripotent stem cells from adult human fibroblasts by defined factors. *Cell* **131**, 861-872 (2007).

303. Carey, B.W.*, et al.* Reprogramming of murine and human somatic cells using a single polycistronic vector. *Proceedings of the National Academy of Sciences of the United States of America* **106**, 157-162 (2009).

304. Park, I.H., Lerou, P.H., Zhao, R., Huo, H. & Daley, G.Q. Generation of human-induced pluripotent stem cells. *Nature protocols* **3**, 1180-1186 (2008).

305. Welstead, G.G., Brambrink, T. & Jaenisch, R. Generating iPS cells from MEFS through forced expression of Sox-2, Oct-4, c-Myc, and Klf4. *Journal of visualized experiments : JoVE* (2008).

306. Nakagawa, M.*, et al.* Generation of induced pluripotent stem cells without Myc from mouse and human fibroblasts. *Nature biotechnology* **26**, 101-106 (2008).

307. Okita, K., Nakagawa, M., Hyenjong, H., Ichisaka, T. & Yamanaka, S. Generation of mouse induced pluripotent stem cells without viral vectors. *Science (New York, N.Y.)* **322**, 949-953 (2008).

308. Sommer, C.A.*, et al.* Induced pluripotent stem cell generation using a single lentiviral stem cell cassette. *Stem cells (Dayton, Ohio)* **27**, 543-549 (2009).

309. Shao, L.*, et al.* Generation of iPS cells using defined factors linked via the self-cleaving 2A sequences in a single open reading frame. *Cell research* **19**, 296-306 (2009).

310. Gonzalez, F.*, et al.* Generation of mouse-induced pluripotent stem cells by transient expression of a single nonviral polycistronic vector. *Proceedings of the National Academy of Sciences of the United States of America* **106**, 8918-8922 (2009).

311. Cheng, L.*, et al.* Low incidence of DNA sequence variation in human induced pluripotent stem cells generated by non-integrating plasmid expression. *Cell stem cell* **10**, 337-344 (2012).

312. Yu, J.*, et al.* Human Induced Pluripotent Stem Cells Free of Vector and Transgene Sequences. *Science (New York, N.Y.)* **324**, 797-801 (2009).

313. Kaji, K.*, et al.* Virus free induction of pluripotency and subsequent excision of reprogramming factors. *Nature* **458**, 771-775 (2009).

314. Woltjen, K. piggyBac transposition reprograms fibroblasts to induced pluripotent stem cells. **458**, 766-770 (2009).

315. Kim, D.*, et al.* Generation of Human Induced Pluripotent Stem Cells by Direct Delivery of Reprogramming Proteins. *Cell stem cell* **4**, 472-476 (2009).

316. Anokye-Danso, F.*, et al.* Highly efficient miRNA-mediated reprogramming of mouse and human somatic cells to pluripotency. *Cell stem cell* **8**, 376-388 (2011).

317. Arnhold, S., Absenger, Y., Klein, H., Addicks, K. & Schraermeyer, U. Transplantation of bone marrow-derived mesenchymal stem cells rescue photoreceptor cells in the dystrophic retina of the rhodopsin knockout mouse. *Graefe's archive for clinical and experimental ophthalmology = Albrecht von Graefes Archiv fur klinische und experimentelle Ophthalmologie* **245**, 414-422 (2007).

318. Steedman, M.R., Tao, S.L., Klassen, H. & Desai, T.A. Enhanced differentiation of retinal progenitor cells using microfabricated topographical cues. *Biomedical Microdevices* **12**, 363-369 (2010).

319. Buchholz, D.E.*, et al.* Derivation of functional retinal pigmented epithelium from induced pluripotent stem cells. *Stem cells (Dayton, Ohio)* **27**, 2427-2434 (2009).

320. Carr, A.J.*, et al.* Protective effects of human iPS-derived retinal pigment epithelium cell transplantation in the retinal dystrophic rat. *PloS one* **4**, e8152 (2009).

321. Aboody, K., Capela, A., Niazi, N., Stern, J.H. & Temple, S. Translating stem cell studies to the clinic for CNS repair: current state of the art and the need for a Rosetta stone. *Neuron* **70**, 597-613 (2011).

322. Cyranoski, D. Japanese woman is first recipient of next-generation stem cells. Vol. 2014 (Nature News, http://www.nature.com/news/japanese-woman-is-first-recipient-of-next-generation-stem-cells-1.15915, 2014).

323. Eiraku, M. & Sasai, Y. Mouse embryonic stem cell culture for generation of three-dimensional retinal and cortical tissues. *Nature protocols* **7**, 69-79 (2012).

324. Eiraku, M.*, et al.* Self-organizing optic-cup morphogenesis in three-dimensional culture. *Nature* **472**, 51-56 (2011).

325. Jin, Z.B., Okamoto, S., Xiang, P. & Takahashi, M. Integration-free induced pluripotent stem cells derived from retinitis pigmentosa patient for disease modeling. *Stem cells translational medicine* **1**, 503-509 (2012).

326. Klassen, H.J.*, et al.* Multipotent retinal progenitors express developmental markers, differentiate into retinal neurons, and preserve light-mediated behavior. *Investigative ophthalmology & visual science* **45**, 4167-4173 (2004).

327. Mah, N.*, et al.* Molecular insights into reprogramming-initiation events mediated by the OSKM gene regulatory network. *PloS one* **6**, e24351 (2011).

328. Schwartz, S.D.*, et al.* Human embryonic stem cell-derived retinal pigment epithelium in patients with age-related macular degeneration and Stargardt's macular dystrophy: follow-up of two open-label phase 1/2 studies. *Lancet* **385**, 509-516 (2015).

329. Song, W.K.*, et al.* Treatment of Macular Degeneration Using Embryonic Stem Cell-Derived Retinal Pigment Epithelium: Preliminary Results in Asian Patients. *Stem cell reports* (2015).

330. Sun, J.*, et al.* Protective effects of human iPS-derived retinal pigmented epithelial cells in comparison with human mesenchymal stromal cells and human neural stem cells on the degenerating retina in rd1 mice. *Stem cells (Dayton, Ohio)*, n/a-n/a (2015).

331. Tokumoto, Y., Ogawa, S., Nagamune, T. & Miyake, J. Comparison of efficiency of terminal differentiation of oligodendrocytes from induced pluripotent stem cells versus embryonic stem cells in vitro. *Journal of bioscience and bioengineering* **109**, 622-628 (2010).

332. Westenskow, P.D.*, et al.* Using flow cytometry to compare the dynamics of photoreceptor outer segment phagocytosis in iPS-derived RPE cells. *Investigative ophthalmology & visual science* **53**, 6282-6290 (2012).

333. Zhou, L.*, et al.* Differentiation of induced pluripotent stem cells of swine into rod photoreceptors and their integration into the retina. *Stem cells (Dayton, Ohio)* **29**, 972-980 (2011).

334. Nguyen, M. & Arnheiter, H. Signaling and transcriptional regulation in early mammalian eye development: a link between FGF and MITF. *Development (Cambridge, England)* **127**, 3581-3591 (2000).

335. Furukawa, T., Kozak, C.A. & Cepko, C.L. rax, a novel paired-type homeobox gene, shows expression in the anterior neural fold and developing retina. *Proceedings of the National Academy of Sciences of the United States of America* **94**, 3088-3093 (1997).

336. Mukhopadhyay, M.*, et al.* Dickkopf1 is required for embryonic head induction and limb morphogenesis in the mouse. *Developmental cell* **1**, 423-434 (2001).

337. Bachiller, D.*, et al.* The organizer factors Chordin and Noggin are required for mouse forebrain development. *Nature* **403**, 658-661 (2000).

338. Lamb, T.M.*, et al.* Neural induction by the secreted polypeptide noggin. *Science (New York, N.Y.)* **262**, 713-718 (1993).

339. Smith, W.C., Knecht, A.K., Wu, M. & Harland, R.M. Secreted noggin protein mimics the Spemann organizer in dorsalizing Xenopus mesoderm. *Nature* **361**, 547-549 (1993).

340. Hemmati-Brivanlou, A., Kelly, O.G. & Melton, D.A. Follistatin, an antagonist of activin, is expressed in the Spemann organizer and displays direct neuralizing activity. *Cell* **77**, 283-295 (1994).

341. Pera, E.M., Wessely, O., Li, S.Y. & De Robertis, E.M. Neural and head induction by insulin-like growth factor signals. *Developmental cell* **1**, 655-665 (2001).

342. Jadhav, A.P., Mason, H.A. & Cepko, C.L. Notch 1 inhibits photoreceptor production in the developing mammalian retina. *Development (Cambridge, England)* **133**, 913-923 (2006).

343. Ikeda, H.*, et al.* Generation of Rx+/Pax6+ neural retinal precursors from embryonic stem cells. *Proceedings of the National Academy of Sciences of the United States of America* **102**, 11331-11336 (2005).

344. Jagatha, B.*, et al.* In vitro differentiation of retinal ganglion-like cells from embryonic stem cell derived neural progenitors. *Biochemical and biophysical research communications* **380**, 230-235 (2009).

345. Hirami, Y.*, et al.* Generation of retinal cells from mouse and human induced pluripotent stem cells. *Neuroscience letters* **458**, 126-131 (2009).

346. Gouras, P., Du, J., Kjeldbye, H., Yamamoto, S. & Zack, D.J. Reconstruction of degenerate rd mouse retina by transplantation of transgenic photoreceptors. *Investigative ophthalmology & visual science* **33**, 2579-2586 (1992).

347. Kwan, A.S., Wang, S. & Lund, R.D. Photoreceptor layer reconstruction in a rodent model of retinal degeneration. *Experimental neurology* **159**, 21-33 (1999).

348. Lakowski, J.*, et al.* Effective transplantation of photoreceptor precursor cells selected via cell surface antigen expression. *Stem cells (Dayton, Ohio)* **29**, 1391-1404 (2011).

349. Schwartz, S.D.*, et al.* Embryonic stem cell trials for macular degeneration: a preliminary report. *Lancet* **379**, 713-720 (2012).

350. Lolley, R.N., Rong, H. & Craft, C.M. Linkage of photoreceptor degeneration by apoptosis with inherited defect in phototransduction. *Investigative ophthalmology & visual science* **35**, 358-362 (1994).

351. Lakowski, J.*, et al.* Cone and rod photoreceptor transplantation in models of the childhood retinopathy Leber congenital amaurosis using flow-sorted Crx-positive donor cells. *Human molecular genetics* **19**, 4545-4559 (2010).

352. Yao, J.*, et al.* XIAP therapy increases survival of transplanted rod precursors in a degenerating host retina. *Investigative ophthalmology & visual science* **52**, 1567-1572 (2011).

353. Eng, L.F. & Ghirnikar, R.S. GFAP and Astrogliosis. *Brain Pathology* **4**, 229-237 (1994).

354. Dahl, D. The radial glia of Müller in the rat retina and their response to injury. An immunofluorescence study with antibodies to the glial fibrillary acidic (GFA) protein. *Experimental eye research* **28**, 63-69 (1979).

355. Zhang, Y., Arner, K., Ehinger, B. & Perez, M.T. Limitation of anatomical integration between subretinal transplants and the host retina. *Investigative ophthalmology & visual science* **44**, 324-331 (2003).

356. Nakatsuji, N., Nakajima, F. & Tokunaga, K. HLA-haplotype banking and iPS cells. *Nat Biotech* **26**, 739-740 (2008).

357. Pappas, D.J*., et al.* Proceedings: human leukocyte antigen haplo-homozygous induced pluripotent stem cell haplobank modeled after the california population: evaluating matching in a multiethnic and admixed population. *Stem cells translational medicine* **4**, 413-418 (2015).

358. Taylor, C.J., Peacock, S., Chaudhry, A.N., Bradley, J.A. & Bolton, E.M. Generating an iPSC bank for HLA-matched tissue transplantation based on known donor and recipient HLA types. *Cell stem cell* **11**, 147-152 (2012).

359. Taylor, C.J*., et al.* Banking on human embryonic stem cells: estimating the number of donor cell lines needed for HLA matching. *Lancet* **366**, 2019-2025 (2005).

360. Rizzino, A. Stimulating progress in regenerative medicine: improving the cloning and recovery of cryopreserved human pluripotent stem cells with ROCK inhibitors. *Regenerative medicine* **5**, 799-807 (2010).

361. Ichikawa, H*., et al.* Gene pathway analysis of the mechanism by which the Rho-associated kinase inhibitor Y-27632 inhibits apoptosis in isolated thawed human embryonic stem cells. *Cryobiology* **64**, 12-22 (2012).

362. Li, H*., et al.* The Ink4/Arf locus is a barrier for iPS cell reprogramming. *Nature* **460**, 1136-1139 (2009).

363. Punzo, C. & Cepko, C. Cellular responses to photoreceptor death in the rd1 mouse model of retinal degeneration. *Investigative ophthalmology & visual science* **48**, 849-857 (2007).

364. Busskamp, V*., et al.* Genetic reactivation of cone photoreceptors restores visual responses in retinitis pigmentosa. *Science (New York, N.Y.)* **329**, 413-417 (2010).

365. Maguire, A.M*., et al.* Age-dependent effects of RPE65 gene therapy for Leber's congenital amaurosis: a phase 1 dose-escalation trial. *Lancet* **374**, 1597-1605 (2009).

366. Maguire, A.M.*, et al.* Safety and efficacy of gene transfer for Leber's congenital amaurosis. *The New England journal of medicine* **358**, 2240-2248 (2008).

367. Matsuda, T. & Cepko, C.L. Analysis of gene function in the retina. *Methods Mol Biol* **423**, 259-278 (2008).

368. Matsuda, T. & Cepko, C.L. Electroporation and RNA interference in the rodent retina in vivo and in vitro. *Proceedings of the National Academy of Sciences of the United States of America* **101**, 16-22 (2004).

369. Cideciyan, A.V. Leber Congenital Amaurosis due to RPE65 Mutations and its Treatment with Gene Therapy. *Progress in retinal and eye research* **29**, 398-427 (2010).

370. Hockemeyer, D.*, et al.* Genetic engineering of human pluripotent cells using TALE nucleases. *Nature biotechnology* **29**, 731-734 (2011).

371. Ding, Q.*, et al.* A TALEN genome-editing system for generating human stem cell-based disease models. *Cell stem cell* **12**, 238-251 (2013).

372. Wang, H.*, et al.* One-Step Generation of Mice Carrying Mutations in Multiple Genes by CRISPR/Cas-Mediated Genome Engineering. *Cell* **153**, 910-918 (2013).

373. Cong, L.*, et al.* Multiplex genome engineering using CRISPR/Cas systems. *Science (New York, N.Y.)* **339**, 819-823 (2013).

374. Maeder, M.L.*, et al.* CRISPR RNA-guided activation of endogenous human genes. *Nature methods* **10**, 977-979 (2013).

9. Appendix

Generation of human ESC and iPSC-derived photoreceptor precursor (PhRP) cells by Ocata Therapeutics

Ocata Therapeutics is a biotechnology company in the field of stem cells and regenerative medicine. Photoreceptor precursors (PhRPs) were generated from human embryonic stem cells (ESC) and induced pluripotent stem cells (iPSC) at Ocata Therapeutics and sent to the Nuffield Laboratory of Ophthalmology, University of Oxford for transplantation studies as detailed in Chapter 6.

Contributing researchers at Ocata Therapeutics: Wang Wei[1], Lu Shi-Jiang[1], Luo Chenmei[1], Huo Hongguang[1] and Lanza Robert[1,2]

1. Ocata Therapeutics, 33 Locke Drive, Marlborough, MA, USA 01752
2. Institute for Regenerative Medicine, Wake Forest University School of Medicine, NC, USA

Methods

1. Culture of undifferentiated human pluripotent stem cells (PSC)

Human H9 ESC lines, derived from blastocyst; and HA iPS cell lines derived from human dermal fibroblasts using non-integrating 6 factor mRNA reprogramming kit (Allele Biotechnology, CA, USA) were maintained on Matrigel® (BD Biosciences, CA, USA) in mTESR1 medium (Stemcell Technology, Vancouver, BC, Canada).

2. Doubling time determination

Cell population doubling time was estimated from cell counting. Each cell population to be tested was harvested with 0.5% Trypsin (life technology). 5×10^5 cells seeded in T-25 flask in 5ml of medium. Medium was changed every 2 days. Cells were harvested at 95% confluent and counted in a hemocytometer.

3. Retinal photoreceptor cell differentiation

To induce neural differentiation, 90% confluent human pluripotent stem cells were split onto the Matrigel at the 1:25 ratio. When cell colonies grew to about 50-100 cells, cell differentiation were initiated by directly switching cell culture medium from mTESR1 to retinal induction medium (RIM) containing

DMEM/F12, N2 and B27 serum-free supplements, 100 units/ml penicillin, 100 µg/ml streptomycin (Life technology), 0.45% glucose (Sigma), 20 µg/ml human insulin (Roche) and 50 ng/ml human Noggin (Peprotech) at 37 °C/5% CO_2. On day 5, RIM medium was switched to neural differentiation medium plus (NDM+), containing Neurobasal, N2 and B27 serum-free supplements, 100 units/ml penicillin, 100 µg/ml streptomycin, Glutamax, MEM Non-essential amino acid (Life technology), 0.45% glucose and 50 ng/ml human Noggin for two weeks. On Day 19, cells were mechanically lifted using a scraper (Corning) and plated into ultra-low attachment dishes in NDM minus (NDM^-, without Noggin). Cells formed neural spheres in the suspension culture. After four days (day 23), neural spheres were collected and plated on Matrigel coated surface in NDM-. Cells were maintained in NDM- until the desired maturation stage for a given experiment.

To generate mature photoreceptor-like cells, photoreceptor precursors (PhRP) were dissociated into single cells using accutase digestion and plated on Matrigel coated dishes at the density of $10^5/cm^2$. Cells were cultured in photoreceptor differentiation medium containing neurobasal, N2 and B27 serum-free supplements, 100 units/ml penicillin, 100 µg/ml streptomycin, Glutamax, MEM none essential amino acid (Life technology), 0.45% glucose, 10 ng/ml human BDNF, 10 ng/ml human CNTF, 2 µM retinoid acid and 10 µM DAPT for two weeks.

4. Gene expression analyses

Total RNA was extracted from cells using an RNeasy kit (Qiagen) following the instruction of user's manual. First-strand cDNA was synthesized with random hexamers using the SuperScript III reverse transcription (RT)-PCR system (Life technology). Reverse transcriptase polymerase chain reaction (RT-PCR) for eye field transcription factors were performed using the following primers: PAX6, F-TCTAATCGAAGGGCCAAATG R-TGTGAGGGCTGTGTCTGTTC; RX1, F-CGGCCAACAAGAAGATGAGT R-GCCATGGAGTTCAAGTCGTT; LHX2, F-TAGCATCTACTGCAAGGAAGAC R-GTGATAAACCAAGTCCCGAG; SIX3, F-GGAATGTGATGTATGATAGCC R-TGATTTCGGTTTGTTCTGG; TBX3, F-TCCGACTCCGTCTCTCTCTC R-CAAATCTTGCTGGGCTCTTC; SIX6, F-TCCCATGGGTATTTCACGTC R-CACACAGAACCCATCACCAC; and SOX2, F-GGAGCTTTGCAGGAAGTTTG R-AATTCAGCAAGAAGCCTCTCC. For real-time RT-PCR, transcripts were assayed using commercially available TaqMan gene expression assays (Life technology) for mash1 (Hs04187546_g1), RORβ (Hs00199445_m1), rhodopsin (Hs00892431_m1), cone-opsin (Hs00241039_m1) and recoverin (Hs00610056_m1), with the data normalized to GAPDH (4352934E). Each data point represents nine technical replicates from three independent biological samples.

5. Flow cytometry analysis

The expression of eye field and retinal neuronal and photoreceptor cell markers were quantified by Flow cytometry on an Accuri C6 flow cytometer

(BD) according to standard procedures. Briefly, single cells were harvested by trypsin digestion. Cells were fixed and permeabilized with intracellular fixation and permeabilization buffer set followed the instruction of the kit manual (e-bioscience). Primary antibodies were freshly prepared in PBS buffer with 5% FBS. Typically 5×10^5 cells were used for antibody labeling. Cells were stained in a 100 µl primary antibody cocktail for 1 h on ice, then washed twice with buffer, and incubated in 100 µl buffer supplemented with appropriate Alexa Fluor® 488 or Alexa Fluor® 647-conjugated secondary antibodies for 30 min on ice. Isotype mouse immunoglobulin G (IgG) or no primary antibody served as a negative control. Data was analyzed using BD Accuri C6 software.

6. In vitro immunocytochemistry

Cells were fixed in 4% paraformaldehyde for 30 min at room temperature. Samples were blocked with 5% normal goat or donkey serum (Jackson ImmunoResearch) and 0.3% Triton X-100 in PBS at room temperature for 1 h, followed by incubation with primary antibodies at room temperature for 1 h. The following antibodies and sources were used: PAX6-specific antibody (1:600, DSHB); SOX2-specific antibody (1:400, Cell Signaling, 3579); RX1/RAX-specific antibody (rabbit polyclonal, 1:100, Abcam, ab23340); human nestin-specific antibody (1:500, R&D, mab1259), TRβ2-specific antibody (1:200, abcam, ab53170); NRL-specific antibody (1:200, Sigma, SAB1100608); Mash1-specific antibody (1:100, Abnova, H00000429-M02); RORβ-specific-

Rabbit antibody (1:50, Millipore, Cat# AB9482); RXRγ-specific antibody (1:100, abcam, ab15518); CRX-specific antibody (1:25, Santa Cruz, SC-30150); NR2E3-specific antibody (1:50, R&D, PP-H7223-00), opsin-specific (red/green) antibody (rabbit polyclonal, 1:300, Millipore, AB5405); monoclonal Rhodopsin-specific (1:400, Sigma, R5403); polyclonal Rhodopsin-specific (1:200, Sigma, R9153), Recoverin-specific (1:200, Millipore AB5585); PDE6α-specific (1:200, Thermo Fisher Scientific, PA5-32974). Appropriate FITC or cy3-conjugated secondary antibodies (Jackson) were used and cell nuclei were counter stained with 4′,6-diamidino-2-phenylindole (DAPI).

Images of immunostaining were obtained by computer-assisted microscopy using a Nikon inverted microscopy (Eclipse TE2000-S) and images were obtained and analyzed using NIS-Element-BR software (Version 4.20, Nikon). Percentage of positive staining was estimated by the number of positive cells divided by total number of cells. 200–300 cells captured from randomly selected field were analysis. In all studies, a minimum of three independent experiments were performed.

7. Photoreceptor precursor cryopreservation

When passage 4 photoreceptor precursor culture become 90% confluent, dissociate cells into single cells using accutase. Plate cells on the ultra-low binding plates at the ratio of 1:1 in NDM medium without Noggin. Collect photoreceptor sphere on the next day and spheres can be frozen down in an

animal-free cryopreservation buffer, Cryostor CS10 (Stemcell Technologies), as neurospheres. Then stored at -80C for 2 days, and transferred to liquid nitrogen.

Results

1. Robust generation of retinal neural precursors from human pluripotent stem cells under defined serum- and feeder-free condition

We developed a simple and efficient method to generate highly enriched retinal cells from human PSCs using a multi-step strategy (Figure 1).

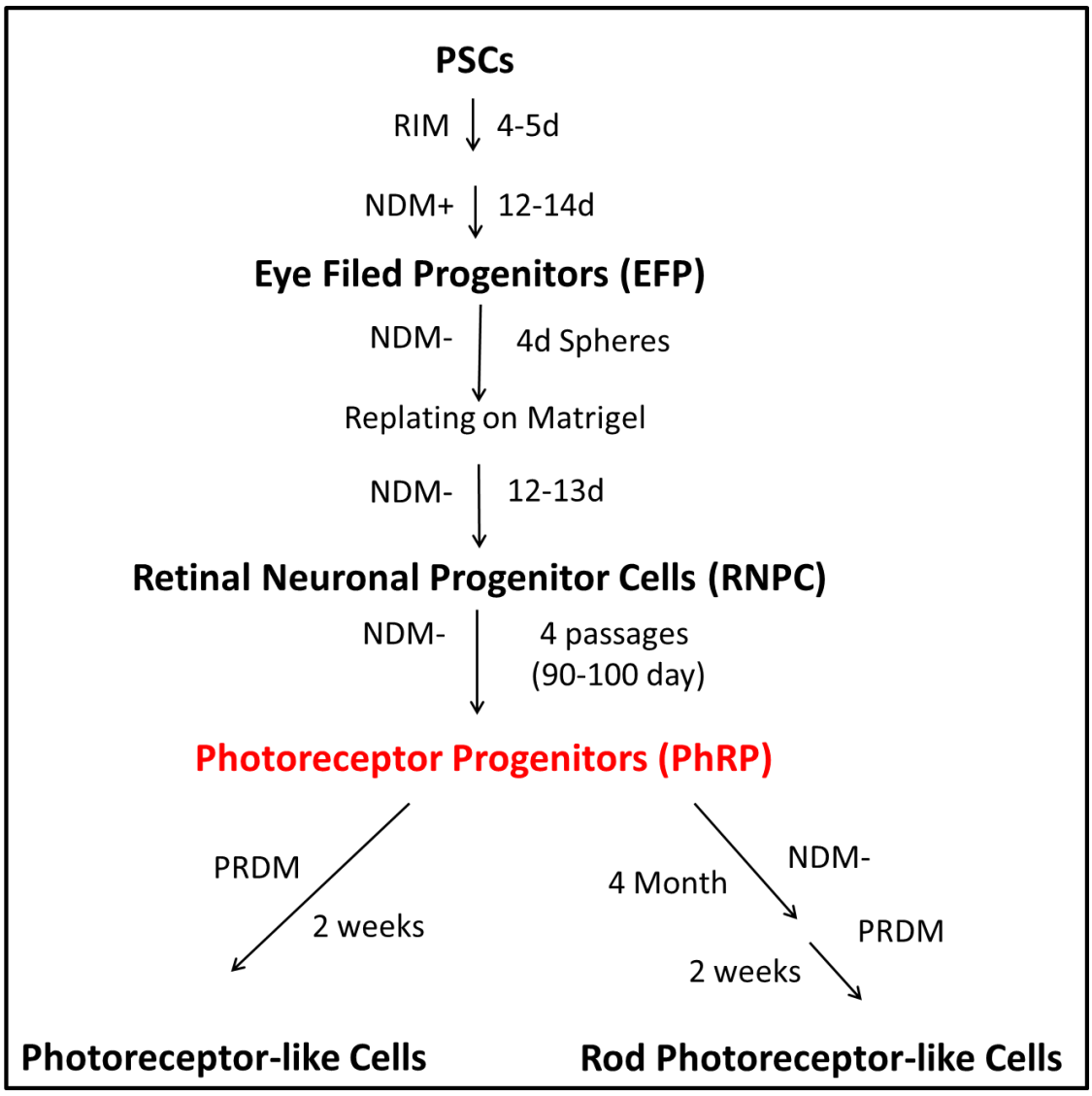

Figure 1: A schematic of the procedure for the generation of RNPCs and PhRPs from human PSCs

PhRPs used in *rd1* study were highlighted in red. RIM, retinal induction medium; NDM, neural differentiation medium with (+) or without (-) Noggin supplement; PRDM, photoreceptor differentiation medium.

First, hESCs were directly induced to differentiation in retinal induction medium (RIM) followed by exposure to neural differentiation medium (NDM) containing Noggin. After short exposure (usually ≈ 4 days) to RIM, cells at the edge of

colonies became elongated and exhibited a columnar phenotype (Figure 2a), and small cells dominated the center of these colonies after further differentiation (Figure 2b). A majority cells at this stage expressed paired box 6 (PAX6), nestin and sex determining region Y-box 2 (SOX2) (Figure 2c-d), suggesting they were committed to neural stem cells. Approximately two weeks after differentiation and expansion in NDM, only a few large cells were observed at the edge of neural stem cell colonies (Figure 2e). Rapid upregulation of PAX6 and retinal homeobox gene 1 (RX1) transcription factors was observed; >95% and >90% of cells at day 13 expressed PAX6 and RX1, respectively (Figure 3a), and most of them (>90%) were double positive for PAX6 and RX1 (Figure 3b-c). RT-PCR analyses showed expression of PAX6, RX1, LIM Homeobox 2 (LHX2), SIX homeobox 3 (SIX3), SIX homeobox 6 (SIX6) and T-Box 3 (TBX3) in these cells (Figure 2f). Real-time quantitative reverse transcription polymerase chain reaction (qRT-PCR) also demonstrated a dramatic decrease in the expression of octamer-binding transcription factor 4 (OCT4) and nanog, two critical pluripotent genes (Figure 2g). These results demonstrated a robust differentiation of hESCs towards retinal neural cells with gene profiles corresponding to eye field progenitors (EFP). After 19-21 days in NDM EFP cells were collected and plated to form neural spheres in suspension culture. After re-plating on Matrigel coated surface, neural spheres rapidly attached to the surface and formed long axon-like neurites, followed by subsequent migration of cell bodies along these extended processes (Figure 2h). Cells continually expanded and formed neural rosettes within a week

(Figure 2i). More than 95% of cells at this stage, including migrated-out neurons or neurons within aggregates, co-expressed PAX6 and Ceh-10 Homeo domain containing homolog (CHX10) (Figure 3d), suggesting they were retinal neural progenitor cells (RNPC).

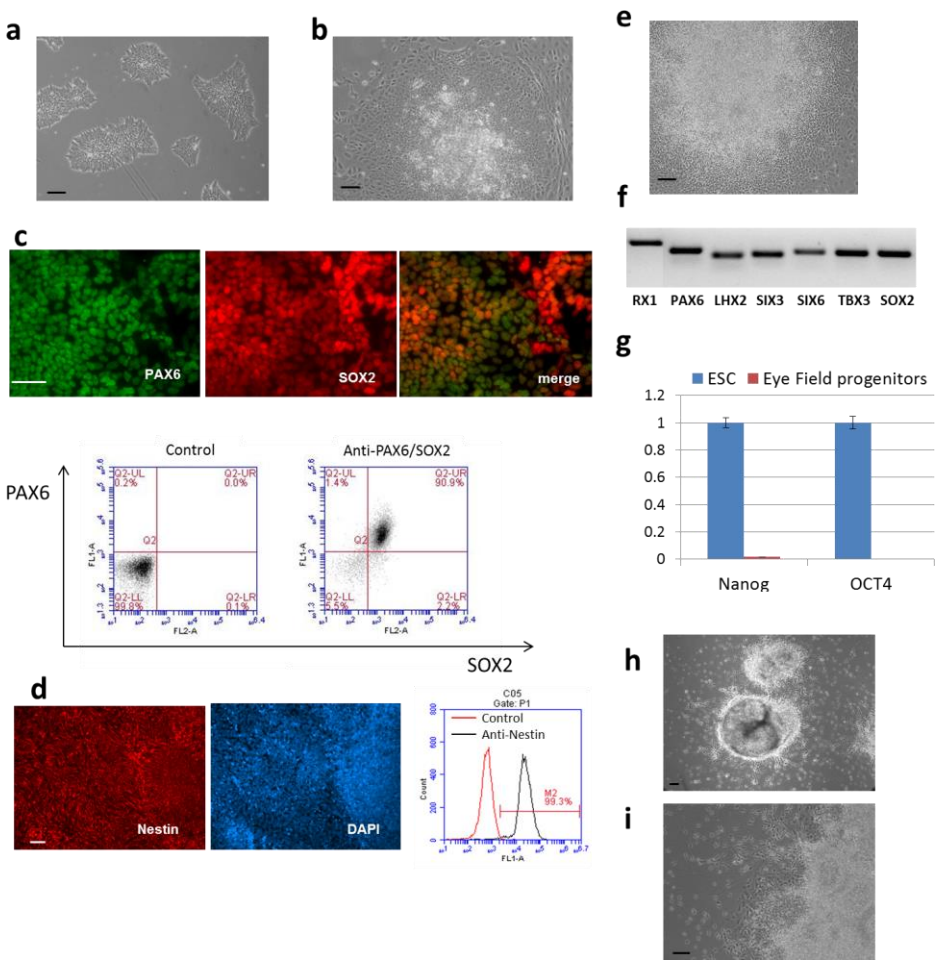

Figure 2: Step wise differentiation of human pluripotent stem cells towards retinal neurons *in vitro*

a, After 1 day cultured in retinal induction medium, cells at the colony margin were column-shaped. **b**, An example of a differentiating ESC colony after 7 days of *in vitro* differentiation. **c**, Up panel, immunofluorescence co-staining of PAX6 and SOX2 on cells after 7 days of *in vitro* differentiation. Low panel, quantification of PAX6 and SOX2 double positive cells by flow cytometry analysis, which shows > 90% of them expressing both PAX6 and SOX2 proteins**. d,** Immunofluorescence and flow cytometry quantification of nestin expression after 7 days of *in vitro* differentiation. **e,** An example of a differentiating eye field progenitor colony after 13 days of *in vitro* differentiation. **f**, RT-PCR analysis of RX1, PAX6, LHX2, SIX3, SIX6, TBX3 and SOX2 on cells after 13 days of differentiation. **g**, Quantitative RT-PCR analyses of ESC pluripotent markers on H9 human ESCs and on day 13 eye field progenitors. **h**, Spheres on Matrigel surface 48 hours after plating eye field progenitors. Note: neurons were migrating out from cell aggregates. **i**, Neural rosettes were formed after 7 days in culture on Matrigel surface. Scale bar, 50 µm.

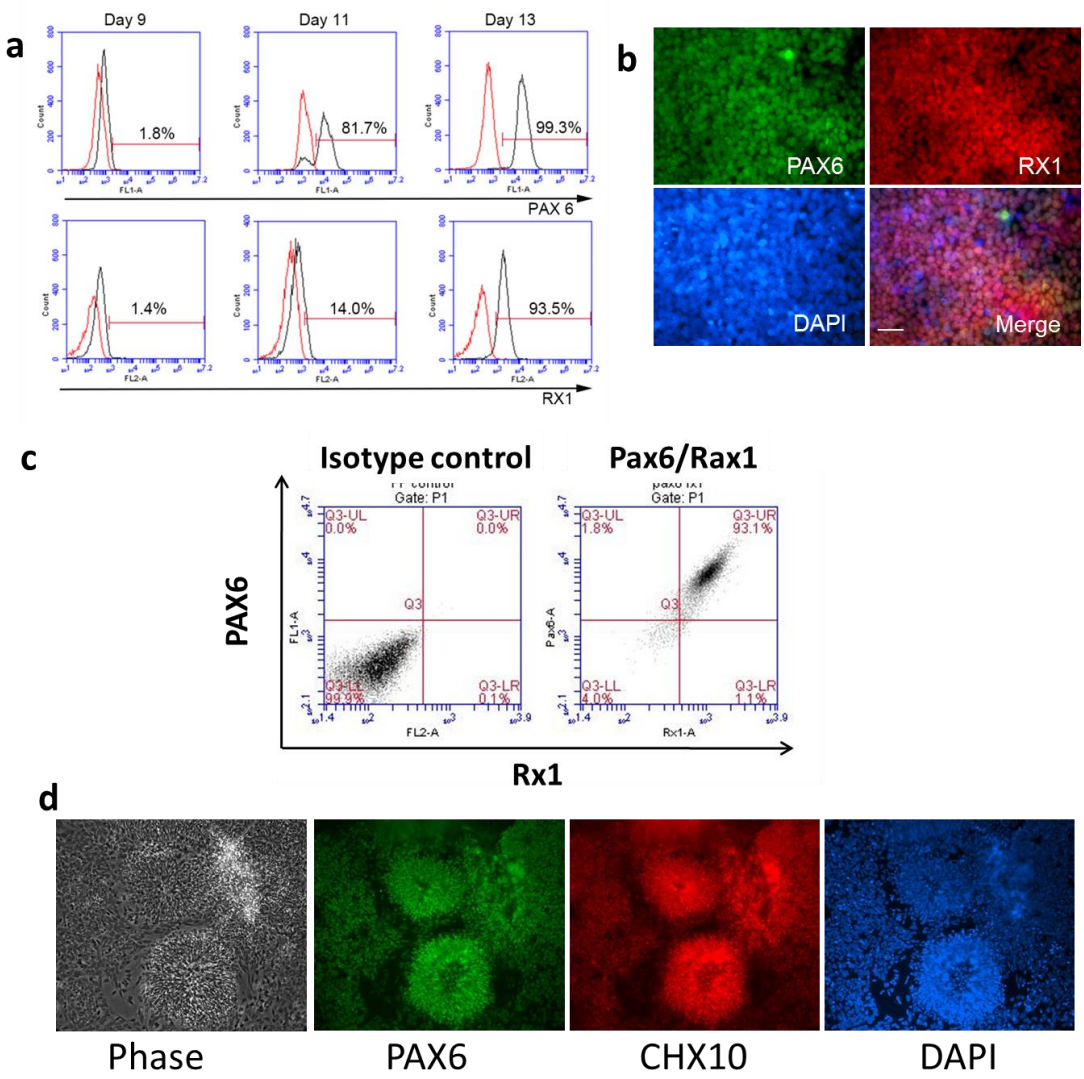

Figure 3: In vitro Differentiation of Human Embryonic Stem Cells towards Retinal Neural Progenitors

(a), Flow cytometry analyses show dynamic changes of PAX6 and RX1 expression on cells from day 9 to day 13 after *in vitro* differentiation. **(b),** Immunofluorescence staining shows co-expression of PAX6 and RX1 on day 13 eye field progenitors. **(c),** Quantification of PAX6 and RX1double positive eye field progenitors by flow cytometry analysis which shows > 90% of them expressing both PAX6 and RX1 proteins. **(d),** Immunofluorescence staining shows homogeneous co-expression of PAX6 and CHX10 on retinal neuronal progenitor cells (RNPC) at about day 30 after initial differentiation *in vitro*. Scale bar, 50 µm. Morphological changes, expression of retinal specific genes and down regulation of pluripotent genes are observed during the differentiation of human pluripotent stem cells towards retinal neural progenitors.

To validate the methodology, multiple hESC and iPSC lines (Table 1), generated with different strategies, were subjected to retinal neuron differentiation and analyzed for the expression of PAX6, RX1 and nestin by flow cytometry. Results demonstrated that all tested cell lines generated a near-homogenous population expressing these markers (Table 1), confirming the robustness of the retinal differentiation platform.

Table 1: Evaluation of eye field progenitor differentiation from multiple human ESC and iPSC lines

Cell lines	Percentage of PAX6/RX1positive cells
ESC lines (N=3), blastocyst: H1, H7 and H9.	92%-98%
ESC lines, single blastomere technology (N=3): MA01, MA09 and NED7.	94%-99%
iPS lines, Episomal Vector (N=4): iPS-1, iPS-2, iPS-3 and iPS-4	90%-99.6%
iPS lines, mRNA (N=2): HA and BJ	92%-98%

2. Generation of photoreceptor precursors and photoreceptor-like cells

We next tested whether PSC-RNPCs were able to further differentiate into more mature retinal neurons such as photoreceptor precursors (PhRP) and photoreceptors. After culturing PSC-RNPCs in NDM without noggin supplementation, cells further differentiated into photoreceptor precursors, as characterized by gradual loss of proliferative capacity as well as expression of transcription factors involved in photoreceptor development. Cell

population doubling time was approximately 10 days at the beginning and extended to 4 weeks by 10 months. After one passage, most cells (>90%) started to express Cone-Rod homeobox (CRX), Neural retina leucine zipper (NRL), retinoid X receptor gamma (RXRγ) and thyroid hormone receptor β2 (TRβ2) (Figure 4a-b), transcription factors that are essential for photoreceptor cell fate determination and development.

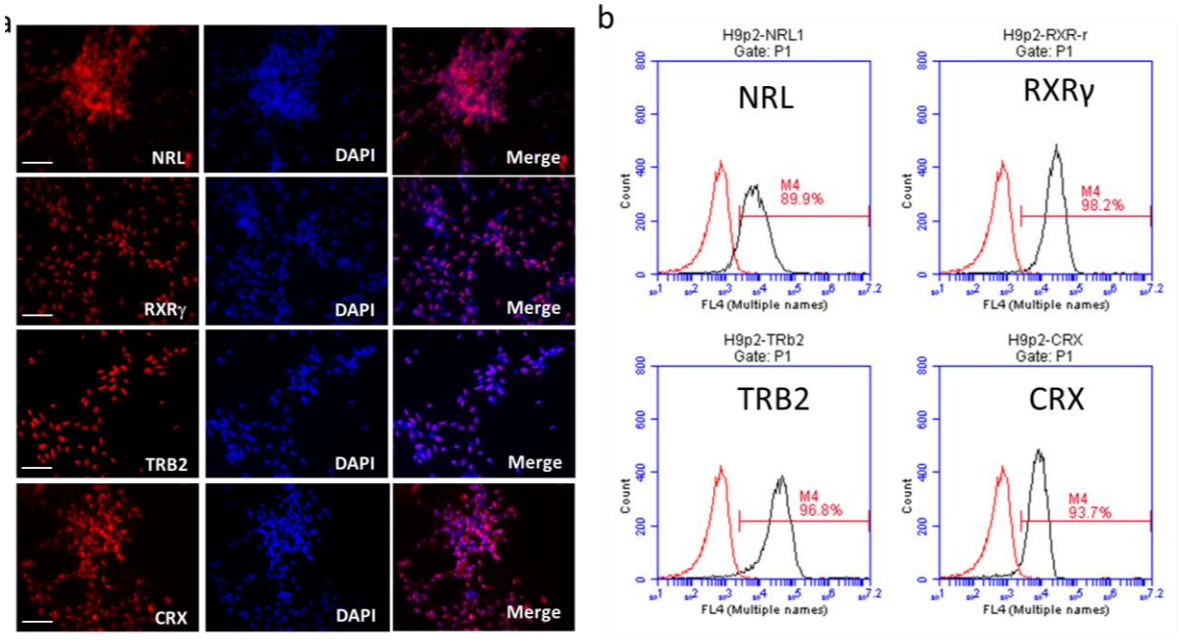

Figure 4: Figure 4 Expression of key photoreceptor transcription factors in differentiating retinal progenitors

(a), Immunofluorescence staining shows the expression of transcription factors NRL, RXRϒ, TRB2 and CRX in cells at 45-50 days after *in vitro* differentiation, Scale bar, 50 µm. **(b)**, Quantification of intracellular staining of NRL. RXRγ, TRB2 and CRX as determined by Flow Cytometry analyses.

At passage 4 (approximately 3 months in NDM without noggin), dramatic morphological changes were observed (Figure 5a). Although a majority of neurons formed short neurites at this stage, neurite branching from the cell body was reduced or absent. Most cells at this stage remained positive for PAX6, NRL, CRX, Nuclear receptor subfamily 2, group E, member 3 (NR2E3) and RXRγ, but lost the expression of CHX10 (Figure 6a and Figure 5c), and less than 10% of them are positive for Ki67, a cellular marker that is strictly associated with cell proliferation (Figure 5b). Real-time RT-PCR revealed up-regulation of Achaete-scute family BHLH transcription factor 1 ASCL1 and RAR-related orphan receptor beta RORβ genes in these cells (Figure 6b). Although recoverin protein was detected at low level (Figure 6c), rhodopsin and opsin proteins remained undetectable, however mRNA levels for both genes were substantially up-regulated in PhRPs in comparison to the levels in RNPCs (Figure 6d). Both neuN antibody and 2^{nd} antibody alone showed negative stains in these cells (Figure 6a). These results indicate that cells were differentiating towards retinal photoreceptors, probably at the stage of PhRPs. Near-homogenous PhRPs were similarly generated from multiple human iPSC lines, which expressed both rod and cone specific transcription factors, NRL and TRβ2 (Figure 5 d-e). Using multiple hESC and iPSC lines, approximately 1-2 X 10^8 PhRPs were generated from10^6 PSCs, therefore a 6-well plate of PSCs (10-12x10^6) could generate 1-2 X 10^9 PhRPs, potentially sufficient for hundreds of patients.

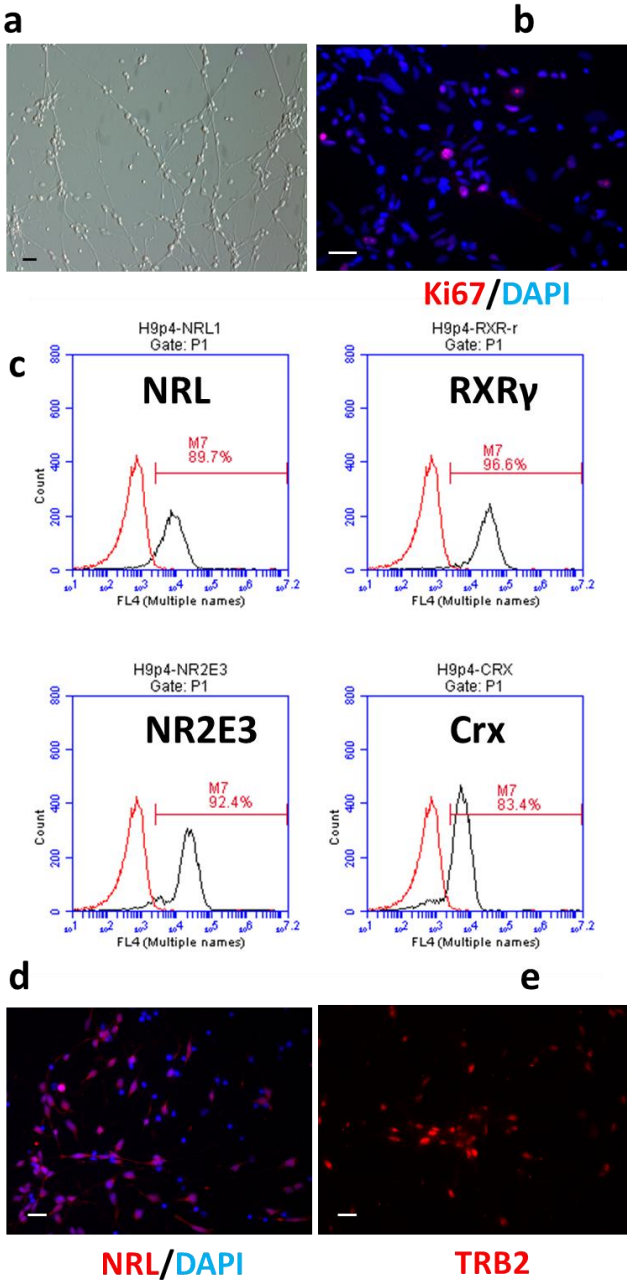

Figure 5: Generation of photoreceptor precursors from human PSCs

a, An example of photoreceptor precursors at day 110 after initiation of *in vitro* differentiation. Scale bar, 50 µm. **b** Immunofluorescence staining of Ki67 in PhRPs. **c**, Quantification of intracellular staining of NRL. RXRγ, NR2E3 and CRX as determined by Flow Cytometry analyses. **d and e**, Photoreceptor precursors derived from human iPS cells; immunofluorescence staining showing the expression of NRL (**d**) and TRB2 (**e**) in HA iPSC-derived photoreceptor precursors at passage 4. Scale bar, 20 µm.

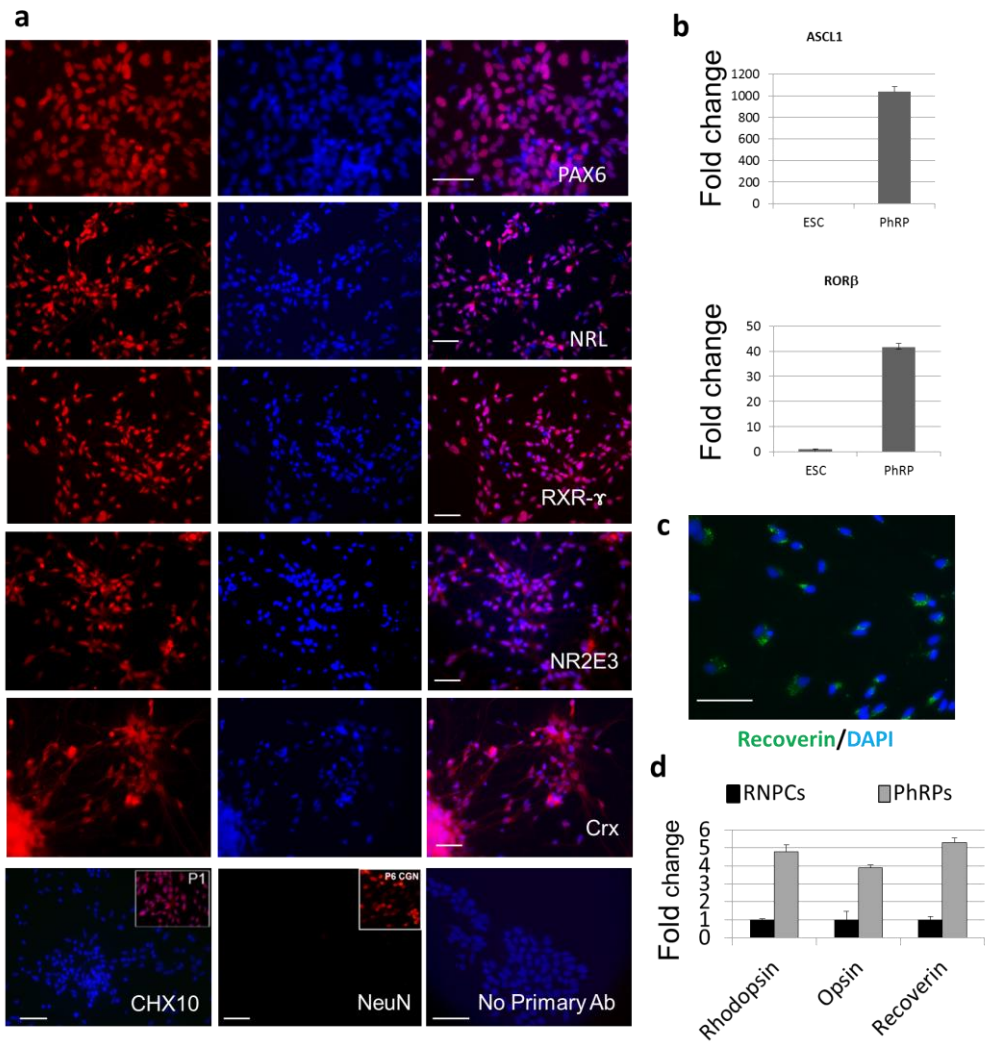

Figure 6: In vitro Differentiation of Retinal Neural Progenitors towards Photoreceptor Precursors

(a), Immunofluorescence staining shows the expression of transcription factors PAX6, CRX, NRL, RXR-ϒ, NR2E3 and CHX10 in PhRPs at 90-100 days after *in vitro* differentiation. The upper right corner of the CHX10 image shows positive expression of CHX10 in RNPCs at day 30, but negative in PhRPs. No positive stain was observed for neuN antibody in these cells (The upper right corner of the neuN image shows positive expression of neuN in mouse central nerve cells). 2nd antibody only also shows no stain. **(b),** Real time-PCR analysis shows up-regulation of photoreceptor transcription factors ASCL1 and RORβ in PhRPs. **(c),** Immunofluorescence staining shows low level expression of recoverin in the cytoplasm of PhRPs. **(d),** Real time-PCR confirms up-regulation of photoreceptor genes rhodoposin, opsin and recoverin in PhRPs as compared to RNPCs. Scale bar, 50 μm. All nuclei are counterstained in blue with DAPI.

To generate photoreceptor-like cells, PhRPs were further cultured in medium containing retinoic acid, DAPT, Brain-derived neurotrophic factor (BDNF) and ciliary neurotrophic factor (CNTF) for two weeks. Most cells (≈95%) expressed rhodopsin, recoverin and phosphodiesterase 6 alpha (PDE6α), markers of rod photoreceptor (Figure 7a), and green/red opsin (M-opsin) protein (Figure 7b), a marker for cone photoreceptors. A majority of cells at this stage co-expressed rhodopsin and M-opsin (Figure 7b right panel), indicating PSC-PhRPs possess potentials to differentiate into both rod and cone photoreceptors. Congruently, cells expressing photoreceptor-specific markers were also generated from iPS-PhRPs (Figure 7c).

Since cone and rod photoreceptors are generated from the same pool of retinal neural progenitors at different developmental stages, with L- M-cone and rod photoreceptors being the last retinal neurons generated, we continually passaged PhRPs *in vitro* for 8 months before commencing differentiation and maturation. After 8 months of culture, PhRPs were able to differentiate into photoreceptor-like cells expressing rod-specific proteins rhodopsin and PDE6α (Figure 7d) but not cone specific markers.

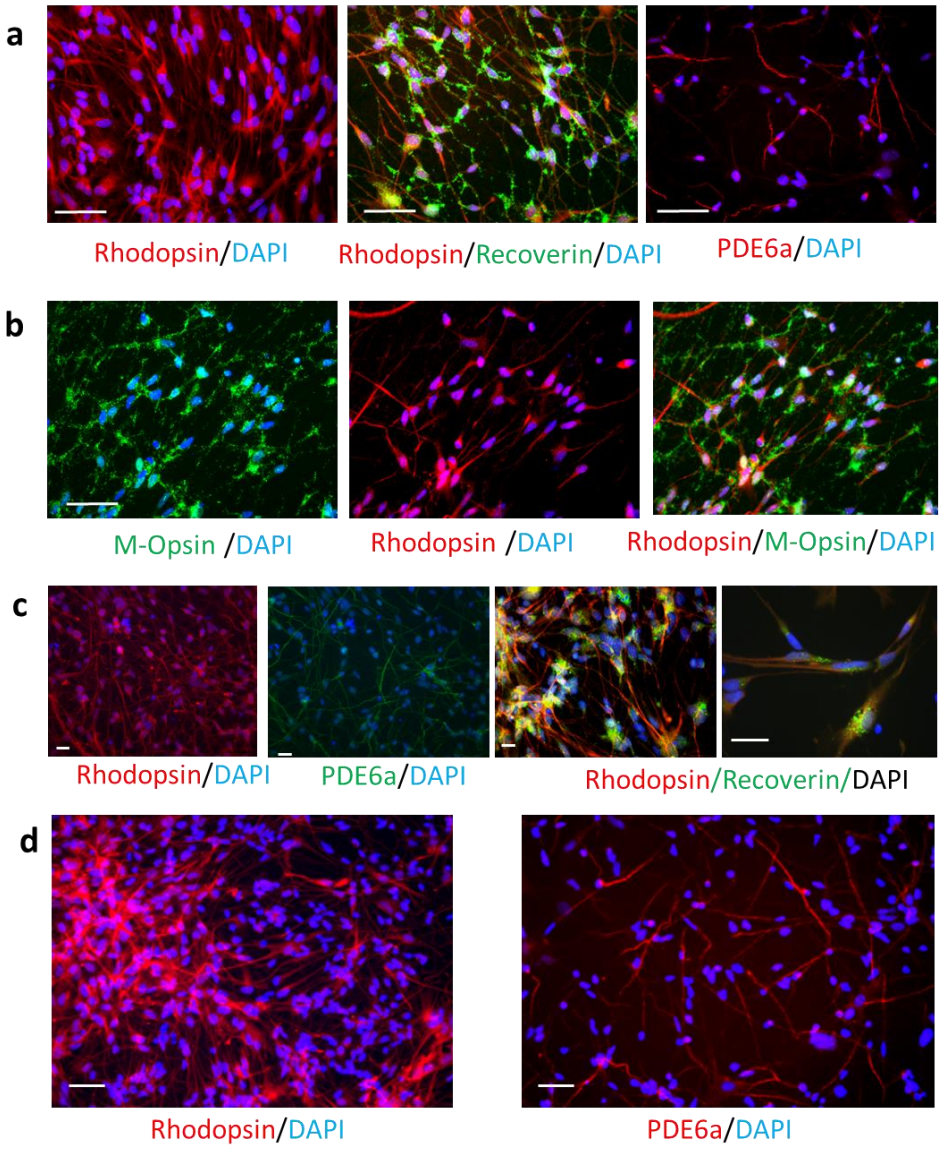

Figure 7: In vitro Generation of Mature Photoreceptor-like cells from Human ESC/iPS-Derived PhRPs

(a), Expression of rod photoreceptor markers, rhodopsin, recoverin and PDE6α and (b), cone photoreceptor markers M-opsin (left panel), Rhodopsin (middle panel) and colocalization of rhodopsin (red) and M-opsin (green, right panel of b) in human ESC-derived photoreceptors after two week *in vitro* maturation of PhRPs (100 days of *in vitro* differentiation) in photoreceptor differentiation medium (Scale bar, 50 μm). (c), Expression of rhodopsin and PDE6α in human iPSC-derived photoreceptors after two week *in vitro* maturation (Scale bar, 20 μm). (d), Human ESC-derived PhRPs cultured *in vitro* for 8 months differentiate into rod photoreceptors expressing rhodopsin and PDE6α, no cone pigment gene expression is detectable in these cells (Scale bar, 50 μm). All nuclei are counterstained in blue with DAPI.